The system CO2-CH4-N2 in fluid inclusions: theoretical modelling and geological applications

van den Kerkhof, A.M.

1988

document version
Publisher's PDF, also known as Version of record

THE SYSTEM CO_2-CH_4-N_2 IN FLUID INCLUSIONS:

THEORETICAL MODELLING AND GEOLOGICAL APPLICATIONS

A.M. van den Kerkhof

THE SYSTEM CO_2-CH_4-N_2 IN FLUID INCLUSIONS:
THEORETICAL MODELLING AND GEOLOGICAL APPLICATIONS

Free University Press is an imprint of:
VU Boekhandel/Uitgeverij b.v.
De Boelelaan 1105
1081 HV Amsterdam
The Netherlands

ISBN 90-6256-694-4 cip
NUGI 816

VRIJE UNIVERSITEIT TE AMSTERDAM

THE SYSTEM CO_2-CH_4-N_2 IN FLUID INCLUSIONS:
THEORETICAL MODELLING AND GEOLOGICAL APPLICATIONS

ACADEMISCH PROEFSCHRIFT

ter verkrijging van de graad van doctor aan
de Vrije Universiteit te Amsterdam,
op gezag van de rector magnificus
dr. C. Datema,
hoogleraar aan de faculteit der letteren,
in het openbaar te verdedigen
ten overstaan van de promotiecommissie
van de faculteit der aardwetenschappen
op maandag 27 juni 1988 te 13.30 uur
in het hoofdgebouw van de universiteit,
De Boelelaan 1105

door

ALFONSUS MARTINUS VAN DEN KERKHOF

geboren te Amstelveen

Free University Press
Amsterdam 1988

Promotor: prof.dr. J.L.R. Touret
Referenten: dr. J. Dubessy
dr. J.B.H. Jansen

DANKBETUIGING

Dit proefschrift is mede tot stand gekomen met de hulp en medewerking van vele mensen, organisaties en instellingen.

In het bijzonder ben ik dank verschuldigd aan mijn promotor prof.dr. J.L.R. Touret voor zijn begeleiding en de belangrijke bijdrage aan het onderzoek. In de afgelopen 3 jaar stond hij altijd klaar om oplossingen te zoeken voor de vele problemen. Het enthousiasme voor "zijn" fluid inclusions was een belangrijke stimulans tijdens mijn werkzaamheden.

Verder dank ik Drs. E.A.J. Burke en de Hr. W.J. Lustenhouwer voor hun uitgebreide begeleiding en advies bij de Raman analyse.

De nauwkeurige waarnemingen, die noodzakelijk waren voor dit onderzoek, waren mogelijk door de goede kwaliteit van de gepolijste doorsneden, vervaardigd door de Hr. H.A. van Egmond.

Het experimentele onderdeel van mijn onderzoek is mogelijk gemaakt door het gebruik van de faciliteiten van het HPT laboratorium van de Universiteit van Utrecht (gedurende 8 maanden). Ik ben vooral dank verschuldigd aan Dr. J.B.H. Jansen die een belangrijke bijdrage heeft geleverd aan mijn onderzoek door zijn adviezen en de stimulerende discussies. Ik wil in het bijzonder de Hr. A.M.J. van der Eerde bedanken voor de grote inzet waarmee hij mij bij de werkzaamheden heeft geassisteerd. Veel zeer kleine kwartsmonsters werden gepollijst door de medewerkers van de slijperij in Utrecht, i.h.b. de Hr. W. Wildenberg.

Gesteentemonsters uit verschillende gebieden vormden de basis voor mijn onderzoek en zonder deze zou dit werk nooit tot stand zijn gekomen. De monsters werden verzameld en beschikbaar gesteld door de volgende personen: Dr. J.J.M.M.M. Coolen (Furua granulietcomplex); Dr. C. Kieft (Harmsarvet); Dr. H.J. Kisch (Appalachen); Dr. R. Kreulen (Dôme de l'Agout); Dr. B. Lasnier (Haut Allier); Dr. H.E.C. Swanenberg (ZW Noorwegen).

Einige Versuche sind gemacht worden im Mineralogisches / Petrographisches Institut der Universität Tübingen (BRD) während eines Besuches von zwei Wochen. Ich danke Prof.Dr. P. Metz und seinen Mitarbeitern herzlich für die Gastfreiheit und für die Benützung der Apparatur. Besonders danke Ich auch Herrn Reinhardt Schultz für die

freundliche Assistenz.

Weiter danke Ich Dr. J. Walther (am Universität Karlsruhe) für die gute Ideen über binäre Systeme und Phasendiagramme.

Je remercie Dr. J. Dubessy pour ses critiques constructives et l'interèt qu'il a montré pour ce travail.

Aussi, je veux remercier Mme. A. Darimont pour mettre à la disposition quelques données originales de sa thèse et pour les discussions concernant la système CO_2-N_2.

Le Microdil-28® de l'Université Libre d'Amsterdam, avec lequel ont été réalisé les spectres Raman, a été l'un des premiers conçu par la Société Dilor. Nous remercions vivement Mr. E. Da Silva et ses collègues pour la qualité et l'efficacité de leurs services.

Fotografische reproducties zijn vervaardigd door de Hr. H.A. Sion. Printer faciliteiten zijn verschaft door de medewerksters van de administratie van het Instuut voor Aardwetenschappen aan de Vrije Universtiteit.

Het huidige onderzoek werd ondersteund door de Nederlandse Stichting voor Aardwetenschappelijk Onderzoek (A.W.O.N., project nr.751.353.014). De faciliteiten voor Raman analyse zijn verschaft door de Vrije Universeit te Amsterdam en door W.A.C.O.M., een werkgroep voor analytisch-chemisch onderzoek van mineralen en gesteenten. Zowel A.W.O.N. als W.A.C.O.M. worden finincieel gesteund door de Nederlandse organisatie voor Wetenschappelijk onderzoek (N.W.O.).

SUMMARY

Carbon dioxide, methane and nitrogen are found in many rocks of metamorphic and magmatic origin and they represent the 3 main gaseous components (besides water) in the earth's crust and upper mantle. These fluids (gases and liquids at high pressure) occur as inclusions of about 5-30μ in size in many rock forming minerals. Although the relative quantities of fluid in rocks is low, they do play an important and sometimes essential role during several geological processes (metamorphic reactions, melting, deformation etc.). Among other possibilities, fluid inclusions can be used for the determination of the depth at which rocks are formed: the density (and molar volume) can be considered as inherited from a high pressure (and temperature) stage at the time of trapping. The density of fluid inclusions is therefore a key parameter for many geological interpretations. It is calculated by means of experimentally determined models (equations of state) and data, obtained by 1) the study of phase transitions at varying temperature ("microthermometry") and by 2) measuring gas compositions by Raman microspectroscopy ("Raman analysis"). The knowledge of phase models for naturally occurring gases and gas mixtures is therefore important for a proper interpretation of measurements.

The application of Raman analysis is a major advantage for the study of fluid inclusions and became possible by the recent development of the Raman microspectrometer (Raman probe). Now, compositions of individual fluid inclusions can be rapidly measured in a non-destructive way. Other analytical methods like gas chromatography result to bulk compositions and give no information about the compositional variation within a sample. The determination of the density is only justified when both phase behaviour (e.g. homogenization temperature) and composition of the individual inclusions are known. The microthermometric data can be directly related to fluid compositions by the use of Raman analysis. Erroneous conclusions were drawn earlier (in particular too high forming pressures), because of the presupposition of pure compositions.

Rock samples from 7 metamorphic areas have been studied: the Furua Granulite Complex (Tanzania), high-grade metamorphic rocks from SW Norway, siliceous marbles from Pusula (SW Finland), granulites from Haut Allier (France), Dôme de l'Agout (France), coal basins of the Appalachians (U.S.A.) and the silver ore deposit of Harmsarvet (central Sweden). The phase behaviour, transitions between solid (S), liquid (L)

and vapour (V), of CO_2-CH_4-N_2 inclusions on cooling and subsequent warming, is more complicated than for the pure components: metastable and partial homogenization and sublimation are typical phase transitions. The interpretation of fluid mixtures (in respect of density and composition) is therefore much more difficult. Phase transitions in fluid inclusions are typical for systems of constant volume (isochoric systems) and they are different from "normal" phase behaviour: traditional terms like boiling, melting and sublimation cannot be simply applied. New definitions are therefore introduced for the description of phase behaviour in fluid inclusions. A classification system is proposed to describe phase behaviour (between -180 and +35°C) of non-aqueous inclusions and to typify the inclusions themselves. This classification is based on a subdivision in two groups according to the final multi-phase equilibrium observed at rising temperature: 1) liquid + gas followed by homogenization (type H) or 2) solid + liquid or gas followed by sublimation (type S). The sequence of phase transitions is fixed for both groups: H-type inclusions show 1 to 5 phase transitions of the sequence S+L → S+L+V → S+L or S+V → S+L+V → L+V → L or V in the studied temperature range; S-type inclusions show 1 to 4 phase transitions of the sequence S+L+V → S+L → S+L+V → S+L or S+V → L or V (both including the final transition). All mentioned types of phase behaviour have been observed in fluid inclusions. It was found that not only homogenization, but the complete phase behaviour (including melting, partial homogenization, metastable homogenization and sublimation) gives a direct indication on the composition and molar volume.

The basic principles of the Raman effect are explained on the hand of a literature study and also the characteristics of Raman spectra of the relevant gases and liquids. The positions and intensities of Raman lines is slightly dependent on the density and especially on the physical state (gas or liquid). The implication for the accuracy of quantitative Raman analysis is limited: measurements can be checked by the comparison with compositions calculated from microthermometric data and available phase models. Furthermore, Raman analysis opens the possibility for the identification of solid (crystalline) compounds. This is especially of interest for minerals which are difficult to analyse by means of the traditional methods (e.g. electron microprobe) like daughter minerals (carbonates, sulphates etc.) in fluid inclusions. Special attention is paid to graphite which is sometimes found in H_2O-CH_4 bearing inclusions: even quantities which cannot be optically observed, but which do also

8

Het equivalent van "retrograde condensatie" voor een systeem van constant volume is homogenisatie naar de gasfase bij een lagere temperatuur voor insluitsels met een lager molair volume (hogere dichtheid).

9

Niet alleen homogenisatietemperaturen, maar ook andere fasenveranderingen (smelten, sublimatie) kunnen worden gebruikt om het molair volume van fluïde insluitsels te bepalen.

10

Het fasengedrag van fluïde insluitsels wordt bepaald door de onderlinge positie van de liquidus en de kritische curve voor een gegeven binair systeem: het snijden van deze curven in het systeem CO_2-N_2 is de oorzaak van een uniek fasengedrag dat zich onderscheid van het systeem CO_2-CH_4 en lijkt op dat van het systeem CO_2-H_2O.

11

Waarnemingen van fasenveranderingen in fluïde insluitsels worden beïnvloed door het te verwachte gedrag op grond van een bekend fasenmodel.

12

"Omnes enim causae effectuum naturalium dantur per lineas, angulos et figuras. Aliter enim impossibile est scire propter quid in illis."
"Alle oorzaken van natuurlijke effecten verschijnen door middel van lijnen, hoeken en figuren. Want anders is het onmogelijk daarin het waarom te kennen."

Umberto Eco (1984) De Naam van de Roos p.229.

STELLINGEN

1

Niet-waterige fluïden in metamorfe en magmatische gesteenten zijn voornamelijk beperkt tot binaire mengsels tussen de eindleden van het system CO_2-CH_4-N_2.

2

Het molair volume van fluïde insluitsels is een belangrijke en soms de enig beschikbare parameter om de vormingsdrukken van gesteenten af te leiden. Daarom is de kennis van de betreffende systemen (fasenmodellen) van belang voor de interpretatie van de evolutie van de korst en bovenmantel.

3

De resultaten van eerdere onderzoeken (b.v. Coolen 1980) waarbij geen gebruik is gemaakt van Raman analyse moeten worden herzien, met name wanneer extreem hoge vormingsdrukken (> 10 kbar) zijn berekend.

Coolen J.J.M.M. (1980) GUA Papers of geology (Univ. Amsterdam), series 1, 13.

4

Het molair volume van gasvormige insluitsels komt overeen met de vormingsdruk en -temperatuur als het watergehalte laag is of als het zoutgehalte van een coexisterende waterige fase hoog is.

5

Bij de gelijktijdige vorming van gasvormige en waterige insluitsels (ontmengingscondities) is de relatieve hoeveelheid water niet van invloed op het uiteindelijk molair volume van de gasfase.

6

De mogelijke aanwezigheid van grafiet in CH_4-H_2O-houdende insluitsels moet altijd worden gecontroleerd met behulp van Raman analyse: hoeveelheden kunnen worden aangetoond die te klein zijn om te worden waargenomen, maar die wel een hoger molair volume van de gasfase tot gevolg hebben.

Fluïde insluitsels met samenstellingen in het systeem CO_2-CH_4-N_2 kunnen meer dan één fase bevatten bij een hogere temperatuur dan kritisch door de aanwezigheid van een kritisch punt van de tweede orde.

9

Not only homogenization temperatures, but also other phase transitions (melting, sublimation) can be used for the determination of the molar volume of fluid inclusions.

10

The phase behaviour in fluid inclusions is determined by the relative position of the liquidus and the critical curve for a given binary system: the intersection of these curves for the system CO_2-N_2 results to an unique phase behaviour which is different from the system CO_2-CH_4 and similar to the system CO_2-H_2O.

11

The observation of phase changes in fluid inclusions is influenced by the expected behaviour, based on a phase model.

12

"Omnes enim causae effectuum naturalium dantur per lineas, angulos et figuras. Aliter enim impossibile est scire propter quid in illis."
"All causes of natural effects are given by lines, angles and figures. Otherwise it is impossible to know the why behind these."

Umberto Eco (1984) De naam van de Roos p.229.

THESES

Non-aqueous fluids in metamorphic and magmatic rocks are mainly restricted to binary mixtures between 2 end-members of the system CO_2-CH_4-N_2.

The molar volume of fluid inclusions is an important and sometimes the only available parameter to deduce the forming pressures of rocks. Knowledge on the systems (phase models) of interest is therefore important for the interpretation of the evolution of the crust and upper mantle.

The results of earlier studies (e.g. Coolen 1980), which were done without Raman analysis should be revised, notably when extremely high forming pressures (> 10 kbar) were calculated.

Coolen J.J.M.M.M. (1980) GUA Papers of geology (Univ. Amsterdam), series 1, 13.

The molar volume of gaseous inclusions corresponds to the forming pressure and temperature if the water content is low or if the salt content of a coexisting aqueous phase is high.

In the case of contemporaneous forming of gaseous and aqueous inclusions (immiscibility conditions), the relative amount of the water phase does not influence the final molar volume of the gas phase.

6

The possible presence of graphite in CH_4-H_2O-bearing inclusions should always be checked by Raman analysis: quantities can be indicated which are too small to be observed, but which result to higher molar volumes of the gas phase.

Fluid inclusions with compositions in the system CO_2-CH_4-N_2 may contain more than one phase at temperatures higher than critical because of the presence of a critical point of the second order.

8

The equivalent of "retrograde condensation" for a system of constant volume is homogenization to the gas phase at a lower temperature for inclusions of lower molar volume (higher density).

determine the total density of inclusions, could be demonstrated.

Theoretical models ("phase diagrams") have been developed showing the correlation between molar volume ($\bar{V}$), composition (X) and temperature (T) for the different phase transitions. Most important are $\bar{V}X$ and TX diagrams, representing isotherms (T = constant) and isochores ($\bar{V}$ = constant) respectively. The latter diagram is firstly introduced here. Models are discussed (besides for the pure systems CO_2, CH_4 and N_2) for the binary systems CO_2-CH_4, CO_2-N_2 and CH_4-N_2; models for the ternary system are tentatively constructed by extrapolation and they can be applied for compositions which highly deviate from binary mixtures.

The systems CO_2-CH_4 and CO_2-N_2 show several similarities, but also some major differences. Both systems are characterized by full miscibility of the liquid and gas phases and the absence of mixed crystals. The solid phase can be considered as pure CO_2 (at temperatures above -180°C). In both systems, and particular for the system CO_2-N_2, multi-phase equilibria (liquid + vapour) are possible at temperatures higher than the critical point (of the first order). This phenomenon ("retrograde condensation") takes place between the critical points of the first and second order. The implication for fluid inclusions is a lowering of the homogenization temperature (to the gas phase) for higher densities.

The major difference between the systems CO_2-CH_4 and CO_2-N_2 is the fact that the critical curve is intersected by the liquidus (3-phase equilibria) in the system CO_2-N_2. This explains why solid CO_2 may be in equilibrium with a critical N_2-rich fluid, but not with a critical CH_4-rich fluid (at melting). Another implication is the impossibility of liquid + gas equilibria (and therefore homogenization) for inclusions containing more than 90 mole% N_2. These fluids are characterized by sublimation at any density.

Special attention is paid to the system CO_2-N_2, because these gases play an important role in rocks and the system is poorly known compared to the system CO_2-CH_4. Partial homogenization is characteristic for CO_2-N_2 mixtures and the corresponding temperatures are calculated by assuming insolubility of CO_2 below the critical temperature of N_2 (-147°C). This assumption is affirmed by the present data.

Experiments have been carried out in order to produce artificial fluid inclusions in quartz. According to the followed method, (micro-)cracks are firstly induced in quartz cores. These cracks are subsequently healed at high temperature (500°C) and pressure (1 to 6 kbar), in the presence

of a fluid of known composition. Only small amounts of water are sufficient for the (re)crystallization of quartz and fluid trapping. Several starting materials have been used for the gas production: silver-nitrate, ammonium-nitrate, silver-oxalate, and their mixtures. All experiments were carried out with a surplus of graphite. In this way, gas compositions could be obtained of about 33, 55 and 77 mole% N_2. The experiments ultimately resulted to the establishment of a $\bar{V}TX$ model, by which the forming conditions of many naturally occurring inclusions can be determined (e.g. from the Furua Granulite Complex and the high-grade marbles of Pusula). The combination of microthermometry, Raman analysis, theoretical models and experiments is therefore indispensable for the interpretation of multi-component gaseous systems.

SAMENVATTING

Kooldioxide, methaan en stikstof worden in veel gesteenten van metamorfe en magmatische oorsprong aangetroffen en vertegenwoordigen de 3 belangrijkste gasvormige bestanddelen (naast water) in de korst en bovenmantel van de aarde. Deze fluïden (gassen of vloeistoffen onder hoge druk) komen voor in veel gesteentevormende mineralen als insluitsels van ongeveer 5-30μ groot. Hoewel de relatieve hoeveelheid van vloeistoffen in gesteenten gering is, spelen zij toch een belangrijke en soms essentiële rol bij verschillende geologische processen (metamorfe reacties, smelten, deformatie etc.). Het onderzoek van fluïde insluitsels is een van de methoden waarmee de diepte kan worden bepaald waarop gesteenten worden gevormd: de dichtheid (en molair volume) van vloeistof-insluitsels kan worden beschouwd als een overblijfsel van een hoge druk (en temperatuur) stadium tijdens hun vorming. De dichtheid van vloeistof-insluitsels is daarom een sleutelparameter voor veel geologische interpretaties. Deze wordt berekend m.b.v. experimenteel vastgestelde modellen (toestandsvergelijkingen) en gegevens, verkregen door 1) het bestuderen van fasenovergangen bij veranderende temperatuur ("micro-thermometrie") en 2) het meten van de gassamenstelling d.m.v. Raman microspectroscopie ("Raman analyse"). De kennis van de fasenmodellen voor natuurlijk voorkomende gassen en gasmengsels is daarom belangrijk voor een juiste interpretatie van de meetgegevens.

De toepassing van Raman analyse is van grote betekenis voor het onderzoek van vloeistofinsluitsels en is mogelijk gemaakt door de recente ontwikkeling van de Raman microspectrometer (Raman probe). Hiermee kunnen de samenstellingen van individuele vloeistofinsluitsels op een non-destructieve en snelle manier worden gemeten. Andere analysemethoden zoals gaschromatografie resulteren in totaalsamenstellingen en geven geen informatie over de samenstellingsvariatie binnen een monster. Een verantwoorde bepaling van de dichtheid is alleen dan mogelijk als zowel het fasengedrag (o.a. homogenisatietemperatuur) en de samenstelling van de individuele insluitsels bekend zijn. Door het gebruik van Raman analyse kunnen de gegevens van microthermometrie direct met de fluïd-samenstelling in verband worden gebracht. In het verleden zijn vaak onjuiste conclusies getrokken (met name te hoge vormingsdrukken), omdat van zuivere fluïdsamenstellingen werd uitgegaan.

Gesteentemonsters zijn bestudeerd uit een 7-tal metamorfe gebieden: het Furua granulietcomplex (Tanzania), hooggradig metamorfe gesteenten

van ZW Noorwegen, kiezelhoudende marmers van Pusula (ZW Finland), granulieten van Haut Allier (Frankrijk), Dôme de l'Agout (Frankrijk), koolbekkens van de Appalachen (U.S.A.) en zilverertsafzettingen van Harmsarvet (centraal Zweden). Het fasengedrag, overgangen tussen vaste (S), vloeibare (L) en gasvormige (V) fasen, van CO_2-CH_4-N_2 insluitsels bij afkoelen en vervolgens verwarmen is gecompliceerder dan voor de zuivere componenten: metastabiele en partiële homogenisatie en sublimatie zijn typische fasenovergangen. De interpretatie van fluïde mengsels (ten aanzien van dichtheid en samenstelling) is daarom veel moeilijker. Fasenovergangen in vloeistofinsluitsels zijn kenmerkend voor systemen van constant volume (isochore systemen) en wijken af van "normaal" fasengedrag: traditionele begrippen zoals koken, smelten en sublimatie kunnen niet zonder meer worden gehanteerd. Nieuwe definities zijn daarom geïntroduceerd om fasenveranderingen in vloeistofinsluitsels te beschrijven. Een klassificatiesysteem is voorgesteld waarmee het fasengedrag (tussen -180 en +35°C) van niet-waterige insluitsels kan worden beschreven en daarmee de insluitsels zelf kunnen worden getypeerd. Deze indeling gaat uit van een verdeling in twee groepen, gebaseerd op het laatste meer-fasenevenwicht dat bij stijgende temperatuur kan worden waargenomen: 1) vloeistof + gas gevolgd door homogenisatie (type H) of 2) vaste stof + vloeistof òf gas gevolgd door sublimatie (type S). De volgorde van fasenovergangen ligt vast voor beide groepen: H-type insluitsels vertonen 1 tot 5 fasenovergangen van de reeks S+L → S+L+V → S+L òf S+V → S+L+V → L+V → L òf V in het bestudeerde temperatuursbereik; S-type insluitsels vertonen 1 tot 4 fasenovergangen van de reeks S+L+V → S+L → S+L+V → S+L òf S+V → L òf V (de laatste fasenovergang vindt altijd voor beide reeksen plaats). Alle genoemde typen van fasengedrag zijn waargenomen in vloeistofinsluitsels. Het is gebleken dat niet alleen homogenisatie, maar het volledige fasengedrag (met inbegrip van smelten, partiële homogenisatie, metastabiele homogenisatie en sublimatie) een directe aanwijzing geeft omtrent de samenstelling en molair volume.

De basisprincipes van het Raman effect worden aan de hand van een literatuurstudie uitgelegd alsmede de belangrijkste kenmerken van de Raman spectra van de betreffende gassen en vloeistoffen. De positie en de intensiteit van Raman lijnen is in geringe mate afhankelijk van de dichtheid en vooral van de fysische staat (gas of vloeistof). Het gevolg voor de nauwkeurigheid van kwantitatieve Raman analyse is beperkt: meetresultaten kunnen worden getoetst door vergelijking met samenstellingen berekend uit microthermometrische gegevens en bestaande

fasenmodellen. Raman analyse opent verder de mogelijkheid om vaste (kristallijne) stoffen te determineren. Dit is vooral van belang voor mineralen die moeilijk met de traditionele methoden (o.a. electronen microsonde) kunnen worden geanalyseerd zoals dochtermineralen (carbonaten, sulfaten etc.) in vloeistofinsluitsels. Bijzondere aandacht wordt besteed aan grafiet dat soms in H_2O-CH_4 houdende insluitsels voorkomt: zelfs hoeveelheden kunnen worden aangetoond, die optisch niet waarneembaar zijn, maar die wel mede de totale dichtheid van de insluitsels bepalen.

Theoretische modellen ("fasendiagrammen") zijn ontwikkeld die de relatie tussen molair volume ($\bar{V}$), samenstelling (X) en temperatuur (T) voor de verschillende fasenovergangen weergeven. Het belangrijkste zijn $\bar{V}$X en TX diagrammen waarin respectievelijk isothermen (T = constant) en isochoren ($\bar{V}$ - constant) kunnen worden gerepresenteerd. Het laatstgenoemde diagram wordt hier voor het eerst geïntroduceerd. Modellen worden besproken (behalve voor de zuivere systemen CO_2, CH_4 en N_2) voor de binaire systemen CO_2-CH_4, CO_2-N_2 en CH_4-N_2; modellen voor het ternaire systeem zijn schematisch opgesteld door extrapolatie en kunnen worden toegepast voor samenstellingen die te zeer van binaire mengsels afwijken.

De systemen CO_2-CH_4 en CO_2-N_2 vertonen veel overeenkomsten, maar ook enkele belangrijke verschillen. Beide systemen worden gekarakteriseerd door volledige mengbaarheid van de vloeistof- en gasfasen en het ontbreken van mengkristallen. De vaste fase kan worden beschouwd als zuiver CO_2 (bij temperaturen boven -180°C). Voor beide systemen, maar i.h.b. voor het systeem CO_2-N_2, geldt dat meer fasen (vloeistof + gas) stabiel kunnen zijn bij temperaturen boven het kritisch punt (van de eerste orde). Dit verschijnsel ("retrograde condensatie") vindt plaats tussen de kritische punten van de eerste en tweede orde. De implicatie voor vloeistofinsluitsels is een verlaging van de homogenisatietemperatuur (naar de gasfase) voor hogere dichtheden.

Het belangrijkste verschil tussen de systemen CO_2-CH_4 en CO_2-N_2 is gelegen in het feit dat de kritische curve wordt gesneden door de liquidus (3-fasen evenwichten) in het systeem CO_2-N_2. Dit verklaart waarom vast CO_2 in evenwicht kan zijn met een kritische N_2-rijke fluïd, maar niet met een kritische CH_4-rijke fluïd (in het smeltpunt). Een ander gevolg is het ontbreken van vloeistof ' gas evenwichten (en dus ook homogenisatie) voor insluitsels die meer dan 90 mol% N_2 bevatten. Deze fluïds worden bij elke dichtheid gekarakteriseerd door sublimatie.

Bijzondere aandacht wordt besteed aan het systeem CO_2-N_2, omdat gasmengsels met deze samenstellingen een belangrijke rol spelen in gesteenten en het systeem veel minder goed bekend is dan bijv. het systeem CO_2-CH_4. Partiële homogenisatie is karakteristiek voor CO_2-N_2 mengsels en de bijbehorende temperaturen worden berekend door aan te nemen dat CO_2 onoplosbaar is beneden de kritische temperatuur van N_2 (-147°C). Deze aanname is bevestigd door de huidige gegevens.

Er zijn experimenten uitgevoerd waarbij kunstmatige vloeistofinsluitsels gemaakt zijn in kwarts. Bij de hier gevolgde methode worden eerst (micro-)barsten geinduceerd in kwartskernen. Deze laat men vervolgens dichtgroeien bij hoge temperatuur (500°C) en druk (1 tot 6 kbar), in aanwezigheid van een fluïd van bekende samenstelling. Slechts kleine hoeveelheden water zijn voldoende om kwarts te laten (re)kristalliseren en daarmee fluïden in te vangen. Voor de productie van het gas zijn verschillende uitgangsstoffen gebruikt: zilvernitraat, ammoniumnitraat, zilveroxalaat en mengsels hiervan. Alle experimenten werden uitgevoerd met een overmaat aan grafiet. Op deze manier konden gassamenstellingen worden verkregen van ongeveer 33, 55 en 77 mol% N_2. De experimenten resulteerden uiteidelijk tot een $\bar{V}TX$ model, waarmee de vormingscondities van veel natuurlijk voorkomende insluitsels kunnen worden vastgesteld (bijv. van het Furua granulietcomplex en de hooggradige marmers van Pusula). De combinatie van microthermometrie, Raman analyse, theoretische modellen en experimenten is daarom onontbeerlijk voor de interpretatie van meersoortige gassystemen.

CONTENTS

I INTRODUCTION

1.1. Historical review

The presence of fluids in rocks have been noticed since antiquity, but their real scientific study began only in the first half of the 19th century. The names of Davy (1822), Brewster (1826), Sorby (1858), Vogelsang (1869) and Hartley (1876) can be mentioned as the most renowned of the early investigators (Roedder 1984; Touret 1982). Their work was mainly confined to descriptions only, but some measurement results could already be obtained (refractive index, spectrographic analysis and even homogenization temperatures). Water and CO_2 were identified as fluid inclusion constituents in this early period, but no further interpretations on the forming conditions could be made. Fluid inclusions were well described in the textbooks on descriptive petrology of the late 19th and early 20th century (Zirkel 1873; Rosenbusch 1923). However, they did not survive the controversy between "magmatists" and "solidists" because fluid inclusions could not be put in a wider context at that time and fell into the background of petrology (Touret 1984). Only a handful of economic geologists continued their study. This may explain why, until now, the systematic bibliography (Fluid Inclusion Research, E. Roedder ed.) is edited under the auspices of the "Commission on Ore-Forming Fluids in Inclusions (COFFI)". It must be noted however that fluid inclusions have always been investigated at a significant scale in the Soviet Union. Many fundamentals have been established by a few Russian scientists, notably Lemmlein and co-workers.

After a period of relative "silence", a renewed interest for fluid inclusions arose around 1960 in the U.S.A. (E. Roedder) and around 1970 in Europe esp. France (A. Weisbrod, B. Poty, J. Touret). The increasing importance of fluids in petrology was accompanied with the development and improvements of the equipment for quantitative analysis. Especially the availability of an advanced device for the observation of fluid inclusions during heating and cooling ("heating/freezing stage") and the measurement of temperatures marking phase transitions was of major importance. This technique known as "microthermometry" is indispensable for the analysis of single inclusions and opens the possibility for the determination of fluid densities and the consequent interpretation on the rock forming conditions. Several analytical methods (e.g. gas

chromatography and mass spectrometry) were applied for measuring fluid compositions in rocks. The disadvantage of the traditional methods is their destructive character and the mixing of many inclusions which may correspond to completely different generations. The introduction of laser Raman micro-spectroscopy (further called: Raman analysis) around 1980 allowed quantitative analysis of single fluid inclusions in a non-destructive way.

Nowadays, the study of fluid inclusions has become an important branch of petrology. Geologists become more and more aware of the fact that fluids are as minerals a given constituent of the earth. Basic principles of fluid inclusion study remain ignored to many petrologists as they are not covered in most current textbooks. In recent years, several review papers and books have partly filled this gap: Hollister & Crawford (1981) and Leeder et al. (1987) which insists on the theoretical principles; Roedder (1984), listing practically all applications until 1983; Shepherd et al. (1985) more devoted to the practical aspects of microthermometry. These works show the widespread occurrence and interest of fluid inclusions: they are found in almost all rock types and their composition and density are in many cases related to the geological environment. The role of fluids during many geological processes (metamorphism, rock melting, ore formation etc.) is significant and sometimes dominant. Data obtained from fluid inclusions cover a wide field of application: they can give more insight in the depth of emplacement of a magma chamber, the source of volcanic rocks, the character of an ore-forming liquid, diagenetic processes and metamorphic PT-conditions. The latter application is most important for this study. Furthermore the accuracy of several geothermometers (e.g. cordierite-garnet), notably used in metamorphic petrology, is dependent on the knowledge of fluid compositions.

The first observations of fluids in rocks concerned water and/or CO_2. Discoveries of other species were made only recently. It became first evident from microthermometric observations that aqueous inclusions are often salt solutions and that CH_4 and N_2 may occur in gaseous inclusions as end-members or in mixtures (Swanenberg 1980; Burruss 1981). This could later be stated and further quantified (Guilhaumou et al. 1981; Kreulen & Schuiling 1982; present work). Further, "fluid" inclusions may not only contain fluid phases, but also solids (daughter minerals) which may be similar or different from the rock forming minerals (e.g. salt in quartz

from granites). The identification of daughter minerals became possible by recording their Raman spectra.

Most works on fluid inclusions rely on the assumption that fluids (especially CO_2) are pure in composition. The common "microthermometric" criterion for purity (coincidence between melting and triple point) is insufficient for some gases, notably CO_2 (present work). In many cases, no serious problems arise; sometimes however (e.g. for CO_2-N_2 mixtures), compositions cannot be ignored as this results to erroneous interpretations on fluid densities. It is stated here that reliable interpretations can only be made if fluid compositions of single inclusions are checked by direct analysis. Several earlier publications should therefore be revised (Touret & van den Kerkhof 1986). This has been done for some examples (Coolen 1980 in: van den Kerkhof 1988; Swanenberg 1980: unpubl. data).

The available equipment has reached a high standard, also after the introduction of laser Raman micro-analysis. A growing amount of fluid inclusion data is being released by many investigators all over the world, sometimes with controversial results. Some recent discussions (e.g. about the interpretation of CO_2 inclusions in granulites) are due to different interpretations of time relations (syn versus post-metamorphic) or calculations of the PT-conditions at the time of trapping. Fundamental knowledge on the physical behaviour of gas and liquid systems at low and high temperature is essential to make reliable interpretations of measurement data and it is this point which is focused on in this work.

1.2. The present study

The aim of this study is the development of models which describe the PVTX relations of fluid mixtures containing CO_2, CH_4 and N_2 and their phase behaviour at low temperatures. Raman analysis showed that these compounds are the most important non-aqueous fluids present in rocks from the crust and upper mantle (Fig.1.1). A compilation of available theoretical models was made for the pure compounds and binary mixtures; models for ternary mixtures could be established in a tentative way. The models could be checked and further developed by adding the data of fluid inclusion studies. It is shown in Fig.1.1 that binary mixtures represent good approximations for many natural fluids. The system CO_2-CH_4

has been much studied (Swanenberg 1980; Ramboz et al. 1984; Heyen et al. 1982) and is complicated by problems of chemical metastability (Kreulen 1986). In this work, the importance of the system CO_2-N_2 is emphasized as N_2 is now known to be a common fluid in many environments. The presence of N_2 carries the considerable risk to confuse pure high density CO_2 with low density CO_2-N_2 mixtures.

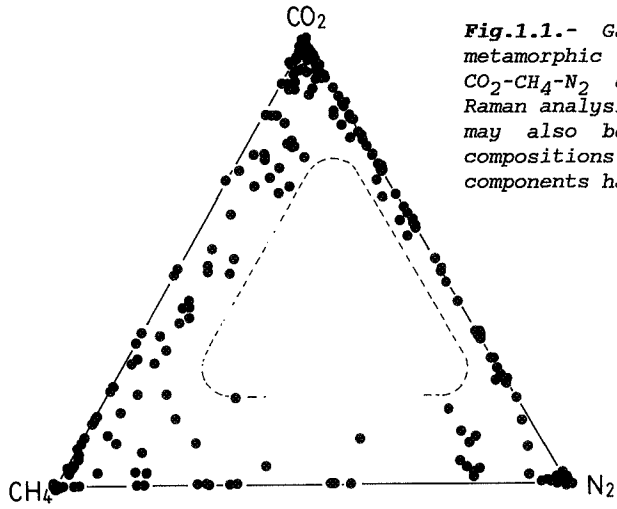

Fig.1.1.- *Gas compositions from 8 metamorphic areas represented in a CO_2-CH_4-N_2 diagram as measured by Raman analysis. Minor amounts of H_2O may also be present. Intermediate compositions between the 3 gaseous components have not been recorded.*

Several ways of graphical representation are demonstrated. Because of the fact that fluid inclusions are constant density systems, the most useful diagrams represent (molar) volume, temperature and composition. Theoretical models of the system CO_2-N_2 could be checked and further improved by the study of experimentally generated inclusions. In some well-documented examples, the study of natural inclusions could also contribute to a better knowledge of the considered systems.

The two methods used for the present study are Raman analysis and microthermometry. This combination is most powerful: both methods allow the study of single inclusions which makes it possible to correlate both phase behaviour of fluid inclusions at low (and high) temperatures and fluid compositions. Better insight could be obtained into the variety of composition and density of natural fluids in rocks (Fig.1.1). The observed compositional limits gave rise to a discussion on the chemical stability of fluids, at their time of formation and after cooling to room temperature.

An extensive and systematic study of microthermometry was made because the large diversity of phase behaviour observed in fluid

inclusions (Chap.III). Phase transitions appeared to be complicated for fluids of mixed composition. Some currently used terms ("homogenization" and "melting") are not uniquely defined and therefore insufficient to describe phase transitions characteristic for systems of constant volume. An increasing number of observations show "strange" phenomena which, not being explained at first sight, are ignored or labelled as "uninteresting". It is shown in this work that detailed observations of phase behaviour can indeed be helpful for further interpretations of fluid density and composition.

The studied material comprises two different types of samples: (1) natural inclusions and (2) quartz samples containing artificially formed inclusions. The results obtained from both groups are complementary as fluid compositions and densities were chosen for artificial inclusions which are missing in the presently selected natural inclusions.

A selection was made of rock samples from 7 metamorphic areas, representative for different geological environments, age and metamorphic grade (see Appendix 3): the Furua Granulite Complex, Tanzania (Coolen 1980); high-grade metamorphic rocks from SW Norway (Swanenberg 1980); siliceous marbles from Pusula, SW Finland (unpubl.); granulites from Haut Allier, France (Lasnier 1976); Dôme de l'Agout, France (Kreulen & Schuiling 1982); coal basins of the Appalachian, U.S.A. (Herskowitz & Kisch 1984; unpubl. data); the silver ore deposit of Harmsarvet, Sweden (van den Kerkhof 1987). It was aimed at finding samples showing the widest variation in composition and density in well documented areas (with known PT-conditions obtained from solid mineral assemblages). It should therefore be noted that these samples are not representative for a "standard" metamorphic area. The rock samples were mainly studied as an application of the treated models to practical cases. The considered regional studies show the possibilities but also the limitations of the use of fluid inclusions for the solvation of geological problems. In some cases, (e.g. Furua Granulites, Tanzania), fluid inclusions of different composition could be assumed to have formed at the same PT-conditions permitting a reversed procedure, namely the modification of an available model from the fluid inclusion data.

The trapping PT-conditions of fluid inclusions can be derived from their homogenization temperature (T_h) and composition (X). The procedure generally followed is threefold i.e. (1) calculation of the molar volume

from an equation of state valid for the low PT-region (2) calculation of the isochore (a curve of constant molar volume) from an equation of state valid for the high PT-region and (3) incorporation of independently derived temperature data (see also section 2.2). It is evident that the molar volume is the key parameter which allows the extrapolation of the present PT-conditions to the geological conditions (Touret 1987). However, the molar volume, which cannot be measured directly, should always be calculated. Presently available equations of state have not been sufficiently checked and they appeared to be inaccurate for many of the fluids playing a role during geological processes. Problems especially arise for fluids of extremely high density, found in some granulite areas, and for fluids of intermediate composition.

The investigated artificial inclusions contain CO_2-N_2 mixtures (see Chap.VI). The forming PT-conditions are experimentally determined and they can reproduce metamorphic conditions. The produced inclusions can be studied for their microthermometric behaviour and checked for their composition by Raman analysis. Contrary to natural inclusions, even when molar volumes are not known, the trapping pressures and temperatures are specified and they can be directly correlated to the temperatures marking phase transitions in the low PT-range (homogenization, melting etc.). In this way models could be established which can be used to derive the trapping conditions from microthermometric data for inclusions of known composition. The discrepancy between these models and those obtained from the literature (e.g. Darimont 1986 for the system CO_2-N_2) may be considerable.

II FUNDAMENTALS

2.1. Fluid inclusions in rocks

Fluids, in more or lesser amounts, are known to be a constituent of many rock types. Some rock forming minerals contain volatile compounds in their lattice: H_2O is present as crystal water in micas and amphiboles; nitrogen (as NH_4^+) in ammonium-micas (Honma & Itihara 1981). Even anhydrous minerals like quartz are capable to contain water at high temperatures (Spear & Selverstone 1983). Gas species which are not bonded to minerals occur as a segregate fluid phase, present as fluid inclusions.

Natural fluids mostly consist of molecular compounds of the system C-O-H-N-S. The "simple" species H_2O, CO_2, CH_4, N_2 and H_2S appear to be most stable in fluid inclusions; more complex compounds are restricted to extreme environments. Water and CO_2 had been known for a long time, but the other gas species have only recently been detected in rocks as a consequence of the improvement of analytical techniques. These gases occur as almost pure inclusions, but more often as mixtures with CO_2 (mostly CO_2-CH_4 or CO_2-N_2) or water.

Fluid inclusions are essentially filled or partially filled cavities, mostly 5-30µ in size. Quartz is the most suitable mineral for fluid inclusion preservation because of the poor development of cleavage, its absence of reaction with the fluid content and its easy (re)crystallization and healing properties. Other examples of alternative host minerals are garnet, apatite, fluorite, halite, calcite and several gem stones like sapphire (Roedder 1984).

At room temperature, a general distinction can be made between aqueous and gaseous inclusions. Both types are often found in the same rock. This might indicate immiscibility between the 2 phases at the time of trapping, but the specific criteria for fluid immiscibility need to be ascertained precisely (Pichavant et al. 1982). Miscibility is a function of both the salt content of the aqueous phase and the gas composition. In other cases, different sources could be indicated for the gas and liquid phases and both may be trapped at different episodes of the rock evolution.

Several criteria concerning fluid inclusion shapes and their textures, showing the time relation between crystallization and tectonic events, are generally used to make a main distinction between primary and secondary inclusions (Roedder 1984 p.43-45). The term "pseudo-secondary" is essentially used for the characterization of a special type of primary inclusions in idiomorphic crystals, but the term is often (mis)used for slightly transposed secondary inclusions. The chronology of fluid trapping is deduced from direct observation of fluid inclusions by translating "primary" versus "secondary" to "early" versus "late": primary inclusions are formed during the mineral growth; secondary inclusions developed after the crystallization of the host mineral. In massive rocks, it is very difficult and sometimes impossible to characterize fluid inclusions as primary or secondary. Many generations of fluid inclusions may occur in one sample as the total fluid content is mostly the result of several stages of rock evolution rather than a single episode. However, the determination of the chronology of fluid generations, although difficult and sometimes even impossible cannot be avoided (Touret 1977, 1981).

Fluids play an important role in many metamorphic reactions. Some examples are dehydration (releasing H_2O) and decarbonization processes (releasing CO_2) taking place during progressive metamorphism. A fluid phase is produced in these cases. The formation of a granitic melt (anatexis) is an example of a water-consuming process as water is more soluble in the melt than any other gas by at least an order of magnitude (Kadik & Lukanin 1973; Kadik & Eggler 1976).

Fluid inclusion compositions are indicative for the chemical environment at the rock forming conditions (wet-dry, oxidizing-reducing etc.); fluid densities are remainders of high pressures and temperatures acting during the entrapment of the fluid. One of the most important topics in fluid inclusion research is the interpretation of the PT-conditions during geological processes (Crawford & Hollister 1986).

Fluid inclusion studies, mentioned in the preceding section, lead to the following conclusions:

1) the complexity of fluid inclusions is indicative for many processes during rock evolution;

2) many problems can only be solved by rigorous treatment of all steps of

investigation, among others, a complete analysis of multi-component fluids (the scope of this work);
3) the difficulties do not preclude the necessity of fluid inclusion investigations: they should be studied at best because they are a given constituent of the rock and give potentially information on the forming conditions which cannot be obtained otherwise.

2.2. The working procedure

As stated earlier, one of the most important parameters in fluid inclusion studies is the density. The use of the molar volume ($\bar{V}$) instead of the density (d) has some advantages, especially for fluids of mixed composition, because the molecular mass of the components can be eliminated. Furthermore, the molar volume varies far less than the density for fluids of different composition, trapped at the same PT-conditions (Holloway 1981). The correlation between $\bar{V}$ and d is expressed by $\bar{V} = M/d$, where M denotes the molecular mass. For a multi-component system, the average molar volume $\bar{V}$ is given by the linear combination of partial molar volumes: for n components

$$\bar{V} \quad \Sigma_i^n X_i.\bar{V}_i \qquad \text{(Eq.2.1.)}$$

where X_i is the molar percentage and $\bar{V}_i$ the molar volume of component i in the mixture (Burruss 1981).

The procedure followed during the systematic study of fluid inclusions is shown in Scheme 2.1 and discussed below:

Descriptions of fluid inclusions by microscope have to be made during the normal petrographic studies (see above). The first step of quantitative fluid inclusion studies aims at the calculation of the molar volume from
a) temperatures marking phase transitions ("microthermometry"), in particular the homogenization temperature (T_h);
b) fluid compositions measured by Raman analysis (X);
c) corresponding PVTX-relations given by a phase model or equation of state valid around the conditions of the homogenization point (mostly below room temperature for gaseous compounds). This equation, which

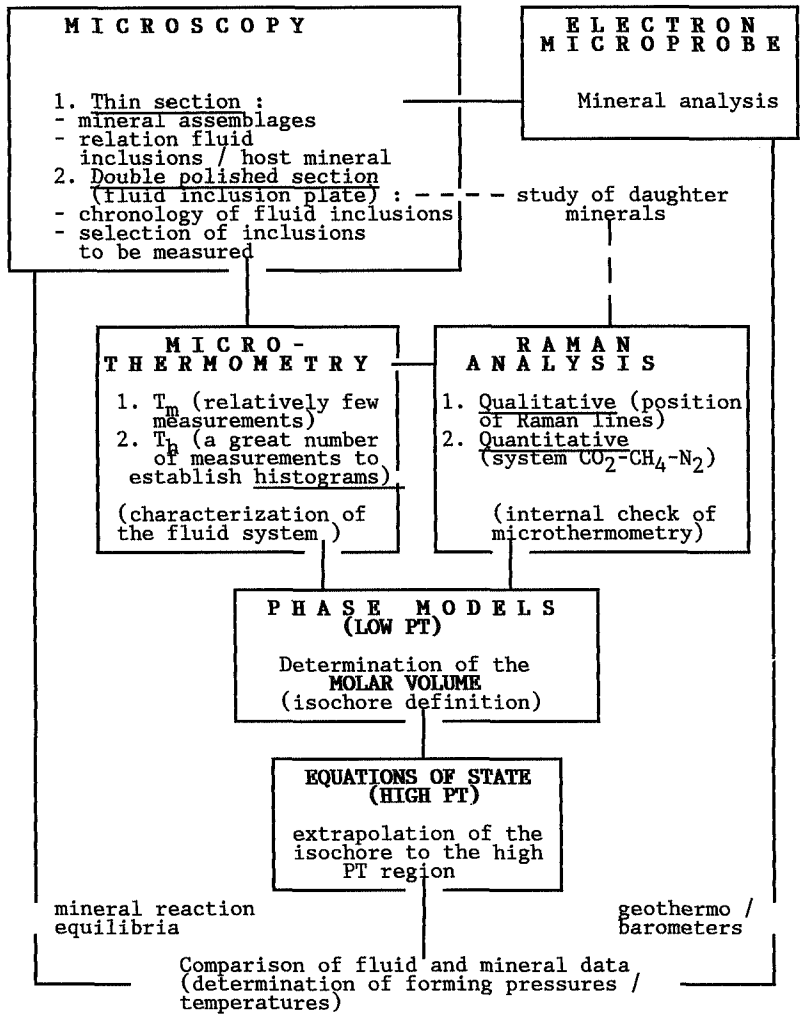

Scheme 2.1.- *Presentation of the working procedure for a systematic study of fluid inclusions (see text).*

relies on experimental data, requires the knowledge of the boiling point and melting point curves.

The determination of molar volumes, directly given by T_h for pure systems, is much more complicated for mixtures. The pure systems H_2O, CO_2, CH_4 and N_2 have been studied in detail and they find a general

application in fluid inclusion studies (see section 5.2.): $\bar{V}$ can be simply read from published thermodynamic tables (Angus et al. 1976a, 1976b, 1979; Vagarftik 1972).

The knowledge of multi-component systems involving water and salt solutions (e.g. H_2O-NaCl) as well as several water-gas systems (e.g. H_2O-CO_2) has been greatly improved during the last decade (Holloway 1977; Bowers & Helgeson 1984, 1985). The study of multi-component gas systems, impossible without Raman analysis, is somewhat behind because of the late recognition of the larger variety of gas species in natural fluids. Several types of diagrams showing the correlations between T, X and $\bar{V}$ are used as a help for the determination of the molar volume in binary mixtures. Diagrams showing the correlation between homogenization and melting temperatures as a function of composition and molar volume (or density) were introduced by Swanenberg (1979) and Burruss (1981) for the system CO_2-CH_4 (see section 5.3.1). These diagrams are isothermal $\bar{V}X$-diagrams or alternatively isochoric TX-diagrams. $\bar{V}X$-Diagrams for the system CO_2-N_2 have been constructed by Darimont (1986) and Darimont & Heyen 1988 (see section 5.3.2).

Some rock samples may contain fluids of mixed composition showing textural evidence for contemporaneous trapping. These fluids of one generation should be trapped at the same PT-conditions. In this case, the corresponding molar volume of the nearest end-member can be obtained by the extrapolation of the homogenization temperatures to one of the pure systems (van den Kerkhof 1988).

The final step of the procedure, after the determination of the molar volume, is the interpretation of the geological forming PT-conditions. These can be calculated from the following fluid inclusion and supplementary data:

a) the molar volume of the fluid (and the fluid composition, already known for the calculation of $\bar{V}$);

b) an equation of state valid for the high PT-region (e.g. the MRK-equation as given by Holloway 1977, 1981);

d) independent metamorphic data, generally the temperatures determined from mineral assemblages (reaction equilibria) and/or geo-thermometry obtained by microscopic studies and mineral analysis by electron microprobe.

The PT-conditions are extrapolated from the homogenization point to the trapping conditions by the construction of the isochore (Fig.2.1).

This curve can be calculated for each inclusion from an equation of state valid for the high PT-region.

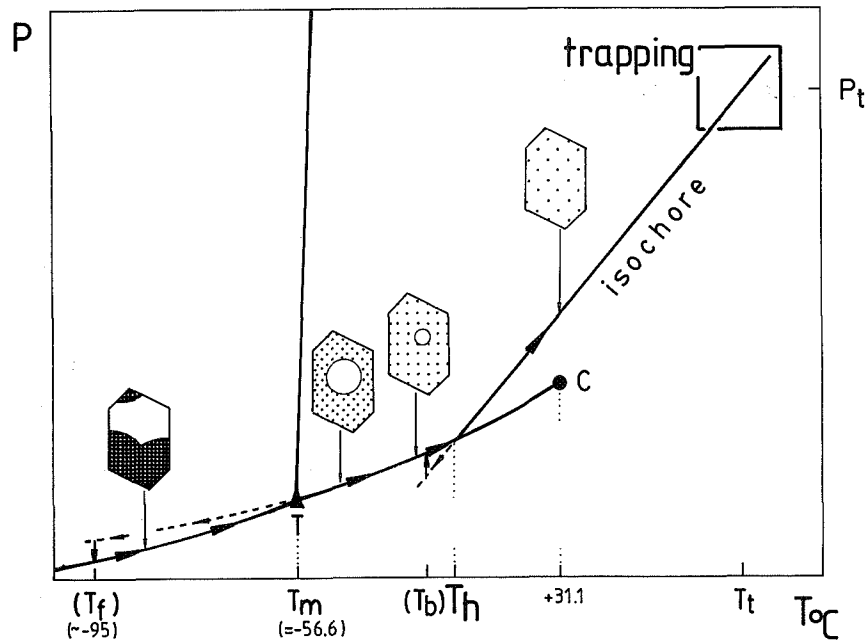

Fig.2.1.- *Sequence of phase transitions of a pure CO_2 inclusion observed during a cooling/warming run: black = solid, stippled = liquid and white = vapour phase. The homogenization temperature (T_h) defines the isochore which can be extrapolated to the PT-conditions of trapping (P_t, T_t). Extrapolated stippled curves denote metastable phase assemblages during cooling and explain freezing (T_f) and heterogenization (T_b) temperatures.*

2.3. Some problems inherent to fluid inclusion studies

Interpretations obtained from fluid inclusion studies rely on the hypothesis that the volume of fluid inclusions is constant from the moment of closure of the cavity to the present day; volume changes during cooling are neglected. Possible partial leakage of inclusions results to erroneous interpretations on the trapping conditions. However, leakage is not a general phenomenon and leaked inclusions can mostly be recognized by a deviant homogenization temperature or by textural evidence ("decrepitation"). Conclusions on possible leakage can only be made after

detailed microthermometric studies and the establishment of a T_h histogram (statistical study).

Metamorphic (or magmatic) temperatures are determined from mineral assemblages and/or mineral chemistry (geo-thermo/barometers). Metamorphic pressures are calculated as a point on the isochore (showing the correlation between P and T), corresponding to the temperature of interest. In the ideal case, the isochore cross-cuts the "PT-box" conditions defined by the appropriate reaction equilibria (Fig.2.1.). This condition is necessary but not sufficient: inclusions might be trapped outside the PT-box, but always along the isochore. In some cases it is possible to determine trapping pressures and temperatures from fluid inclusion data only, namely by the intersection of isochores constructed for gaseous and aqueous inclusions of the same generation (Hollister 1981; Roedder & Bodnar 1980) or by inclusions containing an "internal" thermometer (e.g. Na^+/K^+ ratios in aqueous inclusions (Poty et al. 1974).

The fluid may change in composition and density during the rock evolution i.e. from the rock deposition to the peak of metamorphism and subsequent cooling/uplift. Textures indicate the time relations between the fluids and the rock-forming minerals and also between possible different fluid types. PT-trajectories can sometimes be developed from the combined data of mineral stabilities (reaction curves) and fluid inclusions (isochores) (Hollister et al. 1979).

Load and fluid pressures should be equal in the case of consistent fluid densities and "PT-box" conditions. However, fluid pressures are sometimes lower (or higher) than load pressure at the time of inclusion forming. Internal pressures in the inclusions generally deviate from load pressure during subsequent isobaric or isothermal cooling (or heating). Fluid pressures are supposed to be adjusted during heating (prograde metamorphism) by (re)crystallization. This process is limited during cooling (retrograde metamorphism) being the reason why high fluid densities are preserved. However, this should always be discussed in detail by comparison with independent data.

III MICROTHERMOMETRY

3.1. The cooling/heating stage

Fluid inclusions in quartz are studied with the help of a cooling/heating stage by observation of phase behaviour at varying temperature. Double polished thin sections, 200-300μ thick, are prepared from quartz samples for further handling. Firstly, descriptions of the thin sections are made and the locations of fluid inclusions to be studied are selected. The slices are subsequently broken into pieces of about 0.5 cm to fit in the sample holder of the stage. The inner size of the cover ring is 1.8 cm in diameter. Drawings of the fluid inclusions are systematically made to make it possible to find them back for further discussion and Raman analysis.

The presently used device for the cooling and warming of samples is the Chaixmeca stage, originally designed by Poty et al. (1976). Several modified models or other stages are available since then (Roedder 1984, p.194-196; Shepherd 1985). Earlier models of the Chaixmeca were cooled by a precooled gas flow of (dried) air or nitrogen; the present model is directly cooled by liquid nitrogen and it has a gold coated body (to prevent oxidation at high temperature). The advantage of direct cooling is a low temperature reach and short cooling times: the lower temperature limit is -180°C; cooling to this temperature takes about 2 minutes. A disadvantage of using liquid nitrogen as a cooling agent is the lesser control on the cooling and heating rates.

The Chaixmeca stage is mounted to a Leitz microscope with a long distance H32/0.40 objective and it is provided with a built-in condenser, directly below the sample. This results in a clear illumination of the sample and a high resolution. The optical properties of the Chaixmeca are certainly its greatest advantage and it can hardly be approached by any cooling stage in this respect. A good optical quality is most important for the present application, namely a detailed observation of several types of phase transitions in fluid inclusions. No cover plate is used between the sample and the objective. The sample holder is closed by a plastic sleeve mounted on the objective and resting on the stage.

The forming of ice and moisture on the sample and on the stage during cooling is one of the most serious problems and may hamper accurate observation. To prevent condensation, the stage is heated to about +100°C

to be sure that it is absolutely dry before cooling is started; the sample itself is cleaned with alcohol and also dried. A plastic tube has been attached below the built in condenser to the lamp of the microscope in order to isolate the back side of the stage and to prevent condensation on the condenser during long runs at low temperature.

Only non-aqueous inclusions have been studied here. The temperatures of interest for phase changes are therefore below 31°C i.e. the highest critical temperature in the system CO_2-CH_4-N_2. Measurements are usually made on warming (after cooling) to get round metastable effects. On warming below -5°C, the stage is getting warmed by its surroundings only; the warming rate is not influenced by extra heating or cooling. Above -5°C, some extra heat is generally supplied. The heating rate is about 0.2°C/sec. at -100°C, 0.1°C/sec. at -65°C and 0.05°C/sec. at -10°C; the heating rate at lower temperatures is much higher: in the order of 1°C/sec. at -150°C. Measurements in the lowest temperature range are therefore less accurate. The total time duration needed for one measurement may be considerable, especially for the detection of CO_2 melting: warming from -100°C (freezing) to -56.6°C (melting) takes about 5.5 minutes.

Calibration of the temperature readings was done by means of compounds of known final melting temperature (T_m). The compounds used here for the low temperature range are methyl-cyclopentane (C_6H_{12}, T_m = -142°C), n-heptane (C_7H_{16}, T_m = -90.6°C), chloroform ($CHCl_3$, T_m = -63.5), CO_2 (in fluid inclusions), tetrachlormethane (T_m = -23.0°C) and water (T_m = 0°C). A drop of liquid is put between two normal cover glasses for calibration. Several other methods have been tried but these appeared to be all less reliable.

Special attention was paid to the calibration of the temperature around the melting point of CO_2 (-56.6°C) because the lowering of this temperature with increasing amounts of CH_4 or N_2 needs a high accuracy (preferably better than 0.5°C). For this purpose 3-phase CO_2-H_2O inclusions in quartz from Camperio (Switzerland) (Wagner et al. 1972; Touray 1968) were used. The purity of CO_2 was checked by Raman analysis: the measurement result is CO_2(99.0) N_2(0.9) CH_4(0.1) stating that CO_2 is almost pure. It is noted that 100% pure CO_2 does probably not exist in nature. A possible lowering of the melting point due to contaminations is small because of low fluid densities (see later). It was found from repeated calibration measurements that corrections varied during a 3 year period (Fig.3.1.). The smaller variations are explained by different

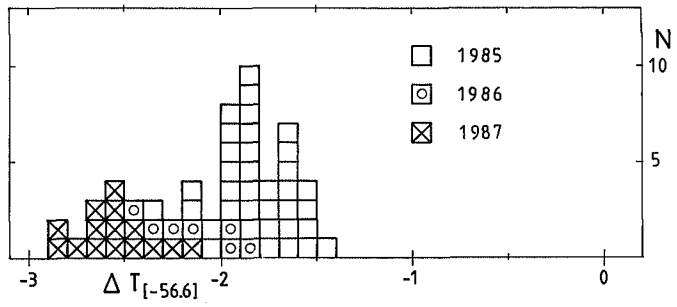

Fig.3.1.- *Histogram showing the frequency of correction temperatures at -56.6°C (the final melting temperature of pure CO_2 inclusions) during a 3 year period for the Chaixmeca cooling stage. Variations stress the necessity of regular calibration for accurate measurements.*

electronic settings which may especially occur by switching the stage on and off. The calibration temperature (ΔT) ranges within a 1.0°C interval (= mean $\Delta T \pm 0.5$°C) within 1 year. The "Camperio standard" has been measured during each series of measurements to obtain the highest possible accuracy around the melting point of CO_2.

The accuracy of the measurements may further be influenced by a) the thickness of the section b) the level of the measured inclusion in the sample c) the location of the sample on the stage (in the middle or at the rim) d) subjective factors depending on the operator. Taking all factors into account it can be assumed that the present measurements of T_m for CO_2 have an accuracy of about ± 0.2°C. The factor of heating rates can be almost eliminated if the standard (CO_2 inclusion or melting compound) and the fluid inclusion sample are warmed at the same rate. Even fast warming at low temperatures (around -150°C) may result to acceptable accuracies (about ± 1°C).

3.2. Phase transitions in systems of constant volume

The study of phase transitions in fluid inclusions at varying temperature since about 1970 resulted to the development of terminology used for the description of observations. Phase transitions at constant volume are mostly different from "normal" (polychoric) transitions. For, major volumetric changes of the phases are normally involved at phase transitions, according to the Clausius-Clapeyron equation:

$$\frac{dP}{dT} = \frac{q}{T\,(V_2-V_1)} \qquad \text{(Eq.3.1.)}$$

where q represents the involved energy of the phase transition, V_2 and V_1 are the specific volumes of the 2 phases and T is the absolute temperature. However, many "isochoric" phase transitions have been only poorly described.

The terms "homogenization" and "melting" are widely used and are sufficient for the description of phase transitions in fluid inclusions of pure composition. Often, only the homogenization temperature is measured and directly translated in terms of fluid densities. However, problems rise when studying fluid inclusions of mixed composition: the traditional terminology appeared to be insufficient to cover the extensive number of phase transitions. Some confusion exists about the proper use of terms, because the traditional terms are often too freely used. A revision of the present definitions is therefore needed. This may have also consequences for the definitions of the commonly used terms.

Some definitions: melting and homogenization

The transitions between the 3 basic physical states (solid, liquid and gas) of one compound are defined as melting, boiling and sublimation. These terms rely on observations at "normal" atmospheric conditions and can be further applied to all systems of varying P, V and T. In these systems, the volume is a function of both pressure and temperature given by an equation of state. Volume changes due to phase transitions are more or less adjusted. However, fluid inclusions represent systems of constant volume (isochoric systems) and P and T are the only variables for a system of constant composition and molar volume. This fact has major implications for the phase transitions especially for those which involve large volume changes (e.g. boiling). I shall state that isochoric systems show a phase behaviour at varying temperature which is typical for these systems. For example, boiling denotes the coexistence of the liquid and gas phases at a given pressure (and temperature) in a system of varying P, V and T. A 2-phase (L-V) inclusion may be seen as a state of permanent "boiling" (or immiscibility). A temperature increase stimulates "condensation" or "evaporation" resulting to a single phase, liquid or gas respectively, defined as "homogenization".

Confusion on the definition of the term "homogenization" may rise if the homogenizing phases are not specified. Strictly speaking, homogenization is the total homogenization of an inclusion resulting to a single phase whatever the preceding phases are. Accordingly, the disappearance of a bubble or a solid (L+V → L, L+V → V or S+L → L, S+V → V) are both denoted as "homogenization" (Burruss pers. comm.). Consequently, "melting" should be defined as any transition from 3 phases to 2 phases. Melting defined in this way, comprises "normal" (final) melting (S+L+V → L+V) as well as the homogenization of liquid and vapour phases in the presence of a solid phase (S+L+V → S+L or S+L+V → S+V). The latter phase transitions are considered then as different aspects of "melting".

Most authors use the term homogenization in a more restricted sense, namely the homogenization of liquid and vapour; melting is generally used for the disappearance of a solid phase. The definitions proposed in the present paper were established by taking into account the following reasonings: a) definitions should concur as much as possible with the traditional use b) all possible phase transitions should be properly named.

Number of possible phase assemblages

The characterization of phase transitions requires proper definitions of the phases. The physical state of a given compound is defined by the character of the molecular bonding. However, the character of the "fluid" phase cannot always be determined in fluid inclusions.

At present, a distinction between a liquid and vapour is not made in fluid inclusions, if these phases do not coexist i.e. in the cases of a single "fluid" phase or a "fluid" coexisting with a solid phase. A "fluid" phase may be preceded by LV-homogenization to the liquid or to the gas phase on warming and the character of the fluid phase can be determined at this point. However, the character of the fluid may change to higher temperatures without any visible evidence: a single phase has the properties of a vapour (or fluid in the proper sense) at temperatures above the critical temperature; liquid may converse to vapour or vise versa in case of changing composition of the liquid during melting.

Only temperatures above -180/-160°C are considered as this is the limit which can normally be reached by cooling with liquid nitrogen.

Solid CH_4 and N_2 cannot be solidified with the present equipment and solid CO_2 is the only solid normally formed. This phase is supposed to be pure in composition.

It can be stated that not more than 2 volatile phases may coexist in the system CO_2-CH_4-N_2 above -160°C i.e. full miscibility of the fluid phases is assumed. Solids of intermediate composition do not form at this temperature (see Chap.V). Consequently, the maximum number of coexisting phases above -160°C is 3: solid (S), liquid (L) and vapour (V). Theoretically, 7 possible combinations between the 3 phases are possible (Table 3.1.). Solid as a single phase is not further considered as inclusions of such high density have never been found. The number of phase assemblages which can be distinguished under the microscope is only 4 as the single liquid or vapour phases are both considered as a "fluid" (F). These 4 assemblages (S+L+V, L+V, S+F and F) are used as the basis for a classification of phase transitions on the understanding that F may denote liquid or vapour.

number of phases	phase assemblage	observed phases
3	S+L+V	S+L+V
2	L+V	L+V
	S+V	S+F
	S+L	
	V	F
	L	

Table 3.1.- *The basic phase assemblages in CO_2-CH_4-N_2 inclusions where S = solid CO_2; L = liquid; V = vapour; F = fluid (liquid or vapour phase). Only 4 assemblages can be observed.*

Stable and metastable phase transitions

Phases in CO_2-CH_4-N_2 inclusions are stable during warming from -160°C and phase transitions more or less gradually proceed. On the contrary, phase transitions during cooling generally represent changes from metastable to stable conditions. The phases are mostly supercooled and phase transitions take place instantaneously, accompanied with a sudden adjustment of the pressure. Phase transitions are generally measured on warming to avoid metastability: the temperature marking a given phase transition on cooling is always lower than measured on warming. The discrepancy between freezing (-90 to -100°C) and melting temperature (-56.6°C) of CO_2 can be taken as an example: the temperature of

appearance of a bubble on cooling (heterogenization) is mostly in the order of 5 degrees lower than homogenization. The direct phase transition L+V → S+V ("freezing") is only possible because of metastable effects and the 3-phase assemblage is "overstepped".

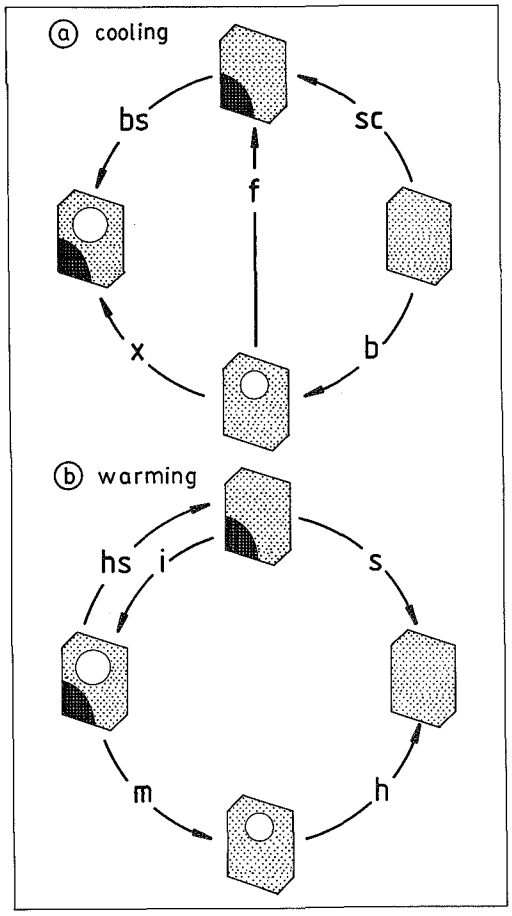

Fig.3.2.- *The possible phase transitions observed during cooling to -180°C (a) and subsequent warming (b) of CO_2-CH_4-N_2 inclusions where black = solid CO_2, stippled = liquid, white = vapour phase. Denotations are identical to the subscripts given in Table 3.2a-b.*

Phase transitions on cooling: definition and symbols

Observed phase transitions in CO_2-CH_4-N_2 inclusions on cooling to -160°C are schematically shown in Fig.3.2a. and listed in Table 3.2a. Some definitions are given below.

1) Heterogenization (T_b) is defined as the point marking a single phase becoming immiscible (F → L+V). This point is characterized by the appearance of a bubble and can be considered as the reverse of

homogenization. Complementary terms (used for non-isochoric systems) are "condensation" (for V → L+V) or "boiling" (for L → L+V).

2) Sublimation (T_{sc}). The term "sublimation" is used here to indicate the transition F → S+F as well as the reverse process S+F → F (see below).

3) Freezing or solidification (T_f) is defined here as the forming of a solid phase from a liquid and a vapour (L+V → S+F). In CO_2-CH_4-N_2 inclusions, freezing can be approached as the crystallization of the liquid phase only (L → S).

4) Crystallization or precipitation (T_x) is defined as the nucleation of a crystal in a liquid phase, coexisting with a vapour (L+V → S+L+V). This phase transition is observed in CO_2-CH_4 inclusions.

5) Partial heterogenization (T_{bs}), the forming of a bubble in the presence of solid CO_2. Heterogenization can be considered as condensation or boiling of the CH_4 and/or N_2-rich fraction, because CO_2 is almost completely partitioning in the solid phase at low temperatures.

a) ON COOLING:	Phase transition			T_x^P x	P
heterogenization	F	→	L+V	b	
sublimation	F	→	S+F	sc	
freezing	L+V	→	S+F	f	
crystallization	L+V	→	S+L+V	x	
partial heterogenization	S+F	→	S+L+V	bs	
b) ON WARMING:					
incipient melting	S+V	→	S+L+V	i	V
	S+L	→	S+L+V	i	L
(final) melting	S+L+V	→	L+V	m	
partial homogenization	S+L+V	→	S+V	hs	V
	S+L+V	→	S+L	hs	L
homogenization / metastable homogenization	L+V	→	V	h/hm	V
	L+V	→	L	h/hm	L
sublimation	S+V	→	V	s	V
	S+L	→	L	s	L

Table 3.2a-b. *Phase transitions in the temperature range from -180 to +35°C a) on cooling and b) on warming in CO_2-CH_4-N_2 inclusions and their denotation. T_x^P is the temperature recorded during a heating/cooling run: x = letter (or group of letters) characterizing the transition; P = involved phase.*

An alternative terminology is suggested by Roedder (1984, p.198): a general denotation "Tn" (nucleation temperature) is used for any forming

of a new phase (solid or vapour), mostly in the liquid phase. According to this nomenclature, freezing (T_f), sublimation (T_{sc}) and crystallization (T_x) for inclusions of the present composition are all denoted as "Tn CO_2 S"; heterogenization (T_b) and partial heterogenization (T_{bs}) can be considered as the nucleation of a vapour phase and these phenomena are accordingly denoted as "Tn V". The advantage of this terminology is its universal application (for both gaseous and aqueous inclusions), but on the other hand it does not decide for the number of involving phases. The presently used terminology is mostly valid for inclusions of the system CO_2-CH_4-N_2.

Phase transitions on warming

Fluid inclusions are cooled until the stabilization of the phase assemblage which is also stable at -160°C. Warming is subsequently started to measure the temperatures marking phase transitions. In the temperature range between -160°C and +35°C, 5 basic phase transitions (1 to 5, see below) can be observed in CO_2-CH_4-N_2 inclusions on warming (Fig.3.2b). Warming mostly results in a decreasing number of phases: 3 phases grade to 2 phases (S+L+V → S+F or S+L+V → L+V) and 2 phases grade to 1 phase (S+F → F or L+V → F). An increasing number of phases on warming is only possible at incipient melting (S+F → S+L+V). "Homogenization" is subdivided in "normal homogenization" and "metastable homogenization" (see below). All phase transitions and their denotations are listed in Table 3.2b. The temperatures marking phase transitions are indicated as T_x^P where the subscript x denotes the abbreviation of the type of phase transition (h, m, s etc.) and the superscript P denotes the phase present before and after the transition (L, V or C).

1) Partial homogenization (T_{hs}) is defined here as the homogenization of the liquid and vapour phases in the presence of solid CO_2 (S+L+V → S+L or S+L+V → S+V). This behaviour has first been described by Guilhaumou et al. (1981) for CO_2-N_2 inclusions. Roedder (1984 p.198) suggests a denotation indicating the 2 homogenizing phases and the resulting phase e.g. Th L-V (V).

2) Incipient (or first) melting (T_i) is defined here as the transition from a solid phase coexisting with liquid or vapour to a

3-phase equilibrium (S+L+V). Incipient melting may show 2 principle types of behaviour: a) T_i^L (S+L → S+L+V) or b) T_i^V (S+V → S+L+V). The latter phase transition is most common: the vapour phase becomes supersaturated and a liquid condensates. The phase transition S+L → S+L+V has been observed in CO_2-CH_4 and sometimes in CO_2-N_2 inclusions (Herskowitz & Kisch 1984; Burruss pers. comm.; present study: inclusions from SW Norway, the Appalachians and artificial CO_2-N_2 inclusions): a tiny bubble appears as the new formed phase becoming larger when melting proceeds. Initial melting into a critical fluid (T_i^C) may occur for some CO_2-CH_4 inclusions (see section 3.3).

It should be pointed here that incipient melting is <u>not</u> identical to <u>eutectic melting</u> (T_e) in non-pure systems. Eutectic temperatures are recorded in salt solutions, but they are normally too low to be detected for gaseous mixtures. T_e is defined as the forming of a first melt after solidification of <u>all</u> compounds of the system of interest (S_1 → S_2+L). Eutectic temperatures are unique for a given system whereas T_i is dependent on the total composition. Eutectic temperatures approximate the melting points of the pure end-members of lowest T_m in the systems CO_2-CH_4 (-183°C) and CO_2-N_2 (-210°C); the eutectic point of the system CH_4-N_2 is located at -210.6°C and a composition of 76.2 mole% N_2 (see section 5.3). Eutectic temperatures cannot be measured with the present equipment because of the cooling limit.

3) <u>Melting</u> (or final melting) (T_m) is defined as the transition from 3 phases (S+L+V) to liquid and vapour by the disappearance of solid CO_2. The melting temperature of pure CO_2 is -56.6°C and T_m is lowered with higher contents of CH_4 or N_2. Note that T_i and T_m coincide at the triple point for 1-component systems. However, "melting paths" (T_m-T_i) of more than 10 degrees have been measured in the system CO_2-CH_4, but they are generally smaller (mostly much less than 5°C) in the system CO_2-N_2. Melting paths are reduced again near the points defined by coinciding homogenization and melting (T_i=T_m=T_h). A special case is melting to a critical fluid (T_i=T_m=T_h^C) found for the system CO_2-N_2 (see section 3.3).

4) <u>Homogenization</u> (normal or stable homogenization) (T_h) is defined as the transition from coexisting liquid and vapour phases to a single phase by shrinkage of the bubble (T_h^L: L+V → L), sometimes referred to as "liquid homogenization" or "homogenization to the liquid", expansion of

the bubble (T_h^V: L+V → V) ("gaseous homogenization") or critical (T_h^C: L+V → L=V).

Metastable homogenization (T_{hm}) is the homogenization of a metastable liquid and vapour. Metastability is characteristic in CO_2-CH_4-N_2 inclusions at temperatures between the melting point (below -56.6°C) and the freezing point (generally -90 to -100°C). For the detection of metastable phase transitions, warming is started before "stabilization" by the forming of solid CO_2. Both T_{hs} and T_{hm} can often be measured for one inclusion i.e. the homogenization of liquid and vapour with and without solid CO_2. The latter temperature is always higher because CO_2 (with a higher critical temperature) is then dissolved in the volatile phases whereas CO_2 is subtracted from the volatiles in the presence of a solid phase.

5) Sublimation (T_s) is defined here as the transition of a solid phase directly to the vapour or liquid(!). Only 2 phases are involved during sublimation according to the present terminology whereas melting involves 3 phases. The transition solid to vapour (S+V → V) has been denoted as "evaporation" by some authors (Kreulen & Schuiling 1982); the transition solid to liquid (S+L → L) has sometimes been denoted as "final melting" (Herskowitz & Kisch 1984) or "dissolution". "Melting" is often used for both transitions (to liquid or vapour). Note that a distinction between both phase transitions cannot be made by observation.

3.3. A classification of phase behaviour: H and S-type inclusions

Determination of the homogenization temperature (T_h) is sufficient for further interpretation as far as pure fluid compositions are concerned. The purity can be checked by accurate measurements (better than 0.5°C) of the melting temperature (T_m) and/or Raman analysis. If there are indications for impure compositions, it is recommended to study the phase behaviour in a more extended temperature range (between -160°C and +35°C). The total phase behaviour expresses both composition and molar volume of fluid inclusions. The phase behaviour may be complicated for some compositions. A classification model is proposed here comprising all possible phase sequences of CO_2-CH_4-N_2 inclusions on warming from -160°C.

The classification is the result of observations made for natural and artificial inclusions.

In the preceding section, 5 basic types of phase transitions (on warming) were distinguished. The number of possible phase transitions during one cooling/warming run is also limited. The phase assemblages to high and low temperatures are fixed: all CO_2-CH_4-N_2 inclusions should be in the fluid state above 31.1°C and only solid phases are allowed at temperatures approaching absolute zero. However, solid phases except solid CO_2 cannot be formed here and are not further considered. At the lowest temperatures (-180/-160°C), one of the following phase assemblages should occur: S+L+V, S+V, S+L or L+V. During subsequent warming, each type of phase transition occurs only once or twice. The order of phase sequences is fixed on warming from this low temperature and appeared to be only related to the final phase transition (homogenization or sublimation). A subdivision in 2 types of fluid inclusions has therefore been proposed (van den Kerkhof 1988):

a) H-type inclusions characterized by homogenization (H) as the final phase transition. The maximum number of phase transitions between -160°C and +35°C is 5 ($T_i \rightarrow Ths \rightarrow T_i \rightarrow T_m \rightarrow T_h$);
b) S-type inclusions characterized by sublimation (S). A maximum of 4 phase transitions may occur ($T_{hs} \rightarrow T_i \rightarrow T_{hs} \rightarrow T_s$).

The complete phase behaviour of a CO_2-CH_4-N_2 inclusion can be described by
a) the final phase transition: homogenization (type H) or sublimation (type S) and
b) the number of phase transitions between -160 and +35°C (subtypes H1 to H5 and S1 to S4).

For example: an inclusion of type H4 is characterized by a 3-phase stability at -160°C and on warming by successive partial homogenization (T_{hs}: S+L+V → S+L or S+V), incipient and final melting (T_i and T_m: S+L or S+V → S+L+V → L+V) and homogenization (T_h: L+V → L or V).

Note that all pure CO_2 inclusions are of type H3; pure CH_4 and N_2 inclusions are of type H1. Metastable homogenization (T_{hm}) can only be measured for S-type inclusions. All possible phase sequences are schematically represented in Table 3.3; examples of the types are shown

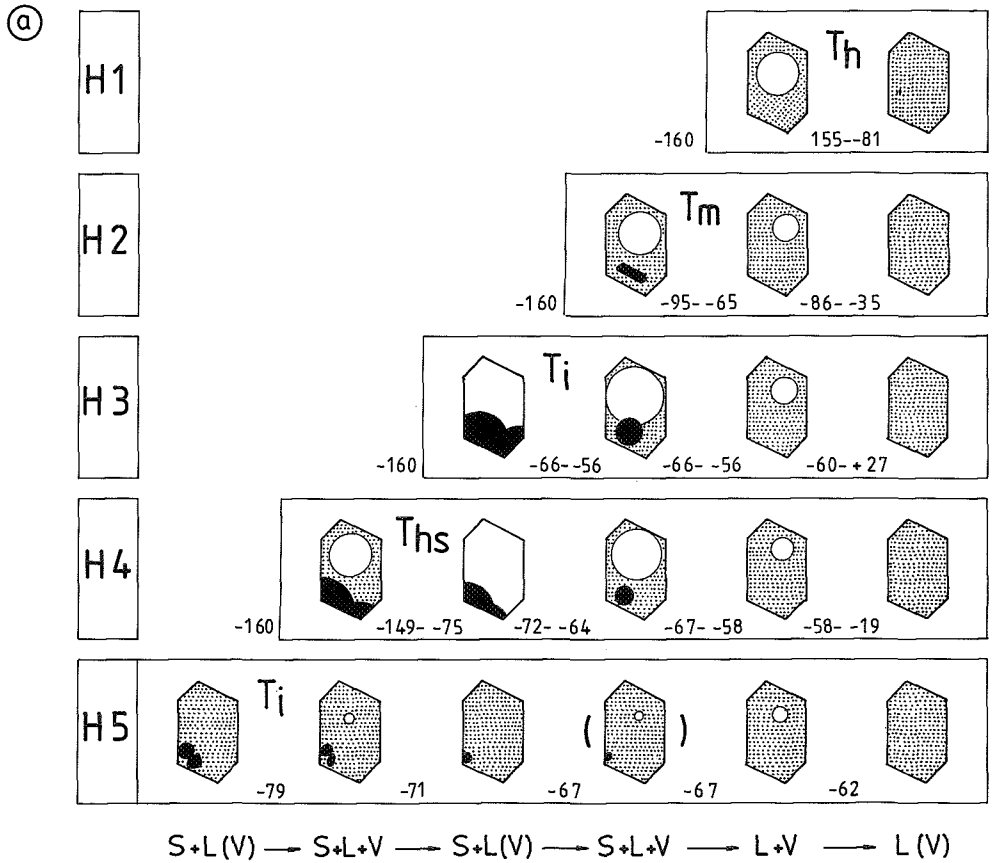

Fig.3.3.- *Types of phase behaviour observed in CO_2-CH_4-N_2 inclusions between -160 and +35°C where black = solid CO_2, stippled = liquid, white = vapour phase. A distinction in 2 groups is made:*
(a) inclusions showing homogenization (H-type);
(b) inclusions showing sublimation (S-type).
The sequence of phase transitions is fixed for both groups: the number of phase transitions may vary from 1 to 5 for H-type inclusions and from 1 to 4 for S-type inclusions. In the latter type, homogenization of the stable or metastable liquid and vapour phases can be observed. The drawings shown are only schematic representations of observations and the volumetric ratios of the phases may be very different. The temperatures indicated are measured ranges in natural inclusions. All fluid mixtures are supercritical above 31.1°C (but generally already supercritical at lower temperatures).

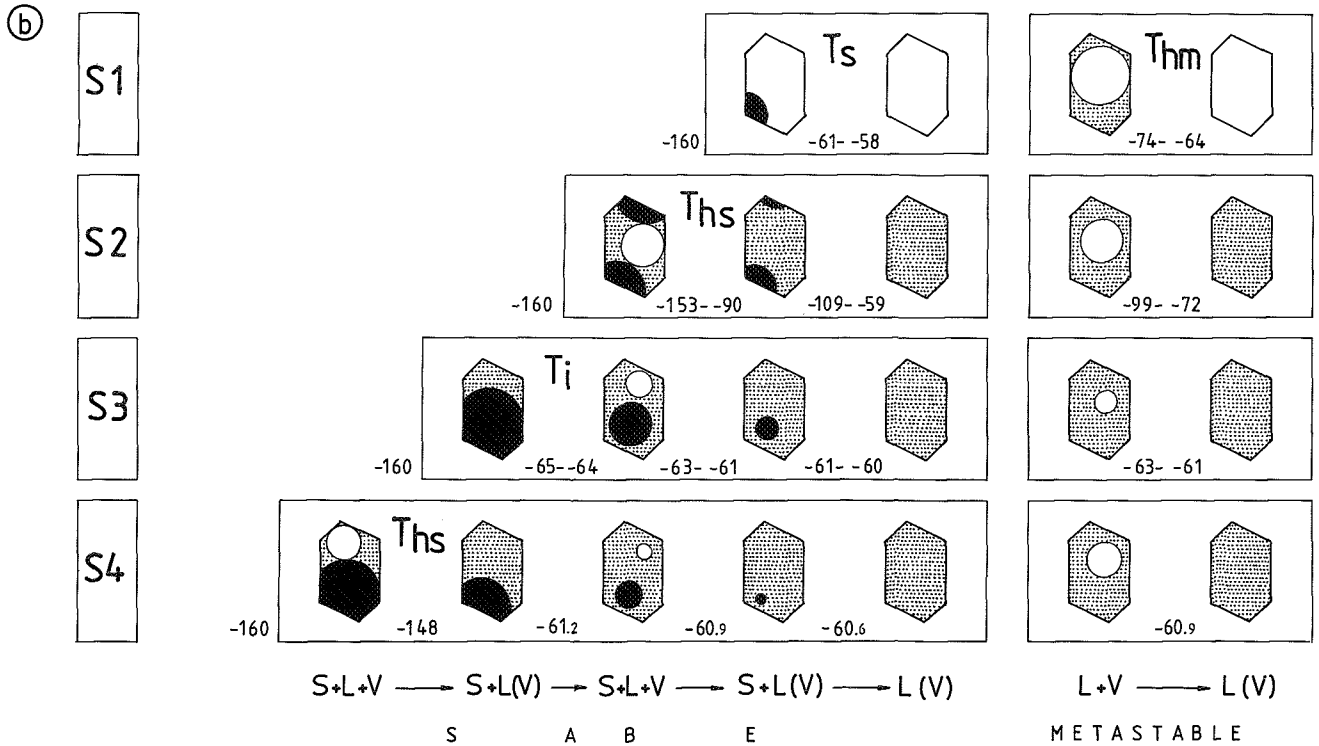
b
S1
S2
S3
S4
Ts
Thm
Ths
Ti
Ths
-160
-61- -58
-74- -64
-153- -90
-109- -59
-99- -72
-65- -64
-63- -61
-61- -60
-63- -61
-148
-61.2
-60.9
-60.6
-60.9
S+L+V → S+L(V) → S+L+V → S+L(V) → L (V)
L+V → L (V)
S
A
B
E
METASTABLE

in Fig.3.3a-b. It is important to realize that the relative amounts of the phases may be very different from the examples shown here. Sometimes, the amount of liquid (or solid) are even too small to be observed (less than about 10 vol% of liquid and 1 vol% of solid cannot be observed). For example, a 3-phase equilibrium is visible as 2 phases (S+V) if the liquid to vapour ratio is less than 10 vol%, and possible partial homogenization (to the vapour phase) cannot be observed. Consequently, an essentially H4 type inclusion can be classified as "H3". However, it is stated that the present classification is meant for practical use and phase behaviour should be classified as observed by optical means.

The final multi-phase assemblage upon warming = L+V (H-type)

	S+L	S+L+V	S+L or S+V	S+L+V	L+V	L or V
H1					... $T_h^{L/V}$	...
H2				... T_m	... $T_h^{L/V}$	...
H3			... T_i^{V}	... T_m	... $T_h^{L/V}$	...
H4		... T_{hs}	... $T_i^{V/L}$	... T_m	... T_h^{L}(V)	...
H5	... T_i	... T_{hs}	... T_i^{L}	(...) T_m	... T_h	...

The final multi-phase assemblage upon warming = S+L or S+V (S-type)

	S+L+V	S+L	S+L+V	S+L or S+V	L or V
S1				... T_s	...
S2			... $T_{hs}^{L/V}$	... T_s	...
S3		... T_i^{L}	... T_{hs}^{L}	... T_s	...
S4	... T_{hs}^{L}	... T_i^{L}	... T_{hs}	... T_s	...

metastable (S-type)

	L+V	L or V
S1 to S4	... $T_{hm}^{L/V}$	...

Table 3.3.- *Table for the classification of CO_2-CH_4-N_2 inclusions according to their microthermometric behaviour. A twofold division is made between H-type and S-type inclusions (see text).*

All types of phase behaviour mentioned above have been observed in natural fluid inclusions, but their frequency of occurrence is very different: H1, H2, H3 and H4 are the most common H-type inclusions; S-type inclusions are mainly restricted to S2. As a general rule, sublimation is favoured at lower molar volumes and higher concentrations of CH_4 and/or N_2 (Burruss 1981). The remaining types are rare and they represent limited compositional and volumetric ranges. The frequency of phase behaviour and also the implications in respect of composition and

molar volume are tentatively indicated in Table 3.4 (see Chap.V for detailed discussion).

TYPE	CO_2	CH_4	N_2	MOLAR VOLUME 40	65	100	200	FREQUENCY
H1	-	var.	var.	xx	xx	xx	xx	common
H2	low	high	low	x	xx	xx	x	common
H3	high	low	low	(x)	x	xx	xx	very common
H4	int.	(int.)	int.	xx	xx	x	(x)	common
H5	int.	int.	-	x	-	-	-	rare
S1	int.	int.	int.	x	-	-	x	rare
S2	low	high	high	xx	xx	x	(x)	very common
S3	int.	(-)	int.	x	-	-	-	rare
S4	int.	(-)	int.	x	-	-	-	rare

Table 3.4. *Some general characteristics of CO_2-CH_4-N_2 inclusions subdivided into types of different phase behaviour (H1-H5; S1-S4): relative proportions of the 3 components (high, intermediate, low or variable content), volumetric ranges (in cm^3/mole) and the frequency of occurence in studied metamorphic rock samples are tentatively indicated.*

Different melting behaviour for H3 and H4 type inclusions

It was mentioned in section 3.2 that initial and final melting may have a very different appearance, dependent on the character of the fluid phases (liquid, critical or vapour). The melting process (between T_i and T_m) can be observed for inclusions of type H3 and H4. Only "normal melting" (see below) is possible for type H3 inclusions, but different melting behaviour has been observed for type H4 inclusions (Fig.3.4).

a) "normal melting" (T_i^V) is defined by the phase sequence S+V → S+L+V → L+V. Inclusions of type H4 showing normal melting should have CO_2-N_2 compositions and are not allowed for the system CO_2-CH_4. However, apparent normal melting is observed for (type H2) CO_2-CH_4 inclusions with a very small amount of liquid below the final melting temperature (see section 5.3.1 and 5.4). Both partial (T_{hs}) and final homogenization (T_h) may be to the liquid, critical or vapour phase.

b) critical final melting ($T_i=T_m=T_h^C$) is only allowed for the system CO_2-N_2 because the critical curve only cross-cuts the liquidus in this system (see Chap.V). Inclusions showing this behaviour are unique in composition and molar volume (XN2~0.57; $\bar{V}$~40 cm^3/mole). Artificial inclusions with properties near this point were made by experiment (see Chap.VI).

c) critical initial melting (T_i^C) is given by the phase sequence $S+V_{crit} \rightarrow S+L+V \rightarrow L+V$). This behaviour may only occur for CO_2-CH_4 and not for CO_2-N_2 inclusions. Partial homogenization was found to be also (near) critical and final homogenization to the liquid phase: an inclusion with $\bar{V}$ ~ 50 cm^3/mole from SW Norway containing $CO_2(49)CH_4(51)$ showed critical initial melting at -67°C (T_m=-64.9; T_h^L=-37°C).

d) initial melting to the liquid (T_i^L) (S+L → S+L+V → L+V) is characteristic for the system CO_2-CH_4 (types H4 and H5). Molar volumes are below about 63 cm^3/mole (section 5.3.1). Both partial and final homogenization are to the liquid phase. In the system CO_2-N_2, T_i^L is only allowed for the special case that T_m-T_h^L, observed in an artificial inclusion (inclusion E333-B6, Chap.VI).

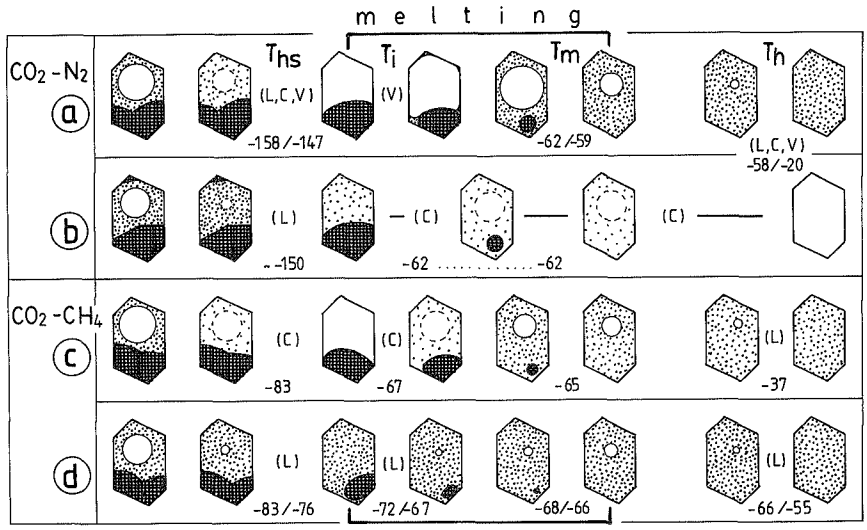

Fig.3.4.- *Schematic representation showing 4 different types of melting behaviour (T_i and T_m) observed in type H4 inclusions. Preceding partial homogenization (T_{hs}) and subsequent final homogenization (T_h) are also shown. Numbers denote temperatures (°C) measured for fluid inclusions. (a) "normal" melting by the forming of a liquid from a supersaturated vapour (b) critical final melting (T_i=T_m=T_h^C) (c) critical initial melting and (d) melting by the forming of a bubble (T_i^L) in a liquid (see text).*

IV RAMAN ANALYSIS

4.1. Introduction

Experimental observations made by Sir C.V. Raman in 1928 first proved the existence of inelastic light scattering which became known as the "Raman effect". The Raman principle has since been applied to fundamental chemical research, mostly in combination with infrared spectroscopy. Its application as a method for quantitative analysis of fluid inclusions by petrologists was introduced at the end of the 1970's (Delhaye & Dhamelincourt 1975; Rosasco & Roedder 1975; Dhamelincourt 1979). Equipment was developed which combined a Raman spectrometer provided with a laser and a microscope (microspectrometer). The non-destructive analysis of small amounts of material present in fluid inclusions became then possible. Several commercially produced types of microspectrometers are available, mostly from 2 firms: Jobin-Yvon (Paris) and Dilor (Lille, France). The advantages of Raman analysis are the non-destructive character of the method and the possibility of measuring single inclusions. Not only gases and liquids can be measured, but also some minerals can be identified which cannot be analysed otherwise i.e. if they occur as small inclusions below the surface of a sample (in particular daughter minerals in fluid inclusions). However, this application of Raman analysis is limited by the fact that purely ionic solids, such as alkali metal chlorides (halite, sylvite etc.) are Raman inactive.

4.2. The principle of the Raman effect

Light illuminating a molecular substance is partly (about 10^{-3}) scattered with the same wavelength (elastic or Rayleigh scattering); a much smaller part (generally 10^{-5} to 10^{-6} of the incident radiation) shows a shift in wavelength due to the interaction between vibrating molecules and the incident light beam. This weak, inelastically scattered light is the Raman effect. Raman frequencies are higher and lower than the frequency of the exciting radiation.

Extensive literature on the theory of the Raman effect is available. A short introduction to the Raman theory is compiled from the literature

(Hibben 1939; Tobias 1967; Alpert et al. 1970; Williams & Fleming 1971; Griffith 1974; Griffith 1975; Brame & Grasselli 1976; Long 1977). Applications of Raman analysis to fluid inclusion studies have been described in several recent publications (Rosasco & Roedder 1979; Dhamelincourt et al. 1979; Rosasco 1980; Delhaye et al. 1980; Guilhaumou 1982; Barbillat 1983; Dubessy 1985; Burke & Lustenhouwer 1987).

4.2.1. The term polarizability

An atom or molecule in an electric field will be distorted and therefore be polarized. This is the induced dipole-moment which is proportional to the applied field according

$$\mathbf{P} = \alpha \mathbf{E} \qquad \text{(Eq.4.1)}$$

where **P** and **E** are vectors indicating the induced dipole-moment and the electric field respectively; α denotes the polarizability. Note that **P** is independent from the permanent dipole-moment. **E** may be the oscillating electric field of a light beam with a frequency ν_0. The polarizability is essentially a bond property, related to the "looseness" of the electron cloud. The numerical value of the polarizability is expressed in volume units. The polarizability is a simple number for atoms, but direction-dependent for molecules: it can be completely described by 3 numbers and visualized by a polarizability ellipsoid.

The Raman effect is due to changes of polarizability during intramolecular vibrations which can be expressed by

$$\frac{\partial \alpha}{\partial Q_V} \neq 0 \qquad \text{(Eq.4.2)}$$

where Q_V is some vibrational coordinate. Only Rayleigh scattering is involved if $\partial\alpha/\partial Q_V$ equals zero. However, not all vibrations are Raman active and their character is strongly dependent on the molecular symmetry.

4.2.2. Vibration and rotation of molecules

The character of molecular vibrations can be elucidated with the example of a simple linear molecule ABA (e.g. CO_2). Here, three possible types of normal vibrations can be distinguished: a) symmetrical (denoted as the Q_1 mode) b) antisymmetrical (Q_2) and c) deformation or bending vibrations (doubly degenerated: Q_{3a} and Q_{3b}) (Fig.4.1). Symmetrical vibrations do not destroy the symmetry of the molecule and they do therefore not influence the dipole-moment. In terms of polarizability: the volume of the polarizability ellipsoid changes with the vibrational frequency while its orientation remains unchanged. It was mentioned above that the polarizability is expressed in volume units and symmetrical vibrations do therefore cause a change in polarizability. It can be stated that symmetrical vibrations are all Raman active whereas antisymmetrical and bending vibrations are not for the linear molecule ABA. However, the latter vibrations may be Raman active for molecules of lower symmetry.

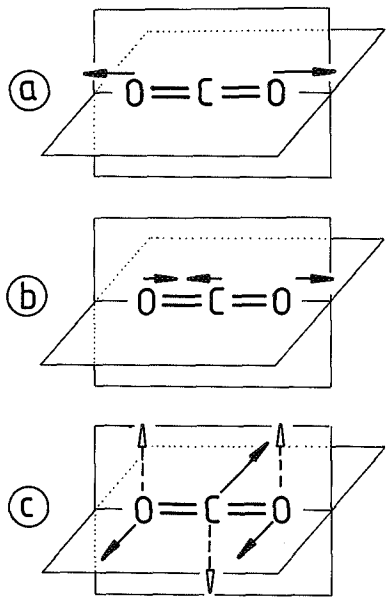

Fig.4.1.- *The 3 normal vibration modes of the carbon dioxide molecule: a) symmetrical b) antisymmetrical and c) bending (doubly degenerate). Only symmetrical vibrations result to polarizability changes and are therefore Raman active (modified after Alpert et al. 1970).*

Not only vibrations, but rotations as well may change the polarizability of a molecule: the polarizability changes with a frequency which is two times the frequency of rotation. A linear molecule has a

rotational axis which coincides with the symmetry axis of the molecule. All rotational Raman lines are situated very near the Rayleigh line and they are therefore very difficult to distinguish. Furthermore, broadening of vibrational Raman lines may be attributed to rotations (Coriolis interaction). Note that rotations are normally absent in the solid state resulting to sharper lines compared to the liquid and gaseous states. Raman shifts due to pure rotations are not further considered in the present study.

4.2.3. Infrared and Raman spectra

The wavelengths of molecular vibrations are mostly between 2500 and 15000 nm and cover the infrared part of the electromagnetic spectrum. Frequencies are generally expressed in terms of wavenumber i.e. the number of vibrations per centimeter being the reciprocal of the wavelength (denoted by $\bar{\nu}$ in cm^{-1}). Consequently, the above mentioned range corresponds to 4000 to 667 cm^{-1}. The method of infrared analysis is based on the fact that a given molecular compound absorbs the light of one or more well-defined wavelengths in this frequency range.

Contrary to the infrared spectrum, the Raman spectrum is an excitation spectrum. The Raman effect in respect of wavenumber is independent on the wavelength of the incident radiation, but only depends on the Raman activity of the compound (the intensity of the Raman scattering may change). Incident wavelengths should be chosen far from the absorption lines to avoid a high noise level. The use of a laser enables the detection of Raman lines for small amounts of material such as fluid inclusions. Monochromatic lasers are generally used with exciting wavelengths between 287 and 633 nm (i.e. in the visible part of the continuous spectrum). The energy (E) of the laser is given by the expression $E = h.\nu_0$ where h is Plank's constant and ν_0 the frequency of the emitted light. The corresponding wavelength is defined as $\lambda_0 = c/\nu_0$ where c is the velocity of light. The intensity of the Raman scattering is higher for higher frequencies of the laser (e.g. green light produces higher Raman intensities than red). The Raman effect results in a pair of lower and higher frequencies compared to the frequency of the incident laser beam (and Rayleigh scattering). These are called the Stokes and anti-Stokes lines, expressed by the equations

$\nu_R \quad \nu_0 - \nu$ ("Stokes") (Eq.4.3a)

and $\nu_R \quad \nu_0 + \nu$ ("anti-Stokes") (Eq.4.3b).

The result of the Raman effect is usually denoted by $\Delta\bar{\nu} = 1/\nu_R$ cm^{-1}. The intensities of the Stokes lines are much higher, and only these are normally measured. An example of a Raman spectrum and its elements are shown in Fig.4.2.

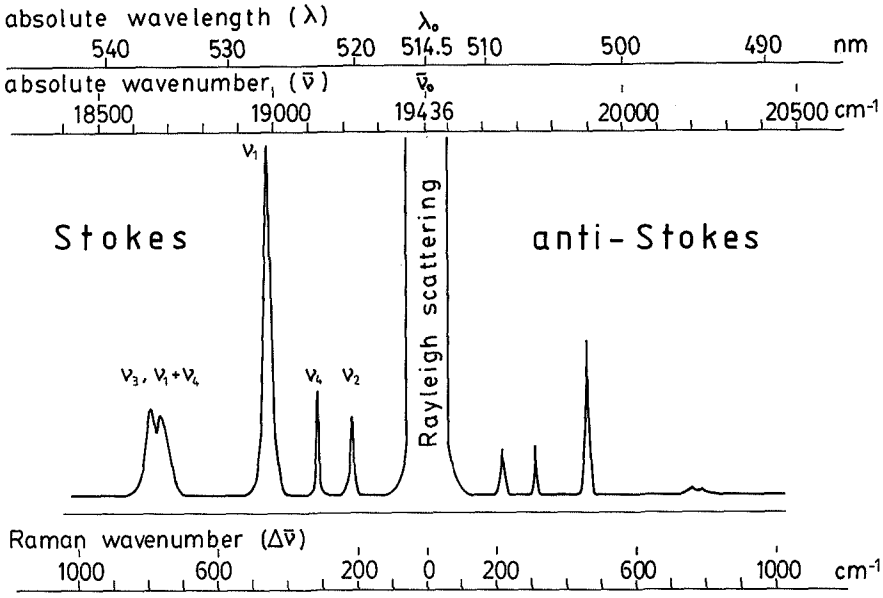

Fig.4.2.- *The Raman spectrum of CCl_4 excited with a wavelength of 514.5 nm, and its elements. The Raman lines may be higher ("Stokes") or lower ("anti-Stokes") in wavelength than Rayleigh scattering. The "Stokes" lines have a higher intensity and only these are normally considered.*

The lines detected in a Raman spectrum may correspond to

a) fundamental vibrations (and rotations) of the molecule;

b) overtones of a given frequency being twice the frequency of the fundamental tone;

c) combination tones (approximately the sum or difference between two simpler frequencies);

d) overtones or combination tones interfering with fundamental tones.

The latter vibrations are denoted as the Fermi resonance effect (or

vibrational perturbation) for which CO_2 serves as a classical example (see section 4.5.1.).

It is common use to designate vibrational types by numerical subscripts (ν_1, ν_2, ν_3 etc.). These types are not unique for all molecules, but only defined within a given class (e.g. molecules of type AB_2 and AB_4); overtones are denoted by $2\nu_1$, $2\nu_2$ etc.

Some elements occur as different isotopes (e.g. H, C and Cl). The substitution of isotopes in a molecule may slightly reduce its symmetry. This may be responsible for the splitting of Raman bands e.g. the spectrum of CO_2 showing an additional line for $^{13}CO_2$. Another example of isotopic splitting is known for CCl_4 (esp. $C^{35}Cl_4$ and $C^{37}Cl_4$).

The principles of Raman and infrared spectroscopy are very similar and both techniques can be considered as complementary. The main difference between infrared and Raman activity is explained by the type of molecular vibration: infrared absorption is due to non-symmetrical vibrations which produce a change of the dipole-moment; the Raman effect is due to symmetrical vibrations by which the polarizability is changed. Highly symmetrical molecules as diatomic N_2 or H_2 are therefore Raman active, but not infrared active. In general, it can be stated for molecules with a symmetry center, that vibrations being Raman active are infrared inactive and v.v. This is known as the rule of mutual exclusion. Raman analysis appeared to be extremely valuable for the detection of inorganic compounds, in particular simple gases.

4.2.4. Absorption and fluorescence

In the case of absorption, the energy of an electromagnetic wave ($h\nu$) is directly related to the vibrations or rotations of the atoms in a molecule. The wavelength(s) of the absorbed light are well defined. Absorption is dependent on the colour of the sample and can be avoided by selecting laser light which is very near to the colour of the sample. Any light colour may be used in the case of a colourless sample.

Fluorescence takes place if quanta (of lower energy) are re-emitted and light is released with a longer wavelength. If occurring during laser illumination, fluorescence can mask completely the Raman effect. The effects of fluorescence are much more likely to occur for higher frequencies (green or blue) than for lower frequencies (red). On the

other hand, the Raman effect is stronger for higher frequency sources. By the analysis of natural fluid inclusions, fluorescence appeared to play only a role for hydrocarbons (Dubessy 1985). No problems in this respect normally occur at present for pure methane inclusions. However, some samples present a natural fluorescence which makes it impossible to record the Raman spectrum. Special care must also be taken to avoid fluorescent resin or other fixing material during sample preparation.

4.3. The Raman spectrometer (Microdil-28®)

Mercury arcs were used as a light source for the early models of Raman spectrometers. The general availability of gas lasers in the 1960's did reduce the time needed for recording spectra by several orders of magnitude and it opened the way for Raman spectroscopy to become a regular analytical method in mineralogy. Several types of laser Raman spectrometers have been developed in the last decade. Since the beginning of the early 1980's, a new generation of microspectrometers became available provided with a multichannel detector. The Microdil-28® is of the latter type and has been used for the present study. The apparatus is produced since 1983 by Dilor Co. (Lille, France). The advantages of multichannel detection are low detection limits and short measurement durations (Burke & Lustenhouwer 1987; Campion & Woodruff 1987).

A scheme of the used Raman spectrometer is shown in Fig.4.3. The elementary parts of the apparatus are

a) the laser;
b) the microscope;
c) the (pre)monochromator;
d) the (multichannel) detector.

The laser source used is an argon-ion laser (Spectra Physics® model 164-06 2-W) with a wavelength of 514.5 nm (green). This laser type has the possibility for an alternative wavelength of 488.8 nm (blue). The output power used is generally between 0.4 and 0.8 W.

The microscope (Olympus® BH-2) can be used as a normal microscope in white light or it focuses the laser beam on the sample during the measurement. The spot of the laser light is about 1-2μ in size. The energy on the specimen is about 10% of the laser power corresponding to

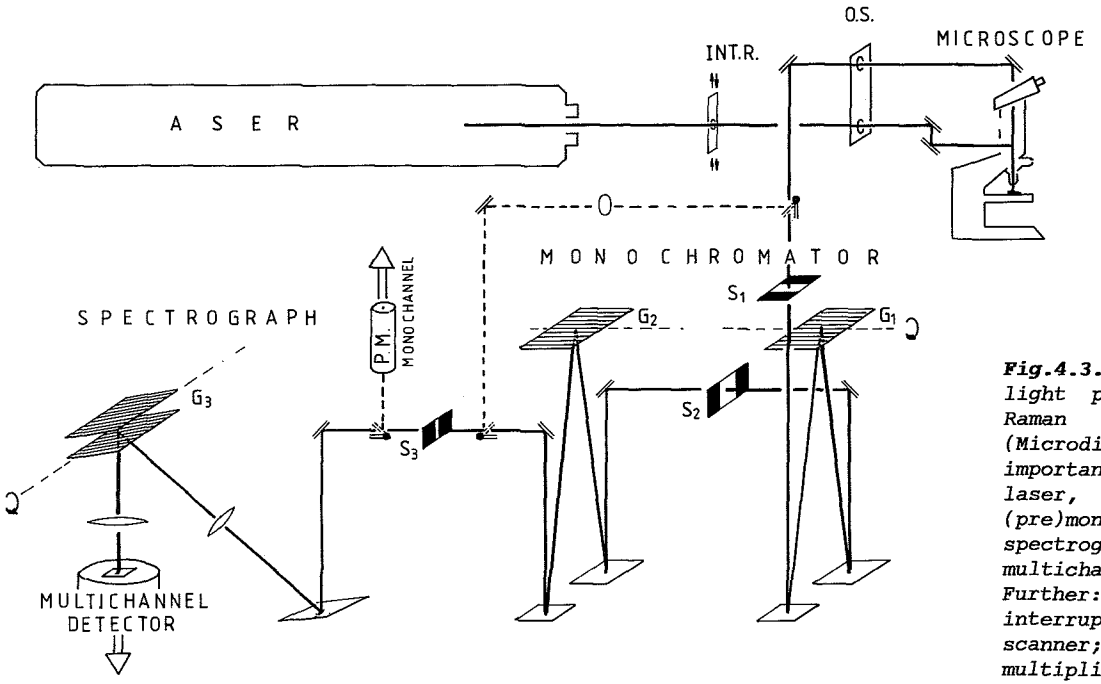

Fig.4.3.- *Scheme of the light path in a laser Raman microspectrometer (Microdil-28®). The most important elements are the laser, microscope, (pre)monochromator, spectrograph and multichannel detector. Further: INT.R = the interrupter; O.S.= optical scanner; P.M.= photo-multiplier; G1-3 = holographic gratings 1 to 3; S1-3 = opening slits 1 to 3.*

an energy in the order of 10^{10} W/m^2 on the sample. The magnification of the objectives used are 50x or 100x. The reflected light is collected at an angle of ~180° through the same objective. The samples used here are normally two-sided polished thin sections, but alternatively capillary quartz tubes containing gas, a cuvette filled with liquid, mineral crystals and powder can be analysed.

A better resolution of Raman spectra is obtained by the incorporation of a (pre)monochromator. The stray light level must be reduced as it interferes with the Raman scattering light: wavelengths which are not to be recorded are rejected. The monochromator consists of two holographic gratings (1800 gr/mm) combined with three slits: the entrance (S_1), intermediate (S_2) and exit (S_3) slit. The width of the exit slit is generally set at 200µ. The spectral resolution is about 7 cm^{-1} for the given slit opening, and 3 cm^{-1} for a slit width of 100µ. A higher resolution is not required for spectra of simple gases as the peaks of interest are generally single. A higher intensity of the Raman signal has a higher priority to obtain accurate quantitative analysis of (small) fluid inclusions.

The spectrograph produces the ultimate spectrum to be recorded. It consists of two combined gratings and two lenses.

The multichannel detector consists of an array of 512 diodes (Reticon®). The part of the Raman spectrum recorded by the detector is 300 to 400 cm^{-1}. The sensitivity of the detector is non-linear and peaks should consequently be recorded at the same position for quantitative analysis. The accuracy of the peak position is $\pm$0.6 to $\pm$0.8 cm^{-1} i.e. the segment of the spectrum between two diodes (see also section 4.5).

It was mentioned above that measurement durations are relatively short: recording one spectrum generally takes between 1 and 5 seconds. An average spectrum is obtained with a much better peak-to-noise ratio by the accumulation of spectra. The number of accumulations is generally taken between 10 and 100. In this way, the detection limit is drastically lowered as it is improved with the square root of the number of accumulations.

Recorded Raman spectra and instrumental setting

Raman analysis with the Microdil-28® results in spectra such as represented in Fig.4.5a, drawn by a HIPLOT DMP-40® plotter. The abscissal scale is the Raman frequency ($\Delta\bar{\nu}$ in cm^{-1}); the ordinate scale plots the

intensity expressed by the number of counts (maximum -1700). The spectra sheets contain a listing of the following operational parameters:

OPERATOR — a short indication;
EXCIT. LINE (nm) — the wavelength of the exciting laser radiation;
SPECT. SLIT WIDTH (cm-1) — the resolution depending on the premonochromator position and the width of slit 3 (automatically inserted);
DATE
LASER POW. (mW) — nominal power of radiation at the laser source;
DETECTOR (Nbr of diodes) — the presently used detector has 512 diodes;
SAMPLE — the indication used here is repeated vertically at the right side of the sheet;
FOREMONO. (cm-1) — the position in absolute wave-numbers of the centre of the premonochromator; usually the same number as for the spectrograph;
FILTER — if any, the number of it;
NUMBER — particular number of the series of spectra measured for one operator. The recorded spectra are saved under the file name composed of the name of the operator followed by the spectrum number.
SPECTRO. (cm-1) — the centre of the spectrograph in absolute wave number; the number is the result of the subtraction of the centre of the abscissa scale (a relative number) from the absolute wavenumber of the exciting radiation (19436 cm^{-1});
INTEGRATION TIME (s) — the time (in seconds) of illumination of the specimen to obtain 1 spectrum;
MODE — monochannel / multichannel (usually MULTICHANNEL);
SLIT WIDTH (μm) — the opening of slit 3, the exit slit of the premonochromator, and also the entry slit of the spectrograph;
NUMBER OF ACCUMULATIONS — the number of spectra (maximum 255) used to obtain the averaged spectrum
REMARK

4.4. The determination of solids

4.4.1. Possibilities and limitations

In general, the significance of Raman spectroscopy is threefold as it enables 1) the identification of polynuclear compounds 2) a better insight in molecular structures by the interpretation of spectroscopic properties and 3) the determination of spatial configurations of a crystal lattice or in the special case of preferentially orientated gas species in minerals (e.g. CO_2 in cordierite, Schreurs 1985). Raman spectroscopy is being applied by physicists, chemists and biochemists etc. mostly for the characterization of molecular properties. The

application by geologists and mineralogists is only in its infancy probably because of the availability of many other analytical methods. Concerning the most important restrictions and disadvantages of the method, it can be mentioned that

1) no sufficient and systematic Raman data on minerals are available (the Raman spectra of the most important rock forming minerals are known, but these data only refer to pure end-members). Moreover, many published spectra give insufficient precision about the composition of the analysed mineral or its physical state (powder, single crystal etc.). The line intensity depends on so many factors (esp. orientation) that it cannot be quantified and the given indications (very strong, strong, weak etc.) are often too vague to be of any real use. Recent attempts were made to create a standard compilation of Raman spectra for rock forming minerals (Smith & Dubessy 1987), but a considerable work of standardization and systematization remains to be done. We normally use the following procedure:

- qualitative appreciation of the most important peaks which, together with other features (shape, refractive index, polarization etc.), indicate possible mineral names;
- recording the Raman spectra of possible minerals under (approximately) the same analytical conditions (laser power, integration time etc.). In most cases, this results in the final determination of the unknown species;

2) the Raman spectra of solids are not easy to interpret: both the symmetry of the molecules and the symmetry of the crystal lattice have to be considered;

3) Raman peak intensities are strongly dependent on the crystallographic orientation due to different polarizations of the light in different directions;

4) no direct quantitative information on the composition of the mineral can be obtained;

5) some minerals are strongly fluorescent;

6) some minerals are not or weakly Raman active (e.g. fluorite).

4.4.2. The identification of daughter minerals

The use of the Raman microspectrometer is very helpful for the identification of minerals if other analytical methods (e.g. electron-

microprobe) fail. This is generally the case for daughter minerals in fluid inclusions or for solids (salts) consisting of elements of lower atomic mass (as H, B, C, O). Best results are obtained for compounds which contain specific molecular groups such as carbonates, sulphates, borates, hydrates etc. Each of these groups shows characteristic Raman bands for the totally symmetrical vibrations e.g. ~1100 cm^{-1} for carbonates and ~990 cm^{-1} for sulphates (Farmer 1974). On the contrary, solids showing only points of symmetry in their crystal structure (cubic packing), as NaCl and CaF_2, do not produce any significant Raman spectrum. Some applications of Raman analysis to the study of daughter minerals (e.g. anhydrite) in fluid inclusions are described by Rosasco & Roedder (1975; 1979). Helpful information on the identification of minerals can be found in Farmer (1974), Griffith (1975) and White (1975).

4.4.3. The Raman spectrum of graphite

Special attention was paid to the Raman spectrum of graphite as this solid has been frequently found in CO_2-CH_4-N_2 inclusions ($\pm$ H_2O) e.g. for compositions with $CO_2/CH_4 < 0.25$ in samples from SW Norway. Graphite is supposed to be mostly a product of the following reaction:

$$CO_2 + CH_4 \quad 2\,H_2O + 2C \qquad \text{(R.4.1.)}$$

The 2 gas species CO_2 and CH_4 should be incompatible in many high density inclusions at room temperature (Kreulen 1987), but the forming of graphite may be hampered by its high nucleation energy. Many fluids containing CO_2 and CH_4 can therefore be considered as chemically metastable. It is important to check the presence of graphite in CO_2-CH_4 inclusions as this may indicate whether the fluid is indicative for the trapping conditions (see section 5.1.1). In some inclusions, reaction 4.1 could proceed spontaneously by induction of the laser beam: a single phase gaseous inclusion (-CH_4(60)-CO_2(30)-N_2(10); $\bar{V}$ 55 cm^3/mole) changed composition shortly after starting Raman analysis. Afterwards, about 12 vol% of water and 4 vol% graphite were formed. Quantitative analysis of CO_2-CH_4 inclusions generally fails in the case of graphite nucleation.

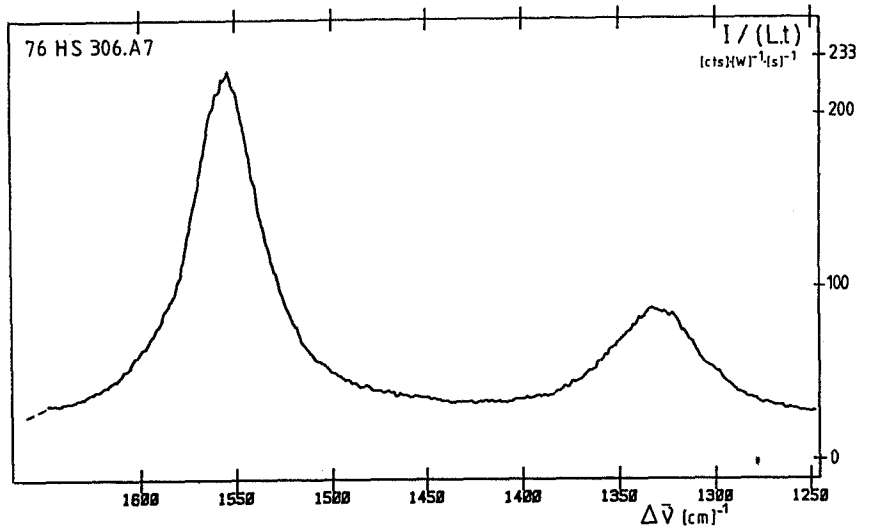

Fig.4.4.- *The Raman spectrum of graphite recorded in a fluid inclusion from SW Norway. Graphite formed in situ from a fluid of intermediate CO_2-CH_4 composition by the induction of the laser. The relative heights of the 2 peaks is a measure for (dis)order of the crystal lattice (see text).*

Graphite is easily detectable by Raman analysis: even amounts which cannot be observed by optical means, appeared to be sufficient to produce a proper Raman spectrum! The spectrum strongly depends on its crystallinity: highly crystalline graphite shows only one Raman band ($\Delta\bar{\nu}$ ~1575 cm^{-1}) due to symmetrical vibrations parallel to the plane of the ring sheets. This band is found to be independent from the crystallographic orientation. An additional peak around 1355 cm^{-1} is produced for graphite of lower crystallinity (Fig.4.4.). The intensity of the 1355-peak gradually increases for higher amounts of distorted carbon and decreasing crystal sizes. It was found by Tuinstra & Koenig (1970) that the relative intensity of the 2 peaks is proportional to the amount of crystallite boundaries within the carbon structure. Another explanation for the spectrum changes are given by Tsu et al. (1978). They found indications that the distortion of the hexagonal ring structures is the dominating factor. Additional peaks (one around 1627 cm^{-1}) have been found by the latter authors and these are explained by the "splitting" of the 1575-peak with decreasing order. Not only intensities, but also peak positions were found to vary with varying crystallinity. A correlation between the two peak intensities with forming temperatures has been

suggested (Michel-Levy & Lautie 1981; Dubessy 1985 p.94) as the degree of crystallinity is temperature dependent. However, this method is unreliable as far as it has not been sufficiently unravelled.

4.5. Raman spectra of gases and liquids

Natural fluid inclusions contain "simple" gases and liquids of the system C-O-H-N-S. The most important species are H_2O, CO_2, N_2, CH_4, possible higher hydrocarbons and hydrogenated sulphur (H_2S and HS^-). The Raman spectrum of H_2O is weak and is not further considered here. The most important Raman spectra relevant to the present study are described in the sections below.

4.5.1. The Raman spectrum of CO_2

It was mentioned above that for the linear molecule O=C=O only one vibration is expected to produce a Raman shift. However, two exciting lines are obtained in the Raman spectrum: a stronger peak around 1388 cm^{-1} and a smaller peak around 1285 cm^{-1} (Fig.4.5a). The appearance of a second peak can be explained as an effect of Fermi resonance, in particular the interaction of $2\nu_2$ (the first overtone of ν_2) and the fundamental line (ν_1). The ν_2-band with a wavenumber of 667 cm^{-1} represents (doubly degenerated) perpendicular vibrations and it is only allowed in the infrared spectrum. Note that two bands are absorbed in infrared with the second being ν_3 at 2349 cm^{-1} (the antisymmetrical vibration). The first overtone of ν_2 can be found at 2 x 667 = 1334 cm^{-1} which is intermediate between the two peaks found in the Raman spectrum ($\pm$ ~ 50 cm^{-1}). A frequency of 1334 is expected for both non-perturbated ν_1 and $2\nu_2$ (Alpert 1970 p.138-140). In the case of Fermi resonance, the fundamental and overtone (or combination) bands are not found at their expected positions: the interaction between the frequencies ν_1 and $2\nu_2$ results to a shift to higher and lower energy levels (the so-called Fermi diad / doublet). ν_1 Is located at a higher frequency, $2\nu_2$ at a lower frequency. However, the assignment of the 2 peaks to ν_1 and $2\nu_2$ is debated: an assignment reversed of the traditional one was proposed by Amat & Pimbert (1965) and Howard-Lock & Stoicheff (1971).

Two peaks of low intensity can be distinguished on both sides of the two main Raman bands, namely around 1265 and 1406 cm^{-1}. In the present study these lines were recorded for fluid inclusions at 1261 and 1407 cm^{-1} (Fig.4.5b). Their frequencies are generally assigned to "hot-bands" due to the thermal energy of the molecules. They should represent interactions between $\nu_1+\nu_2$ and $\nu_1+3\nu_2$ (Howard-Lock & Stoicheff 1971). Their frequencies are expected to be located at the lower sides of the main peaks. Contrary to expectations, the hot band near the highest peak appeared to have a higher frequency. This can be explained as an effect related to Fermi resonance.

A peak of extreme low intensity is generally noticed at the lower frequency side of the 1388-peak (Fig.4.5b). The wavenumber of this line is presently found to be 1367 cm^{-1}, about 18 cm^{-1} below the position of the main peak. It is explained by isotopic splitting due to the presence of $^{13}CO_2$. It is known that the $^{13}CO_2$-content in natural carbon dioxide is 1.11%. Quantitative isotope analysis fails because of the general low intensity of the $^{13}CO_2$-peak. The possibility of detecting Raman spectra in a high dispersion mode is promising in this respect.

The peak positions in Raman spectra of gases are generally available for pressures of 1 atm. However, pressures in fluid inclusions are generally much higher (up to about 1 kbar) and it follows from microthermometric observations that "fluids" in fluid inclusions most often have the character of a liquid. A shift in peak positions might be expected when going to higher pressures and especially when passing the transition gas to liquid. Electron distributions and even symmetries may be distorted because of the influence of the neighbouring molecules, resulting to a (generally small) change in polarizability. Not only the peak positions are expected to change, but also the peak intensities (Schrötter & Klöckner 1979). It was stated in the latter paper that the Raman cross-section generally increases from the gaseous to the liquid state. An additional effect is the change of refractive index by which the focus of the laser beam is somewhat influenced (see section 4.6.3.).

The positions of Raman peaks in the spectrum of CO_2 have been determined in the present study by selecting a number of fluid inclusions of known density and composition from several areas. The results are presented in Table 4.1. Inclusions were chosen which contain more than 95 mole% CO_2 and show a wide range of homogenization temperatures. All detections of Raman spectra were carried out at room temperature (~20°C): CO_2-inclusions are in the liquid state, gaseous

state or two-phase as the critical temperature of CO_2 (31.1°C) is higher than room temperature. Two-phase inclusions show homogenization temperatures (to liquid or vapour) higher than 20°C. The internal pressure of the fluid inclusions (at 20°C) can be calculated (Angus et al. 1976). The highest pressure presently found is 860 bar in a sample from the Furua Granulite Complex (Tanzania).

Calibration of peak positions is done by detecting the Raman spectrum of diamond, showing a single peak at 1332 cm^{-1} which is well in the spectral range of the Fermi diad (Fig.4.5c). The Raman lines can be measured with an accuracy of $\pm$ 0.8 cm^{-1} in this range with the present

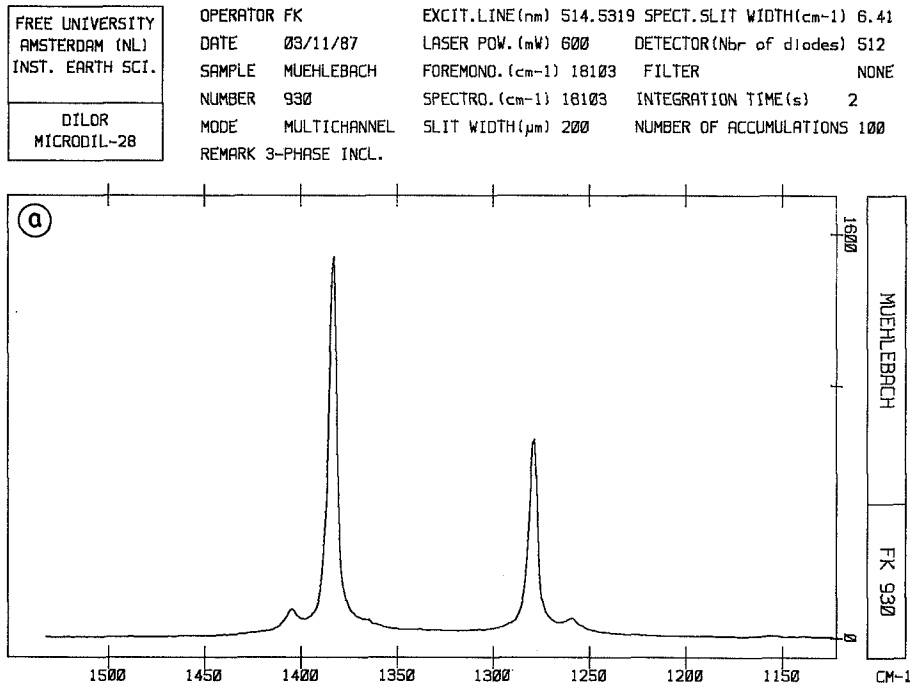

Fig.4.5.- a) *The spectrum of CO_2 measured in the gas phase of a 3-phase inclusion as recorded with the Microdil-28®. The peaks at $\Delta\bar{\nu}$ = about 1280 and 1385 cm^{-1} form the so-called Fermi diad. The parameter list gives the measurement conditions (see text for explanation). The sample was taken from Mühlebach, Wallis, Switzerland.*
b) *Enlargement of the spectrum shown in Fig.4.5a. Note the 2 "hot bands" at 1261 and 1407 cm^{-1} and the small $^{13}CO_2$ peak at 1367 cm^{-1}.*
c) *The Raman spectrum of diamond with a single peak at $\Delta\bar{\nu}$ =1332 cm^{-1}. The total time of recording of the present spectrum is only 10 seconds! (laser power = 50 mW). This line is used for calibration of the peak positions of CO_2.*

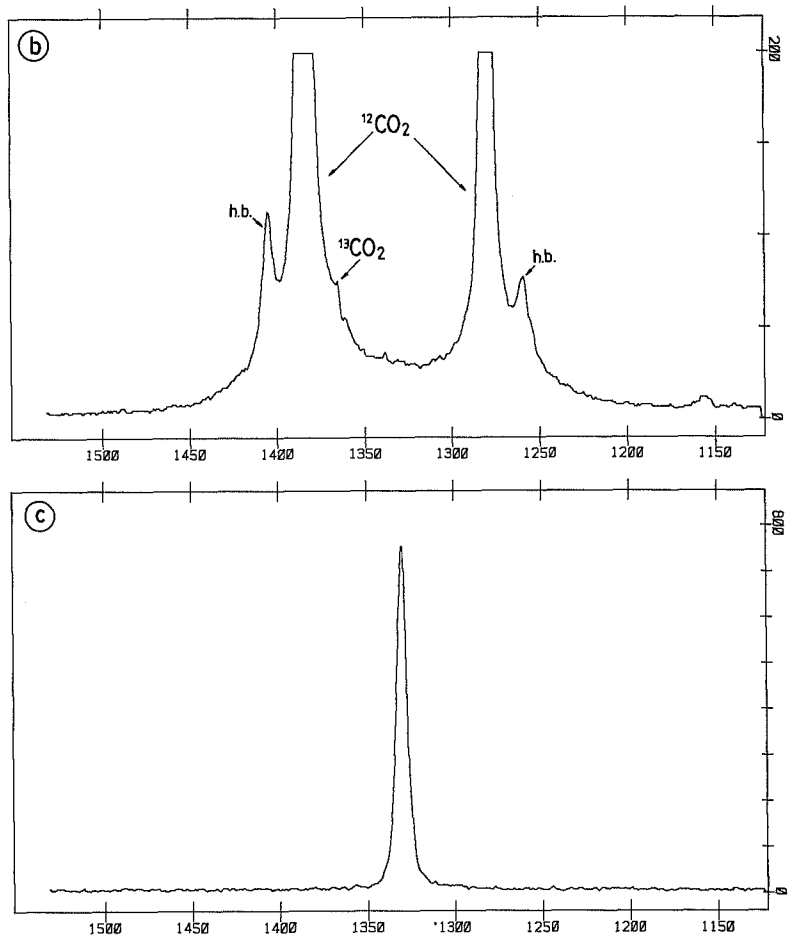

equipment. Graphical representations showing the correlation between the found Raman shifts and T_h are shown in Fig.4.6a-b. A tendency for lower frequencies is noticed for both peaks going to higher densities. This change is drastic at the transition from liquid to gas (i.e. in the two-phase field). The lowering of the frequency is more pronounced for the lower intensity peak (with a shift of 6 cm^{-1}); the larger peak shows a shift of about 4 cm^{-1} for the same spectra.

The absolute change of intensity of Raman peaks with pressure could not be studied because of the lack of standards. In the present study, only the relative intensities of the Fermi diad could be measured. Each peak was recorded separately in the same position because of the non-constant sensitivity of the multichannel detector. Values for the ratio

of peak intensities given in the literature for gaseous CO_2 are 1.52 (Howard-Lock & Stoicheff 1971) and 1.55 (=1.21/0.78) (Schrötter & Klöckner 1979). The ratio found for the present liquid inclusions is around 2.4 which is considerably higher than the given values for the gaseous state (Fig.4.6c).

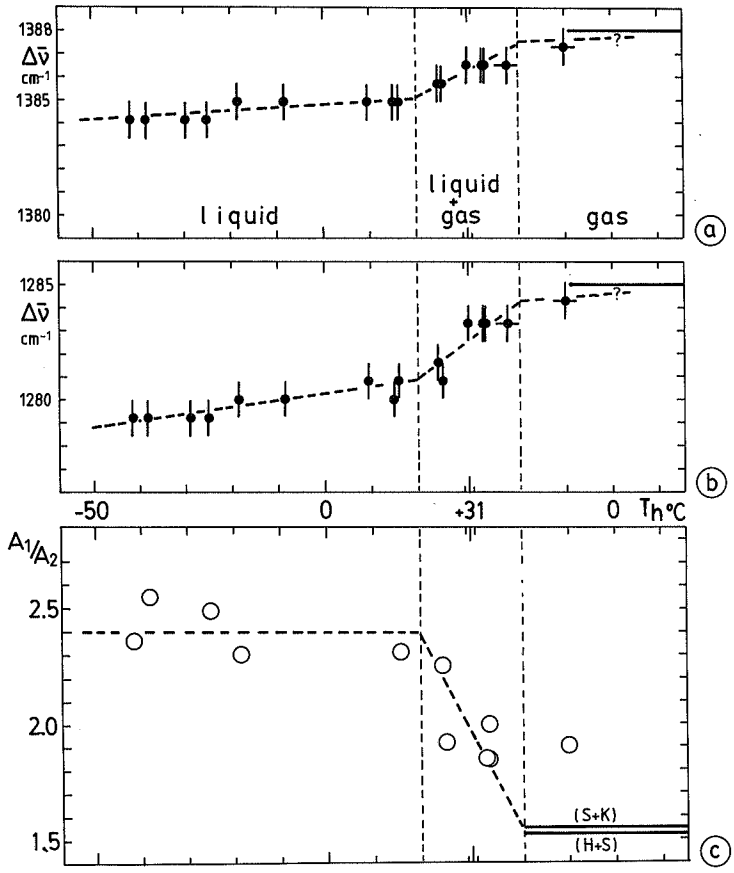

Fig.4.6.- *The peak positions of the Fermi diad in the CO_2 Raman spectrum as a function of homogenization temperature (T_h):*
a) *the main peak ($\Delta\bar{\nu}$ = 1388 cm^{-1} at 1 atm.) and*
b) *the lower intensity peak ($\Delta\bar{\nu}$ = 1285 cm^{-1} at 1 atm.).*
All recordings were made at 20°C; the exciting wavelength of the laser is 514.5 nm and power of the laser output is 600 mW. Note the drastic shift of peak positions at the transition from the liquid to the gaseous state.
c) *The relative Raman peak intensities (A_1/A_2) of CO_2 inclusions plotted against the homogenization temperature. The 1285-peak is relatively smaller (A_1/A_2 ~ 2.4) for inclusions in the liquid state compared to the given value for the gaseous state (A_1/A_2 ~ 1.54) (Schrötter & Klöckner 1979; Howard-Lock & Stoicheff 1971).*

4.5.2. The Raman spectrum of N_2

The high symmetry of the N=N molecule allows only symmetrical vibrations: a permanent dipole-moment is absent because positive and negative charges are always symmetrically distributed on the molecule.

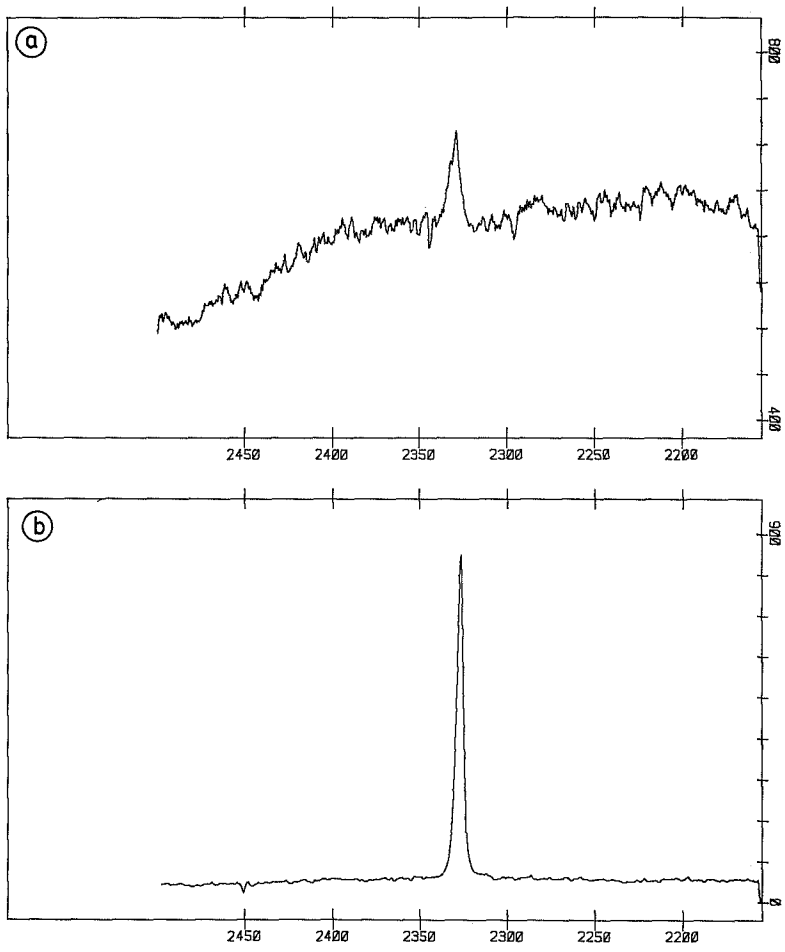

Fig.4.7.- *The Raman spectrum of nitrogen.*
a) *Atmospheric nitrogen ($\Delta\bar{\nu}$ = 2331 cm^{-1});*
b) *The Raman spectrum of N_2 recorded in a high density inclusion from SW Norway ($\bar{V}$ = 52 cm^3/mole). The peak position is significantly lower ($\Delta\bar{\nu}$ = 2328 cm^{-1}) than for atmospheric nitrogen (inclusion 75HS191-A3, Table 4.2).*

Consequently, nitrogen does not produce an infrared band. On the other hand the polarizability is variable and N_2 should therefore be Raman active. The vibrational Raman spectrum consists of a single line at 2331 cm^{-1} for gaseous nitrogen at 1 atm. (Schrötter & Klöckner 1979). The Raman spectrum of atmospheric nitrogen is shown in Fig.4.7a, recorded with the present equipment by focussing the laser beam a few microns above a highly reflecting surface; an example of a Raman spectrum for a high density fluid inclusion is shown in Fig.4.7b. A shift of the peak position to lower frequencies was noticed for inclusions of higher density (and higher pressure). A selection was made of inclusions containing more than 95 mole% N_2 (Table 4.2a). The maximum shift compared to atmospheric N_2 is about 3 cm^{-1} for fluid inclusions with calculated pressures of 840 bar at 20°C. The peak position for N_2 dissolved as a minor constituent (<5 mole%) in liquid CO_2-inclusions is about the same as for high density N_2-inclusions (Table 4.2b).

4.5.3. The Raman spectrum of CH_4

Molecules of type BA_4 (as CH_4 and CCl_4) show the configuration of a tetrahedron. These molecules have 9 degrees of vibrational freedom, but only 4 modes are fundamental (Fig.4.8). The first mode (ν_1 = 2917 cm^{-1}) is totally symmetric and represents the expansion and contraction ("breathing") of the tetrahedron. ν_2 (1534 cm^{-1}) is the doubly degenerated "skating" mode. Vibrations ν_3 and ν_4 (at 3019 and 1309 cm^{-1} respectively) are both triply degenerated. ν_3 denotes motions of the central atom relative to the outer atoms.

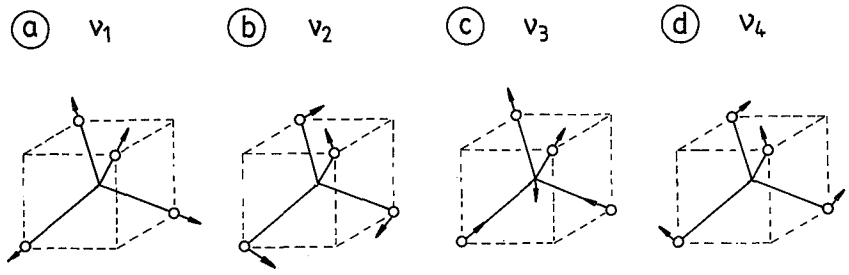

Fig.4.8.- *The fundamental normal modes of a tetrahedral XY_4 molecule like CH_4: a) the totally symmetric "breathing" mode ν_1 b) the ν_2 mode (doubly degenerated) c) the ν_3 mode (triply degenerated) and d) the ν_3 mode (triply degenerated). The "breathing" mode is by far strongest Raman active; the remaining "skating" modes should also be Raman active, but this could not be stated with the present equipment.*

Only modes ν_3 and ν_4 are infrared active, but all the 4 fundamental frequencies should be Raman active (c.f. the spectrum of CCl_4, Fig.4.2). However, ν_1 appeared to be by far the most dominant frequency in the Raman spectrum of CH_4 and the other frequencies are generally not found at all. Only ν_3 has been sometimes observed and seems to be more pronounced in low density inclusions (Fig.4.9a). The intensity of this peak was calculated by Schrötter & Klöckner (1979) to be about half the intensity of the main peak. A sufficient explanation for the present low intensities has not yet been found.

A drastic shift of the (main) peak position of CH_4 to lower frequencies with increasing pressure is known for some time (May et al. 1959; Dhamelincourt et al. 1979; Fabre & Couty 1986; v.d.Kerkhof 1987). For the present quantification of this shift, a selection of natural inclusions was made containing more than 95 mole% CH_4. Fluid pressures at 20°C could be calculated (Angus et al. 1976). The lowering of the Raman peak position is most drastic in the lower pressure range. It was found that the lowering of the Raman peak position is about 7 cm^{-1} for inclusions with internal pressures of almost 1 kbar (Th_L = -125°C) compared to methane of 1 bar (Table 4.3; Fig.4.10); CH_4-inclusions characterized by critical homogenization (internal pressures around 170 bar at 20°C) show a lowering of the peak position of about 5 cm^{-1}. A reliable calibration of the peak position could not be achieved in this part of the spectrum because of the lack of a standard (a systematic correction should probably be made). The present values for $\Delta\tilde{\nu}$ are about 3 cm^{-1} higher compared to the data published by Fabre & Couty (1986); peak shifts are consistent with these data (Fig.4.10). Dhamelincourt et al. (1979) found a more drastic lowering of 4 cm^{-1} (from 2916.1 to 2912.1 cm^{-1}) for a pressure increase from 1 to 70 bar. Peak positions of CH_4 dissolved in CO_2 in the liquid state are comparable with those of intermediate density methane (Table 4.3b); in 2-phase CO_2-rich inclusions, CH_4 is preferably partitioning in the gaseous state which is expressed by the higher Raman frequencies.

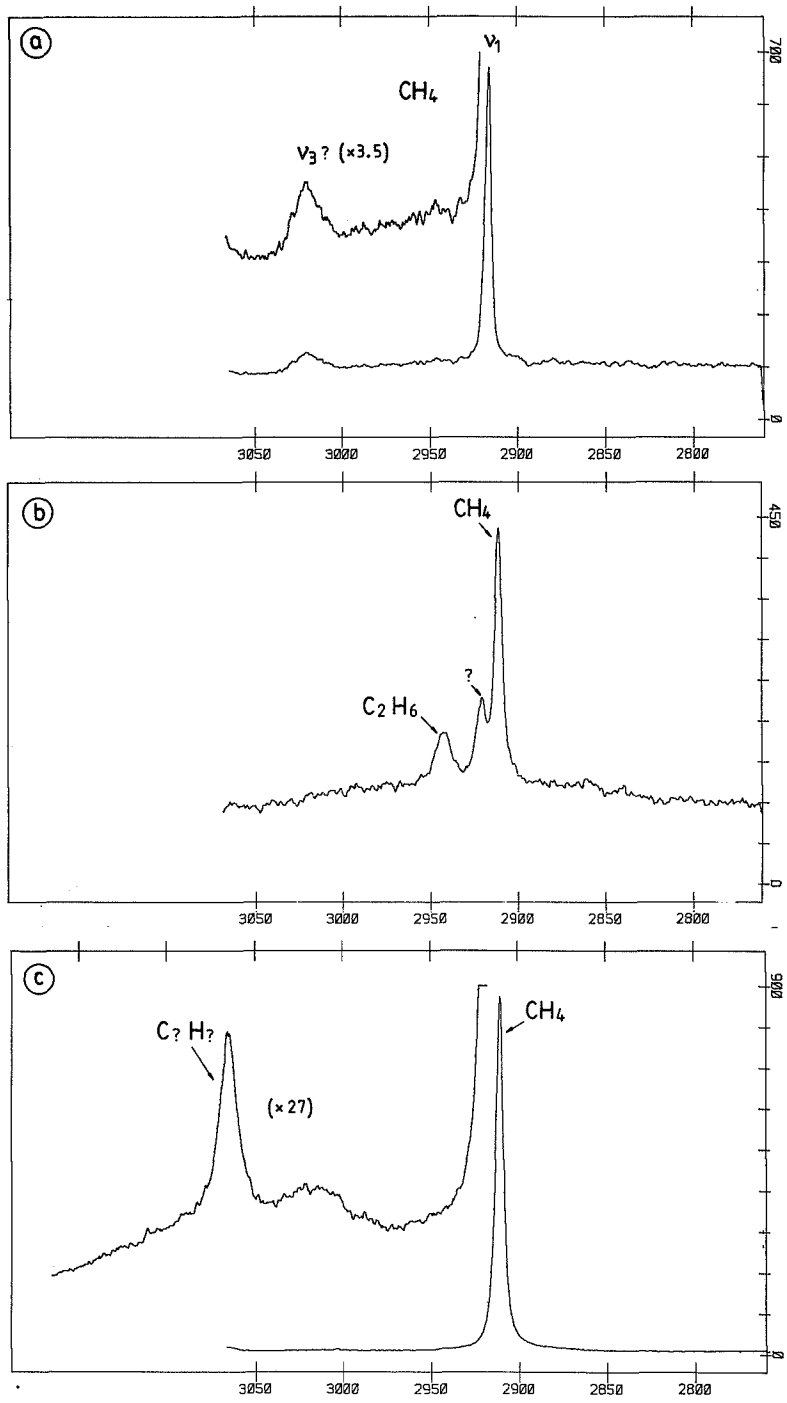
a
ν_1
CH_4
ν_3 ? (×3.5)
700
0
3050
3000
2950
2900
2850
2800
b
CH_4
?
C_2H_6
450
0
3050
3000
2950
2900
2850
2800
c
$C_?H_?$
(×27)
CH_4
900
0
3050
3000
2950
2900
2850
2800

Fig.4.9.- *The Raman spectra of methane and some other hydrocarbons in natural fluid inclusions.*
a) *The main peak of methane at 2918 cm^{-1} (ν_1); a peak of much lower intensity around 1330 cm^{-1} is attributed to the ν_3 mode of methane (low density inclusion 80.28I-B15, Table 4.3).*
b) *The Raman spectrum of methane and probably ethane ($\Delta\tilde{\nu}$ ~ 2940 cm^{-1}) (CO_2-N_2 rich inclusion from Pusula, SW Finland). The small peak at the shoulder of the CH_4-peak could not be explained.*
c) *The Raman spectrum of methane and unidentified hydrocarbon(s) showing a peak at 3067 cm^{-1}. The low intensity ν_3-peak of methane can also be distinguished (inclusion 79.7b-A1, Table 4.3).*

The relatively small values of Raman shift of CH_4, CO_2 and N_2 with varying density and also the low accuracy of the peak positions do not allow the determination of the density from Raman analysis only and microthermometry cannot be replaced in this respect. However, peak positions may be used as an internal check for densities determined from homogenization temperatures (e.g. in the case of low T_h due to the presence of gases which are not Raman active like He and Ar).

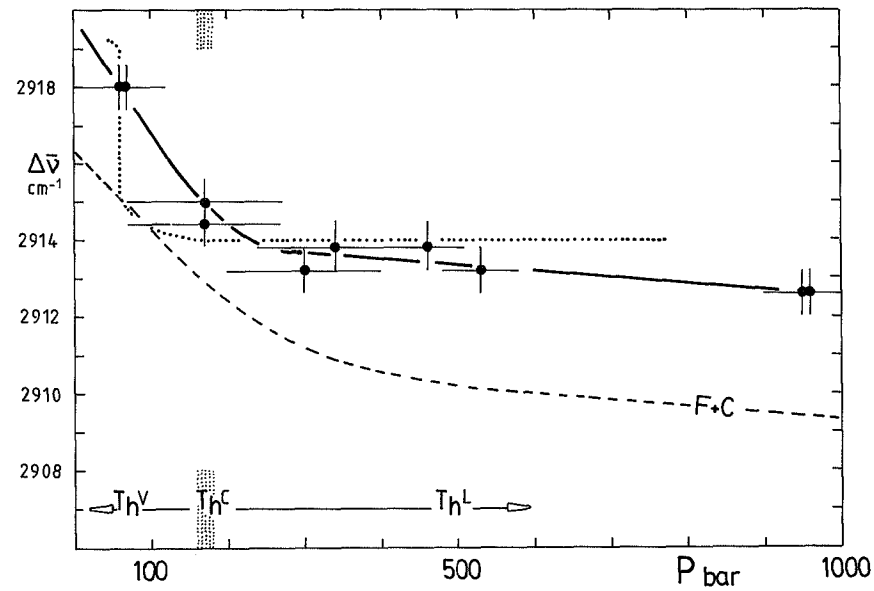

Fig.4.10.- *The position of the Raman peak of CH_4 in natural fluid inclusions as a function of pressure calculated (at room temperature) from homogenization temperatures (Angus et al. 1976). The solid curve denotes (>95 mole%) pure CH_4 inclusions; the dashed curve = the Raman shift as calculated by Fabre & Couty (1986); the dotted curve = CH_4 (< 5 mole%) in liquid CO_2. The lowering of the Raman peak for the highest density inclusions is about 7 cm^{-1}.*

Table 4.1-3.- *The position of the Raman lines for CO_2 (Table 4.1), N_2 (4.2) and CH_4 (4.3) as measured in natural fluid inclusions at room temperature. The selected fluid inclusions contain >95 mole% of the given compound. Tables 4.2b and 4.3b comprise CO_2-rich inclusions containing <5 mole% of dissolved N_2 and CH_4 respectively, and >95 mole% CO_2. N_2 and CH_4-rich fluids are supercritical at room temperature; CO_2 has the character of a liquid or vapour (s.s.).*

The exciting wavelength of the used laser is 514.5 nm. The laser output was taken 0.6 W for all measurements.
The origin of the samples is given by [1] Harmsarvet, Sweden [2] Mühlebach, Switzerland [3] SW-Norway [4] SW-Finland (coll.: T. Hartel) [5] Camperio, Switzerland [6] Furua Granulite Complex, Tanzania [7] Bergslagen (coll.: Drs. A. Damman) [8] Pusula quarry, SW-Finland [9] Appalachian Mountains (coll.: Dr. H. Kisch).

Further: T_h = homogenization temperature (°C) to the (L)iquid, V(apour) or C(ritical (= partial homogenization (T_{hs}) of CH_4-rich inclusion); $\bar{V}$ = molar volume (cm^3/mole); P = pressure at 20°C (bar) (after Angus et al. 1976a, 1976b, 1979); $\Delta\bar{\nu}$ = Raman wavenumber (cm^{-1}).*

For CO_2 (Table 4.1), the positions of both peaks of the Fermi diad are measured. The ratio of the peak integrals (R) was calculated as well. Each peak was seperately recorded (in the middle of the recorded spectrum) because of the non-equal sensitivity of the detector.

The position of the Raman lines of CO_2 are adjusted relative to the position of the diamond line at 1332 cm^{-1}; the position of both N_2 and CH_4 lines are adjusted relative to the peak position of atmospheric N_2 at 2331 cm^{-1}. Accuracies range from about 0.8 cm^{-1} for the CO_2 spectrum to about 0.6 cm^{-1} for CH_4.

Table 4.1. (CO_2)

Loc	Nr.		T_h	$\bar{V}$	P	$\Delta\bar{\nu}$	$\Delta\bar{\nu}$	R
[7]	DA.G.11	V	~+10.	325	49	1284.3	1387.3	1.90
		V	+20.	225	57			
[5]		V	+20/25	200	61	1283.3	1386.5	
[4]	TH643-4	V	+27.4	158	67	1283.3	1386.5	2.00
[4]	TH643-4	V	+27.6	155	67			1.85
[4]	TH643-4	V	+27.7	155	67	1283.3	1386.5	1.85
		C	+31.06	94.4	73.8			
[5]		L/C	+31.	90	73	1283.3	1386.5	
[2]		L	+25.5	63	65	1280.8	1385.7	1.92
[1]	A1-5	L	+24.7	61	64	1281.6	1385.7	2.25
		L	+20.	57	57			
[1]	A1-1	L	+16.1	54	71	1280.8	1384.9	2.31
[3]	HS250-A1	L	+15.0	53	78	1280.0	1384.9	
[3]	HS256-A5	L	+9.5	51	110	1280.8	1384.9	
[3]	HS250-A12	L	-8.5	45	280	1280.0	1384.9	
[1]	B1-4	L	-18.5	43	410	1280.0	1384.9	2.30
[1]	B1-9	L	-24.9	42	530	1279.2	1384.1	2.49
[3]	HS256-A10	L	-29.8	41	600	1279.2	1384.1	
[6]	ME268.1-A5	L	-38.2	40	790	1279.2	1384.1	2.55
[6]	ME268.1-A12	L	-41.6	39	860	1279.2	1384.1	2.36

Table 4.2a (N_2)

Loc	Nr.		T_h	$\bar{V}$	P	$\Delta\bar{\nu}$
[8]	Pu2A-1	V	-148.1	~100	200-300	2329.6
[1]	T1-2	V	-145.9	~100	200-300	2329.6
[1]	L1-9	V	-142.9	~100	200-300	2329.6
[1]	L1-8	V	-142.0	~100	200-300	2329.0
[8]	Pu2A-2	V/C	-147.4	89	315	2329.6
[8]	L1-3	C/V	-148.4	89	315	2329.0
[3]	75HS191-A2	L	-144.4	~80	370	2329.0
[3]	75HS191-A3	L	-154.3	52	840	2328.3

Table 4.2b (N_2 in CO_2)

[1]	81.58c.A2-1	L	+11.4	51	110	2327.7
[3]	75HS191-B10	L	-11.3	45	280	2327.6
[1]	81.58c.B1-9	L	-24.9	42	530	2328.3

Table 4.3a (CH_4)

[9]	80.28I-C10	V	-96.3	300	60	2918.0
[9]	80.28I-B15	V	-94.7	280	70	2918.0
[9]	80.28I-C9	C	-82.0	99	170	2915.0
[9]	79.7b-A2	L/C	-77.5	~99	~170	2914.4
[9]	79.7b-A1	L	-86.6	67	300	2913.2
[1]	81.57.P1-12	C/L	-89.4	62	340	2913.8
[1]	81.57.P1-5	L	-97.9	55	460	2913.8
[1]	81.57.P1-11	L	-100.3	53	530	2913.2
[9]	79.7b-A3	L*	-123.5	45	950	2912.6
[9]	79.7b-A4	L*	-124.2	45	960	2912.6

Table 4.3b (CH_4 in CO_2)

[2]		L	+25.5	63	65	2917.4
[1]	81.57.P2-5	L	+20.5	57	57	2915.0
[1]	81.58c.H1-7	L	+17.7	55	65	2915.6
[1]	81.58c.A2-1	L	+11.4	52	95	2914.4
[1]	81.58c.H1-23	L	+4.2	48	170	2913.8
[1]	81.58c.B1-4	L	-18.5	43	410	2913.8
[1]	81.58c.B1-9	L	-24.9	42	530	2914.4

4.5.4. Raman spectra of higher hydrocarbons

Raman bands are sometimes found in the vicinity of the CH_4-peak and they are attributed to several other species of hydrocarbons. Methane is mostly the only hydrocarbon present in natural fluid inclusions and higher hydrocarbons may only occur in accessory amounts. Recorded Raman peaks could be identified as members of the alkane-series. For example, ethane was detected in fluid inclusions from the Pusula-quarry (SW-Finland) (Fig.4.9.b). The presence of propane has only been suspected in some inclusions. The position of the main peak of ethane is 2954 cm^{-1}; the main peak of propane is 2890 cm^{-1}. In many cases it is not easy to identify Raman bands of unknown hydrocarbons. An example of a spectrum is shown in Fig.4.9c with an unidentified peak at 3067 cm^{-1}. Similar peaks in this range of the Raman spectrum have been found by Guilhaumou (1982 p.28-29). They are attributed to complex aliphatic or aromatic hydrocarbons.

A small peak was sometimes found at a position of about 10 cm^{-1} higher than the CH_4-peak (Fig.4.9b), sometimes only visible as a shoulder of the main peak. This peak could not be identified so far.

4.5.5. Raman spectra of hydrogenated sulphur

The Raman spectra of hydrogenated sulphur obtained from natural fluid inclusions were described by Rosasco & Roedder (1979), Bény et al. (1982), Dubessy et al. (1984) and v.d.Kerkhof (1987). In the present study, these compounds are found in minor amounts in fluid inclusions from several metamorphic areas. Hydrogenated sulphur occurs as molecular H_2S or ionic HS^-. Gaseous and liquid H_2S produces only one vibrational Raman frequency as was explained for linear AB_2 molecules. The position of the Raman peak of H_2S is 2911 cm^{-1} at 1 atm. (Schrötter & Klöckner 1979), but significantly lower in fluid inclusions; peak positions around 2585 cm^{-1} are attributed to the ionic species HS^- (Rosasco & Roedder 1979). In the present study two spectral ranges are distinguished: 1) between 2607 and 2610 cm^{-1} for H_2S and 2) between 2580 and 2584 cm^{-1} for HS^-. Examples of both types are shown in Fig.4.11a-c.

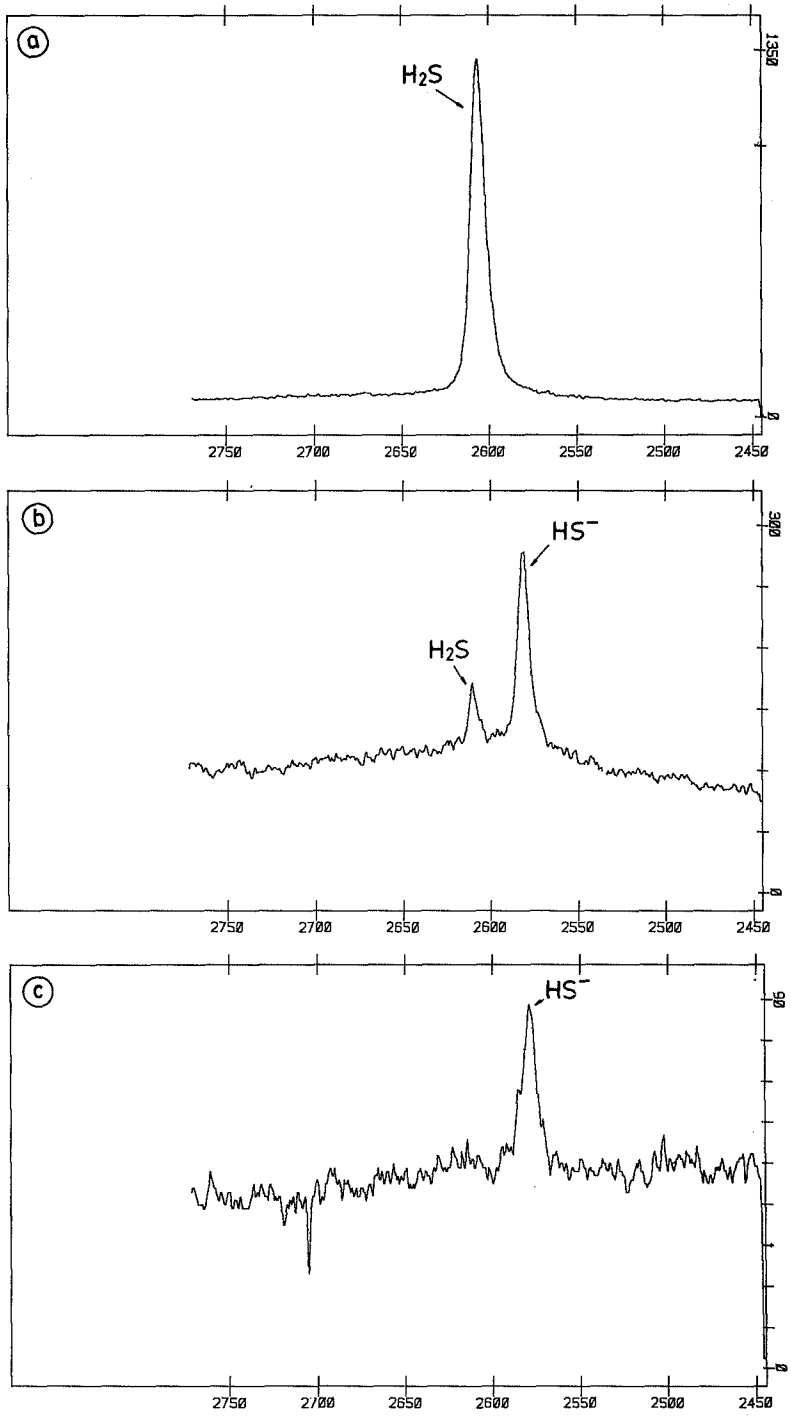
a
H2S
1350
0
2750
2700
2650
2600
2550
2500
2450
b
HS⁻
H2S
300
0
2750
2700
2650
2600
2550
2500
2450
c
HS⁻
90
0
2750
2700
2650
2600
2550
2500
2450

(Fig.4.11)

Fig.4.11.- *Raman spectra of hydrogenated sulphur.*
a) *H_2S ($\Delta\bar{\nu}$ = 2608 cm^{-1}) in a fluid inclusion from Pusula, SW Finland. The total gas composition of the inclusion is N_2(67.3) H_2S(23.6) CO_2(6.5) CH_4(2.4) C_2H_6(0.1).*
b) *H_2S + HS^- ($\Delta\bar{\nu}$ = 2610 and 2581 cm^{-1}) (<1 mole%) in a fluid inclusion from Dôme de l'Agout. The gas composition is CH_4(79.2) CO_2(16.2) N_2(4.6).*
c) *HS^- ($\Delta\bar{\nu}$ = 2578 cm^{-1}) (< 1 mole%) in an inclusion from the Appalachians, U.S.A. The gas composition is CH_4(92.0) CO_2(6.5) N_2(0.7).*

It is remarkable that H_2S and HS^- are restricted in respect of bulk composition of the inclusion (CO_2-CH_4-N_2): H_2S is found as the only modification of hydrogenated sulphur in CO_2-N_2 and CO_2-rich CO_2-CH_4 inclusions (Pusula, SW-Finland; Dôme de l'Agout, France); HS^- is only found in CH_4-N_2 and CH_4-rich CO_2-CH_4 inclusions (Dôme de l'Agout; Appalachian Mountains, U.S.A.). Both H_2S and HS^- are found in CO_2-CH_4 inclusions of intermediate composition (Dôme de l'Agout) (Fig.4.12). All inclusions may contain small amounts of additional water. The relative amounts of H_2S and HS- are only related to the CO_2 to CH_4 ratio; N_2 is a non-reactant gas. The equilibrium

$$H_2S + H_2O \quad HS^- + H_3O^+ \qquad \text{(R.4.2.)}$$

will shift to the left in a more acid environment due to the presence of carbonic acid (H_2CO_3) (with a somewhat higher dissociation constant than H_2S). The ratio H_2S/HS^- can therefore be used as a tracer for the pH of the system.

Fig.4.12.- *The state of hydrogenated sulphur (molecular or ionic) in correlation with the bulk gas composition (CO_2-CH_4-N_2): fluid inclusions from Dôme de l'Agout (France), Pusula (SW Finland) and the Appalachians (U.S.A.). H_2S occurs in CO_2-N_2; HS^- in CH_4-N_2 fluids. Both H_2S and HS^- are only found in fluid inclusions of intermediate CO_2-CH_4 composition.*

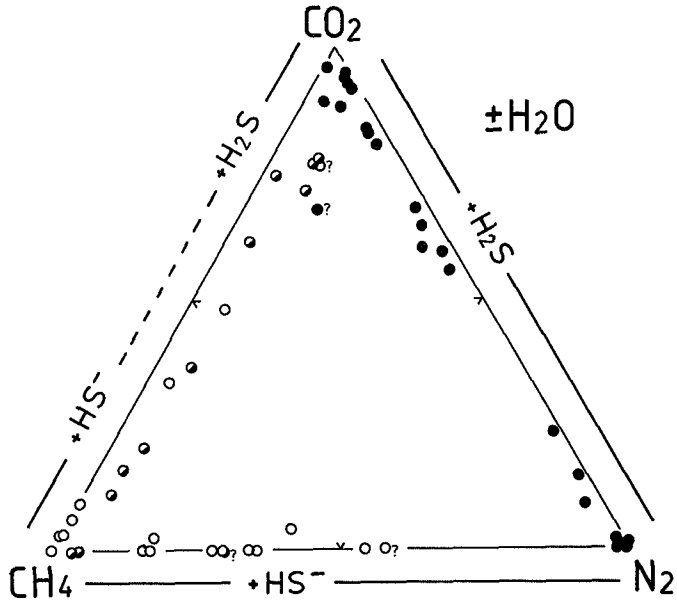

(Fig.4.12)

4.6. Quantitative analysis in gaseous systems

The possibility of quantitative analysis of fluid inclusions by means of Raman microspectroscopy is of fundamental interest for this study. The gas species to be considered are CO_2, CO, CH_4 (and higher hydrocarbons), N_2, O_2, H_2 and H_2S which are all Raman active. Nitrogen oxides and NH_3 have not been detected in natural inclusions. The Raman spectrum of water appeared to be extremely weak.

The first attempts of quantification were published by Rosasco & Roedder (1975, 1979) and concerned the analysis of salt solutions. Concentrations of poly-atomic ions as SO_4^- could be calculated. Later Raman studies on brines were made by Dubessy (1982). A disadvantage of the method is the impossibility to detect most monatomic ions (like K^+, Na^+, Ca^{2+}).

Data of quantitative Raman analysis of gaseous fluid inclusions are available from the end of the 1970's (Dhamelincourt et al. 1979; Bény et al. 1982; Guilhaumou et al. 1984). A review of published data is given by Touray et al. (1985) and Roedder (1984 p.104-108).

4.6.1. Theoretical considerations

The flux of scattered Raman light (in $W.cm^{-3}$) radiated by a molecule is given by the so-called Placzek equation (Placzek 1934):

$$\Phi \qquad I_o \cdot \sigma_i \cdot N_i(V) \cdot \Omega \qquad \text{(Eq.4.4.)}$$

I_o = the intensity if the incident light at the location of the molecule ($W.cm^{-2}$);
σ_i = the Raman scattering cross-section of molecule i for a given Raman line ($cm^2.mole^{-1}.sr^{-1}$);
$N_i(V)$ = the number of molecules in an irradiated volume V ($mole.cm^{-3}$);
Ω = a factor expressing the part of the Raman light collected by the optical system (sr).

The determination of absolute quantities is not possible as I_o can only roughly be estimated. Furthermore, Ω is not known because of the numerous reflection and absorption effects in the sample and in the optical system of the apparatus. Nevertheless it is possible to determine the relative amounts of the compounds present in a liquid or gas. It can be assumed that the intensity of the Raman light (Φ) is proportional to the surface (A) of the recorded peak. These peak integrals are calculated with the help of the program delivered with the Microdil-28®. Further, the intensity I_o is proportional to the used laser power (L). The relative Raman scattering cross-section (σ_r) is commonly used for gaseous compounds rather than the absolute values. σ_r^i Is a dimensionless number being a measure for the specific Raman activity of a compound i relative to nitrogen (for which σ is defined as 1). The values for σ_r are experimentally determined and can be found in the literature (Schrötter & Klöckner 1979) for the frequencies of the emitted Raman line (ν_o-ν) and for the used frequency of the laser (ν_o). A list of relative Raman cross-sections for some compounds of interest is represented in Table 4.4. The term $N_i(V)$ in Eq.4.4 can be taken as a constant if the focus of the laser is not changed for the spectra which have to be compared.

The factor Ω can be ignored as the given values for σ_r include both the absolute Raman cross-section and the correction due to the scattering geometry. Ω can therefore be considered as an instrumental factor which is constant for the analysis of one fluid inclusion, but it

may be different for different measurement conditions (objective, sample etc.).

An additional factor which has to be taken into account is the measurement duration (t) being the recording time of one spectrum. It was confirmed that both the measurement duration and the laser power show linear correlations with the intensity of the Raman light (Burke & Lustenhouwer pers.comm.). L and t are considered as the instrumental setting parameters which have to be selected for each spectrum. The output of the laser power is generally taken between 0.4 and 0.8 W for the analysis of gases and liquids; measurement durations are taken between 1 and 5 seconds. These parameters can be ignored for further calculations if Raman spectra of all compounds are recorded at the same instrumental setting conditions. However, one or both of these parameters are often reset to get proper spectra of both main and minor constituents. In these cases, the adjusted peak integral (A^*_i) for a compound i can be defined as follows:

$$A^*_i : \frac{A_i}{L.t} \qquad \text{(Eq.4.5.)}$$

When the considerations above are taken into account, Eq.4.4. can be re-written for practical use:

$$A_i \quad L \,.\, t \,.\, \sigma_i \,.\, N_i \qquad \text{or} \qquad \text{(Eq.4.6a)}$$

$$N_i \quad \frac{A_i}{L.t.\sigma_i} \quad \frac{A^*_i}{\sigma_i} \qquad \text{(Eq.4.6b)}$$

In the latter equation, the number of molecules is only proportional to the peak integral (detected at the same measurement conditions) divided by the relative Raman cross-section. The total number of molecules can be taken as 100% for the calculation of the composition. If the total number of components is denoted by C, the mole fraction (X) of a component i is given by the general expression

$$X_i \quad \frac{N_i}{\Sigma_{j=1}^{C} N_j} \qquad \text{(Eq.4.7)}$$

For a mixture consisting of only 2 components, the following correlations are found by combining Eqs.4.6 and 4.7:

$$N_1 \quad \frac{A^*_1 \cdot \sigma_2}{A^*_2 \cdot \sigma_1} \cdot N_2 \qquad \text{and} \qquad \text{(Eq.4.8a)}$$

$$N_1 + N_2 = 100\% \qquad \text{(Eq.4.8b).}$$

4.6.2. Measurement accuracies

It is difficult to quantify the accuracy of the calculated fluid compositions because many factors may influence the ultimate result. The limitations of quantitative Raman analysis were discussed by Wopenka & Pasteris (1985). It can be stated that results are limited by the specific conditions of each measurement. The accuracy of both peak intensities (A) and relative Raman cross-sections (σ_r) have to be considered. First, a review is given of the limitations inherent to the technique itself; the accuracy of the Raman cross-section is discussed in section 4.6.3.

The intensity of Raman signals is determined by some practical limitations: peak intensities are strongly dependent on the nature of the sample. In general, two-sided polished thin sections are used, but results for capillary quartz tubes and (covered) cuvettes appeared to be also successful. For the fluid inclusion sections, the following aspects have to be taken into account: a) the size and shape of the inclusion b) the depth of the inclusion below the surface c) the quality of the polished section. d) the density of the fluid e) the species of host mineral which is generally quartz, but other minerals may also contain fluid inclusions and f) the colour and possible fluorescence of the host mineral and the fluid. Fluorescence is mainly of influence on the peak-to-background ratio.

Some instrumental factors have been mentioned earlier, namely the laser power (L) and the measurement duration (t). The quantity of the scattered light which is collected by the instrument is dependent on the used objective. Highest Raman intensities are presently obtained with a 50x objective.

The peak integral is calculated by counting statistics. This matter is extensively discussed by Wopenka & Pasteris (1985). The multichannel detector is provided with 512 diodes and wavenumber steps of a spectrum of 300 to 400 cm^{-1} long is therefore 0.6 to 0.8 cm^{-1} (wavenumber steps are smaller at higher Raman frequencies). The integral is the calculated surface between two given points delimiting the Raman peak; the base is

defined as the tie-line between these points. The choice of the lower and upper limits is more or less subjective. The shape of the peak, the height-to-width ratio and the overlap of two or more peaks are restricting factors. The resulting analytical errors due to the counting statistics are assumed to be small as far as good peak-to-background ratios are obtained.

4.6.3. The relative Raman scattering cross-section

The accuracy of quantitative analysis is directly related to the Raman activity of the measured compound expressed by the relative Raman scattering cross-section (σ_r). Uncertainties in σ_r are probably most important for the ultimate measurement accuracies. The uncertainty of the available literature values (Table 4.4.) was stated to be about 10% for the presently used exciting frequencies (Schrötter & Klöckner 1979).

The detection limit is lower for a compound with higher σ_r. For example, small amounts of methane (σ_r = 8.9) in a CO_2-rich inclusion can be easily detected whereas small amounts of nitrogen (σ_r = 1) in the same inclusion may be overlooked. The detection limits determined for the present equipment are 0.1-0.2 mole% for N_2 and 0.02-0.04 mole% for CH_4 in a "normal" inclusion (Burke & Lustenhouwer 1987). As a general rule, it can be stated that only the difference between the Raman cross-sections of 2 components is important for the accuracy of the measurement: small amounts of CH_4 in CO_2 results to accurate measurements whereas small amounts of CO_2 in CH_4 results to inaccurate measurements. The largest discrepancies in measured compositions (in absolute mole%), due to the accuracy of σ_r, occur for compositions of intermediate (50-50 mole%) composition in binary mixtures (Wopenka & Pasteris 1985).

It was shown earlier for CO_2, N_2 and especially for CH_4 that Raman peak positions shift to lower frequencies with increasing pressure (and increasing density). Schrötter & Klöckner (1979) demonstrated that also Raman intensities are influenced with varying pressure. The relative Raman cross-sections are generally given for gaseous compounds at 1 atm. However, "fluid" inclusions contain much higher pressures (up to 1 kbar) and their content may have the character of a gas, a liquid, a supercritical fluid, or more phases may be present. σ_r was stated to be higher for a compound in the liquid state compared to the gaseous state (Schrötter & Klöckner 1979). This was explained by the internal field

effect and (less) by intermolecular interactions. The major implication is a change in the scattering geometry which is related to the refractive index of the liquid: σ_r^L can be approximately calculated as a function of the refractive index of the liquid. However, the latter quantity is difficult to determine for fluid inclusions and the relative Raman cross-section for the present compounds in the liquid state remain therefore unknown.

Compound	$\Delta\bar{\nu}$	σ_r
CO_2	1285	0.78
CO_2	1388	1.21
O_2	1555	1.0
CO	2143	0.93
N_2	2331	1.
H_2S	2611	6.8
CH_4	2917	8.9
C_2H_6	2954	13 ?
C_3H_8	2890	6.6
H_2	4156	3.45

Table 4.4.- *Relative Raman scattering cross-sections for the most important gas species found in natural fluid inclusions given for an exciting wavelength of 515 nm (mean data after Schrötter & Klöckner 1979).*

Fluid compositions can independently be derived from microthermometric data and a given equation of state. This method is reliable as far as the equation of state is well known for the considered compositional range. In the system CO_2-N_2, compositions can alternatively be obtained from the estimated volume of solid CO_2 at temperatures below -150°C (Guilhaumou et al. 1981). The latter results appeared to be in good agreement with Raman analyses. Also the data presented in this work (especially for CO_2-CH_4 fluids, Fig.4.13) do not show major deviations from the compositions determined from microthermometry. The values for the relative Raman cross-sections as listed in table 4.4 can therefore be taken as acceptable for both gaseous and liquid phases, although one has to bear in mind that the physical state of an inclusion is possibly one of the most important factors which may influence the accuracy of quantitative Raman analysis.

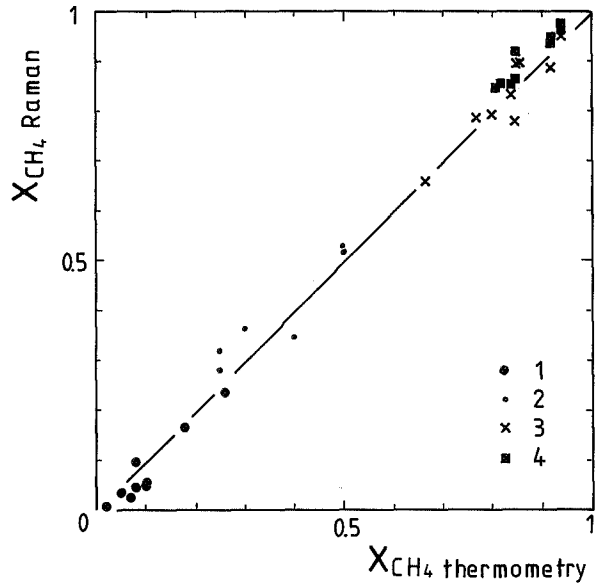

Fig.4.13.- *The correlation of CO_2-CH_4 compositions measured by Raman analysis and determined from microthermometric data: (1) type H3 inclusions, according to the Heyen equation; (2) H3 (or H4/H5) inclusions, according to present PVTX-diagrams (Chap.V); (3) type H2 inclusions, present model; (4) type S2 inclusions, Herskowitz & Kisch (1984).*

V THEORETICAL MODELS

5.1. Principles

5.1.1. The fluid inclusion system

A system of variable state is determined by the 4 quantities pressure (P), temperature (T), volume (V) and composition (X). A fluid inclusion represents a closed system and its variance is restricted by the constancy of both volume and total mass (m). The composition can also be taken as a constant factor as far as chemical equilibria do not (significantly) change with temperature i.e. if the system remains isochemical. This assumption is allowed as a first approximation for many fluids: pure compounds (e.g. CO_2 or H_2O) are generally stable over a large temperature range. However, compositional changes with varying temperature might be expected in fluid mixtures representing unstable reaction equilibria e.g. fluids containing CO_2, CH_4, water and graphite (Kreulen 1987). These compounds mostly represent metastable compositions. It was demonstrated by Dubessy (1984) that the $\bar{V}X$ properties of fluid inclusions are representative for the trapping conditions at high temperature in the following cases: a) in absence of graphite b) in the presence of graphite, but a fluid containing >90 mole% CO_2 or CH_4. However, the $\bar{V}X$ properties might have considerably changed during cooling for intermediate CO_2-CH_4 compositions. It was found in the presently studied inclusions from SW Norway that molar volumes gradually change with composition: from pure CO_2 ($\bar{V}$ = 40-45 cm^3/mole) to $CO_2(50)$ $CH_4(50)$ ($\bar{V}$ = 70-80 cm^3/mole). In these inclusions, small amounts of graphite could only be indicated by Raman analysis.

Compositional variations are not further taken into account in this chapter and all compounds are considered as chemically stable. Consequently, temperature and pressure are the only changing variables in an inclusion of given composition. The acceptance of constant volume and mass implies a constant density as d = m/V. It is preferred here to consider the molar volume instead of the density in fluid inclusions. The molecular mass (M) can be left out of account for further calculation. This is especially advantageous for fluids of mixed composition as the molecular mass should be calculated as an extra parameter in more-

component systems ($M = \Sigma X_i \bar{V}_i$). The correlation between $\bar{V}$ and d is given by the expression

$$\bar{V} \quad (M/m).V = M/d \qquad \text{(Eq.5.1.)}$$

Molar volumes in natural fluid inclusions are mostly lower than 100 cm^3/mole; the corresponding fluid pressures at room temperature are between 100 and 500 bar. Most fluids in rocks do therefore <u>not</u> behave as ideal gases.

5.1.2. Equations of state

The correlation between P, V, T and X for single (mostly supercritical) fluids is given by an equation of state. These equations are empirically determined from experimental data and enable the extrapolation of physical conditions outside the experimental range. The number of data on fluids of geological interest (especially the multi-component fluids) are poor (see following sections) and the equations established with the help of these data may therefore be inaccurate. Furthermore, the mathematical forms of all present equations do not allow validity for large PT-ranges: the parameters of the equations should be adjusted for different ranges of application. A general distinction can be made for equations of state valid for the high PT-region (supercritical fluids) and the low PT-region (liquid and multi-phase behaviour).

An equation of state for a compound for which experimental data are lacking can be approached by the law of <u>corresponding states</u> stating that the properties of all real gases are the same at the critical point. This is only valid for non-polar substances; polar substances deviate from ideality. The method of corresponding states can be used by taking the compressibility factor Z, defined as PV/RT, as a constant at the critical conditions. An equation of state describing any fluid can be obtained by filling in the reduced temperature (T/T_C), pressure (P/P_C) and volume (V/V_C) (Fraser 1977; Wood & Fraser 1978; Saxena & Fei 1987).

Several mathematical forms of equations of state are presently available. The classical and most simple equation is given by the gas law

of Boyle - Gay Lussac: P = R.T/V where R denotes the gas constant (= 83.12 cm^3bar/deg.mole) and T the absolute temperature. This equation is only valid for ideal gases; many other equations have been developed to describe the behaviour of gases at high pressure, in the domain where interaction between molecules becomes important. The van der Waals equation includes corrections for attractive and repulsive forces between the molecules:

$$P \quad \frac{R.T}{V-b} - \frac{a}{V^2} \qquad \text{(Eq.5.2.)}$$

The parameters a and b are constants expressing the cohesion and volume of the molecules, respectively. The term a/V^2 is the cohesive pressure, becoming larger for higher values of a, and zero for ideal gases. The van der Waals equation is used as a basic form for later and more advanced equations. Three of the most popular forms are discussed below: a) the Redlich-Kwong b) the Peng-Robinson and c) the Heyen equation. Several variants of these equations exist, especially for the first mentioned one.

a) The Redlich-Kwong equation (Redlich & Kwong 1949) achieves better fittings with experimental data for high density gases:

$$P \quad \frac{R.T}{V-b} - \frac{a}{V(V+b)(T)^{1/2}} \qquad \text{(Eq.5.3.)}$$

where a and b are constants, as for the van der Waals equation. Their numerical values can be found with the corresponding state method. This equation is a good approximation for non-polar compounds like N_2 and CH_4. However, for polar compounds (CO_2 and H_2O), the equation significantly deviates from the PVT data because the parameters a and b are temperature dependent. Several variants of the Redlich-Kwong equation are presently in use. Some of these modifications were discussed and compared by Saxena & Fei (1987). The most important modifications are those given by a) de Santis et al. (1974) used by Holloway (1977) b) Touret & Bottinga (1979) and Bottinga & Richet (1981) c) Kerrick & Jacobs (1981) d) Halbach & Chatterjee (1982). These modified equations result to reasonably good fittings at pressures above 1 kbar and temperatures higher than about

125°C (Saxena & Fei 1987), although each equation may have its specific range of application.

De Santis et al. (1974) made the proposition to consider b as a constant and a as a function of temperature. The result became known as the Modified Redlich-Kwong (MRK) equation which finds a wide application by geologists (Swanenberg 1980). Holloway (1977, 1981) used this equation for a computer program which can be used for several polar and non-polar fluid mixtures of geological interest (especially for the system CO_2-H_2O).

The establishment of an equation of state for fluid mixtures requires the application of mixing rules. A distinction can be made in non-polar, non-polar + polar and polar mixtures. a and b for non-polar mixtures can be determined from the following expression (Redlich & Kwong 1949):

$$a = \Sigma_i \Sigma_j X_i X_j a_{ij} \quad \text{where } a_{ij} = (a_i a_j)^{1/2} \qquad \text{(Eq.5.4a)}$$

$$b = \Sigma_i X_i b_i \qquad \text{(Eq.5.4b)}$$

The calculation of the parameters a and b in mixtures including polar compounds is more complicated. De Santis et al. (1974) proposed that for 2 components 1 and 2

$$a_{12} = (a_1^{o} a_2)^{1/2} \qquad \text{(Eq.5.4c)}$$

where a_1^{o} is a constant for one of the 2 components and a_2 is a function of temperature for the other component.

b) An alternative equation of state was proposed by Peng & Robinson (1976). The Peng-Robinson equation has the form

$$P = \frac{R.T}{V-b} - \frac{a}{V(V+b)+b(V-b)} \qquad \text{(Eq.5.5.)}$$

Herskowitz & Kisch (1984) found this equation to be most reliable for the construction of a VX [T] diagram for the system CO_2-CH_4 in the range $T_h < T_m$ (i.e. at low molar volumes and high CH_4 contents).

c) The Heyen equation of state (Heyen 1980, 1981) was developed for high density liquids and covers the range of multi-phase equilibria of the system CO_2-CH_4-N_2. The equation has been applied to the systems CO_2-CH_4 (Heyen et al. 1982) and CO_2-N_2 (Darimont 1986; Darimont & Heyen 1988) in the low PT-region. L-V and S-L-V equilibria could be characterized and diagrams were developed showing the XVT correlations at the homogenization and melting points. The form of the equation includes a third parameter (e):

$$P \quad \frac{R.T}{V-e} - \frac{a}{V^2 + (b+e)V - be} \qquad \text{(Eq.5.6.)}$$

The equation reduces to the Peng-Robinson equation for e = b. The parameters a and b are both functions of temperature and can be found from corresponding state equations (Heyen 1980, 1981); e is taken as a constant. The mixing rules applied for the Heyen equation are

$$a \quad \Sigma_i X_i \frac{\Sigma_j X_j \tau_{ij} (a_i a_j)^{1/2} (1-\delta_{ij})}{\Sigma_k X_k \tau_{ik}} \qquad \text{(Eq.5.7a)}$$

$$b \quad \Sigma_i X_i b_i \qquad \text{(Eq.5.7b)}$$

$$e \quad \Sigma_i X_i e_i \qquad \text{(Eq.5.7c)}$$

The parameters τ_{ij} and δ_{ij} are constants which are empirically found for binary mixtures. At random mixing, the values of these parameters are $\tau_{ij}=1$ and $\delta_{ij}=0$.

It is not possible to decide which of the mentioned equations is best in general. Their accuracy depends on the range of application in respect of P, V, T and X. The Heyen equation is preferred here for the characterization of fluids at low temperatures i.e. in the region of phase transitions; the modified Redlich-Kwong equation as proposed by de Santis (1974) and Holloway (1977) is mostly used in the present study to calculate high PT conditions (isochore extrapolation).

5.1.3. Phase theory

Phase changes, the disappearance or the forming of a phase, can be effected by changing one or more of the parameters P, V, T or X. The stability of a phase assemblage is determined by the number of variables which can be changed independently. This is expressed by the phase rule (Eq.5.8.): the number of phases is a function of the composition and the variance of the system. In fluid inclusions, 2 variables of state (temperature and volume) are externally fixed; pressure is a dependent variable. The number of possible phase equilibria (n), for a given number of phases, is given by Eq.5.9 i.e. the number of forms (points, curves etc.) in phase diagrams. Eq.5.8 together with Eq.5.9 are used for the characterization of a theoretical model of a given system (Campbell & Smith 1951; Smith 1963).

$$p \quad c + 2 - f \qquad \text{(Eq.5.8.)}$$

$$n = \binom{N}{p} : \frac{N!}{(N-p)!\ p!} \qquad \text{(Eq.5.9.)}$$

p = number of phases;
N = maximum number of possible phases (for f=0);
c = number of components (CO_2, CH_4 etc.);
n = number of possible phase equilibria (for given p);
f = variance or degree of freedom.

It is further stated that $p \geq 1$ and $f \geq 0$. The variance is the number of independent variables (P, T, X or V) which have to be fixed to define a system or to characterize phase equilibria within a system. The number of variables needed for the expression of the composition (X) is c-1. Phase equilibria are given by an invariant point for f = 0, univariant curves for f = 1, divariant surfaces for f = 2 and trivariant volumes for f = 3. The implications of the phase rule for systems of 1, 2 or 3 components are given below and in Table 5.1a-c:

Unary or pure systems (c=1) have a maximum variance of 2, for the single phase (S, L or V). It is most convenient to take P and T as the 2 variables. Alternatively, P-V or V-T can be chosen. The third parameter is determined by an appropriate equation of state e.g. isochores (curves

of constant volume) are uniquely defined in a PT-field. 2-Phase assemblages (S+L, S+V or L+V) are univariant. The pressure and, more important, the molar volume of a pure, 2-phase inclusion can therefore be determined from temperature readings only. The invariant point of a pure system is characterized by the coexistence of the 3 phases S+L+V (triple point). The critical point (L=V) is also invariant.

a) Unary systems (c=1)

f	p	n		form
0	3	1	invariant	triple point
1	2	3	univariant	2-phase curves
2	1	3	divariant	monophase surface
3	-	1	universal representation	

b) Binary systems (c=2)

0	4	1	invariant	quadruple point
1	3	4	univariant	3-phase curves
2	2	6	divariant	2-phase surfaces
3	1	4	trivariant	monophase volumes
4	-	1	(universal representation)	

c) Ternary systems (c=3)

0	5	1	invariant	quintuple point
1	4	5	univariant	4-phase curves
2	3	10	divariant	3-phase surfaces
3	2	10	trivariant	2-phase volumes
4	1	5	-	-
5	-	1	-	-

Table 5.1.- *Characteristics of* ***a)*** *unary* ***b)*** *binary and* ***c)*** *ternary systems and implications for graphical representations. f = the variance of the system; p = the number of phases; n = number of possible phase equilibria.*

The binary system (c=2) of 2 components A and B has a maximum variance of 3: the composition (X_{AB}) is normally chosen as the additive variable to P and T. For fluid inclusions however, the pressure is mostly ignored because it cannot be measured and X, V and T are taken as the variables. It follows from the phase rule that binary systems show an invariant quadruple point (p=4): the coexisting phases are generally a liquid, vapour and 2 solids. The elements of 2 pure systems and the corresponding binary system are schematically represented in Fig. 5.1a.

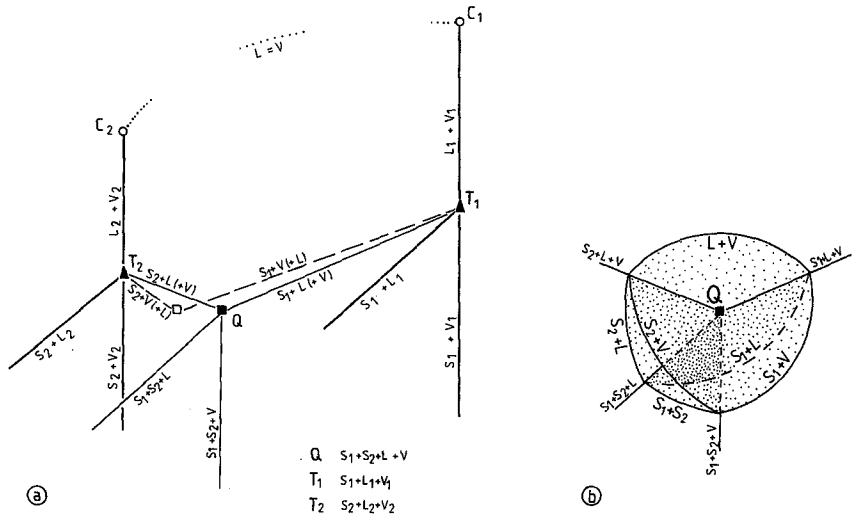

Fig.5.1.- a) *Elements of a binary system and its pure subsystems in a PTX space. Point Q denotes the invariant quadruple point, T_1 and T_2 the invariant triple points of the pure systems; C_1 and C_2 denote the critical points. Univariant equilibria are represented by 3-phase equilibria in the binary system and 2 phases in both pure systems, and the critical curve. Dashed lines indicate vapour compositions coexisting with solid and liquid.* ***b)*** *Detail of the quadruple point showing the grouping of univariant (3-phase) and divariant (2-phase) equilibria.*

The 3 dimensions of this diagram correspond to 3 independent variables. The 3-phase assemblages are univariant. The composition of coexisting liquid and vapour phases is generally different and both are indicated. A detailed illustration of the quadruple point (S_1+S_2+L+V) is shown in Fig.5.1b. The critical conditions (L=V) are univariant and are given by the critical curve.

The ternary system (c=3) of the components A, B and C has a maximum variance of 4. The composition can be expressed as two concentrations between 2 end-members (X_{AB} and X_{BC}), or as partial pressures. P and T or alternatively V and T can best be chosen to make 4 independent variables together with X_{AB} and X_{AC}. The invariant point is defined by a the coexistence of 5 phases (quintuple point). Several solids are in equilibrium here.

5.1.4. Graphical representation of systems and phase diagrams involving molar volume

The graphical representation of multi-phase systems (phase diagrams) is restricted to the 2 dimensions of paper and human imagination. The number of variables is generally higher than 3, meaning that 1 or more variables should be taken as a constant to make illustration possible. It was mentioned earlier that curves of constant molar volume are defined as isochores; other curves denote constant P (isobars), constant T (isotherms) or constant X (isopleths).

The construction of phase diagrams for unary systems is most simple as they are completely defined by only 3 variables of state (1, 2 or 3 between P, T and V). An universal representation of the system can be obtained in a 3-dimensional PTV diagram (Burruss 1981). The stability of monophase equilibria is determined by only 2 variables and a 2-dimensional diagram (one of the 3 principle sections of the PVT-space) therefore represents a complete illustration of the system. Most convenient is the use of the PT diagram because isochores can be constructed which enable extrapolation from low PT (the laboratory conditions) to high PT conditions (of geological interest); alternative illustrations are VT or PV diagrams (Roedder 1984, p.225-230).

Binary systems are defined by 4 degrees of freedom: P, V, T and X. Single phase equilibria are defined by fixing 3 variables of state. 4 possible diagrams with 3 independent parameters can be chosen for illustration. It is convenient to use 2-dimensional projections of these diagrams where 2 variables are kept constant e.g. in a PT diagram both isochores and isopleths can be represented. A selection of two basic types of diagrams was presently made for the representation of multi-phase equilibria (in the low temperature region) namely 1) PTX diagrams and 2) $\bar{V}$TX diagrams.

The principle sections of the PTX diagram are the traditional phase diagrams to visualize binary systems: the PT, XT and XP sections showing isopleths, isobars and isotherms respectively. Although the molar volume is not presented in these diagrams, they are added here because many workers are familiar with them whereas the $\bar{V}$TX diagrams are unconventional in petrology. The isobaric XT diagram (for the system CO_2-

CH_4) was discussed by Donnely & Katz (1954) and Burruss (1981). Special attention is paid to the PT-projection (see later).

Diagrams involving the molar volume, temperature and composition ($\bar{V}$TX diagrams) are most useful for the application to fluid inclusion studies, because the pressure in fluid inclusions cannot be measured in a direct way. The principle sections of the $\bar{V}$TX diagram are employed for the characterization of fluid inclusions: it is not aimed at finding the pressure in a fluid inclusion, but to find its molar volume (and density). These diagrams are essentially polybaric because the pressure is a dependent parameter, defined at each point. The 2 diagrams selected here are a) the $\bar{V}$X diagram and b) the XT diagram.

The $\bar{V}$X diagram (showing isotherms) was firstly introduced by Burruss (1981) for fluid inclusion work. It appeared to be most suitable for the description of phase behaviour observed by microthermometric studies. A fluid inclusion is plotted as a point in the diagram. Phase behaviour (H and S-types) can be indicated in respect of $\bar{V}$ and X (see sections 5.3.1 and 5.3.2).

The XT diagram (showing isochores) is introduced here because the data obtained from microthermometry and Raman analysis can be simply plotted (even without knowing the topology of the system). This is especially useful for the presentation of fluid inclusion data of one sample (or one region) showing varying composition, but about constant molar volume. The advantage of the TX diagram is the possibility to present all observed phase transitions in one diagram, whereas a succession of several $\bar{V}$X diagrams is needed for the visualization of phase changes. The resemblance between the isochoric and the isobaric XT diagram was noticed by Touret (1982), but it must be stressed that they should not be confused: an empirical TX diagram obtained from measurement data of fluid inclusions may represent an isochoric section, but is never isobaric. Presentation of such data in isobaric diagrams is therefore not allowed. The basic difference between the isobaric and the isochoric TX diagram is indicated by the statement that compositions of the individual phases (e.g. the compositions of coexisting liquid and vapour) can be read at any temperature in an isobaric diagram, but not in an isochoric diagram (pressures are the same for all phases whereas their molar volumes are not). This makes the isobaric diagrams more accessible and easier to read, but they are of lesser importance for fluid inclusion studies.

Isochoric PT diagrams are employed, as for the unary systems, for

supercritical fluids (in the high temperature region) in order to extrapolate low PT conditions to trapping conditions.

The ternary system cannot be completely represented in 3-dimensions as there are 5 variables (X_{AB}, X_{AC}, P, V, T) of which 4 are independent. It is most convenient to construct a diagram for constant pressure or constant molar volume with the composition in the XY-plane (as a triangle with the apices A, B and C) and the temperature in the Z-direction. The latter diagram is discussed for the system CO_2-CH_4-N_2 in section 5.4. Projections in the compositional plane are normally represented.

5.2. Unary systems

5.2.1. The system CO_2

Available PVT data for CO_2 are more limited than might be expected from its general importance. The data for the low PT-region are taken from Angus et al. (1976a). Most important for fluid inclusion studies is the situation of the boiling point curve: the molar volume of a CO_2 inclusion is directly determined from its homogenization temperature (Hollister & Crawford 1981; Roedder 1984 p.227-230). The critical temperature of CO_2 is 31.1°C; the melting temperature (at the triple point) is -56.6°C.

Fig.5.2.- *Isochores of CO_2 (molar volumes between 30 and 500 cm^3/mole) compiled from Angus et al. (1976) (A), Vagarftik (1972) (V), Juza et al. (1965) (J) and Shmonov & Shmulovich (1974) (SS^1 = measurement data; SS^2 = extend range). Numerals in brackets indicate homogenization temperatures (°C).*

(Fig.5.2)

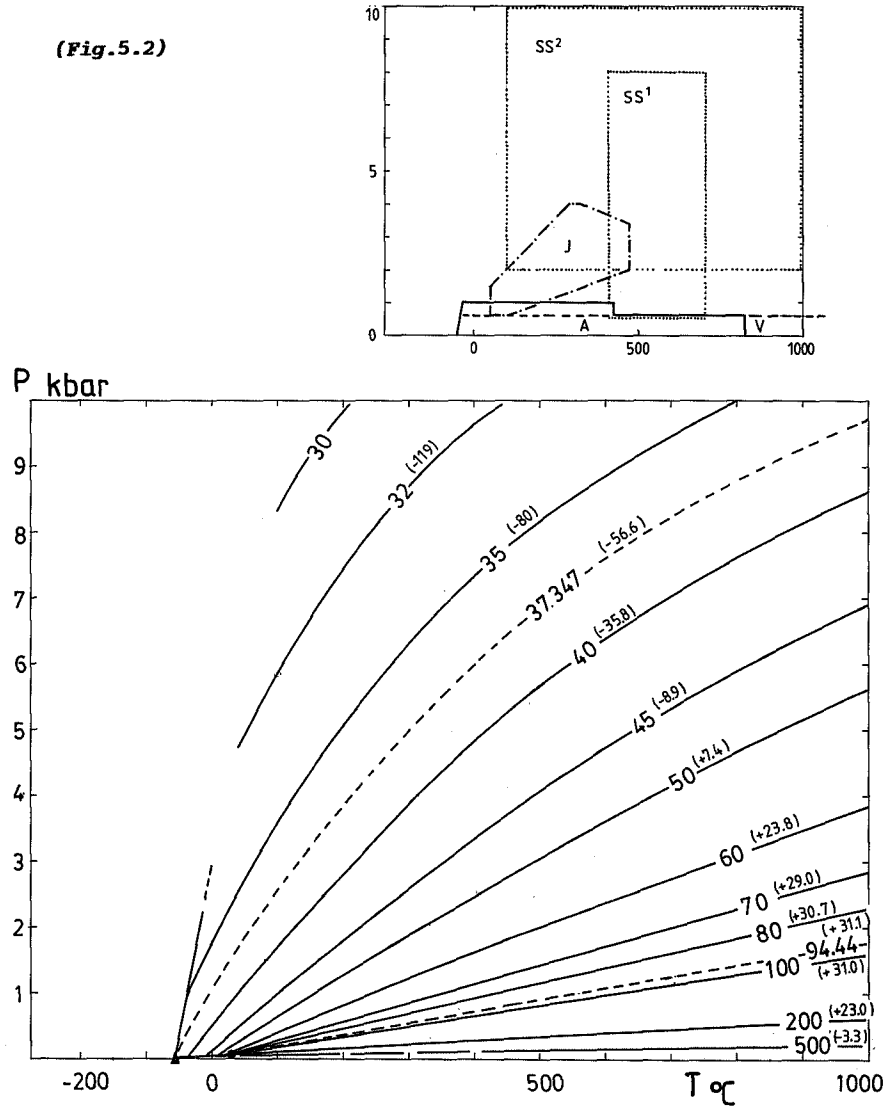

A selection was made of the literature presenting data covering the high PT conditions: Angus et al. (1976a), Juza et al. (1965), Shmonov & Shmulovish (1974) and Vagarftik (1972). A compilation of these data resulted to the PT diagram of Fig.5.2 (showing isochores). Data for the highest temperatures (and pressures below 600 bar) are available from Vagarftik: from 0 to 3725°C. Data for the highest pressures are taken from Shmonov & Shmulovish: 2 to 8 kbar at temperatures between 100 and 700°C. The latter study mostly contributes to the conditions of

geological interest. A compilation of literature data was also made by Touret & Bottinga (1979), Swanenberg (1980) and Roedder (1984 p.229).

Several equations of state have been applied to the system CO_2. Angus et al. (1976a) and Shmonov & Shmulovish (1974) applied pure mathematical equations to achieve (limited) extension of their experimental data. Most important are the MRK equations as revised by Holloway (1977) and Bottinga & Richet (1981). These equations agree with the experimental data to about 2 kbar (at 1000°C) and to 500°C (at 6 kbar), but deviations become more significant to higher PT (Touret & van den Kerkhof 1986).

5.2.2. The system CH_4

The knowledge on the system CH_4 in the low PT region mostly relies on the data of Angus et al. (1976b) and Vagarftik (1972). The critical temperature of CH_4 is -82.6°C; the melting temperature -182.5°C.

The references mentioned above are also the only available for high pressures or high temperatures. Thermodynamic data are lacking for high P and T, the conditions of geological interest. The knowledge on the PVT correlations in this region are only dependent on equations of state based on low PT data. Swanenberg (1980) and Holloway (1977) both employed the MRK equation for the calculation of isochores of CH_4 by using constant values for the parameters a and b (see section 5.1.2). These parameters are a = $40.06.10^6$ bar.$cm^6.\sqrt{K}.mole^{-2}$, b = 32.71 cm^3/mole (Swanenberg) and a = $31.59.10^6$; b = 29.703 (Holloway).
The resulting isochores are straight lines in the PT-field. The isochores calculated by Swanenberg indicate systematic higher pressures than the isochores of Holloway. The latter equation shows better agreement with the data of Angus et al. (1976b) for the higher density fluids. The (mathematical) equation of state used for the construction of the tables given by Angus et al. (1976) cannot be guaranteed for temperatures higher than 200°C, but it is probably the best equation available in this region. Isochores calculated by the equations of Angus and Holloway almost coincide for molar volumes higher than 60 cm^3/mole; the Angus equation results to strongly curved isochores for lower molar volumes (higher densities) (Fig.5.3). The equations of both Holloway and Swanenberg give erroneous results for densities higher than the triple point. Tomilenko & Chupin (1983) constructed straight-line isochores (as for CO_2 and N_2) up to pressures of 15 kbar and 1200°C.

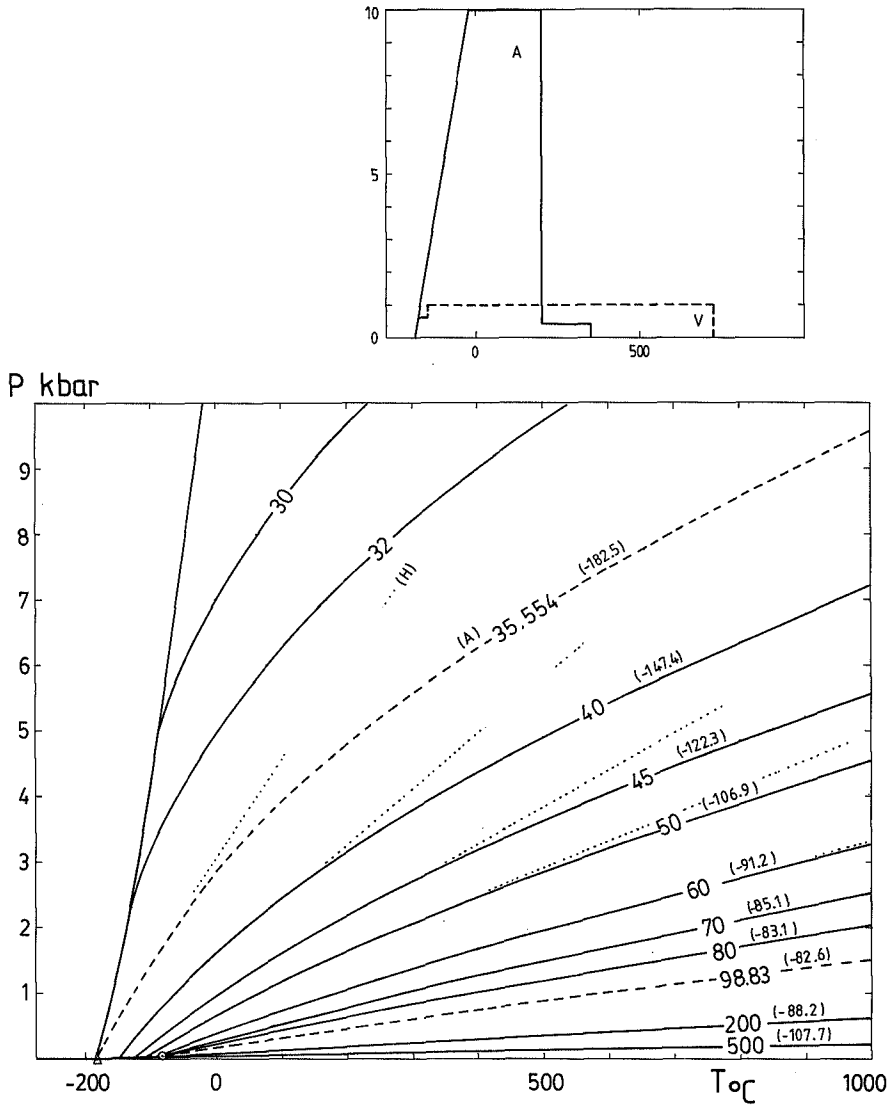

Fig.5.3.- *Isochores of CH_4 (molar volumes between 30 and 500 cm^3/mole) compiled from Angus et al. (1976) (A) and Vagarftik (1972) (V). Isochores in the high PT range are extensions of the equation used by Angus; dotted lines are the (linear) isochores produced by the "Holloway equation". Numerals in brackets indicate homogenization temperatures (°C).*

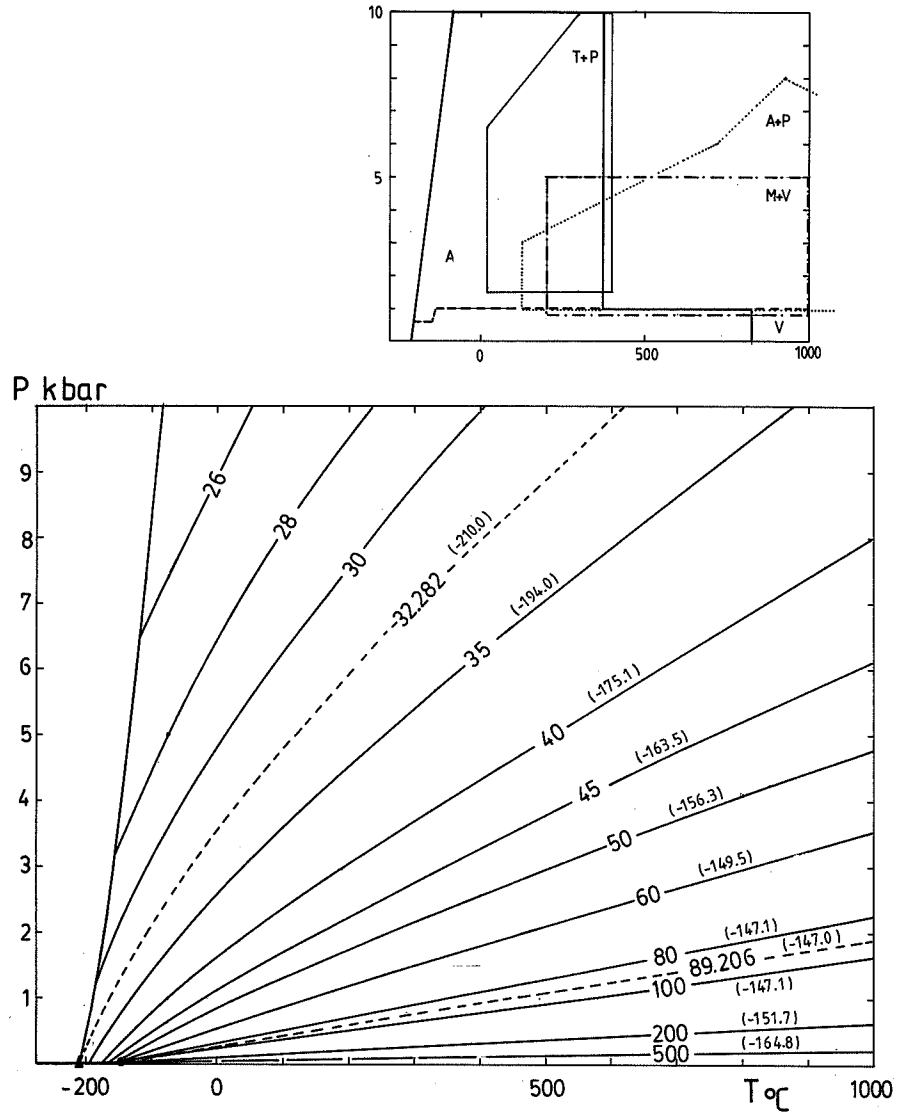

Fig.5.4.- *Isochores of N_2 (molar volumes between 26 and 500 cm^3/mole) compiled from Angus et al. (1979) (A), Vagarftik (1972) (V), Malbrunot & Vodar (1973) (M+V), Tsiklis & Polyakov (1968) (T+P) and Antanovish & Plotnikov (1976) (A+P). Numerals in brackets indicate homogenization temperatures (°C).*

5.2.3. The system N_2

Data of the low temperature region are given by Angus et al. (1979) and Vagarftik (1972). The critical temperature is -147.0°C; the melting temperature -210.0°C (Angus).

Present literature data cover a large part of the high PT-range: Angus et al. (1979), Antanovish & Plotnikov (1976), Malbrunot & Vodar (1973), Tsiklis & Polyakov (1968), Vagarftik (1972). A graphical representation of isochores is shown Fig.5.4.

Swanenberg (1980) calculated the parameters of the MRK equation for data of the low and high PT-region: isochores at high PT could be well reproduced with the MRK equation by setting a=0 and b as a function of temperature and pressure. In the computer program of Holloway, constant values for a and b give reasonable good results with a = $15.38.10^6$ bar.$cm^6.\sqrt{K}.mole^{-2}$ and b = 26.8 cm^3/mole.

5.3. Binary systems

5.3.1. The system CO_2-CH_4

No miscibility between the solid phases and full miscibility between the liquid and the gas phases (without azeotrope) is assumed for the system CO_2-CH_4. The system is relatively well known compared to the other binary systems treated here. The following discussion relies on the data obtained from Donnely & Katz (1954), Davis et al. (1962), Arai et al. (1971), Hwang et al. (1976) and Mraw et al. (1978). The traditional geometrical representations are diagrams showing correlations between the variables P, T and X. These PTX diagrams are most suitable to visualize the topology of the system.

PTX diagrams

The 3 principle sections of the PTX diagram are shown in Fig.5.5a: the PT, TX and PX diagram. Only univariant and divariant equilibria are illustrated for simplicity. The general characteristics of the system are discussed by Campbell & Smith (1951, p.250-254) and Smith (1963, p.119-122). Coexisting liquid and vapour phases generally differ in composition

meaning that any 2-phase equilibrium is represented by 2 surfaces, one for the liquid and one for the vapour; each 3-phase equilibrium is represented by 3 curves (for the solid, liquid and vapour phases). Compositional differences between liquid and vapour are of major importance for the topology of the system. The 2 solid phases are assumed to be pure CO_2 and pure CH_4; the vapour is always richer in CH_4 than the liquid. In a multi-phase system the composition of the individual phases is different; pressure and temperature are the same for all phases.

The PT diagram is treated here in more detail and was already published by Swanenberg (1979), Burruss (1981) and Roedder (1984, p.242). Curves of constant composition are constructed (Fig.5.5b). A compilation of literature data resulted to the diagram of Fig.5.6. showing isopleths for the 2-phase equilibria: the boiling point curves, L(+V), dew point curves, V(+L) and sublimation curves, V(+S). This diagram was proposed by Swanenberg (1979) with the indication of the isochores. The PT diagram illustrates the strong curvature of the 3-phase curve with a pressure maximum at 49 bar for T = -69°C, $X_{CH4}(V)$ = 0.89 and $X_{CH4}(L)$ = about 0.76 (Hwang et al. 1976; Davis et al. 1962). The curve intrudes the region of L+V immiscibility, but it does not intersect the critical curve. Consequently, solid CO_2 cannot melt into a critical or supercritical fluid. This fact is the most basic difference with the system CO_2-N_2 (see section 5.3.2.).

Experimental data are poor in the region of the assumed eutectic (quadruple point). Donnely & Katz (1953) estimated the position of the eutectic by the extrapolation of experimental data. However, a considerable discrepancy was noted between these data and those from Davis et al. (1962), Hwang et al. (1976) and Mraw et al. (1978). The existence of any significant eutectic was doubted by Davis et al. (1962) because the "eutectic" appeared to coincide or nearly coincide with the triple point of CH_4. Their data show that pressures along the 3-phase curve approximate the vapour pressure of pure CH_4 at temperatures below-120°C; the CO_2-content of the liquid phase was measured to be less than 0.2% below -143°C. The acceptance that liquidus compositions approximate pure CH_4 implies that even the smallest amounts of CO_2 present in CO_2-CH_4 inclusions can be solidified upon cooling; the data of Donnely & Katz indicate that solid CO_2 cannot be formed in a liquid containing less than 4 mole% CO_2 (at about -100°C and at any pressure) i.e. for compositions between the liquidus composition and pure CH_4. However, it should be noted that small particles of solid CO_2 are often difficult or even

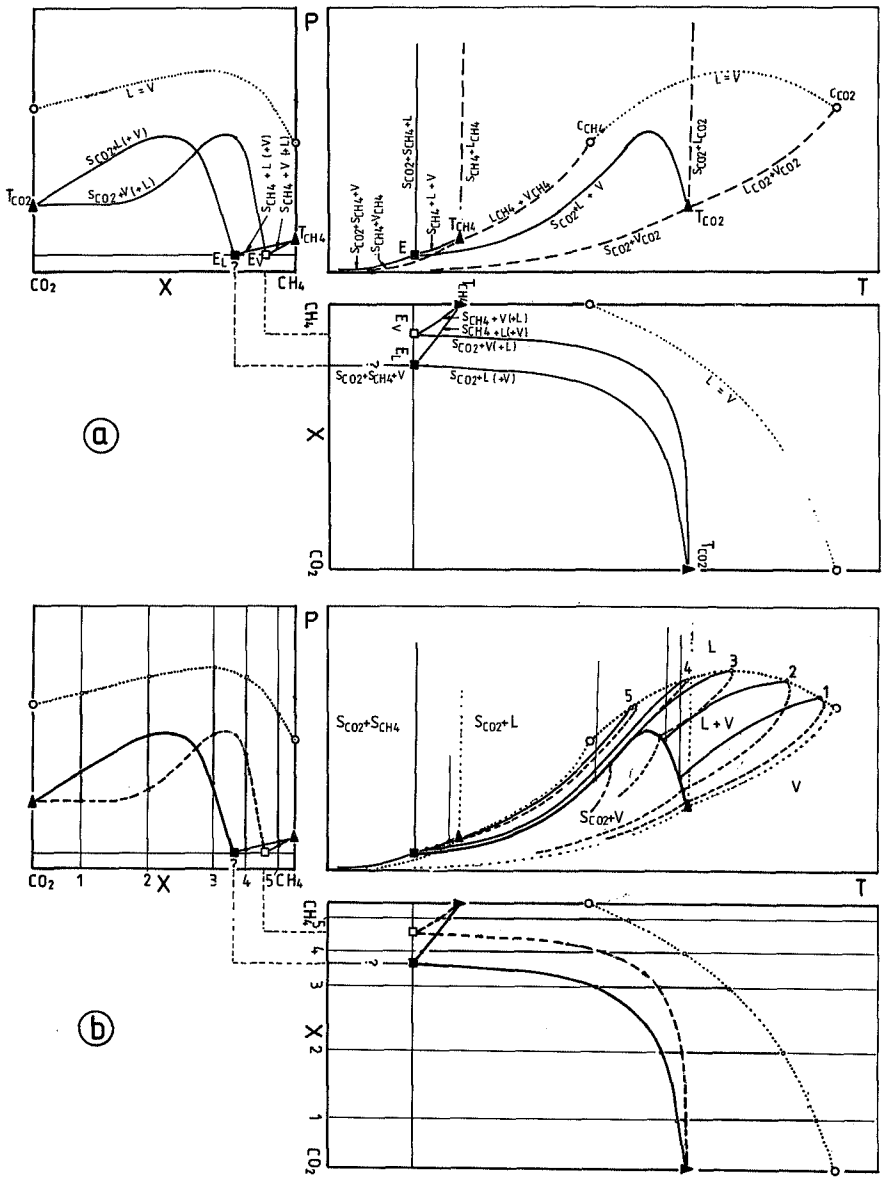

Fig.5.5.- The 3 principle sections of the PTX diagram (PT, PX and TX) for the system CO_2-CH_4 (schematic).
***a)** The univariant equilibria of the binary system (solid curves and the dotted critical curve). Compositions of the eutectic or quadruple point are indicated for the liquid (E_L) and vapour (E_V) phases. The pure systems are illustrated by the triple points (T_{CO2} and T_{CH4}), critical points (C_{CO2} and C_{CH4}) and univariant equilibria (dashed curves).*
***b)** Isopleths indicated for 5 compositions (1, 2, 3, 4 and 5) in the PT, PX and TX diagram. L+V equilibria (in the PT diagram) are defined by boiling point curves (solid) and dew point curves (dashed). Solid and dashed curves in the PX and TX diagrams denote the liquid and vapour compositions of the 3-phase equilibria respectively.*

impossible to observe. In natural CO_2-CH_4 inclusions, solid CO_2 has been presently observed for CO_2-contents as low as 3 mole%.

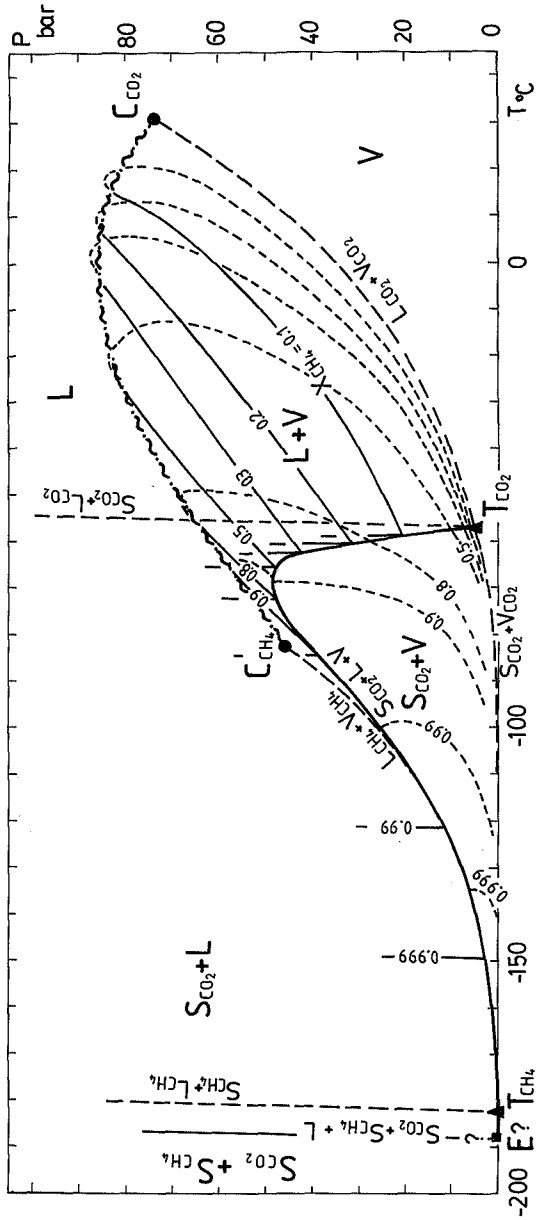

Fig.5.6.- *PT diagram (isopleths) of the system CO_2-CH_4 compiled from Donnely & Katz (1953), Davis et al. (1961), Arai et al. (1971), Angus et al. (1976a, 1976b).*

The $\bar{V}TX$ diagram

The volumetric data of phase equilibria are poor and mostly rely on the paper of Arai et al. (1971). These data comprise measurements for liquid-vapour equilibria for T>-20°C, X_{CH4}<0.55 and $\bar{V}$<700 cm^3/mole. Experimental data for the molar volume for 3-phase equilibria are not available and either for S+V and S+L equilibria. The $\bar{V}TX$ relations of 3-phase equilibria can be obtained by extrapolation of the L-V data of Arai et al. (1971) to the liquidus conditions. Heyen et al. (1982) applied his equation to construct a $\bar{V}TX$ diagram which is only valid for CO_2-rich compositions, below 50°C and 100 bar. Herskowitz & Kisch (1984) used the Peng-Robinson equation for the construction of a diagram valid for CH_4-rich compositions below -70°C and 50 bar (in the S+L region).

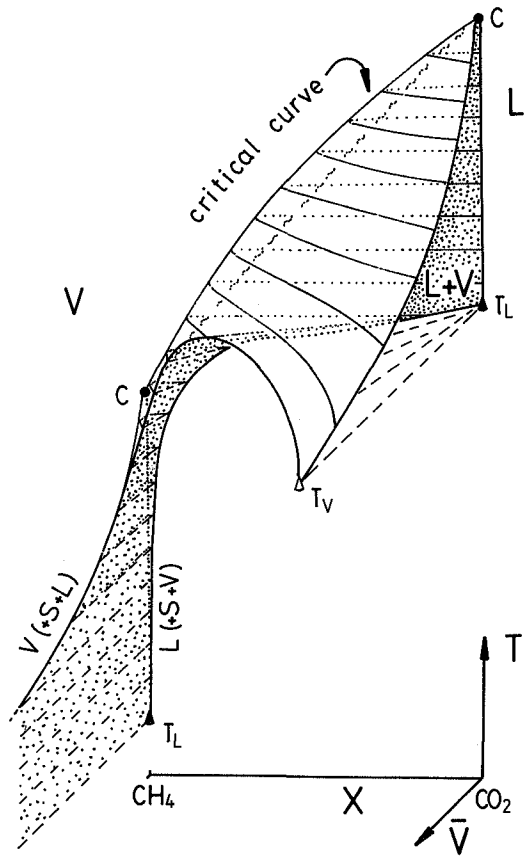

Fig.5.7.- *The configuration of liquid-vapour immiscibility in the system CO_2-CH_4 in respect of $\bar{V}$, X and T. Note the relative position of the 3-phase curves for liquid and vapour compositions (L(+S+V) and V(+S+L)). Some isothermal sections are also shown: solid curves indicate L+V to L or V boundaries; dashed lines connect coexisting L and V for the 3-phase assemblages.*

The $\bar{V}TX$ diagram is introduced here for the presentation of the fluid inclusion system. Fig.5.7 shows the shape of the immiscibility gap between liquid and vapour in a $\bar{V}TX$ space. The boundaries of LV-immiscibility are 2 surfaces representing bubble and dew points, joining at the critical curve (L=V). The critical curve does not form the hinge of the curved LV-surface (defined as the critical curve of the second order), but is situated at the "liquid side" of the surface. The 3-phase curves were constructed by the extrapolation of data (Davis et al. 1962; Arai et al. 1971). Some isothermal sections, parallel to the $\bar{V}X$-plane, are shown as well in the figure. Orthogonal projections parallel to the T-axis result to $\bar{V}X$ diagrams. This type of diagram, first introduced by Burruss (1981), is suitable for the presentation of fluid inclusion properties: any fluid inclusion should plot as a point in the diagram and phase equilibria are indicated for a given temperature. A schematic illustration of the $\bar{V}X$ diagram is shown in Fig.5.8. The 3-phase equilibria are given by 2 (polythermal) curves, for the liquid and for the vapour phases, denoted by L(+S+V) and V(+S+L) respectively; the solid phase consists of pure CO_2. The 3-phase curves show a maximum and a minimum in respect of molar volume. Solid CO_2 (S) has a molar volume of 28.2 cm^3/mole ($d = 1.56\ g/cm^3$; $\bar{V} = M/d = 44/1.56 = 28.2$). The 3-phase stability field is limited by the 3 tie-lines connecting S and the corresponding liquid and vapour phases on the liquidus (lines 1, 2 and 3 in Fig.5.8). The situation of the 2-phase stability fields L+V, S+L and S+V and the single phase field (L or V) are also determined for a given temperature. Lines and curves marking phase transitions (on warming) are denoted as indicated in Fig.5.8. For example: melting (T_m) is defined as the transition S+L+V → L+V (line 3); homogenization (T_h) as L+V → L or V (curve 4). Inclusions with $\bar{V}X$ plotting exactly on one of the 3-phase curves are characterized by coinciding homogenization and melting temperatures ($T_h=T_i=T_m$).

A part of the $\bar{V}X$ diagram for the system CO_2-CH_4 in the correct proportions was obtained from the assembled data (Fig.5.9a). Most tie-lines are omitted here to keep the figure readable. The $\bar{V}$-maximum of the L(+S+V) curve was calculated to be 65 cm^3/mole at $X_{CH4} = 0.87$ (Herskowitz & Kisch 1984); the minimum of the V(+S+L) curve was estimated to be about 225 cm^3/mole at $X_{CH4} \simeq 0.9$. The critical curve (C_1) shows a slight minimum and connects the critical points of the pure components. The critical curve of the second order (C_2), given by the highest homogenization temperature possible for fluids of given composition, is

constructed by connecting the tangents of the homogenization curves parallel to the $\bar{V}$-axis. All fluid inclusions plotting in the area between C_1 and C_2 are characterized by retrograde condensation. Arai et al. (1971) measured these points for +15, 0 and -20°C. The term "retrograde condensation" is properly defined as condensation at releasing pressures (by volume expansion), but at constant temperature (Ypma 1963). In fluid inclusions however, de volume is constant and the pressure can only be lowered by also lowering the temperature. Retrograde condensation and "normal" condensation by cooling can therefore not be distinguished. The implication of retrograde condensation for the isochoric system is the rise of homogenization temperatures to the vapour phase with higher molar volume (lower density) (T_h^V "normally" decreases with higher molar volumes); homogenization temperatures to the liquid phase always rise with higher molar volumes.

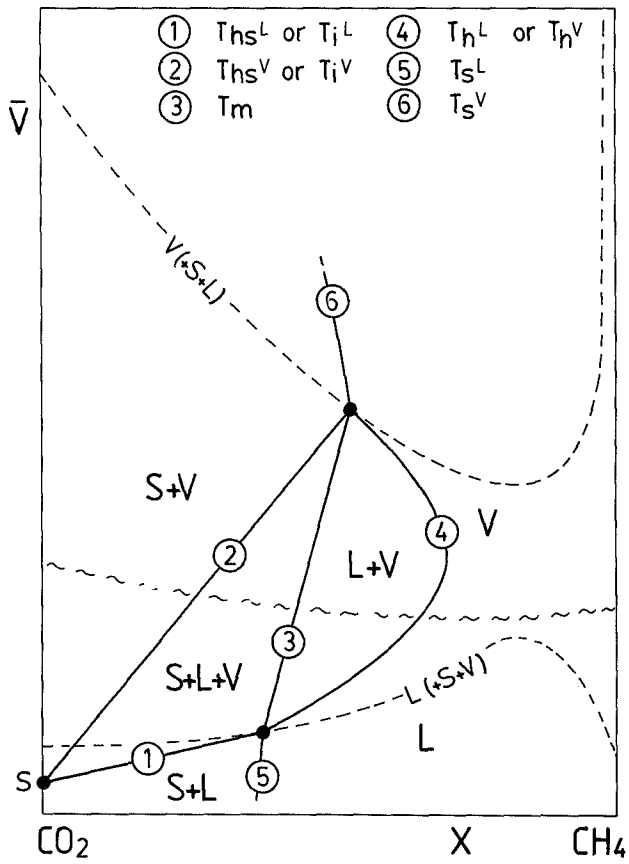

Fig.5.8. *- Phase fields in the system CO_2-CH_4 at constant temperature represented in a $\bar{V}X$ diagram (schematic). Dashed curves are the (polythermal) 3-phase equilibria for liquid and vapour compositions; critical conditions plot on the wavy curve. Point S indicates the properties of the solid phase ($\bar{V}$ = 28.2 cm^3/mole). The 3-phase stability field is delimited by tie-lines 1, 2 and 3; curves 4, 5 and 6 mark transitions to the single phase. The presently used denotations for all curves marking phase transitions are shown at the top of the figure (see table 3.2b for explanation).*

Systematics of phase behaviour (H and S types)

The $\bar{V}X$ diagram is most appropriate to illustrate the distribution of fluid inclusion types as distinguished by microthermometric observations (types H1-5 and S1-4, see Chap.III). Inclusions plotting in the areas above and below the liquidus conditions (L(+S+V) and V(+S+L)) are characterized by sublimation; inclusions plotting in the area between these curves show final homogenization (Fig.5.9a-b). Type H2, H3 and S2 behaviour are most frequently found; type H1, H4, H5, S1 behaviour is less frequent or rare because of their limited $\bar{V}X$; type S3 and S4 behaviour has not been observed in CO_2-CH_4 inclusions. Phase behaviour and specifications of CO_2-CH_4 inclusions are given below:

H1-type inclusions consist of pure CH_4. It was mentioned earlier that even very small amounts of CO_2 can be solidified because the eutectic point (almost) coincides with the triple point of CH_4.

H2-type inclusions are CH_4-rich, or CO_2-rich with a high density. The $\bar{V}X$-conditions are bounded by the lines 1 and 2 of Fig.5.9a. The 2-phase equilibria S+V or S+L cannot be stabilized at any temperature: tie-lines between S and V(+S+L) or L(+S+V) do never cross-cut the $\bar{V}X$-conditions of a H2-type inclusion. Consequently, a 3-phase equilibrium remains stable over a long temperature range. Complete solidification is not possible at temperatures above -180°C. An example of the successive phase assemblages is schematically shown in Fig.5.10a. At the lowest temperature (T_1), a 3-phase equilibrium (S+L+V) exists, followed by melting at T_2. The resulting phase assemblage (S+L) after melting is shown at T_3. T_4 denotes the homogenization temperature. In the case of Fig.5.10a, homogenization is to the liquid phase, but homogenization to the vapour phase is observed if the $\bar{V}T$-conditions plot at the other side of the critical curve.

H3-type inclusions theoretically only comprise pure CO_2 inclusions and low density inclusions of low CH_4-content. However, the amount of liquid around -180°C for all inclusions plotting above curve 1 (Fig.5.9a) appears to be too small for observation and only solid and vapour can be seen. These inclusions are therefore classified as apparent H3 ("H3") although H4 behaviour is expected. The successive phase assemblages on warming are schematically shown in Fig.5.10b. The theoretical partial

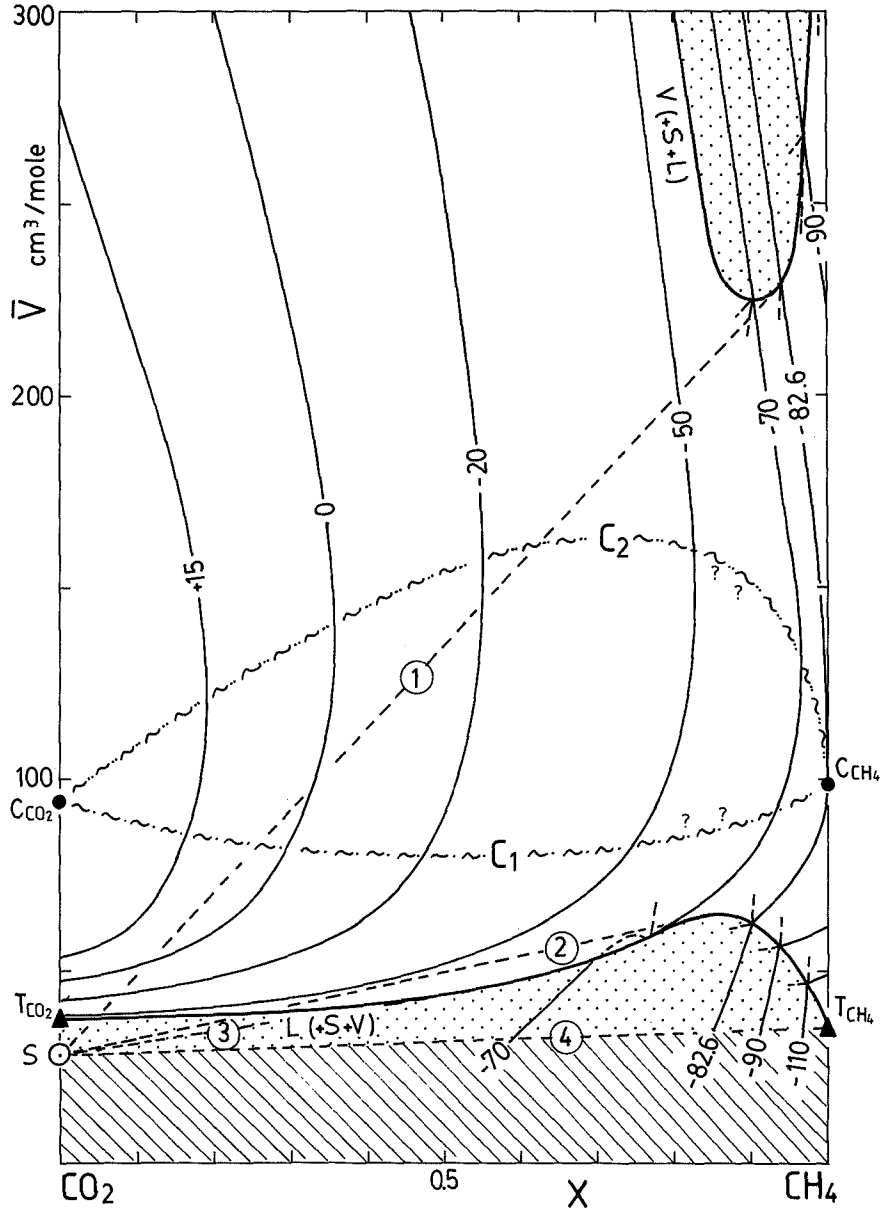
300
200
100
$\bar{V}$ cm³/mole
V (+S+L)
-90
-82.6
-70
-50
-20
0
+15
C_2
C_1
①
②
③
④
L (+S+V)
C_{CO_2}
C_{CH_4}
T_{CO_2}
T_{CH_4}
S
-70
-82.6
-90
-110
CO_2
0.5
X
CH_4

(Fig.5.9a)

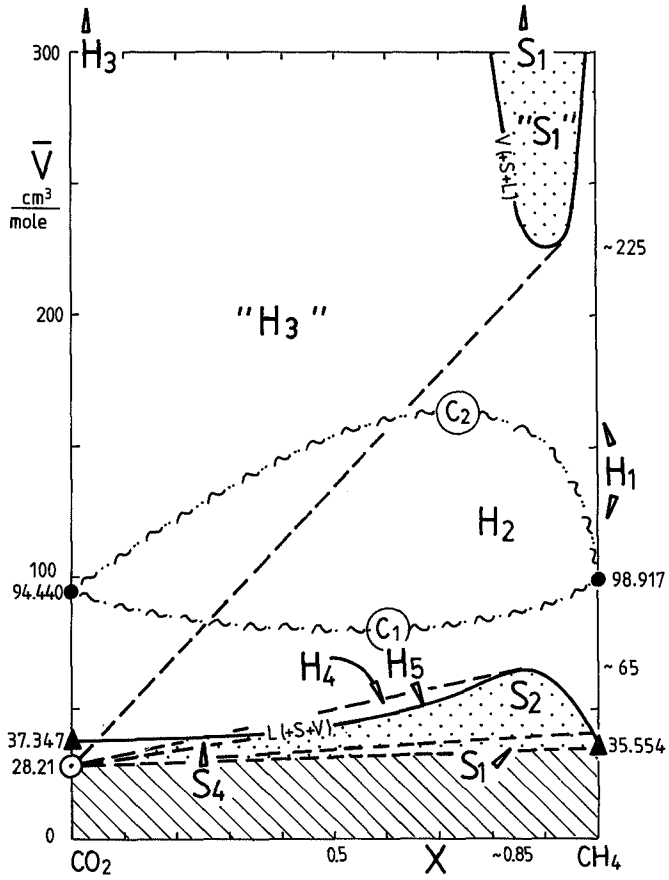

(Fig.5.9b)

Fig.5.9.- $\bar{V}X$ *diagrams of the system* CO_2-CH_4 *for molar volumes between 28 and 300* cm^3*/mole.*
a) *The 3-phase curves for the liquid and vapour phase (L(+S+V) and V(+S+L)) delimit the regions characterized by sublimation (stippled) and homogenization (open). The wavy-dotted curves* C_1 *and* C_2 *are the critical curves of the first and second order respectively. Fluids with* $\bar{V}X$ *properties plotting in the region between these curves are characterized by retrograde condensation. A selection of isotherms (°C) marking homogenization and sublimation temperatures is shown; most tie-lines marking initial and final melting are not extended for simplicity. Lines 1, 2 and 3 denote tangents connecting S and V(+S+L): lines 1 and 2 delimit type H2 inclusions, lines 2 and 3, H4 (or S4) inclusions (Fig.5.9b). Molar volumes below that of line 4 are not possible.*
b) *(as Fig.5.9a) also indicating the distribution of phase behaviour (H and S types) (see text).*

homogenization point T_{hs} (always to the vapour phase!) is visualized at T_2. The first clearly observed phase transitions on subsequent warming are initial and final melting (at T4 and T_6). T_5 illustrates the 3-phases during the melting process. Final homogenization is observed at T_8 by entering the single phase field. Homogenization may be to the liquid or to the vapour phase for inclusions with molar volumes lower or higher than the critical curve respectively.

H4-type inclusions (really observed as H4) show a remarkable behaviour which is unique for CO_2-CH_4 inclusions and does not occur in CO_2-N_2 inclusions: initial melting is characterized by the forming of a bubble (T_i^L). This phenomenon is explained by the concave shape of the L(+S+V) curve (Herskowitz & Kisch 1984). As a result, a part of the tie-lines between S_{CO2} and L(+S+V) run above the L(+S+V) curve. Inclusions with $\bar{V}X$-conditions plotting in the wedge-shaped region bounded by line 2 (Fig.5.9a) and the L(+S+V) curve will show twice a 3-phase equilibrium during warming. The $\bar{V}X$-conditions are very limited: $38<\bar{V}<63$ cm^3/mole and $0.24<X_{CH4}<0.85$. An example of H4-behaviour in a CO_2-CH_4 inclusion is shown in Fig.5.10c. Around -180°C (T_1), 3 phases coexist grading to S+L at T_3 (T_{hs} is always to the liquid: S+L+V → S+L). At T_4, a bubble appears and the 3-phase field is entered again. Melting can be observed at T_6 shortly followed by homogenization (at T_8). Final homogenization is also always to the liquid phase.

H5-type inclusions can be considered as a special type of H4 namely in the case of $\bar{V}X$ conditions plotting on the L(+L+V) curve. The type is therefore very uncommon, but it has been observed in a few inclusions. They are characterized by the almost direct transition L+S → L+V, without any detectable 3-phase assemblage.

Sublimation is less common for CO_2-CH_4 than for CO_2-N_2 inclusions, but it has been observed in some samples. Almost only S2 behaviour is of real importance in the system; the other types are subordinate.

S1-type inclusions may only occur for inclusions of extremely low (or high) density and this type is therefore rare. Theoretically, all CO_2-CH_4 inclusions should contain 3 phases around -180°C, but small amounts of liquid (< 10 vol%) cannot be observed for higher molar volumes.

Fig.5.10.- *Phase sequences in CO_2-CH_4 inclusions at rising temperature as exemplified in $\bar{V}X$ diagrams (schematic). Denotations of the phase fields are as indicated in Fig.5.8.* ***a)*** *Type H2 inclusion* ***b)*** *type H4 (apparent H3) inclusion* ***c)*** *type H4 inclusion* ***d)*** *type S2 inclusion* ***e)*** *type S2 (apparent S1) inclusion (see text).*

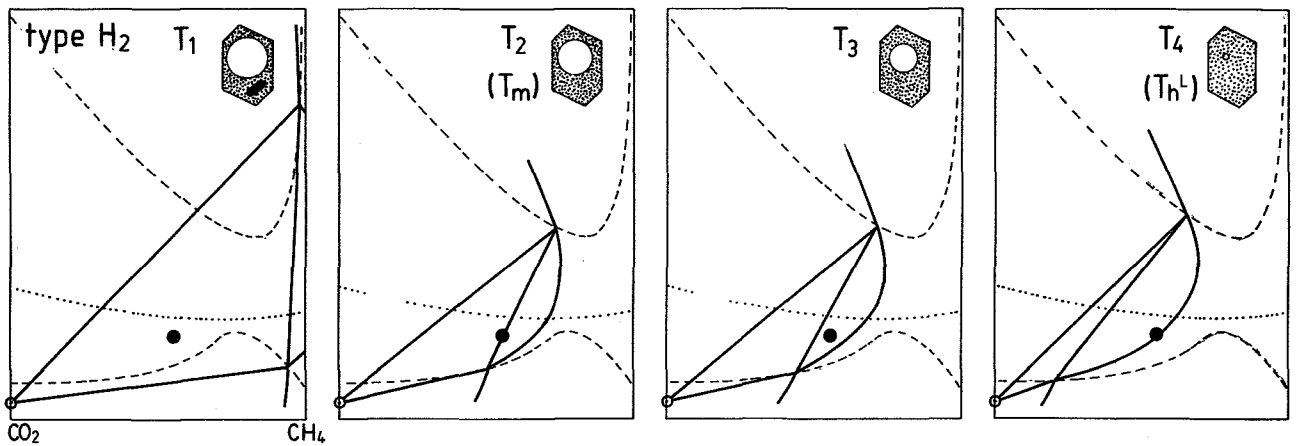

(Fig.5.10a)

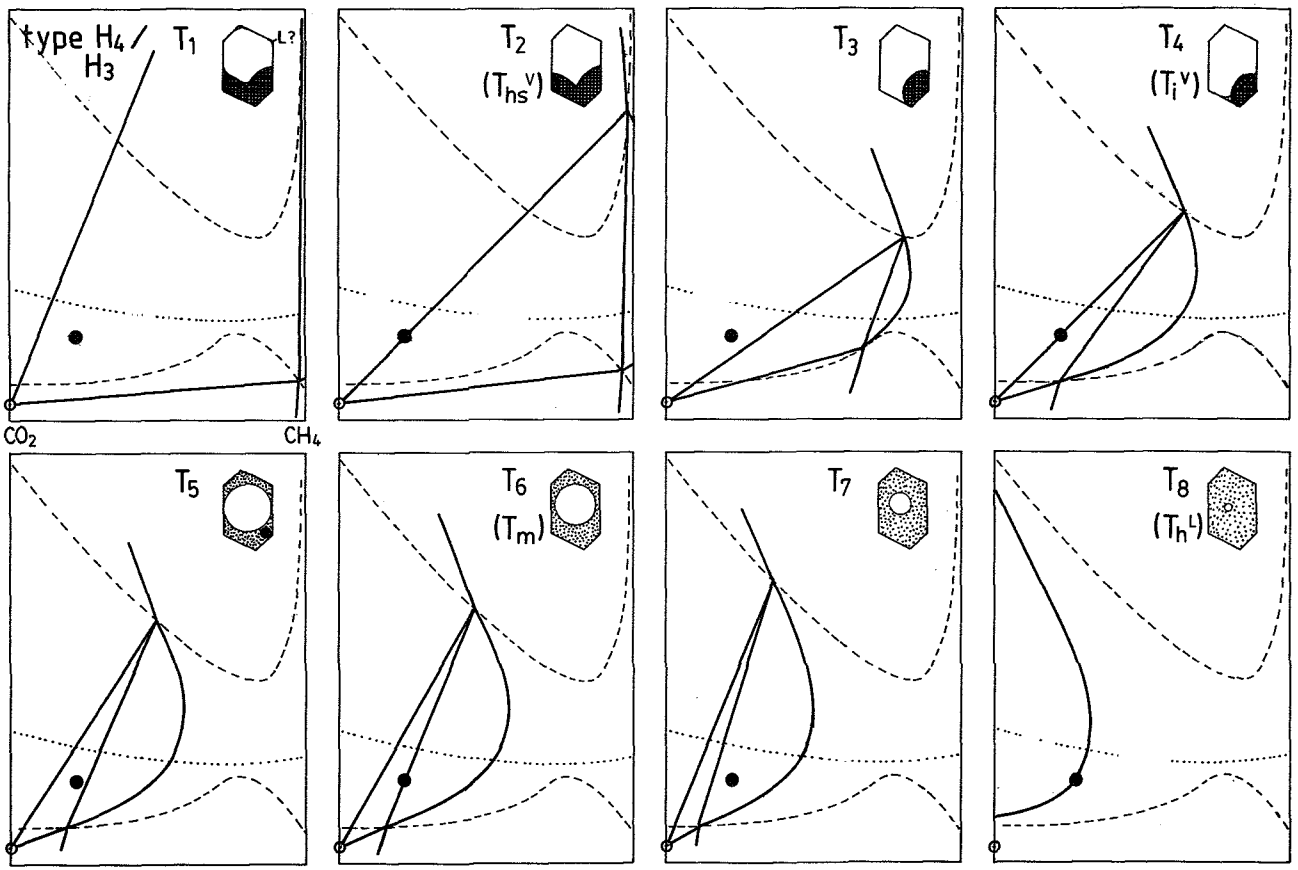

(Fig.5.10b)

(Fig.5.10c)

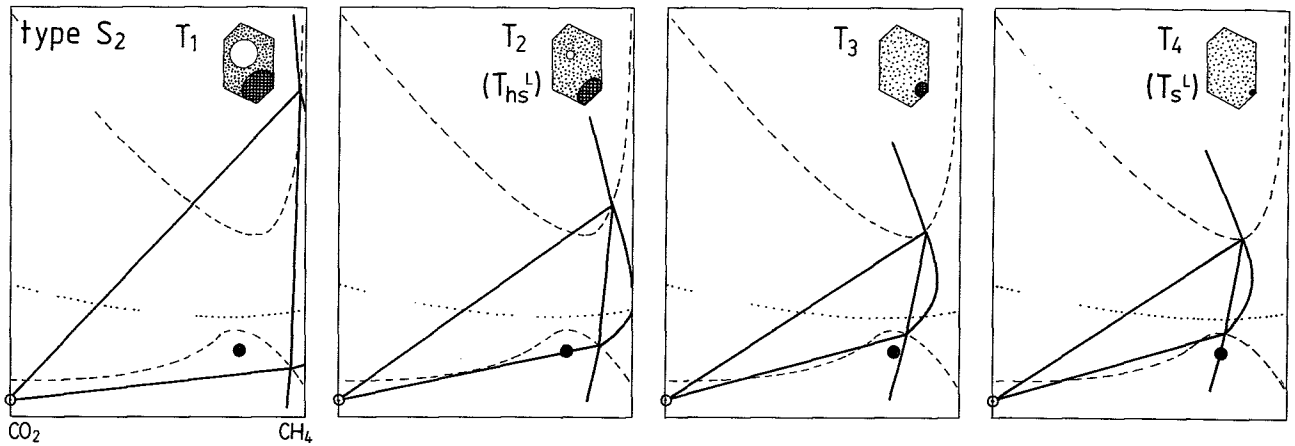

(Fig.5.10d)

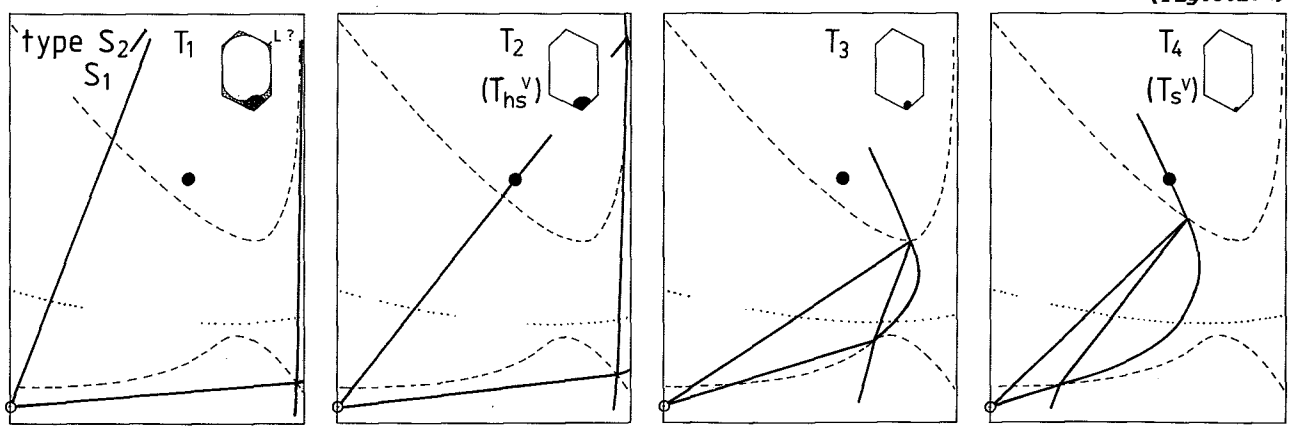

(Fig.5.10e)

2 Examples of S2-type inclusions (for high and low density) are shown in Figs.5.10d-e. The latter is probably observed as type S1; only inclusions characterized by sublimation to the liquid phase (S+L → L) can be clearly recognized as type S2. The $\bar{V}X$-conditions should plot between the L(+S+V) curve and line 4 in Fig.5.9a: $\bar{V}<63$ cm^3/mole and X_{CH4} is mainly restricted to CH_4-richer compositions. In Fig.5.10d, a 3-phase equilibrium is shown at T_1; successive homogenization (to the liquid) in the presence of solid CO_2 and sublimation (to the liquid) are represented at T_2 and T_4 respectively.

S3 and S4-type inclusions have not been observed for CO_2-CH_4 inclusions. This behaviour might be expected for extremely dense fluids as the equivalent of H4-type conditions below the L(+S+V) curve.

The XT diagram

Any fluid inclusion with a CO_2-CH_4 composition can now be classified by means of microthermometric studies and the $\bar{V}X$ diagram: indications can be obtained on composition and molar volume. Compositions can be checked by Raman analysis. Both the isothermal $\bar{V}X$ and the isochoric TX diagram can be used to find the numerical value of the molar volume. The use of the TX diagram is preferred here because it is more suitable for plotting microthermometric and Raman data. A theoretical model of the isochoric XT diagram for the system CO_2-CH_4 is shown in Fig.5.11. Shown are the liquidus conditions for the liquid and vapour compositions and the critical curves of the 1st and 2nd order (C_1 and C_2). The same stability fields as in the $\bar{V}X$ diagram are indicated, namely S+L+V, S+L, S+V, L+V and L or V. One isochoric section for $\bar{V}$ = 50 cm^3/mole is shown in Fig.5.12. The denotations of the phase transitions are also indicated in the latter figure. The homogenization point curve intersects the liquidus twice for $\bar{V}<65$ and $\bar{V}>225$ cm^3/mole. Homogenization can therefore be observed for both CO_2-rich compositions (type H3 and H2) and CH_4-rich compositions (type H1 and H2). The intermediate part, for $T_h < T_m$, is characterized by sublimation. Homogenization point curves do not intersect the liquidus for molar volumes between about 65 and 225 cm^3/mole and sublimation is forbidden for any composition.

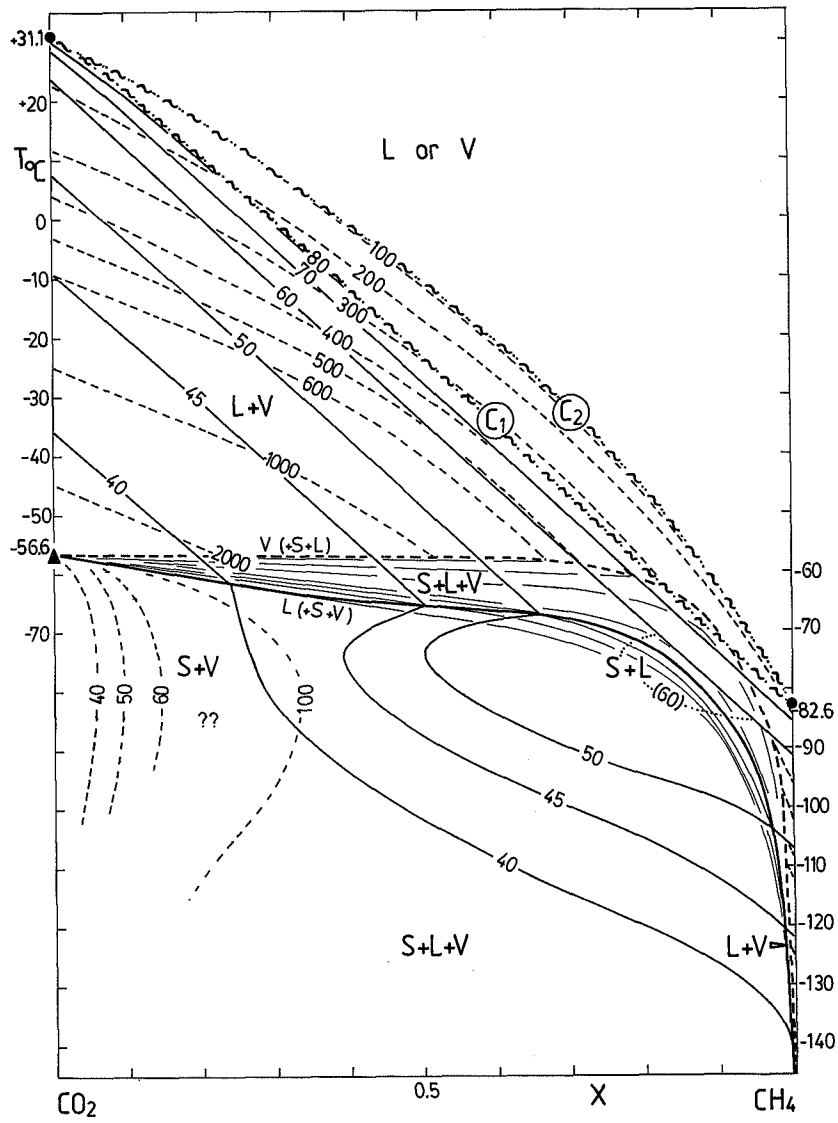

Fig.5.11.- *Isochoric projections (cm^3/mole) in the TX diagram for the system CO_2-CH_4. Phase transitions at varying temperature can be read for inclusions of given (total) molar volume and composition from the corresponding vertical (constant X) section; not indicated are the molar volumes and compositions of the single phases. The following phase fields are distinguished: S+L+V, S+L, S+V, L+V and L or V. Homogenization points are shown for the liquid (solid curves) and vapour phase (dashed curves). C_1 and C_2 denote the critical curves of the first and second order respectively. Solid CO_2 is only stable below the melting curves (intermediate between the liquidus conditions (L(+S+V) and V(+S+L)).*

Homogenization point curves do not intersect the liquidus for molar volumes between about 65 and 220 cm^3/mole: sublimation is not allowed at any composition for these values. The S+L field is reduced to higher molar volumes and does not exist for $\bar{V}$ > about 65 cm^3/mole; the S+V field expands to higher molar volumes, replacing S+L+V. The boundary between S+V and S+L+V is not sharply defined as it is also determined by the minimum amount of liquid which can be observed in a fluid inclusion (generally 10 vol%): the apparent S+V field is therefore more extended than is shown here.

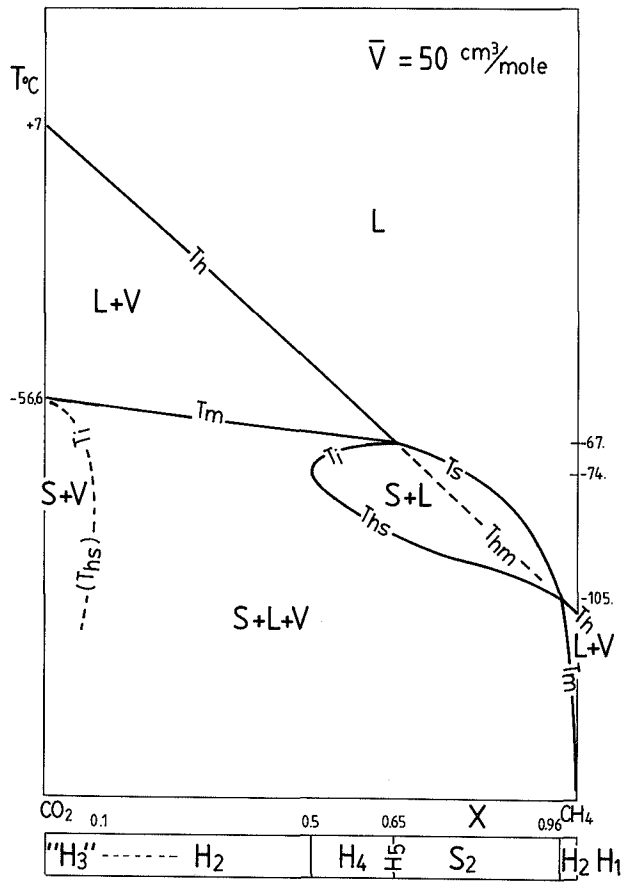

Fig.5.12.- *Isochoric section of the TX diagram for $\bar{V}$ = 50 cm^3/mole, showing the phase fields and the denotations of phase transitions as defined in Chap.III. Types of phase behaviour (H1-5 and S2) are determined for a given compositional range. A part of the theoretical H2 inclusions are observed as H3 because of the optical restriction to observe small amounts of liquid for the phase assemblage S+V+L.*

5.3.2. The system CO_2-N_2

The importance of the system CO_2-N_2 for the study of natural fluid inclusions is emphasized in this work; the system was also studied in more detail by experimental methods (Chap.VI). The experimental data from the literature are more limited than for the system CO_2-CH_4 and mainly rely on the paper of Arai et al. (1971). They comprise the PVTX-relations

of bubble and dew curves including critical data (for -20<T<+15°C) and parts of the monophase liquid and vapour regions for the same temperature range. The earlier work of Muirbrook (1964) contains PVTX-data for a temperature of 0°C only. His volumetric data generally deviate less than 10% from the data of Arai et al. (1971). The only equation of state applied to the system CO_2-N_2 is given by Darimont (1986) and Darimont & Heyen (1988). The calculated parameters of this equation are also based on the data of Arai et al. (1971). The equation was used for the extrapolation of experimental data to the region of the liquidus (around -56.6 to -70°C).

The two binary systems CO_2-N_2 and CO_2-CH_4 are very similar in many respects (Guilhaumou et al. 1981; Touret 1982): both systems are characterized by immiscibility of the solid phases and full miscibility of the liquid and vapour phases. The latter statement implies the presence of a continuous critical curve which was already shown in the preceding section for the system CO_2-CH_4. However, the pressure maximum of the 3-phase equilibria is at least 5 times higher for the system CO_2-N_2. This pressure rise can be explained by the more preferential partitioning of N_2 in the volatile phases. The critical curve shows only slightly higher pressures and is intersected by the 3-phase curve. In general, the continuity of the critical curve and therefore of the L+V-equilibria is determined by the relative positions of the 3-phase and critical curve (Campbell & Smith 1951 p.258-259; Smith 1963 p. 119-122). This can be illustrated with the help of a PT diagram (Fig.5.13a-c). Only invariant and univariant equilibria are shown for simplicity in this figure. A model of a binary system (with the properties mentioned above) can be obtained by selecting one of the shown examples for the critical curve (1, 2 or 3) and one of the examples for the 3-phase curve (a, b or c) in Fig.5.13a. The combinations 2b and 2c are representative for the systems CO_2-CH_4 (Fig.5.13b) and CO_2-N_2 (Fig.5.13c) respectively (A=CO_2; B=CH_4 or N_2). In the latter figure, the critical curve intersects the 3-phase curve twice, at points P and Q. Only the assemblage of solid CO_2 coexisting with one fluid phase is allowed at PT-conditions between these points; the 3-phase curve does not extend in this part. Critical conditions do neither occur between P and Q, except in the case of metastability i.e. if solid CO_2 is not yet formed during cooling below the melting temperature. Solid CO_2 is in equilibrium with a critical fluid <u>at</u> the conditions of points P and Q. The occurrence of this

assemblage (at melting) is characteristic for the system CO_2-N_2 and is not allowed in the system CO_2-CH_4.

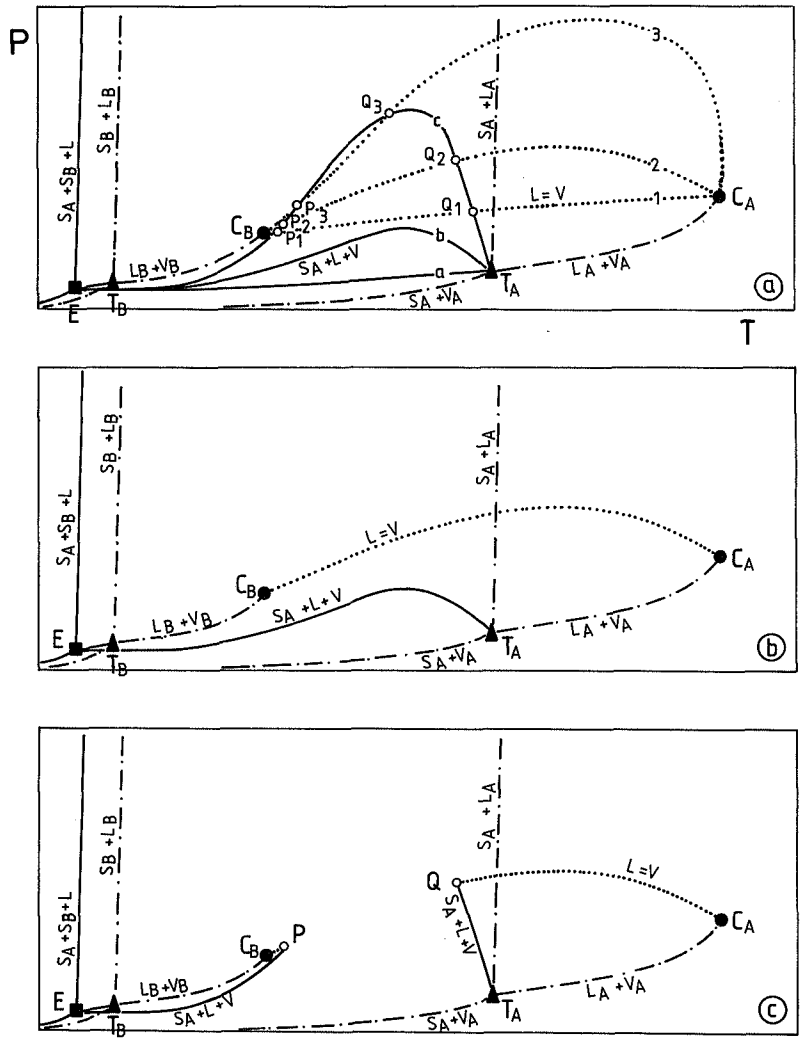

Fig.5.13.- ***a)*** *Schematic projections of univariant curves in binary systems with limited or no miscibility in the solid state and full miscibility in the liquid state (modified after Smith 1963). Three examples of melting curves (S+L+V) and three critical curves (L=V) are shown. The combination of b with 2 has a continuous critical curve* ***(b);*** *the combination of c with 2 has lower and upper critical endpoints (P and Q)* ***(c).*** *The two examples are representative for the systems* CO_2-CH_4 *and* CO_2-N_2 *respectively.*

PTX diagrams

The PT diagram discussed above can be considered as one of the 3 principle sections of the more general PTX diagram. The univariant curves of the system CO_2-N_2 represented in the remaining PX and TX diagrams are shown in Fig.5.14. The discontinuity of the system is evident in all sections. A more detailed PT diagram could be obtained from the Heyen equation (Fig.5.15). Shown are the 3-phase curve, the critical curve and some isopleths for the L+V equilibria. It was mentioned for the system CO_2-CH_4 that most probably no realistic eutectic point exists. This is the more true for the system CO_2-N_2 as the solubility of CO_2 in N_2 is even less than in CH_4: the eutectic should therefore coincide with the triple point of N_2. Accordingly, point P, the theoretical intersection point of the critical curve with the liquidus at the low temperature side, should coincide with the critical point of pure N_2. No solubility of CO_2 in N_2 is assumed at temperatures below that of the critical temperature of N_2 (-147°C), meaning that the composition of the volatile phases coexisting with solid CO_2 in this range consist of (almost) pure N_2 ($S+L_{N2}+V_{N2}$). Coexisting liquid and vapour (without solid CO_2) are restricted to pure N_2 inclusions. The position of point Q, the intersection of the critical curve and the liquidus at the high temperature side, can be estimated from the Heyen equation: T -70°C, P - 250 bar and X_{N2} - 0.75. These values are the result of extrapolations far outside the range of experimental data and are inaccurate. The results of the present experiments (see Chap.VI) indicate the following values: T - -62°C, P - 200 bar and X_{N2} - 0.57; the molar volume at point Q is around 40 cm^3/mole (see later in this chapter).

Fig.5.14.- *Univariant equilibria projections in the 3 principle sections of the PTX diagram (PT, PX and TX) for the system CO_2-N_2 (schematic). The melting curve (solid) is intersected by the critical curve (dotted) at P and Q. Dashed curves (in the PT diagram) indicate equilibria of the pure end-members.*

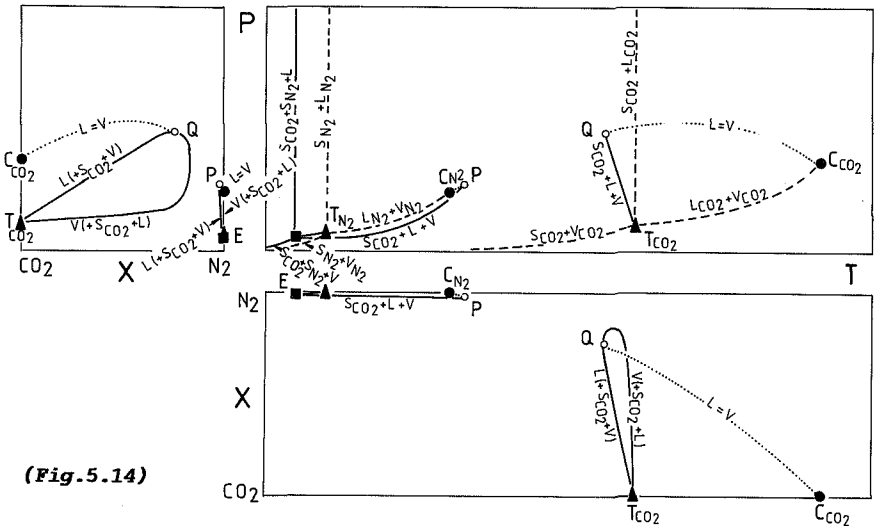

(Fig.5.14)

The $\bar{V}TX$ diagram

The advantage of the $\bar{V}TX$ diagram was discussed already for CO_2-CH_4 inclusions. A 3-dimensional representation of L+V immiscibility conditions of the system CO_2-N_2 is shown in Fig.5.16. This volume is bounded by melting and homogenization surfaces. A selection of some isothermal sections is also shown. Melting and homogenization temperatures are fixed for inclusions of given composition and molar volume. Projections parallel to the temperature axis result to the $\bar{V}X$ diagram. Fig.5.17a shows the part of this diagram covering the region of lower molar volumes, most interesting for the present use. This diagram was compiled from the data of Arai et al. (1971) for the higher temperatures (>-20°C); the conditions around the liquidus are derived from the Heyen equation; low temperature conditions (<-147°C) are obtained from present calculations (see later). The resemblance with the topology of the $\bar{V}X$ diagram compiled for the system H_2O-CO_2 is striking (Walther 1981, p.77). Both binary systems H_2O-CO_2 and CO_2-N_2 are discontinuous because of the limited solubility of their end-members. The system CO_2-H_2O is somewhat more complicated because the amount of H_2O cannot be assumed as zero below the critical temperature of CO_2 (+31.1°C) whereas the amount of CO_2 in the volatile phases below the critical temperature of N_2 (-147°C) can be neglected. A fundamental difference with the system CO_2-CH_4 (Fig.5.9a) is the twofold division of the curves

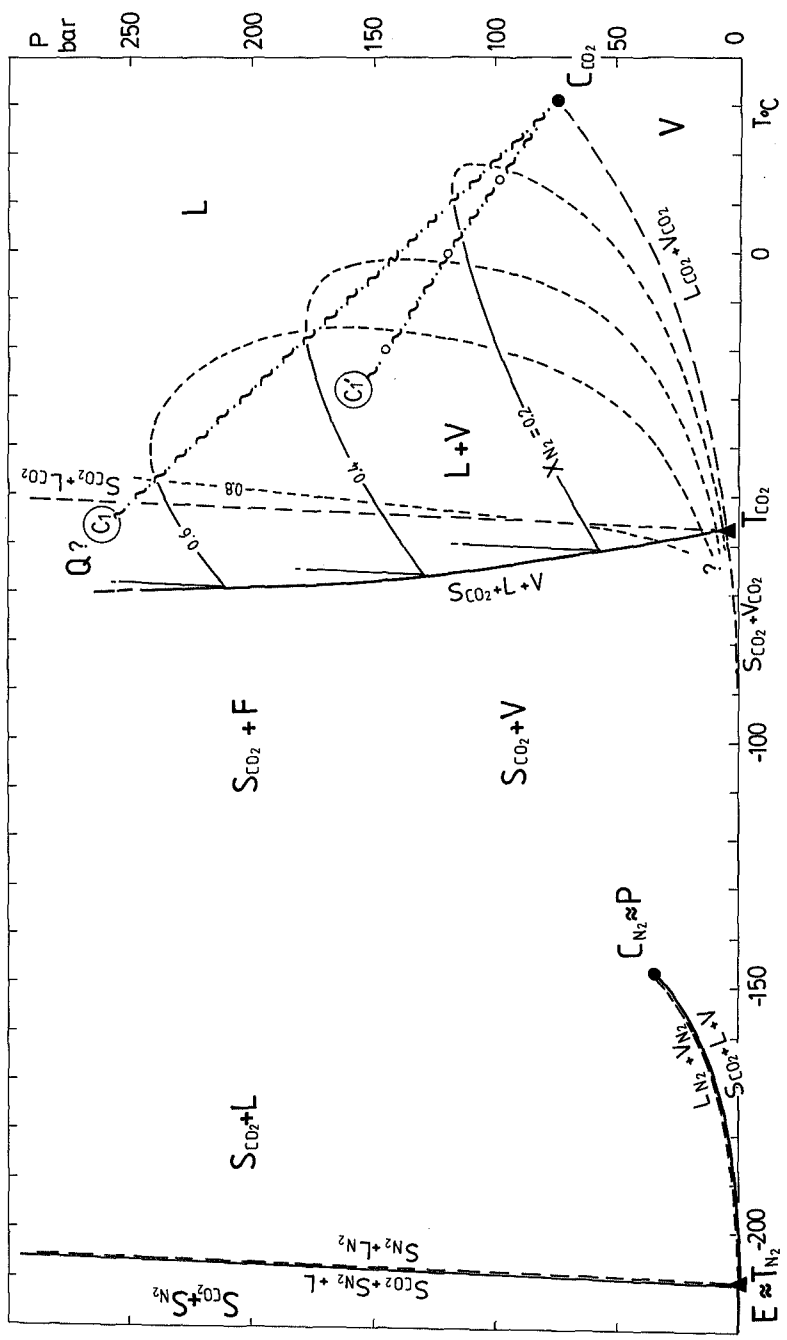
P bar
250
200
150
100
50
0
T°C
C_{CO_2}
L
V
$L_{CO_2}+V_{CO_2}$
C_1'
C_1
$S_{CO_2+L_{CO_2}}$
Q?
0.8
0.6
0.4
0.2
X_{N_2}
L+V
$S_{CO_2}+L+V$
T_{CO_2}
?
$S_{CO_2}+V_{CO_2}$
$S_{CO_2}+F$
$S_{CO_2}+V$
$C_{N_2}\approx P$
$L_{N_2}+V_{N_2}$
$S_{CO_2}+L+V$
-100
-150
-200
$S_{CO_2}+L$
$S_{CO_2+N_2}+L$
$S_{N_2}+L_{N_2}$
$S_{CO_2}+S_{N_2}$
$E\approx T_{N_2}$

(Fig.5.15)

Fig.5.15.- *The system CO_2-N_2 compiled from Arai et al. (1971), Angus et al. (1976, 1979) and Darimont (1986) (Heyen equation). Immiscibility of liquid and vapour is shown by (solid) boiling and (dashed) dew point curves. C_1 and C_1' denote the critical curve as estimated from the Heyen equation and from the experimental data of Arai et al. (1971) respectively. The system is somewhat disintegrated below the critical temperature of N_2 (-147°C): liquid and vapour are (almost) pure N_2. Consequently, the equilibria of the binary system coincide with the pure N_2 system in respect of pressure and temperature. Point P approximates the critical point of nitrogen (C_{N2}); the position of point Q is somewhat uncertain and could be better specified by the generation of synthetic inclusions (Chap.VI).*

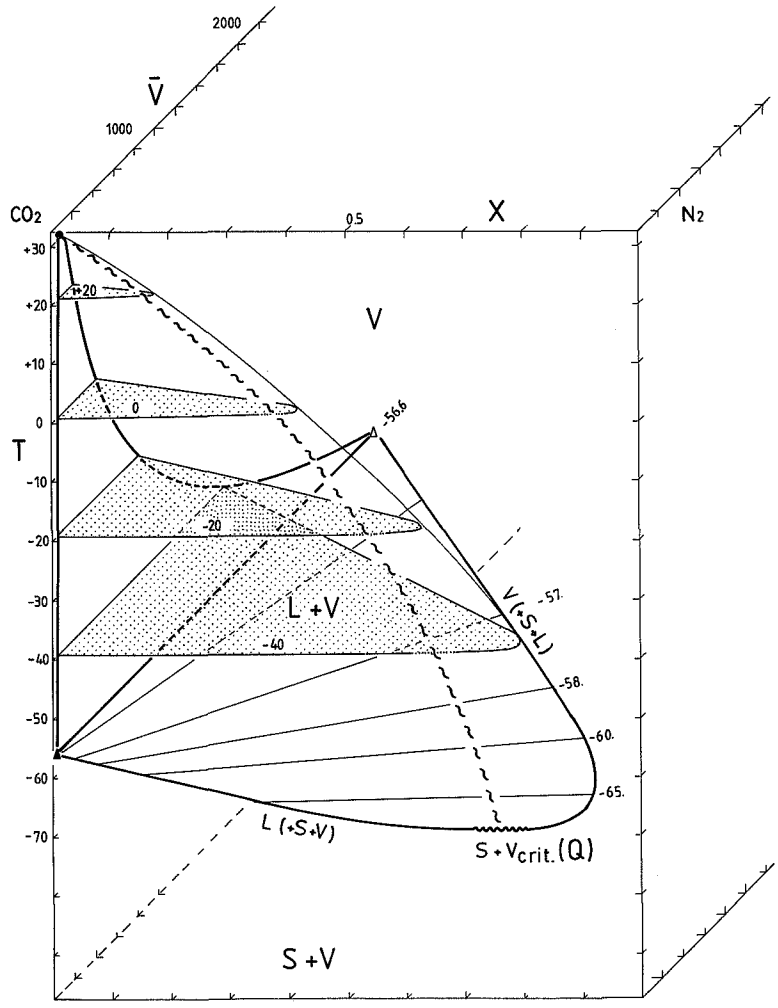

(Fig.5.16)

Fig.5.16.- *A part of the CO_2-N_2 system as represented in a 3-dimensional $\bar{V}TX$-diagram. Selected sections show isothermal conditions of LV immiscibility (stippled surfaces). Some tie-lines between coexisting L and V at melting are also indicated. Critical conditions plot along the wavy curve which intersects the 3-phase equilibria at point Q, characterized by the phase assemblage S_{CO2} + critical fluid.*

representing the vapour and liquid phases at the 3-phase stability conditions (V(+S+L) and L(+S+V)). The regions characterized by sublimation, S+L and S+V, are splitted for the system CO_2-CH_4, but joined for the system CO_2-N_2 (the stippled areas in Fig.5.9a and 5.17a). Sublimation (S-type behaviour) is characteristic for all inclusions with compositions of more than about 90 mole% N_2 (except for the pure N_2 inclusions). All inclusions with $\bar{V}X$-conditions plotting in the non-stippled area are characterized by homogenization (H-type). The critical curve of the 1st order (C_1) intersects the 3-phase curve around X_{N2} = 0.75 (point Q) and around the critical point of N_2 (point P). Fluid inclusions with $\bar{V}X$ properties plotting between the critical curves of the 1st and 2nd order are characterized by higher homogenization temperatures to the vapour phase with higher molar volume (lower density) (i.e. the constant volume equivalent of "retrograde condensation"). The points of retrograde condensation for T=+15, 0 and -20°C are given by Arai et al. (1971). This phenomenon might be expected for molar volumes between about 40 and 140 cm^3/mole and is more common for the system CO_2-N_2 than for the system CO_2-CH_4 as the two critical curves are much more divergent in the first system. Inclusions with lower molar volume than about 40 cm^3/mole (approaching the molar volume of the triple point of CO_2 at 37.347 cm^3/mole) always homogenize to the liquid phase. The most important forms shown in Fig.5.17a mark the phase transitions a) homogenization, b) melting and c) partial homogenization:

a) the curves marking homogenization temperatures (T_h) are isotherms for temperatures between -70 (point Q) and +31.1°C (the critical temperature of CO_2). The curves denote the phase transition L+V → L (below the 1st order critical curve) or L+V → V (above the critical curve).

b) the lines marking melting temperatures (T_m) (the dashed lines in Fig.5.17a) denote the phase transition S+L+V → L+V. Note that melting temperatures are not only influenced by the composition, but also by the molar volume: T_m is lowered by both higher N_2-contents and lower molar volumes (higher densities).

c) the lines marking partial homogenization temperatures of the N_2 fraction in the presence of solid CO_2 (T_{hs}) (S+L+V → S+L or S+V) were calculated by assuming no partitioning of CO_2 in the volatile phases below -147°C (see section 6.7.2). They are essentially tie-lines connecting solid CO_2 and LV-conditions at the "boiling" conditions of pure N_2. A fluid inclusion characterized by critical T_{hs} should plot on the tie-line connecting S_{CO2} and the critical point of N_2 (C_3 in Fig.5.17a).

Systematics of phase behaviour (type H and S)

The most important types of phase behaviour presently observed in CO_2-CH_4-N_2 inclusions are H3, H4 and S2; type S1, S3 and S4 behaviour was only found for extremely low molar volume ($\bar{V}$ ~ 40 cm^3/mole, van den Kerkhof 1988). Type H1, H2 and H5 inclusions have not been found for inclusions of mixed composition. The distribution in respect of $\bar{V}$ and X of the types of phase behaviour expected for CO_2-N_2 inclusions (discussed in Chap.III) is indicated in Fig.5.17b. The implications of these types for the system CO_2-N_2, are described below.

Type H1 inclusions are characterized by homogenization only in the temperature range between -180°C and +35°C. They should consist of pure N_2. Even the smallest amounts of CO_2 are assumed to be solidified at low temperature. However, solid CO_2 is not visible if its volume is too small. It is assumed from experience that a solid particle taking less than 1 vol% of the cavity cannot be observed. This value corresponds to a CO_2-N_2 inclusion containing 3 mole% of CO_2 with a molar volume around the critical $\bar{V}$ of N_2. Inclusions plotting at the right side of line 2 and below line 1 (in Fig.5.17b) are apparently of type H1 (see below); pure N_2 inclusions with a molar volume higher than about 310 cm^3/mole seem to be empty. Up to about 10 mole% of solid CO_2 may be overlooked for inclusions of molar volumes around 280 cm^3/mole and these are described as type H1; smaller amounts (< 3 mole%) of solid CO_2 should be possible to observe for the lowest molar volumes (<89.206 cm^3/mole).

Type H2 inclusions are characteristic for the system CO_2-CH_4 and do not occur for CO_2-N_2 inclusions.

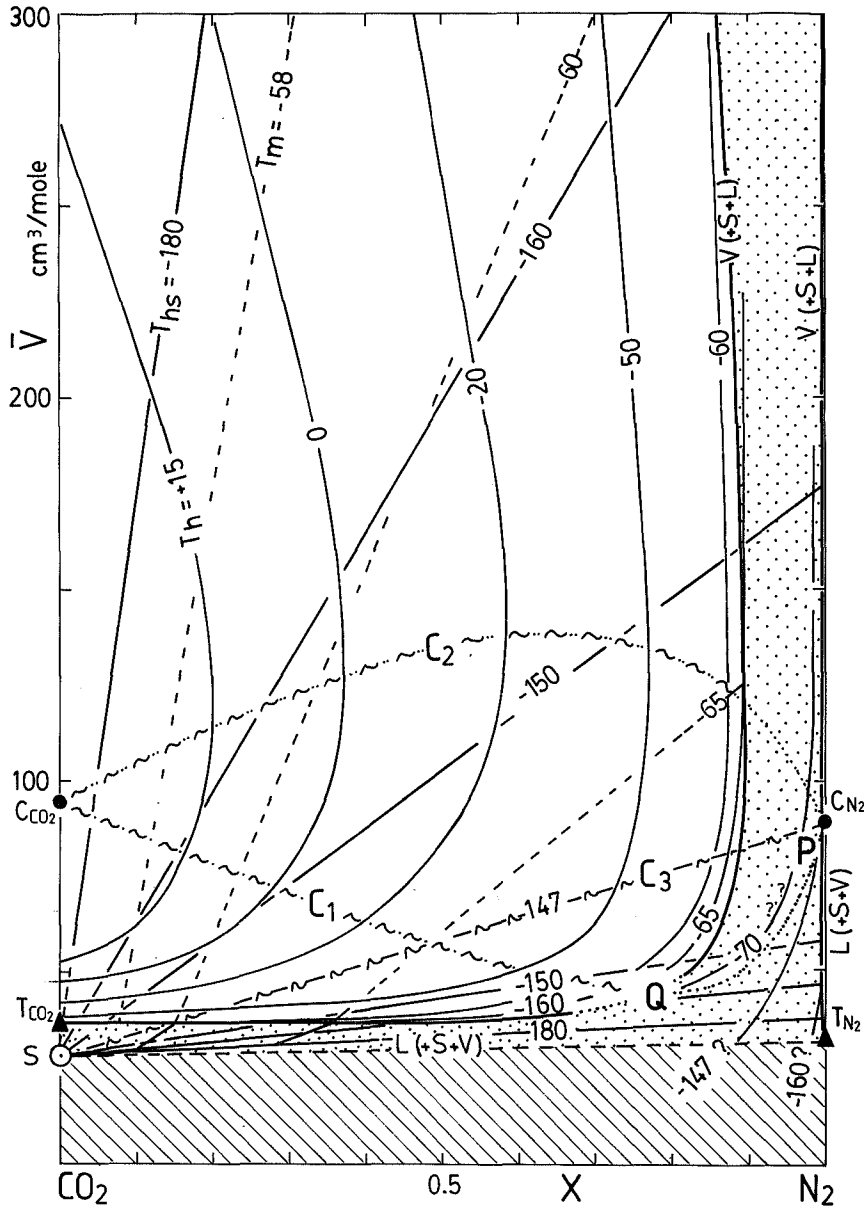
300
200
100
$\bar{V}$ cm³/mole
T_{hs} = -180
T_m = -58
T_n = +15
0
-20
-50
-60
-160
V (+S+L)
-60
V (+S+L)
C_2
-150
-65
C_{CO_2}
C_{N_2}
P
C_1
C_3
147
-65
-70
L (+S+V)
-150
-160
Q
T_{CO_2}
T_{N_2}
S
-180
L (+S+V)
-147 ?
-160 ?
CO_2
0.5
X
N_2

(Fig.5.17a)

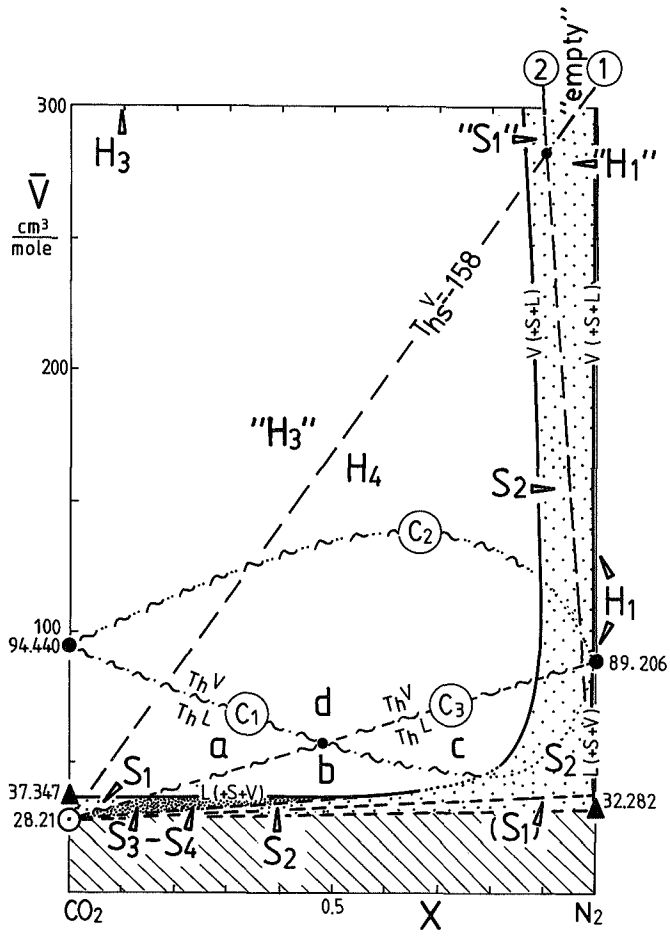

(Fig.5.17b)

Fig.5.17.- *Proportional $\bar{V}X$ diagrams of the system CO_2-N_2 for molar volumes between 28 and 300 cm^3/mole.*
a) *The 3-phase curves for the liquid and vapour phase (L(+S+V) and V(+S+L)) delimit the regions characterized by sublimation (stippled) and homogenization (open). The wavy-dotted curves C_1 and C_2 are the critical curves of the first and second order respectively. Fluids with $\bar{V}X$ properties plotting in the region between these curves are typified by retrograde condensation. Line C_3 indicates critical partial homogenization (T_{hs}^{C} = -147°C). A selection of isotherms (°C) marking final (>-70°C) and partial (<-147°C) homogenization temperatures is shown; dashed lines mark final melting.*
b) *(as Fig.5.17a) also indicating the distribution of phase behaviour (H and S types) (see text). Lines 1 and 2 delimit the observation of the liquid (<10 vol%) and solid phase (< 1 vol%) due to optical restrictions: N_2-rich inclusions with $\bar{V}$ > about 290 cm^3/mole may appear completely empty.*

Type H3 inclusions theoretically occur for pure or almost pure CO_2 compositions only. However, a part of the H4 inclusions are apparently classified as H3, because partial homogenization (T_{hs}) cannot be observed for higher values of the molar volume and lower N_2 contents (see below).

It was shown in section 5.3.1 that type H4 inclusions have restricted $\bar{V}$ and X for the system CO_2-CH_4, showing an exceptional behaviour (initial melting by the appearance of a bubble). Type H4 behaviour appeared to be much more characteristic for the system CO_2-N_2: most of the H-type inclusions (showing final homogenization) theoretically belong to this type. However, a part of the H4 inclusions are observed as H3, if the amount of liquid at low temperatures is too small to be observed. The tie-line representing T_{hs}^V = -158°C in the $\bar{V}X$ diagram (line 1 in Fig.5.17b) is taken as the boundary between the H4 and (apparent) H3 types. Inclusions plotting on this line show a liquid to vapour ratio of 10 vol% at -180°C, the lowest temperature which can normally be reached by cooling with liquid nitrogen. It is generally accepted that 10 vol% of liquid is the minimum amount which can be observed by optical means (Roedder 1984). Calculations are explained in Appendix 1. It is shown here that homogenization of N_2 (pure, or in the presence of solid CO_2) to the vapour phase cannot be observed below -158°C. However, lower temperatures are sometimes measured for irregular inclusions. Inclusions with higher $\bar{V}$ and/or higher X_{CO2} are observed as H3; those plotting at the other side of the line T_{hs} = -158°C (lower $\bar{V}$ and/or higher X_{N2}) are observed as H4.

The behaviour of type H4 inclusions is schematically illustrated with the help of the example of Fig.5.18a: at temperature T_1 (around -160°C), 3 phases are observed. Partial homogenization to the vapour phase (S+L+V → S+V) occurs during subsequent warming at T_2 (around -150°C). A liquid starts to form again at T_4 (around -65°C) by entering the 3-phase stability field (S+V → S+L+V). Contrary to CO_2-CH_4 inclusions, the liquid is the new formed phase during melting (except for the extremely dense S3 and S4 types). The stability of the 3 phases during melting is illustrated at T_5. The L+V field is entered at the temperature of final melting (T_6). Ultimately, final homogenization to the liquid phase is illustrated at T_8.

The relative positions of the 1st order critical curve (C_1 in Fig.5.17b) and the line defining critical partial homogenization (C_3 = S+Vcrit) give rise to make a distinction of 4 types of H4 behaviour

showing different combinations (a, b, c and d) of the homogenization (T_h) and partial homogenization (T_{hs}) character: curve C_1 separates homogenization to the liquid and to the vapour (L+V → L or V); line C_3 separates partial homogenization to the liquid and vapour (S+L+V → S+L or S+V). An inclusion with $\bar{V}T$-conditions plotting exactly on the intersection point show both critical homogenization (T_h^C) and critical partial homogenization (T_{hs}^C). The following types are distinguished (Fig.5.17b):

a) T_h to the liquid; T_{hs} to the vapour phase. The $\bar{V}X$-conditions of these inclusions plot below curve C_1, but above C_3. N_2-contents are lower than about 50 mole% and molar volumes are lower than 94.44 cm^3/mole;

b) both T_h and T_{hs} are to the liquid phase ($\bar{V}X$-conditions plot below curves C_1 and C_3). The compositions of these inclusions are intermediate between CO_2 and N_2 ($0.1<X_{N2}<0.8$); molar volumes should be lower than about 60 cm^3/mole;

c) T_h to the vapour; T_{hs} to the liquid phase ($\bar{V}X$-conditions plot above C_1, but below C_3). These inclusions are rich in nitrogen ($X_{N2} > 0.5$) and molar volumes should be lower than about 80 cm^3/mole;

d) both T_h and T_{hs} are to the vapour phase ($\bar{V}X$-conditions plot above curves C_1 and C_3). N_2-contents are between about 0.1 and 0.9; molar volumes are higher than about 60 cm^3/mole (low density).

It should be noted that C_1 and C_3 do not represent sharply defined curves and they should be seen as a transition zone between liquid and vapour: critical conditions cover a wider region than indicated by the curves. Homogenization to liquid or vapour has been frequently observed as "near" critical.

Type H5 behaviour has only been noticed as a special type of H4 in CO_2-CH_4 inclusions and do not occur in CO_2-N_2 inclusions.

Inclusions showing sublimation are rich in N_2 (covering a large volumetric range), or poor in N_2 (limited to extremely low molar volumes):

Type S1 inclusions occur for fluids of extremely low (S+L → L) or extremely high molar volume (S+V → V). Contrary to the system CO_2-CH_4, even small amounts of solid CO_2 may sublimate (without the forming of a

melt). S1 behaviour has been found in the high density inclusions from the Furua Granulite Complex, Tanzania. Homogenization temperatures can be measured only "metastably". The N_2-content of these inclusions is about 30-40 mole%, but S1 behaviour is expected to be also possible for higher N_2-contents.

Type S2 inclusions have been frequently observed in CO_2-N_2 inclusions. Guilhaumou et al. (1981) described both S2 and H4 behaviour for inclusions from Tunisia. S2 is also one of the most frequently occurring types in the experimentally produced fluid inclusions of higher N_2-content (see Chap.VI).

The phase behaviour of type S2 is illustrated with the help of Fig.5.18b (showing sublimation to the liquid) and Fig.5.18c (showing sublimation to the vapour). Sublimation is preceded by partial homogenization (T_{hs}) to the liquid and vapour respectively. Sublimation is detected in the temperature range between -147 and -70°C. "Final" homogenization temperatures can sometimes be measured metastably. It should be noted that small particles of solid CO_2 may be overlooked and S2 inclusions may be observed as type H1. Sublimation has been observed for fluid inclusions containing less than 3 mole% CO_2 (see also Darimont 1986). Tie-line 2 in Fig.5.17b represents a solid content of 1 vol% assumed that all CO_2 is present in the solid phase. The line points to $\bar{V}$ = 2820 cm^3/mole for pure CO_2 (see App.1, application 3). The solid phase can only be observed for inclusions plotting left of line 2 (type S2); a solid is not visible for inclusions plotting at the other side of the line and they are apparently of type H1. It is interesting to consider the intersection point of line 1 (discussed above) and line 2 which plots in the S2 field. Around this point, 4 types of apparent phase behaviour can be grouped (Fig.5.17b):

a) S2 type inclusions (also be observed as such), plot below line 1 and left of line 2;

b) apparent H1 type ("H1") inclusions plot below line 1 and to the right of line 2;

c) inclusions plotting above line 1 and to the right of line 2 seem to be empty at -180°C (but the amounts of solid and liquid are too small to be observed);

d) apparent S1 ("S1") inclusions plot above line 1 and to the left of line 2.

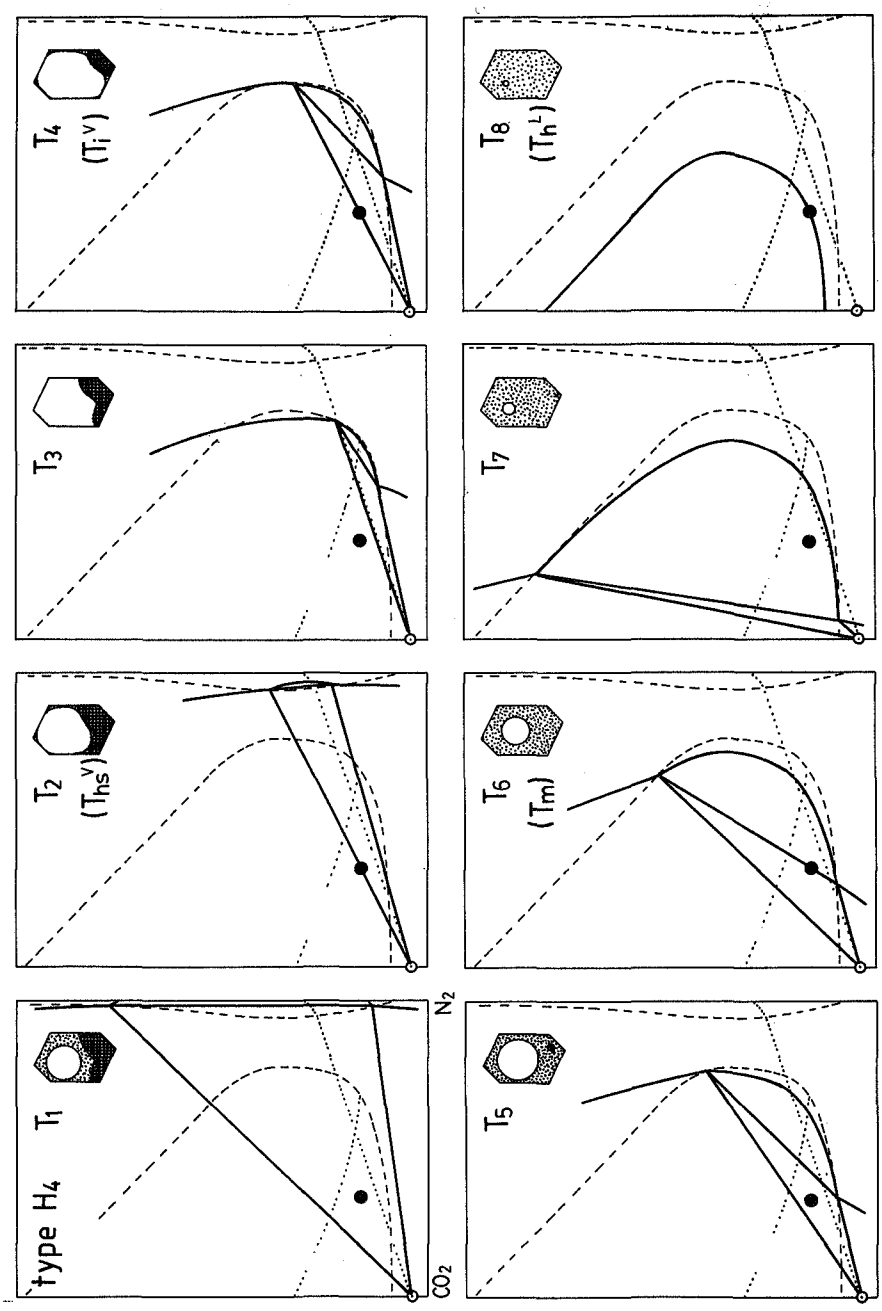

(Fig.5.18a)

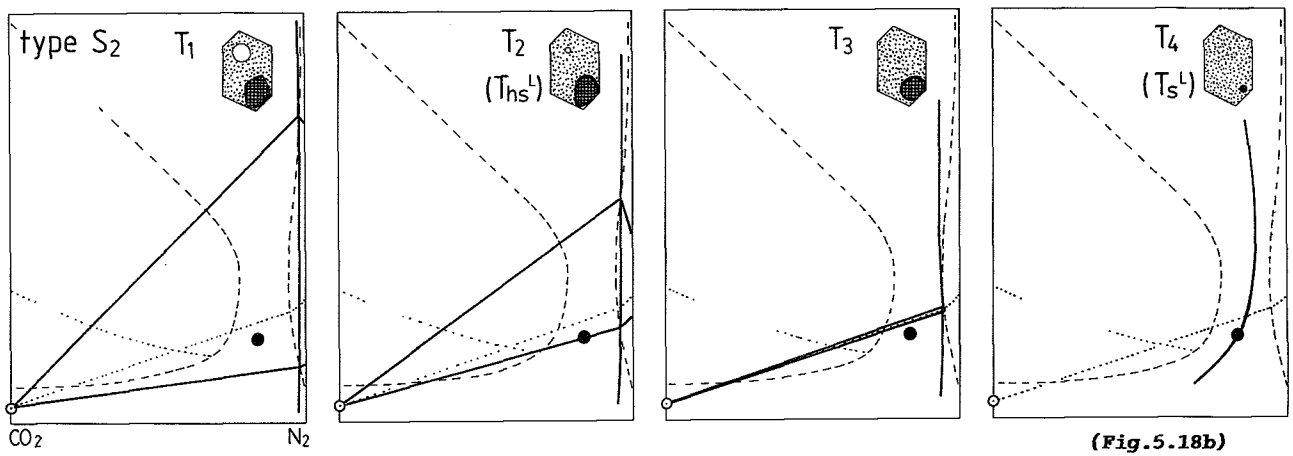

(Fig.5.18b)

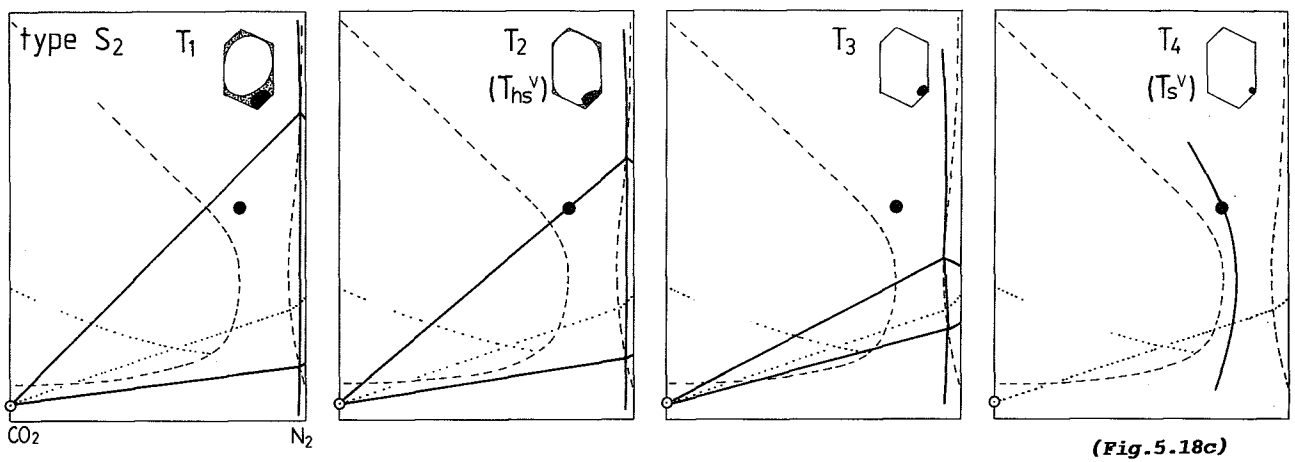

(Fig.5.18c)

Fig.5.18.- *Examples of phase sequences in CO_2-N_2 inclusions at rising temperature in the $\bar{V}X$ diagram (schematic). Denotations of the phase fields are as indicated in Fig.5.8.* ***a)*** *Type H4 inclusion* ***b)*** *type S2 inclusion (low molar volume)* ***c)*** *type S2 inclusion (high molar volume) (see text).*

Type S3 and S4 inclusions both represent extremely dense CO_2-N_2 fluids. This type has only been observed in the samples from Furua (Tanzania). Characteristic is the homogenization of liquid and vapour phases to the liquid during melting (S+L → S+L+V → S+L) in the temperature range from -65 to -61°C. Partial homogenization (T_{hs}^{L}) is observed as well for type S4 inclusions (of somewhat higher N_2-content). The $\bar{V}X$-conditions are very limited and should plot below the L(+S+V) curve, in the wedge-shaped area between line C_3 and the tangent tie-line (S_{CO2} L(+S+V): N_2-contents are less than about 50 mole% and molar volumes are around the value for the triple point of CO_2.

It was shown in the foregoing how the microthermometric behaviour of "gaseous" inclusions are interpreted in respect of composition and molar volume. Some types of phase behaviour are characteristic for one of the 2 systems CO_2-CH_4 or CO_2-N_2: H4-type inclusions (showing "normal" initial melting) are unique for the system CO_2-N_2 whereas H2-type inclusions are unique for CO_2-CH_4.

The TX diagram

The temperatures measured by microthermometry together with the compositions can be plotted in a TX diagram. A theoretical model of an isochoric TX diagram is shown in Fig.5.19. Note that this diagram is, as the isothermal $\bar{V}X$ diagram, only an alternative section of the $\bar{V}TX$ diagram. The most marked forms of the diagram are the L+V and the S+L+V fields, both characterized by the existence of a bubble. The curves marking partial homogenization (T_{hs}) are constructed by calculations demonstrated in section 6.7.2. T_{hs} to the liquid phase (S+L+V → S+L) is only found for inclusions of higher N_2-contents; T_{hs} grades to critical homogenization (S+L+V → S+V_{crit}) and subsequently to the vapour phase (S+L+V → S+V) going to CO_2-richer compositions. It was mentioned earlier that partial homogenization to the vapour below -158°C can generally not be observed. Curves C_1 and C_2 denote the critical curves of the first and the second order. It can be seen that homogenization

temperatures are drastically lowered with increasing amounts of N_2. This lowering is accompanied with homogenization to the liquid phase grading to homogenization to the vapour phase when passing the 1st order critical curve. Homogenization to the vapour phase does therefore not always indicate low fluid densities, but may also indicate high N_2-contents of a high density fluids. Melting temperatures are only slightly lowered with increasing N_2-contents and even hardly lowered for inclusions of high molar volume (low density).

One section of the TX diagram, for $\bar{V}$ = 50 cm^3/mole, is shown in Fig.5.20. The phase stability fields and the denotations of the curves are also shown. Note the differences between the systems CO_2-N_2 and CO_2-CH_4 at a constant molar volume of 50 cm^3/mole (cf. Figs.5.12 and 5.20): the 3-phase field is restricted to temperatures below -147°C and to temperatures just below final melting for the system CO_2-N_2.

The positions of the sublimation curves (T_s) are not exactly known, but fluid inclusion studies indicate that sublimation temperatures mostly plot on the extrapolated melting curves; T_s is only drastically lowered for almost pure N_2 compositions.

The stability field of L+V in Fig.5.19 was obtained from the Heyen equation of state (Darimont 1986). This equation appeared to produce somewhat deviant results than the original data of Arai et al. (1971). The critical curve obtained from the latter source is also shown in the figure (C_1'). However, critical conditions are generally difficult to reproduce by equations of state and are not beforehand indicative for the accuracy of the equation. Deviations from the other LV-data show that the equation becomes inaccurate for extrapolations below -20°C. A similar diagram was therefore constructed from the results of presently made experiments (Chap.VI, Fig.6.20). A comparison between this model and the model of Heyen/Darimont is made in section 6.7.4. The most noticeable discrepancies concern a) the position of the intersection point of C_1 and the liquidus (point Q) at N_2-richer compositions b) a much less lowering of melting temperatures c) the position of the critical curve and d) a more widespread occurrence of retrograde condensation for the experimental model.

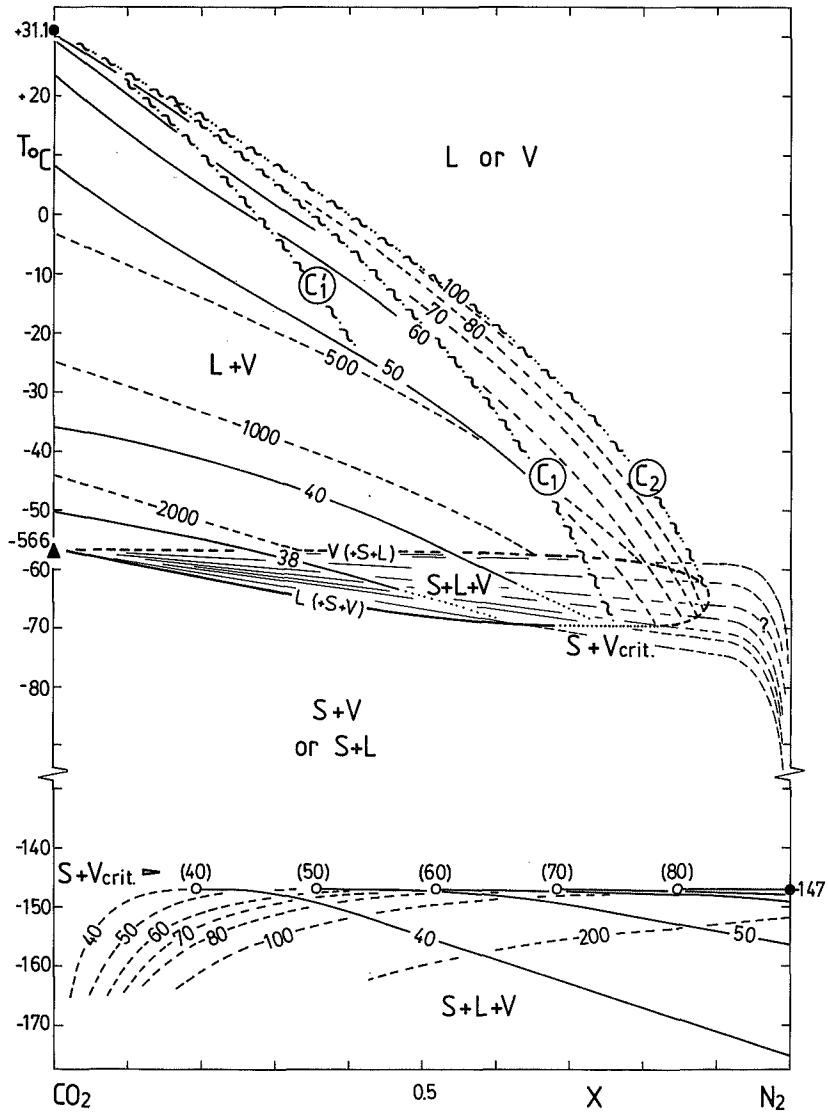

Fig.5.19.- *Isochores (cm^3/mole) in the TX diagram for the system CO_2-N_2 compiled from Darimont (1986) and present calculations. Phase transitions at varying temperature can be read for inclusions of given (total) molar volume and composition from the corresponding vertical (constant X) section; molar volumes and compositions of the single phases are not indicated. The following phase fields are distinguished: S+L+V (divided into 2 parts), S+L or S+V, L+V and L or V. Partial and final homogenization is shown to the liquid (solid curves) and vapour phase (dashed curves). C_1 and C_1' denote the critical curve (of the first order) obtained from the Heyen equation and from Arai et al. (1971) respectively; C_2 denotes the critical curve of the second order.*

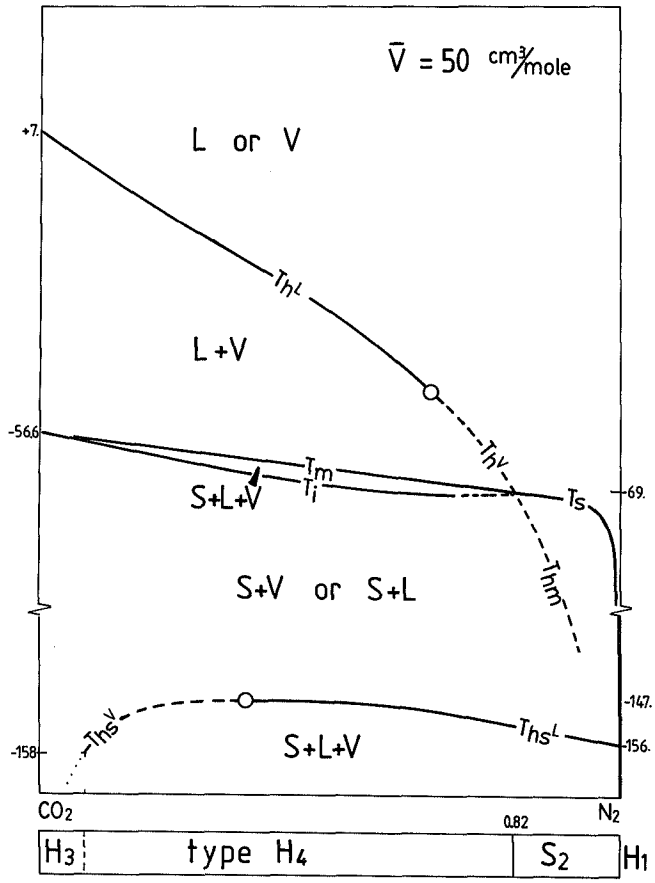

Fig.5.20.- TX diagram with the isochoric section for $\bar{V}$ = 50 cm³/mole, showing the phase fields and denotations of phase transitions as defined in Chap.III. Types of phase behaviour (H1, H3, H4 and S2) are defined for given compositions. Open circles denote critical partial and final homogenization. Partial homogenization (to the vapour phase) can generally not be observed below -158°C.

5.3.3. The system CH_4-N_2

Phase transitions in the system CH_4-N_2 only occur at temperatures below -82.6°C (the critical temperature of methane). Only liquid-vapour immiscibility can be observed by using equipment cooled by liquid nitrogen; freezing temperatures (below -182.5°C) can normally not be reached. According to the present definitions, all CH_4-N_2 inclusions are classified as type H1. It was found by Raman analysis that small amounts of CO_2 may be present in natural fluid inclusions mainly consisting of CH_4-N_2 (see below). These inclusions are apparently of type H1 (if the solid is too small to be observed), or they are classified as type H2 (mostly CH_4-rich) or S2 (mostly N_2-rich) to somewhat higher CO_2-contents.

Data on the binary system CH_4-N_2 in the low temperature region could be obtained from the literature. PVTX-data on liquid-vapour equilibria as well as the critical conditions are published in the Landolt-Börnstein tables (1960); data on solid-liquid equilibria (freezing and melting points) are published in Timmermans (1960), Stephen & Stephen (1963) and Omar (1962). In the latter publication 3-phase equilibria and an extensive description of the system are given. Swanenberg (1980) calculated the molar volumes in the region of L-V-immiscibility by the extrapolation of the MRK-equation of state to the boiling point curves.

General characteristics of the system

Solid methane and nitrogen are partly miscible, contrary to the systems CO_2-CH_4 and CO_2-N_2 where the solid phases are pure components; the liquid and gas phases are fully miscible in all mentioned systems. A distinction can be made between 2 phase complexes: 1) LS-equilibria denoted by freezing (L+S → S) and melting point curves (L+S → L) and 2) LV-equilibria denoted by boiling point and dew point curves. These complexes interfere at temperatures below -183°C (and P<0.68 bar): the L+V and L+S fields intersect favouring the stability of S+V (i.e. the "sublimation" field). Sublimation of solid CH_4 or N_2 is only possible for inclusions of extremely high or low molar volume and is not further considered here.

The system CH_4-N_2 is discussed below with the help of 1 principle section of the PTX diagram (isoplethic PT) and 2 principle sections of the $\bar{V}$TX diagram (isochoric TX and isoplethic $\bar{V}$T diagrams).

The PT diagram

Multiphase equilibria in an isoplethic PT diagram are shown in Fig.5.21. A similar diagram was constructed by Swanenberg (1980, Fig.10). It can be seen that the critical curve has a pressure maximum at P=50 bar (T=-105°C; X_{N2}=0.44). Boiling and dew point curves indicate the limits of LV-immiscibility for a given composition. 3-Phase equilibria occur at temperatures between -211 and -183°C and have a pressure maximum of about 0.68 bar (T=-191°C).

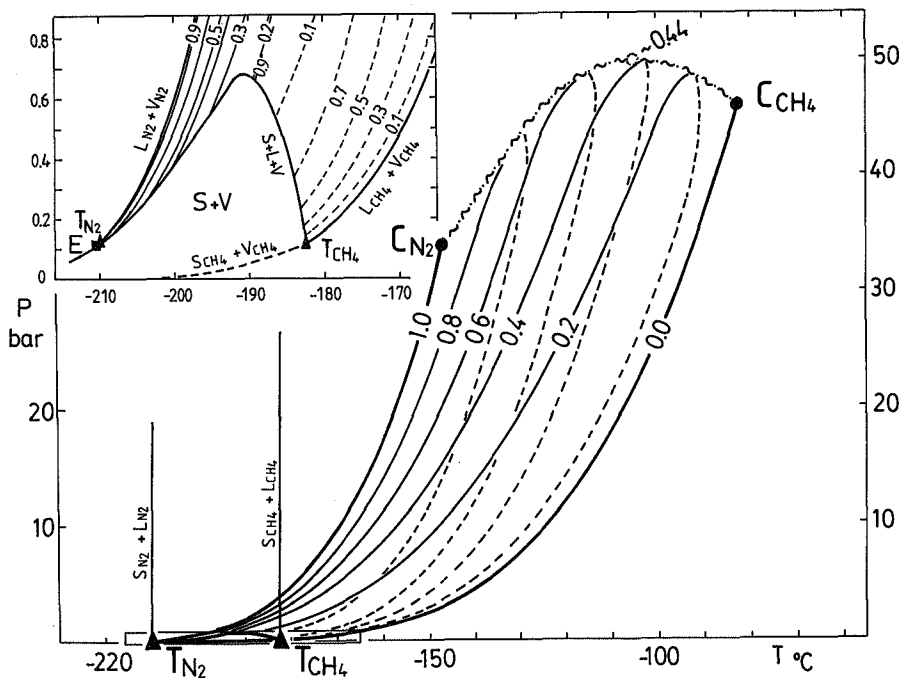

Fig.5.21.- *The system CH_4-N_2 compiled from Landolt-Börnstein (1960), Omar (1962) and Angus et al.(1976, 1979). Isopleths show LV immiscibility for the intermediate compositions. The inset shows 3-phase equilibria in detail.*

VTX diagrams

Representation of LS-equilibria in a TX diagram is most illustrative (Fig.5.22). The positions of the freezing and melting curves are about pressure independent and these curves can therefore be considered as polybaric (and polychoric). The system shows an eutectic (quadruple point) at X_{N2} = 0.762 and T = -210.6°C (Omar 1962). This temperature approximates the temperature of the triple point of pure N_2 (-210.0°C). Melting temperatures for compositions between 76.2 and 100 mole% N_2 are about constant. Crystals of mixed composition (up to $CH_4(55)N_2(45)$) may form showing that the amount of N_2 which is soluble in solid methane is less than 45 mole%. There is no evidence for the forming of an other condensed phase of intermediate composition (Omar 1962). The L+S-field is somewhat degenerated to N_2-rich compositions as freezing and melting points differ less than 0.6°C. The solid phase may occur as 2 modifications: cubic crystals (α) of CH_4-rich composition or (at

temperatures higher than -237.7°C) hexagonal crystals (β) of N_2-rich composition.

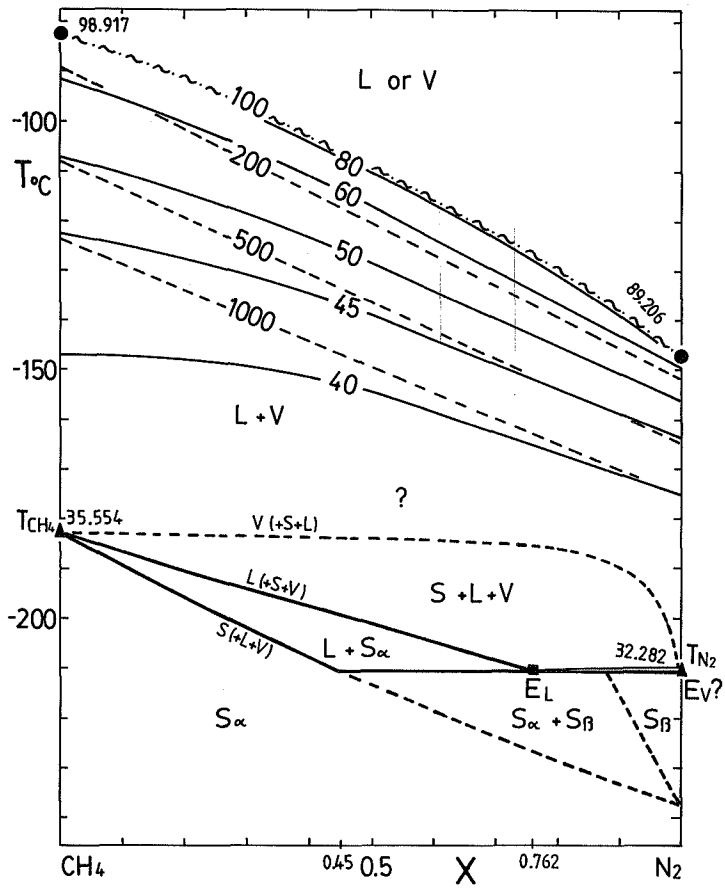

Fig.5.22.- *Isochores (homogenization point curves) for CH_4-N_2, indicated for molar volumes between 40 and 1000 cm^3/mole: solid curves are homogenizations to the liquid, dashed curves to the vapour phase. The wavy-dotted curve indicates the critical conditions. (Polychoric) LS equilibria occurring at temperatures between -211 and -183°C are also shown. Note the existence of mixed crystals which may occur as different modifications (α and β).*

Swanenberg (1980) estimated the molar volume of LV-equilibria by extrapolation to the conditions of interest by using the MRK equation of state. The molar volume of intermediate compositions between CH_4 and N_2 could be calculated by this method. The results represented as homogenization point curves in an isochoric TX diagram are shown in

Fig.5.22. It can be seen that T_h is gradually lowered with higher amounts of N_2. Isochores representing higher molar volumes (to the vapour phase) are estimated by linear extrapolation between the 2 end-members as it can be assumed that these fluids approximate ideal gas behaviour; isochores are slightly curved to lower molar volumes. Molar volumes for fluid inclusions of known homogenization temperature and composition can be read from Fig.5.22 or from the isoplethic $\bar{V}X$ diagram (Fig.5.23). Note that the determination of the molar volume is inaccurate around the critical conditions because $\bar{V}$ drastically changes with T_h in this region.

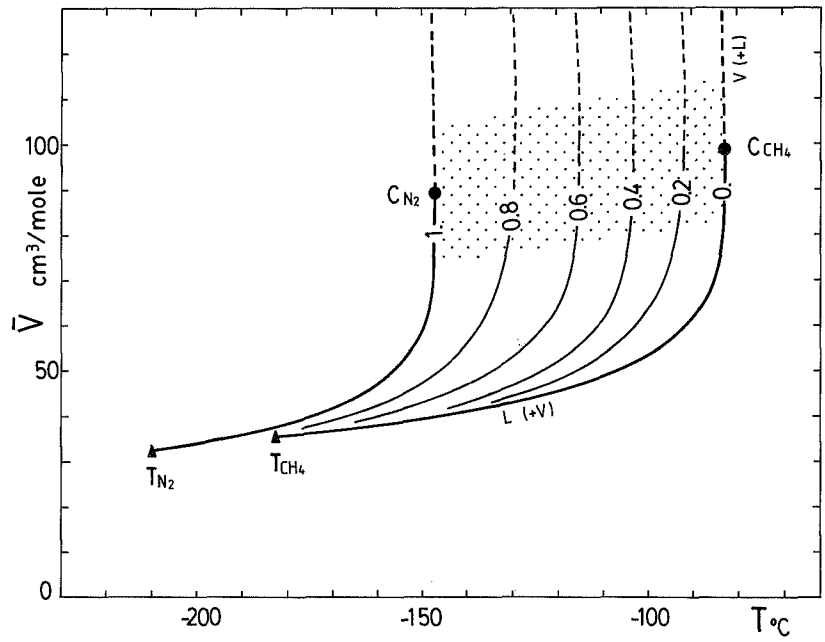

Fig.5.23.- *The molar volume of CH_4-N_2 mixtures as a function of homogenization temperature (revised after Angus et al. 1976, 1979 and Swanenberg 1980). The stippled area indicates (near) critical conditions.*

Molar volume of CH_4-N_2 (± CO_2)

The presence of small amounts of CO_2 (< 20 mole%) affects the total molar volume of the fluid: $\bar{V}$ as calculated from T_h or T_{hs} will therefore be too high. A correction of the molar volume can be made by assuming that all CO_2 is partitioning in the solid phase at the temperature of

homogenization. The total molar volume ($\bar{V}_t$) can be expressed by

$$\bar{V}_t \quad X_S.\bar{V}_S + X_V.\bar{V}_V \qquad \text{(Eq.5.10a)}$$

where X_S and X_V denote the molar fractions of solid CO_2 and vapour (or liquid) phase (CH_4-N_2) respectively; $\bar{V}_S$ and $\bar{V}_V$ denote the molar volume of the phases. Taking $X_V = 1-X_S$ and $\bar{V}_S = 28.2$ cm^3/mole, Eq.5.10a can be re-written as

$$\bar{V}_t \quad \bar{V}_V - X_{CO2}\cdot(\bar{V}_V-28.2) \qquad \text{(Eq.5.10b)}$$

Example: A fluid inclusion shows a homogenization temperature of -130°C to the liquid phase (near critical); Raman analysis results to a composition of X_{N2}=0.75, X_{CH4}=0.15 and X_{CO2}=0.10. The molar volume of the fluid fraction (with a composition of X_{N2}= about 0.8) at low temperatures is about 80 cm^3/mole (Fig.5.23). The total molar volume of the inclusion is estimated to be 80-5 = 75 cm^3/mole (Eq.5.10b).

Note that the effect of small amounts of CO_2 on $\bar{V}_t$ is not very large compared to the accuracy of the molar volume: the molar volume of inclusions showing about critical homogenization, determined for CH_4-N_2, differs less than 10% for $X_{CO2}<0.15$.

Observations of phase equilibria below -180°C

The use of liquid helium as a coolant permits the detection of freezing and melting temperatures of CH_4-N_2 inclusions. The only fluid inclusion data known to the author for these low temperatures are given by Kreulen & Schuiling (1982) for samples from Dôme de l'Agout (France). Solidification ("freezing") temperatures were recorded of about -220°C, 10 degrees below the eutectic temperature. This can be explained by the metastability of the liquid phase or by incorrect calibration in this temperature range (Kreulen pers. comm.). Temperatures of final melting were found between -207 and -198°C corresponding to N_2-contents of 42 to 68 mole%.

Some examples of natural inclusions

Fluid compositions of (almost) pure CH_4 or N_2 frequently occur in rocks. These fluids are often found as end-members of mixtures with CO_2

(e.g. fluids found in samples from the Appalachian Mountains, U.S.A. and from silicious marbles from Pusula, SW Finland). Intermediate compositions between CH_4 and N_2 are sometimes found, mostly associated with CO_2-CH_4 fluids. CH_4-N_2 fluids could be indicated by Raman analysis in samples from the following 3 areas (in order of increasing densities):

a) Dôme de l'Agout, France (Kreulen & Schuiling 1982). Fluids inclusions occur in quartz segregations in pelitic gneisses. H1-type inclusions show homogenization temperatures ranging from -95 to -84 (critical) and from -111 to -83°C (vapour); N_2-contents are 0 to 0.6 ($\pm$ CO_2). Molar volumes were calculated to be 70-200 cm^3/mole.

b) SW Norway (Swanenberg 1980). CH_4-N_2 fluid inclusions ($\pm$ CO_2) of type H1 and S2 were locally found in highly metamorphic tonalites and granodiorites showing homogenization (or partial) homogenization from-154 to -91°C (liquid) and from -148 to -83°C (critical); the N_2 to CH_4 ratio may cover the full range between the 2 components. Molar volumes of the CH_4-N_2 fluids was calculated 52-100 cm^3/mole.

c) Haut Allier, France (Lasnier 1976). S2 type inclusions in basic granulites (quartz bearing "pyrigarnite") show (partial) homogenization temperatures between -137 to -128°C (to liquid, vapour or critical). The CH_4-N_2-CO_2 fluids found in these rocks contain about 70-80 mole% N_2 and about 15 mole% CH_4; CO_2-contents are less than 17 mole%. The molar volume of these fluids is around 90 cm^3/mole.

All mentioned examples represent high-grade metamorphic rocks. However, the molar volumes of the CH_4-N_2 fluids are not in agreement with the peak metamorphic conditions. This can be explained by retrograde re-equilibration of a multi-component fluid by the forming of solid or liquid phases (graphite, carbonates, H_2O etc.). The fluid phase may become enriched in CH_4 and N_2 and is considered as a rest fluid.

5.4. The ternary system CO_2-CH_4-N_2

Experimental data on intermediate compositions in the CO_2-CH_4-N_2 system are not available, but a model can be established from the 3 binary "subsystems" discussed in the preceding sections and also from measurement data obtained by fluid inclusion studies.

A ternary system can be visualized by a 3 dimensional representation given for constant pressure or constant molar volume (see section

5.1.3/4). Isochoric diagrams are most interesting for the present use. The TX diagram is chosen here for the representation of the ternary system: the composition is plotted in a plane formed by a triangle with apices CO_2, CH_4 and N_2; the temperature extends in the third direction (Campbell & Smith 1951 p.277). The diagram formed in this way has the shape of a trigonal prism. Fig.5.24 shows a schematic diagram of the system CO_2-CH_4-N_2 for $\bar{V}$ 100 cm^3/mole. The 3 sides of the prism represent the isochoric sections for the binary systems CO_2-CH_4, CO_2-N_2 and CH_4-N_2. Only the relative positions of the melting and

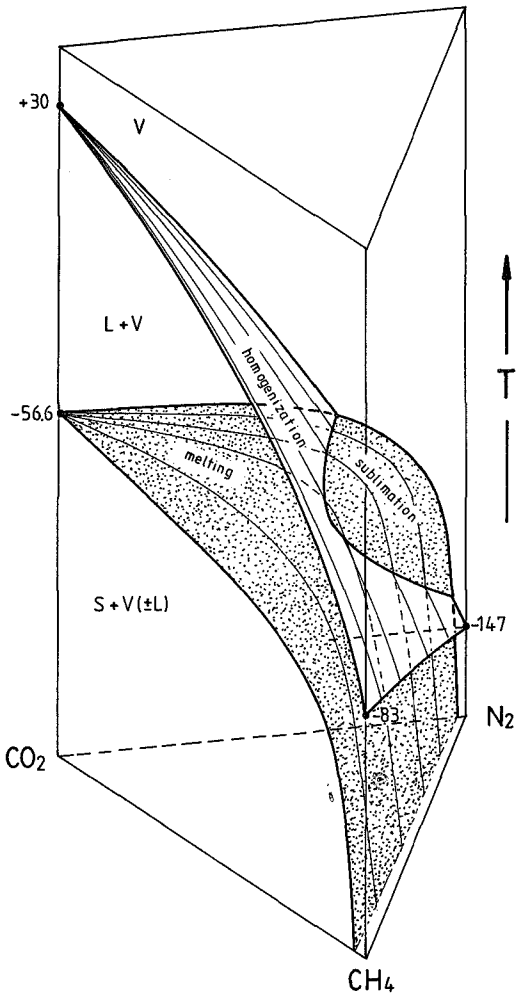

Fig.5.24.- *Schematic TX-diagram for the ternary system CO_2-CH_4-N_2 at constant molar volume (~ 100 cm^3/mole). The 2 surfaces represent "melting" (stippled) and homogenization points. Their intersection results to a division into parts distinguished by "$T_m < T_h$" (melting) and "$T_m > T_h$" (sublimation).*

homogenization point surfaces are shown for simplicity. The homogenization point curve does not intersect the liquidus for the system CO_2-CH_4 (at the given molar volume), but it does intersect (at any molar volume) for the system CO_2-N_2. Homogenization points of the ternary system partly run below the melting points ("$T_h<T_m$"). This part is defined as the sublimation region; homogenization is characteristic in the remaining part ("$T_h>T_m$"). In general, all vertical sections through a prismatic diagram represent binary systems, but of particular interest are sections taken through the CO_2-composition i.e. systems consisting of CO_2 and a gas mixture between CH_4 and N_2 (CO_2-(CH_4+N_2)).

It is common use to employ projections parallel to the T-axis on the compositional plane by constructing isotherms. These triangular diagrams are also isochoric in this case. Some examples as established for several molar volumes are shown in Fig.5.25. The diagrams were tentatively constructed by extrapolation from the binary systems. The results could be checked by microthermometric studies and Raman analysis of fluid inclusions (natural inclusions from 8 studied areas and synthetic inclusions). The compositional distribution of these inclusions is in agreement with the expected phase behaviour. Fluid inclusions from Dôme de l'Agout are used for the construction of the diagram for $\bar{V}$ - 100 cm^3/mole, inclusions from SW-Norway for $\bar{V}$ - 50 cm^3/mole.

Type S and H inclusions

The most important types of phase behaviour are those characterized by
a) sublimation: S2-type inclusions;
b) homogenization: H2-type and H4 type inclusions;
c) identical behaviour as for the pure end-members: apparent H3 type (similar to pure CO_2) and H1-inclusions (similar to CH_4 and N_2). These types of phase behaviour partly override the H2 and H4-fields.
All other types of phase behaviour (S1, S3, S4 and H5) have a more limited distribution in respect of molar volume and composition.

The stippled areas of Fig.5.25 denote the fluid compositions of S-type inclusions, whereas fluids of the remaining compositions are characterized by homogenization (H-type). The sublimation region drastically expands to lower molar volumes: sublimation may only occur for the N_2-richer CO_2-CH_4-N_2 fluids at molar volumes higher than 65 cm^3/mole (and below 225 cm^3/mole); both N_2 and CH_4-richer fluids may show

sublimation for molar volumes below 65 cm^3/mole. S-type inclusions are dominant for the lowest molar volumes (around 40 cm^3/mole).

The final homogenization temperatures are visualized by isotherms (Fig.5.25); the temperatures (isotherms) marking other phase transitions are not shown. Dashed curves denote homogenization to the vapour; solid curves denote homogenization to the liquid phase. For the examples shown at $\bar{V}$ = 200 and 100 cm^3/mole, homogenizations are to the vapour phase only; homogenizations to the liquid phase gain importance for $\bar{V} < 100$ cm^3/mole and only homogenizations to the liquid phase are possible for $\bar{V}$ - 40 cm^3/mole. The phase transitions observed at temperatures below final melting (or sublimation) temperature are symbolized as defined in chapter III e.g. a H4-type inclusion shows a total number of 4 phase transitions (3 phase transitions below T_h) in the temperature range from -180°C upwards. The shown distributions of the types of phase behaviour are only tentatively located. Note that H2-type inclusions are unique for CH_4-rich fluids, loosing importance at lower molar volume; H4-type inclusions are unique for N_2-rich compositions. The boundary limit between H2 and H4 is determined by the stability field of solid CO_2 coexisting with one volatile phase (S+V or S+L): this assemblage is extensive for the system CO_2-N_2, but highly reduced for the system CO_2-CH_4; on the other hand, the 3-phase stability field covers a long temperature interval for the system CO_2-CH_4 (Fig.5.12) and is splitted into 2 restricted temperature ranges for the system CO_2-N_2 (Fig.5.20). Partial homogenization and initial melting become identical to final melting (T_m=T_{hs}=T_i) along the boundary curve between H2 and H4: the volatile fraction is just saturated at this point (CH_4-richer fluids are supersaturated; N_2-richer fluids are undersaturated).

Fig.5.25.- *Isochoric projections of the system CO_2-CH_4-N_2 for molar volumes between 40 and 200 cm^3/mole (tentative). The stippled regions are characterized by sublimation (S-type); the remaining regions by homogenization (H-type). Isotherms mark homogenization to the liquid (solid) or to the vapour phase (dashed). H2 and H4-type inclusions are typical for CH_4-rich and N_2-rich compositions respectively; (apparent) H3 and H1-type inclusions are typical for CO_2-rich and CH_4-N_2-rich compositions.*

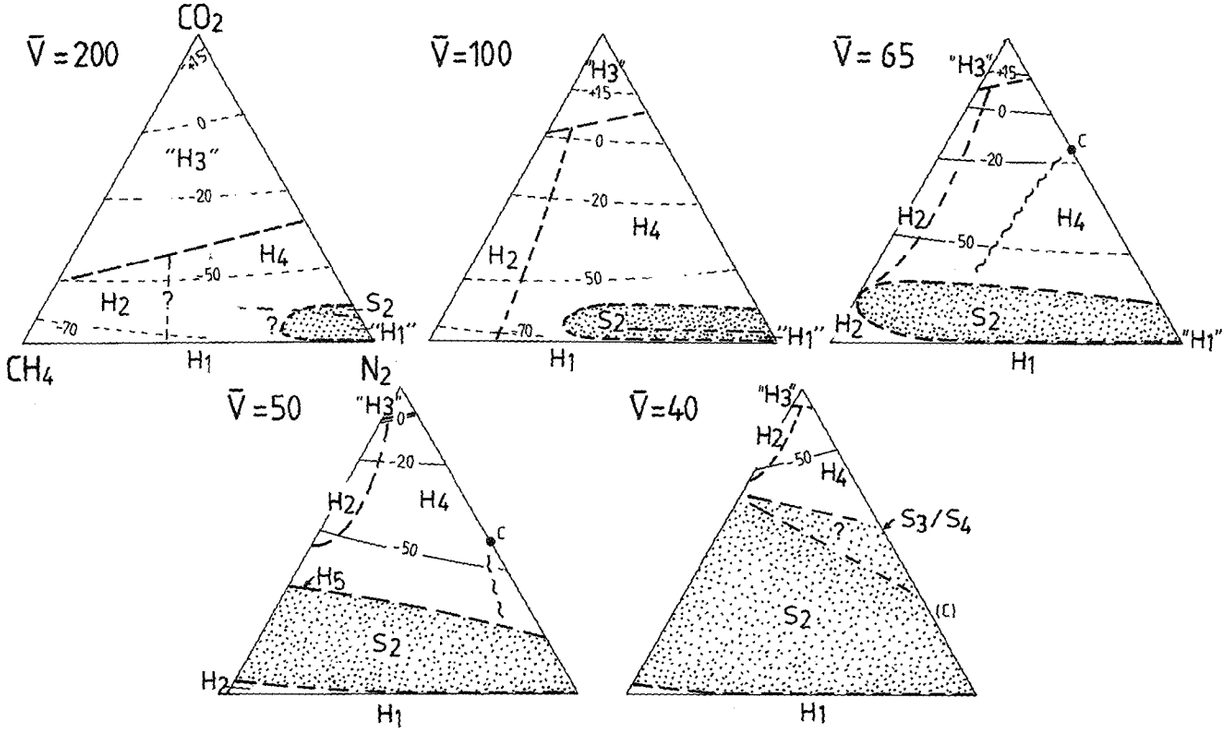
V̄ = 200
CO2
+15
0
"H3"
-20
H4
-50
H2
?
S2
-70
"H1"
CH4
H1
N2
V̄=100
"H3"
+15
0
-20
H4
H2
-50
S2
-70
"H1"
H1
V̄= 65
"H3"
+15
0
C
-20
H2
H4
-50
H2
S2
"H1"
H1
V̄=50
"H3"
0
-20
H2
H4
C
-50
H5
S2
H2
H1
V̄=40
"H3"
H2
-50
H4
S3/S4
?
S2
(C)
H1

(Fig.5.25)

Phase observations and optical restrictions

Inclusions showing phase behaviour similar to pure components CO_2 (type H3) and CH_4 or N_2 (type H1) cover the upper and lower parts of the shown triangular diagrams respectively. Both of these types are more common for higher molar volumes because of the more reduced absolute volumes of the phases. The distribution of inclusions showing apparent H3-type (or "normal" CO_2 behaviour) was estimated by the assumption that less than 10 vol% of liquid cannot be observed. This limit appeared to be too optimistic in many cases and apparent H3 behaviour may cover a larger part of the diagram. An inclusion of essentially type H4 is observed as type H3 if the amount of liquid at T_{hs} is extremely small. A type H2 inclusion may also be mistaken as H3 if the inclusion seems to be completely frozen at -180°C (a very small amount of liquid should be present!); initial melting (T_i) does not take place, but (apparent) T_i is detected at the temperature at which the amount of liquid becomes large enough to be observed.

H1-type behaviour is restricted to inclusions containing no CO_2. Inclusions of type S2 (and also of type H2 and H4) may be observed as H1 if the amount of solid CO_2 is very small. It was assumed than less than 1 vol% of a solid particle cannot be observed by optical means.

VI ARTIFICIAL CO_2-N_2 INCLUSIONS

6.1. Introduction

Fluid inclusions are generally studied for the determination of their trapping PT-conditions which are obtained from the homogenization temperature, composition and an adequate equation of state. Synthetic fluid inclusions produced by means of HPT-experiments, are formed at fixed temperature and pressure. These inclusions of known trapping conditions are studied and further characterized. Pressures in fluid inclusions, which can generally not be measured, are known for synthetic inclusions at the experimental temperature. The formation of synthetic fluid inclusions opens the possibility to establish or to modify equations of state for multi-component systems.

Fluid inclusions are generated by healing of "cracked" quartz in the presence of a fluid of known composition (Bodnar et al. 1985). Experimental temperatures are limited because quartz does not (re)crystallize at low temperatures, especially for fluids of low water content. On the other hand, it is not possible to form high density inclusions at high temperatures because the required pressures cannot be realized. All present experiments were carried out at 500°C; pressures could be chosen in the range from 0 to 6 kbar.

Fluids were generated by the decomposition of one or more starting compounds. Several possibilities have been tried out by studying decomposition reactions in more detail. Three compositions within the system CO_2-N_2 were selected by the choice of the following compounds:

a) X_{N2} - 0.33 - silver-nitrate ($AgNO_3$);
b) X_{N2} - 0.55 - ammonium-nitrate (NH_4NO_3) + silver-oxalate ($Ag_2C_2O_4$)
   or
   - guanidine-nitrate ($NH_2C(=NH)NH_2.HNO_3$) silver-oxalate;
c) X_{N2} - 0.77 - ammonium-nitrate.

All gas compositions were in equilibrium with graphite during the experiments.

The formed inclusions and healing textures give insight in the forming processes of fluid inclusions during the experiments. Similar

processes are supposed to be responsible for the forming of fluid inclusions in natural rocks. A study on the phase behaviour upon cooling ("microthermometry") was made afterwards. A direct correlation between these observations and trapping PT-conditions could then be derived. Gas compositions were measured by Raman analysis.

Temperatures marking phase transitions at low temperatures (T_h, T_m, T_{hs}, T_{hm}) were correlated to the trapping pressures (P_t) for fluids of constant composition (X) and trapping temperature (T_t). These correlations are graphically represented in "T_h-P_t" diagrams. Furthermore, isochores in the high PT-region were established by the construction of tie-lines connecting the PT-conditions during the experiment (T_t, P_t) and at the point of homogenization (T_h, P_h) (Fig. 6.1.). The experimental PT-conditions constitute a point on the isochore. The pressure at T_h cannot be measured directly, but can be taken less than 255 bar for the system CO_2-N_2 (Darimont 1986; Darimont & Heyen 1988) i.e. very low compared to the experimental pressures.

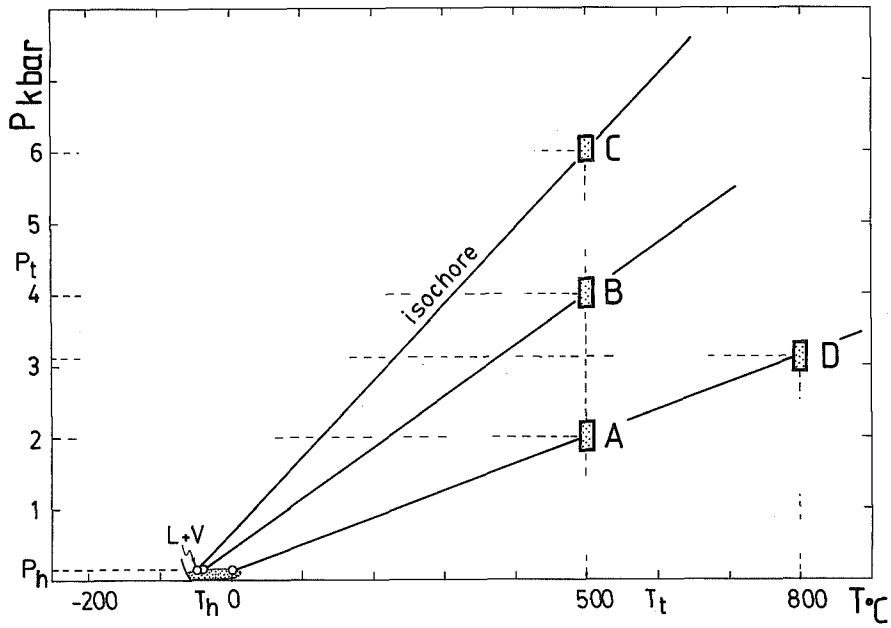

***Fig.6.1.**- Schematic presentation of experimental forming conditions of fluid inclusions (P_t, T_t) and the conditions of homogenization (P_h, T_h). Fluid inclusions formed at the same temperature, but at different pressures (A, B and C) have different molar volumes; fluid inclusions formed at conditions defined by the same isochore (A and D), have the same molar volume and therefore show the same phase behaviour at low temperatures.*

Diagrams valid for a wide compositional range were established by the compilation of data obtained from inclusions of the 3 different compositions mentioned above. This was done by the construction of a diagram showing correlations between T_h-X-P_t. Molar volumes cannot be measured directly by means of the present experimental method. An equation of state valid for the high temperature range should therefore be applied for the calculation of $\bar{V}$. These calculations finally result to the construction of an isochoric T_h-X diagram.

6.2. The experimental method

The present method is based on the fact that small amounts of fluid are trapped during "healing" of cracks in quartz (Shelton & Orville 1980; Smith & Evans 1984; Roedder 1984 p.343; Bodnar et al. 1985). This process is assumed to be also responsible for the generation of so-called "secondary inclusions" during metamorphism (Lemmlein & Kliya 1952). The widespread occurrence of these inclusions may therefore indicate that healing (or annealing) is a common geological process. During the experimental procedure, cracks are artificially induced. It was affirmed by earlier experimenters (Shelton & Orville 1980) that the densities of fluid inclusions formed in this way are consistent with the experimental conditions.

The degree of quartz healing is a function of temperature, time, initial silica-concentration of the fluid and crack dimensions (Smith & Evans 1984). These authors further state that micro-cracks in quartz have geologically short lifetimes at temperatures above 200°C: healing could not experimentally be reproduced at lower temperatures. Extensive healing was found at temperatures between 400 and 600°C in a time interval of several days and in the presence of an (aqueous) pore fluid.

Annealing takes place by dissolution and precipitation of quartz. Water plays an essential role as a solvent and transport medium during this process. Earlier experimental studies concerned only water inclusions and brines. As far as known to the author, the present work constitutes the first attempt to produce artificial gaseous inclusions. However, small amounts of water must be added as water is indispensable for the mineral growth. It was found for the present experiments that the salts (used for gas production) partly dissolve in water resulting to concentrated brines. It is assumed that high salt contents influence the

speed of quartz growth: the high concentrations of the aqueous fluid at high PT may explain slow healing rates (in the order of weeks).

The present experiments were carried out at the HPT-laboratory of the Institute of Earth Sciences of the State University of Utrecht (Dr. J.B.H. Jansen); some experiments were made for comparison at the Mineralogical / Petrographical Institute of the University of Tübingen, FRG (Prof.Dr. P. Metz).

A description of the followed experimental procedure is given below.

The quartz samples used for the experiments consist of large euhedral crystals from Brazil, (almost) free of fluid inclusions on microscopical observation. Cylinders of 0.38 cm in diameter are drilled, most commonly parallel to the crystallographic c-axis.

Cracks are induced by means of quenching, according to the method described by Bodnar et al. (1985): the quartz cores are firstly heated to about 350°C and subsequently dropped in cold water. Surprisingly, it was found out that alternative cooling by means of liquid nitrogen did not result in the forming of cracks. The "cracked" quartz cylinders are subsequently cut into pieces of about 1 cm length. Possible sharp edges are smoothed to prevent damage of the gold capsules.

Quartzes together with starting material are put in noble metal capsules (tubes) made of gold, platinum or Ag-Pd. The tubes used here are 0.58 and 0.45 cm in (outer) diameter and their lengths are taken between 2.5 and 4 cm; the thickness of the walls is 0.02 cm. After closing one side of the tubes, starting materials (e.g. silver-nitrate, graphite and water) and the quartz cylinder are added. Finally, the tubes are sealed with the help of a graphite arc-welder.

The capsules are placed in an autoclave of the type described by Tuttle (1949). Autoclaves are connected to a high pressure gas (argon or CO_2). The maximum pressure which can be hold in the autoclaves is 6000 bar at 650°C and 1000 bar at 750°C. The accuracy of the pressure readings (below 6000 bar) is ±10 bar; the accuracy of the temperature readings is ±5°C for the present experimental set ups. An extensive description of the experimental set up in Utrecht is given by Bos et al. (1987). Argon or carbon dioxide are applied as a pressure medium in Utrecht and Tübingen respectively. The application of argon has the advantage of higher possible pressures (up to 6 kbar for the present set up, but considerably higher for alternative set ups); CO_2 will become partly solid at pressures around 6 kbar with the possible risk of stopping up

the tube system. The experimental conditions are commonly reached by first setting the pressure (at room temperature). Connections and taps are checked for leakage during one day ("dummy pressure"). Subsequently, the temperature is set by putting the furnace over the autoclave. Some gas should be released during warming to prevent overpressure. The duration of one experimental run is taken between 2 and 14 days. The best results are obtained for the longer periods. The autoclaves are cooled before pressure release (non-isobaric cooling). A schematic representation of the experimental PT-path is shown in Fig.6.2.

The "healed" quartz samples are treated for further studies by the preparation of double-polished thin sections.

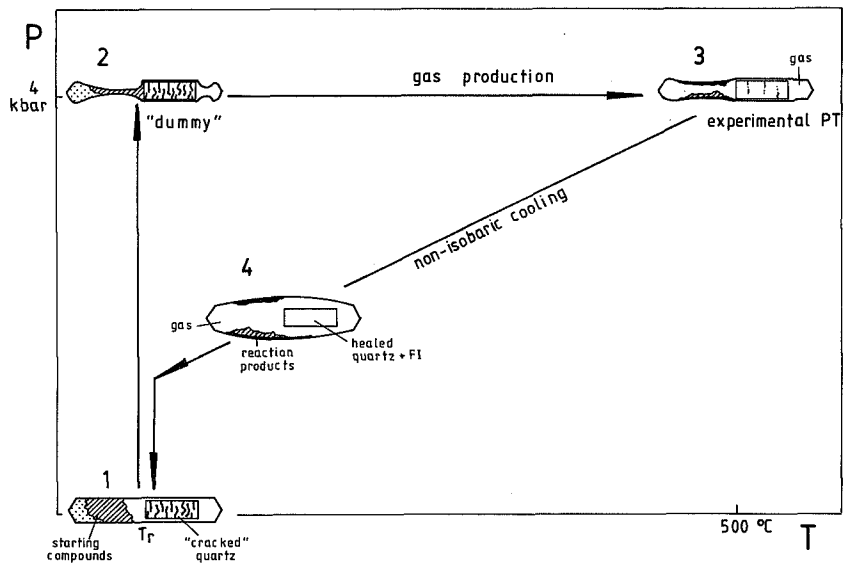

Fig.6.2.- *The PT-path (1 to 4) during experimental runs (schematic). The volume of the gold capsule is adjusted by distortion in order to equalize internal and external pressures. Gas production inside the capsule takes place at high temperatures by the thermolysis of starting compounds. Quartz healing and the forming of fluid inclusions at the experimental PT (at 3) take 1 to 3 weeks.*

6.3. Chemical reactions for gas mixture production

Liquids of wished composition can simply be used for the formation of aqueous inclusions. However, gases or gas mixtures have to be produced by one or more starting compounds. They should decompose and/or react at the

experimental PT-conditions. The choice of starting compounds is therefore an essential aspect of this study.

Several potential starting compounds for the production of CO_2-N_2 mixtures are known (Holloway & Reese 1974). Equilibria calculations were made by these authors for several systems starting from selected compounds. They assumed complete decomposition into gas species, but their calculations have not been checked by experiments so far. It follows from the present experiments that decomposition and reaction equilibria are much more complicated than firstly assumed: several solid reaction products generally form in addition. The stability of these compounds is dependent on the acting PT-conditions, the surrounding gas species etc.

Good results are achieved for starting compounds producing nitrogen and oxygen on heating; oxygen is reduced by (a surplus of) graphite to produce CO_2.

Reaction processes have been studied in capillary quartz tubes ("HT-experiments"). In these tubes, solid, liquid and gaseous reaction products and physical changes can be observed; gas compositions can be measured afterwards by Raman analysis. The used quartz tubes are 0.20 and 0.10 cm in outer and inner diameter respectively (the wall thickness is 0.05 cm); their lengths are taken about 3 cm. The tubes were closed by melting their ends in the flame of a methane-oxygen burner. After filling and sealing, the tubes are put in a furnace and heated to a few hundred degrees centigrade to start decomposition and/or reactions of the starting compounds. Some reactions need longer periods to reach equilibrium conditions (sometimes several days). Heating is limited by the pressure rise in the quartz tubes. The tube strength could be determined by filling them with pure water to a given filling degree. Pressures are calculated from the water isochores in the HPT-region (Fisher 1976; Crawford 1981). It was found that the quartz tubes are able to hold pressures in the order of 1 kbar. However, quartz tubes filled with other compounds than water may explode already at a much lower pressure possibly due to sudden pressure increments (some reaction products are explosive!). The results of HT-experiments are most successful if a) the amount of starting compound is not too high b) temperatures are kept below about 600°C c) the heating rate is moderate d) experimental durations are long enough to achieve completion of chemical reactions.

One should be aware of the fact that chemical equilibria at high temperatures (and pressures) are generally not the same as equilibria at room temperature (Dubessy 1984). The compositions measured by Raman analysis do therefore not necessarily represent the compositions at high PT. "Retrograde" reactions may take place during cooling resulting to different phase contents and compositions. The forming of new phases has implications for the (partial) molar volume of the gas phase (see section 6.8.). Many retrograde reactions do not or slowly proceed. Fluids containing CO_2, CH_4 and H_2O can be mentioned for example (see section 6.5.4.). Fluid compositions at room temperature are then considered as chemically "metastable".

6.4. Experiments with silver-nitrate and graphite

6.4.1. Decomposition reactions

Silver-nitrate ($AgNO_3$) and graphite produce N_2 and CO_2 during complicated decomposition reactions. These reactions have been studied in more detail: silver-nitrate and graphite were introduced in capillary quartz tubes and subsequently heated. Complementary information was obtained from Gmelins Handbuch (1971) and Weast (1975).

The decomposition behaviour of $AgNO_3$ on heating and progressive reactions is illustrated in Fig.6.3.

$AgNO_3$ melts forming a colourless liquid. The melting point is +209.5°C at 1 atm., but higher at higher pressures: about 230°C at 2 kbar, about 255 at 5 kbar and about 295°C at 10 kbar. The dissociation into ions (Ag^+ and NO_3^-) is complete above the melting point.

Thermal decomposition ("thermolysis") already starts just above the melting point and proceeds very slowly if temperatures are kept a few degrees above this temperature. The first stage of decomposition is characterized by the forming of $AgNO_2$ and oxygen according to the reaction

$$2\ AgNO_3 = 2\ AgNO_2 + O_2 \qquad \text{(R.6.1.)}$$

This reaction would take place at temperatures above 250°C, but it cannot be observed.

The thermal instability of $AgNO_3$ becomes more evident above 300°C and strongly increases from 450°C. The development of nitrous gases starts at temperatures above 444 (469)°C when decomposition becomes complete: NO_2, N_2 and O_2 may all be released.

The colourless melt becomes yellowish from about 400°C, indicating the first forming of NO_2 (in solution). The gas phase, at first colourless, is replaced by a pale brown gas on further heating. Gas (NO_2) is colourless again when cooled (favouring the stability of N_2O_4). In the vicinity of graphite, brown gas grades to colourless gas indicating the proceeding of the following NO_2-consuming reaction:

$$2\ NO_2 + 2\ C = N_2 + 2\ CO_2 \qquad \text{(R.6.2.)}$$

At the same time, possible oxygen may be reduced by forming carbon dioxide:

$$O_2 + C = CO_2 \qquad \text{(R.6.3.)}$$

The brown colour of the gas will have completely faded away after some period; the yellowish liquid (a mixture of Ag^+, NO_3^- and NO_2 ?) may longer persist. The amounts of liquid slowly decrease until complete disappearance. In some cases (at higher temperature) the brown gas is more persistent.

An alternative way of nitrogen forming is the decomposition of NO_2 according

$$2\ NO_2 = N_2 + 2\ O_2 \qquad \text{(R.6.4.)}$$

This equilibrium is supposed to shift to the right at lower pressures; the stability of NO_2 is favoured at higher pressures.

A white fine-grained solid (probably Ag_2O or Ag_2CO_3) is formed as a reaction product during the forming of NO_2. Most remarkable is the absence of silver at first sight. This is probably due to high gas pressures.

Experiment QB16

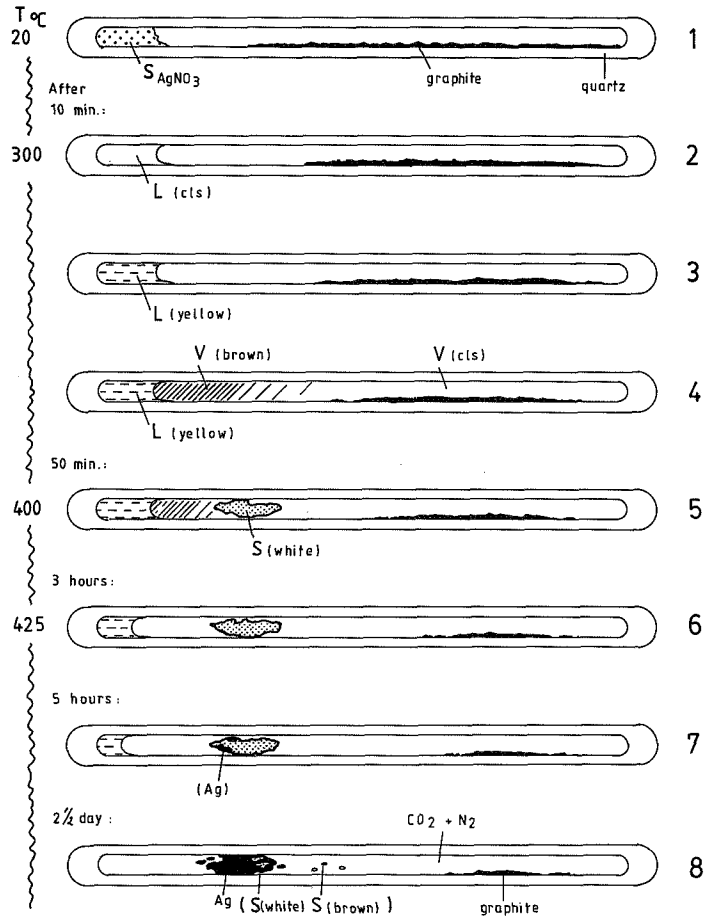

Fig.6.3.- *Observations upon heating in a capillary quartz tube (3 cm long) of silver-nitrate ($AgNO_3$) (6.8 mg) with a surplus of graphite (0.9 mg). The estimated inner volume of the tube is 0.02 cm^3. Most remarkable are melting (1-2); the forming of the brown gas NO_2 (3-4); reduction of NO_2 by graphite to (colourless) CO_2 and N_2 and contemporaneous forming of a white solid, most probably silver-carbonate (Ag_2CO_3) (5-6); replacement of Ag_2CO_3 by metallic silver (7-8). The final gas composition after 2 to 3 days at 425°C (in mole%) is $CO_2(67.4)N_2(32.6)$.*

The following phases can be distinguished during the early stage of the reaction process: a yellowish liquid (decreasing in amount), a brownish gas (gradually replaced by a colourless gas, at first near graphite), a white powder and graphite (partly reacted). Further reactions appeared to proceed very slowly.

On longer heating durations (in the order of days), the white solid is gradually replaced by silver precipitating on the glass walls. Some white powder may remain. It was mentioned in Gmelins Handbuch (1971) that decomposition of $AgNO_3$ into Ag, O_2 and NO_2 needs an induction period of about 1 hour at 450°C (and 1 atm.!) becoming shorter at higher temperatures. The reaction proceeds in a first-order interval after this period.

In addition, small amounts of a dark brown solid of unknown composition may be formed. This compound has especially been observed when heated to higher temperatures (about 600°C). At this temperature, a dark brown liquid also formed, rapidly crystallizing on cooling.

The following compounds are observed at the end of the experiments: metallic silver, small amounts of white powder (?), some small brown spots (solid ?), graphite (which was added in access) and colourless gas. During cooling to room temperature, the tube may be wetted by small amounts of water (?) which was probably present as crystalline water in $AgNO_3$.

The gas content of the quartz tube was analysed by Raman analysis. The measurement result in molar percentage is $CO_2(67)$ $N_2(33)$.

It is evident from the descriptions given above that the decomposition of $AgNO_3$ and the reduction of oxygen and nitrogen oxides by graphite represent dynamic and complex equilibria. However, the resulting reaction products at low temperature are most interesting. Total reactions can therefore be written considering 3 solid reaction products: Ag, Ag_2O and Ag_2CO_3:

$$2\ AgNO_3 + 3\ C \rightarrow N_2 + 3\ CO_2 + 2\ Ag \qquad (R.6.5a)$$

$$2\ AgNO_3 + 5/2\ C \rightarrow N_2 + 5/2\ CO_2 + Ag_2O \qquad (R.6.5b)$$

$$2\ AgNO_3 + 5/2\ C \rightarrow N_2 + 3/2\ CO_2 + Ag_2CO_3 \qquad (R.6.5c)$$

These reactions result to the following respective gas compositions: $CO_2(75)N_2(25)$ (R.6.5a); $CO_2(71.4)N_2(28.6)$ (R.6.5b); $CO_2(60)N_2(40)$ (R.6.5c). The ratio of CO_2 and N_2 is therefore related to the solid species formed. It was found by Raman analysis of synthetic fluid inclusions that gas compositions cover the full range between X_{N2} = 0.25 and 0.40 showing evidence for possible gas production by all three reactions 6.5a-c (section 6.4.5.). It is assumed that reactions 6.5b and 6.5c are favoured at higher pressures and higher activities of CO_2.

6.4.2. HPT-experiments (P = 1 to 6 kbar; T = 500°C)

Synthetic CO_2-N_2 inclusions have been made by the healing of "cracked" quartz in gold capsules filled with $AgNO_3$, graphite and some water. Temperatures were about 500°C for all experiments; pressures were set at about 1, 2, 4 or 6 kbar. The durations of the experimental conditions were taken between 7 and 15 days. Fluid inclusions appeared to develop insufficiently in a period of less than 1 week; best results were obtained for the longer periods (about 2 weeks).

The amount of $AgNO_3$ can be widely chosen taking into account that a minimum amount of gas is needed to fill the capsule at HPT-conditions (not all volume can be adjusted by distortion of the capsule); a maximum amount should not be exceeded because of the danger of bursting of the capsule by internal overpressure. Argon -used as a pressure medium- may penetrate then into the capsule and mix with the present gases (sample E232). Capsules often burst during pressure release after the experiment (e.g. samples E263, E274, FK1); they remain generally tight by using smaller amounts of $AgNO_3$ (in the order of 50 mg) and the capsule should be degassed before opening.

Supposed that silver is the only solid reaction product, it can be calculated from reaction R.6.5a that 1 gram of $AgNO_3$ produces 0.4706 (= (3x44 + 28)/(2x170)) gram of gas which is in agreement with the present findings. The weight loss by degassing may be somewhat (to 15%) higher probably due to the escape of a few milligrams of graphite and/or water.

The solid reaction products were studied after opening the capsules. A typical example of a gold capsule before and after the experiment is shown in Fig.6.4a-b. The most remarkable observations inside the capsule are

a) a silver coating, precipitated in the middle part of the Au capsule;

b) a silver-rich aggregate (a tough, porous, white to metallic rod) consisting of silver, Ag-compounds and graphite. Note that silver precipitated on or in the vicinity of graphite and not around the original site of $AgNO_3$;

c) remaining graphite, generally found at one side of the capsule.

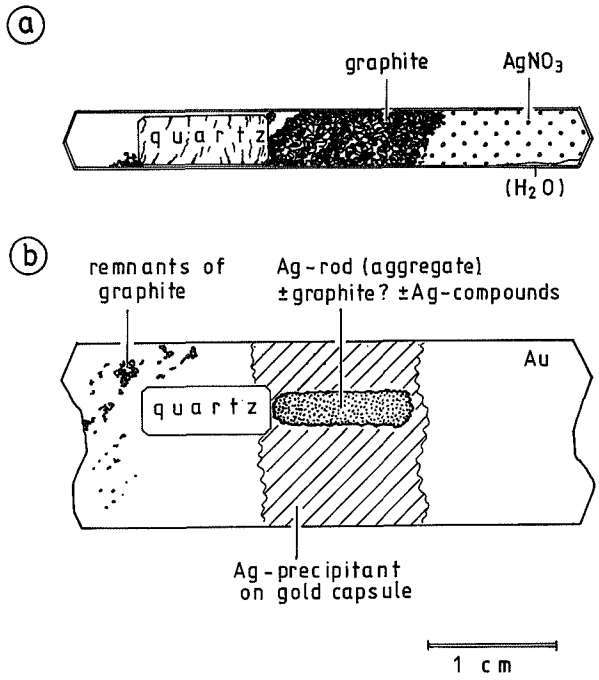

Fig.6.4.- *HPT experiment with silver-nitrate and graphite: starting compounds and solid reaction products.* ***a)*** *Cross-section of a filled and sealed gold capsule before the experiment.* ***b)*** *The capsule opened after the experiment (1-6 kbar; 500°C). Silver formed in the part of the capsule which was taken by graphite.*

6.4.3. Fluid inclusion textures

In the present samples, several stages can be distinguished being representative for the development of fluid inclusions. Note that, in our experiments, the quartz samples are not subjected to stress. Minor amounts of water (~10 mg) appear to be sufficient for quartz growing. The textures of the partially healed cracks and fluid inclusion forms give a better insight in the forming process of fluid inclusions (see also Smith & Evans 1984). A selection of photographs is shown in Fig.6.5. The healing process can be reconstructed by the interpretation of textures

which give rise to a distinction in three types of fluid inclusion development (A, B and C). Differences are supposed to be due to the speed and degree of quartz growing ("slow", "moderate" and "fast"). Many inclusions are transitional between the 3 basic types. Their characteristics are given below.

A. "slow healing" starts with the forming of "quartz-pillars" joining both sides of a crack. The occurrence of hexagonal crystal shapes is common. Parts of the fluid may become isolated and angular inclusions are formed. The outline of fluid inclusions often show concave shapes. These inclusions are generally the largest in size within a sample (up to several 10ths of microns); they are however extremely flat (their thickness is only a few microns). The inclusions may be connected by very small or almost invisible "canals". It may be difficult to decide in some cases if an inclusion is really isolated.
B. "moderate healing" results to the forming of irregular fluid canals. These canals may be of several order of magnitude (generations?) within one crack. Remarkable is the local development of circular shapes. Worm-like inclusions may be formed after complete closure. Strings of "droplets" locally form at regular distances. The larger and more isolated inclusions show rounded shapes. Inclusions with a negative crystal shape do not form, probably because the experimental durations are too short.
C. "fast healing" is supposed to be the case for the finely dispersed fluid inclusions present in most samples and is related to the smallest cracks. Inclusions are only a few microns in size and too small for microthermometric studies.

The healing process resulting to textures of "type B" is described by Smith & Evans (1984): mass transport and mineral growth takes place along crack tips. Here, cylindrical voids are formed which are pinched off into spherical voids. Crack regression results to a zonal distribution of fluid inclusions and to the forming of inclusion "strings". The healing process denoted here as "type A", is characterized by a more or less contemporaneous quartz grow at many locations in larger cracks, seen the more equal distribution of quartz "pillars". These textures mostly do not show a distinct growing direction.

The fluid content of most present inclusions is gas-rich; water has only been observed in small amounts. It was found that the quantity of

added water does not affect the water content of the inclusions. It is therefore concluded that immiscibility between a gas-rich fluid and a brine exist during the trapping conditions. The amount of aqueous inclusions in the present samples is scarce. This can be explained by the concentration of the liquid phase at the bottom of the capsule, not in contact with quartz. Two distinct fluid inclusion types can be distinguished in sample E274 (formed at 6 kbar): 1) gaseous inclusions with accessory water and 2) aqueous inclusions showing a gas bubble and a small salt crystal ($AgNO_3$?). Salt most probably forms upon cooling of a saturated solution (daughter mineral). Indications for immiscibility were also found in sample E232 (formed at 4-2 kbar): gaseous inclusions coexist with a salt-rich brine. Fluid inclusions of both types are sometimes connected by a small "canal" (Fig.6.5.). In the samples formed at 2 kbar, several inclusions are found containing large amounts of salt crystals; water leaked from these inclusions.

It can be concluded that 2 fluids are immiscible during the experiments: a gaseous fluid, and a brine ($AgNO_3$ solution?). There is evidence for decreasing salt concentrations in the brine to higher experimental pressures. All gaseous inclusions show low water contents regardless the total amount of present water. Note that high density gaseous inclusions are only possible to form because of the immiscibility of the gas and liquid phases at high PT.

***Fig.6.5.**- Photographs of textures showing fracture healing in quartz and several types of synthetic fluid inclusions. The experiments were carried out at 500°C and up to 6 kbar. The parameters (pressure, used starting material, water content of the fluid) for the samples can be read from Tables 6.1-4. The sections are taken about perpendicular to the crystallographic c-axis in all samples.*

Experiments with silver-nitrate

***a)** sample E232-B (5 days). Aqueous and gaseous inclusions show evidence for immiscibility at the time of trapping: a multi-phase inclusion (L+V+salts) and a pure gas inclusion (dark) are connected by a fracture, indicating contemporaneous trapping. The gas phase shows the same homogenization temperature (-7°C) in both inclusion types. The large gas inclusion is contaminated with argon by leakage during the experiment (T_h = -42°C).*

***b)** sample E245-A (7 days). Well developed gaseous inclusions (water only accessory) representing a late stage of fracture healing ("type B", see text). Inclusions mostly show rounded shapes.*

***c)** sample FK4-A (8 days). A partly healed fracture showing hexagonal quartz crystals, joining both sides of the crack ("type A", see text).*

Fluids are only trapped in the smallest parts of the crack; the larger part of the crack is "empty" after the experiment.

d) *(sample FK4). Irregular fluid canals (partly closed) in cracks showing "moderate" healing ("type B"). Remarkable are the circular forms.*

e) *sample E263 (14 days). Inclusions partly filled with crystals (probably $AgNO_3$). Two types of inclusions are present affirming immiscibility at trapping: 1) inclusions with a high salt content and 2) gaseous inclusions. The "solid" inclusions do not contain observable water which probably evaporated.*

f) *(sample E263). An example of textures showing "slow" fracture healing ("type A"). Quartz forms hexagonal forms at growing. The intermediate fluid canals are locally closed and the first fluid inclusions start to form.*

g) *sample E304 (14 days). Euhedral quartz growth in a fracture. It is remarkable that 2 of the 6 faces of the prism do not develop here. Note that the "low quartz" modification (hexagonal) should be stable at the present experimental temperature of 500°C. Quartz growth is equally distributed in the fracture.*

h) *(sample E304-A). Well developed gaseous inclusions (water accessory). The crack is larger from lower left to upper right: fluid inclusion sizes grade from small to large in this direction.*

i) *(detail of h). Inclusions are transitional between "type A and B" (roughly from top to bottom). Note the occurrence of inclusions showing concave and rounded shapes. Almost all inclusions are closed and contain a gas mixture of constant composition.*

j) *sample E274-A (15 days). "Type B" healing showing strings of small fluid inclusions, indicating successive regression of the crack during the healing process. Strings mark former crack tips.*

Experiments with ammonium-nitrate (± silver-oxalate)

k) *sample E318 (14 days). Quartz grow textures indicating an early stage of healing, from the rim to the central part of the crack. Note the serrated forms of quartz crystals. The intermediate spaces are not closed and therefore "empty".*

l) *sample E269-A (15 days). Well developed 2-phase inclusions with a high water content. Inclusions show concave shapes ("type A" healing). Note that more than one bubble is present in some inclusions.*

Experiments with guanidine-nitrate

m) *sample E286 (13 days). Healing textures showing several directions of crystal growth, parallel and perpendicular to the fracture.*

n) *(sample E286). A later stage of fracture healing characterized by the forming of the first fluid inclusions. The fracture is open in the lower half, but almost completely healed in the upper half of the photo.*

o) *(sample E286-A). Well developed fluid inclusions. Many inclusions also contain small salt crystals.*

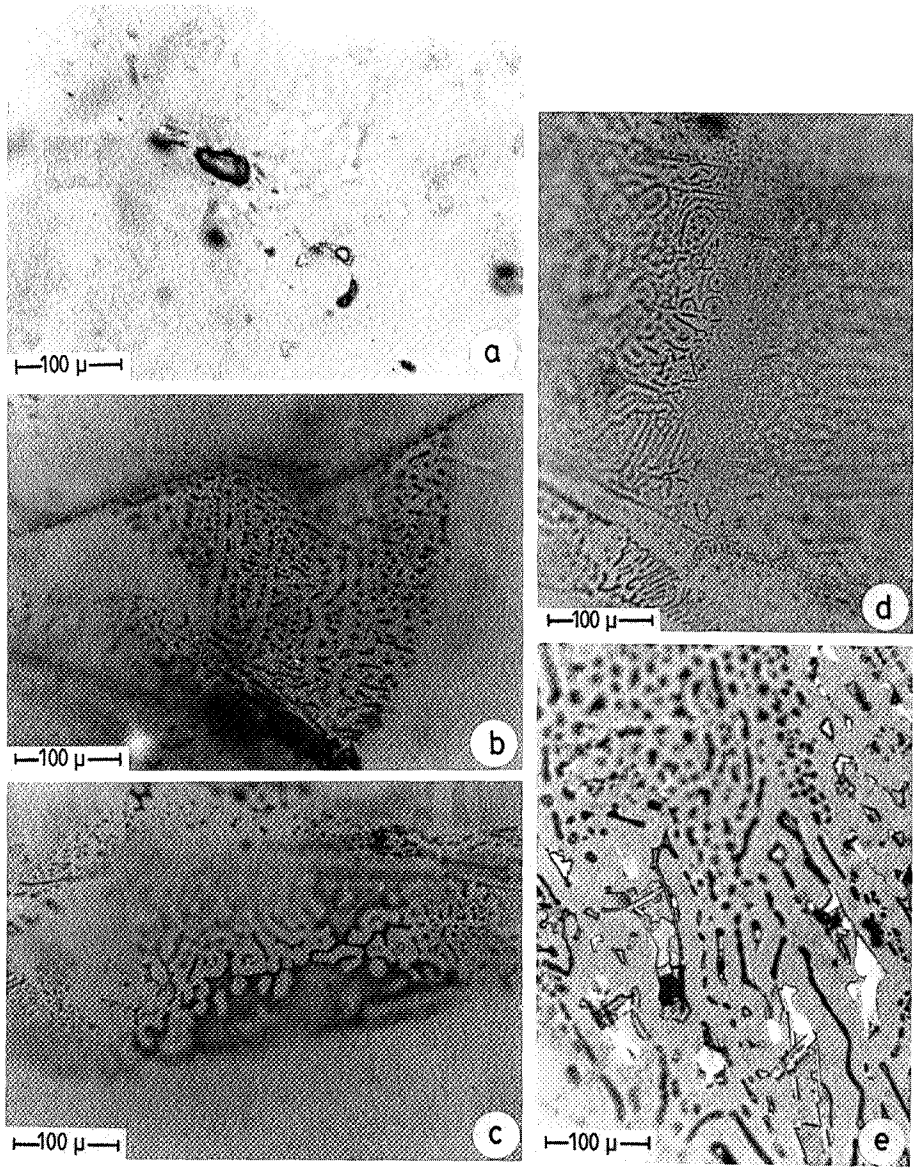
100 µ
a
b
c
d
e

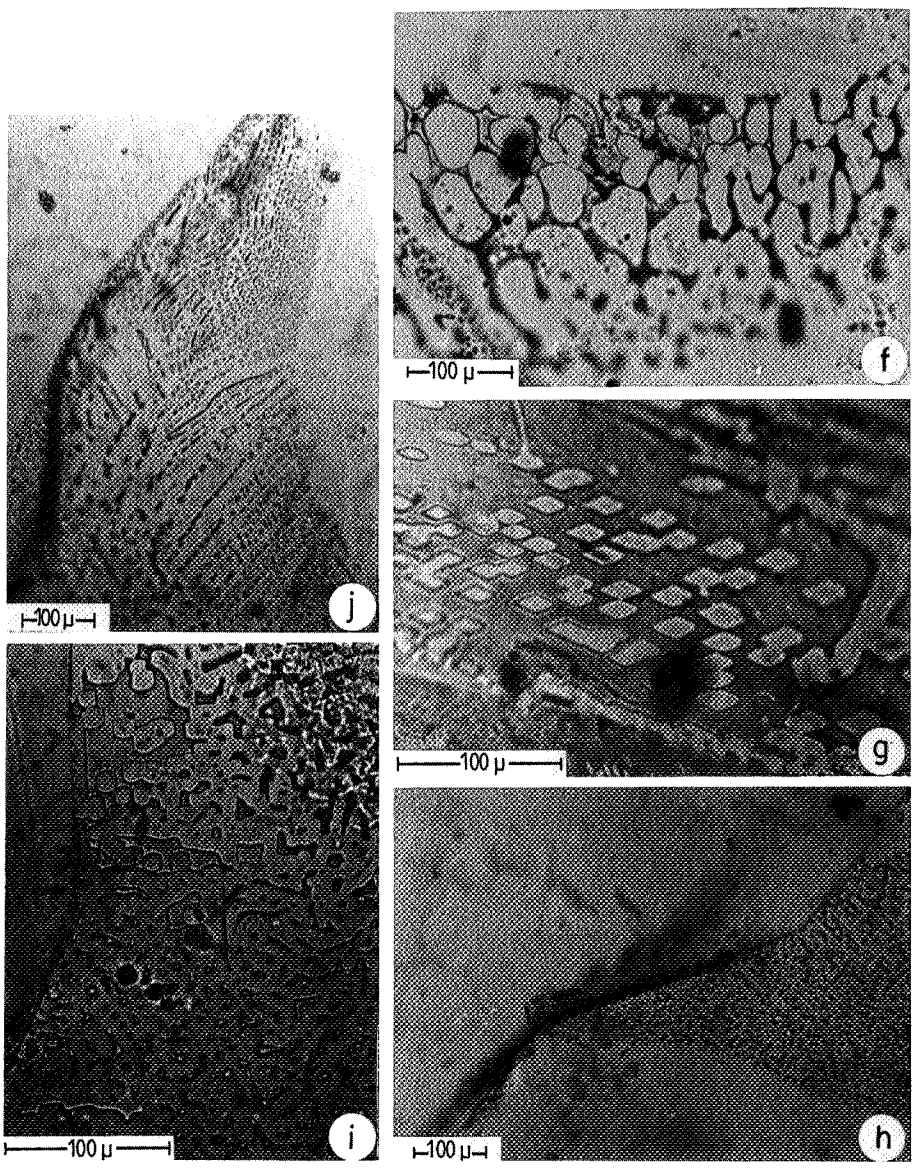
100 µ
f
100 µ
g
100 µ
h
100 µ
j
100 µ
i

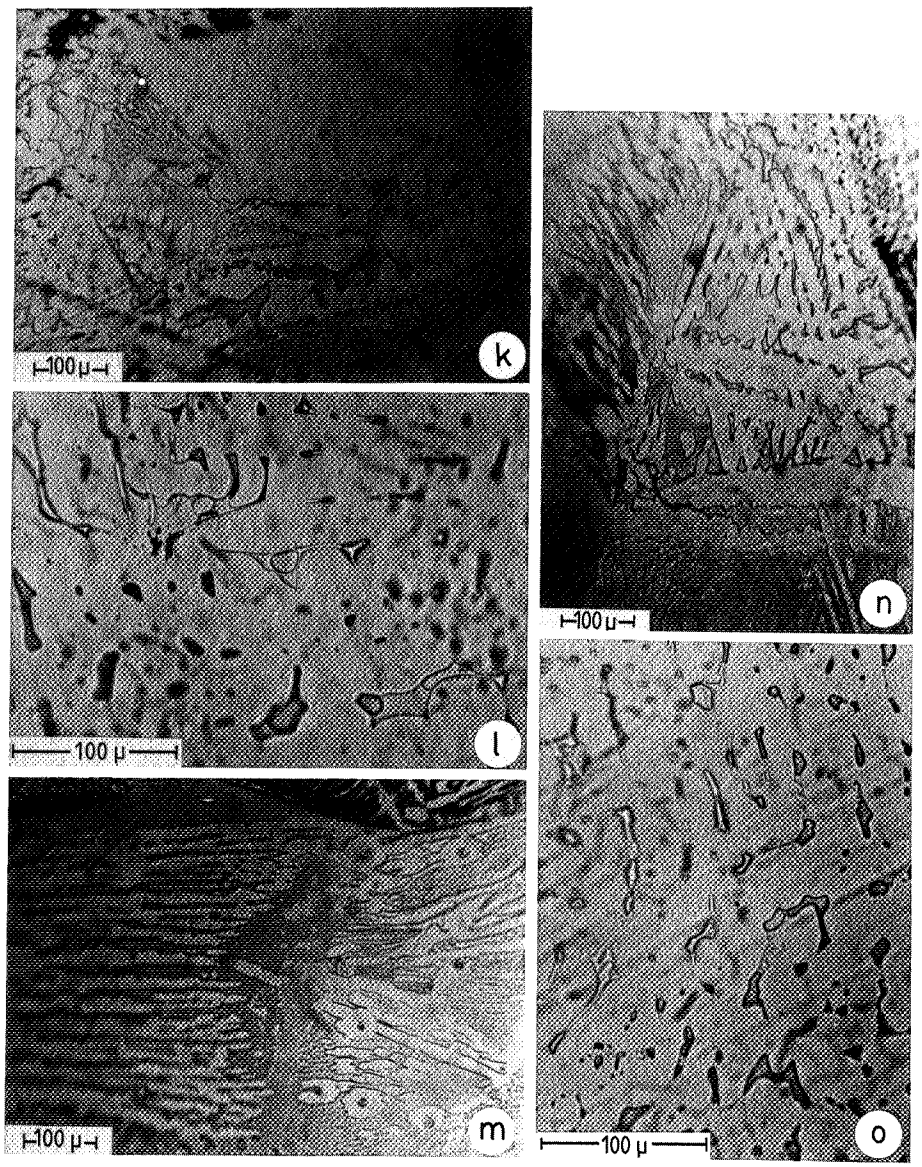
k
100 µ
l
100 µ
m
100 µ
n
100 µ
o
100 µ

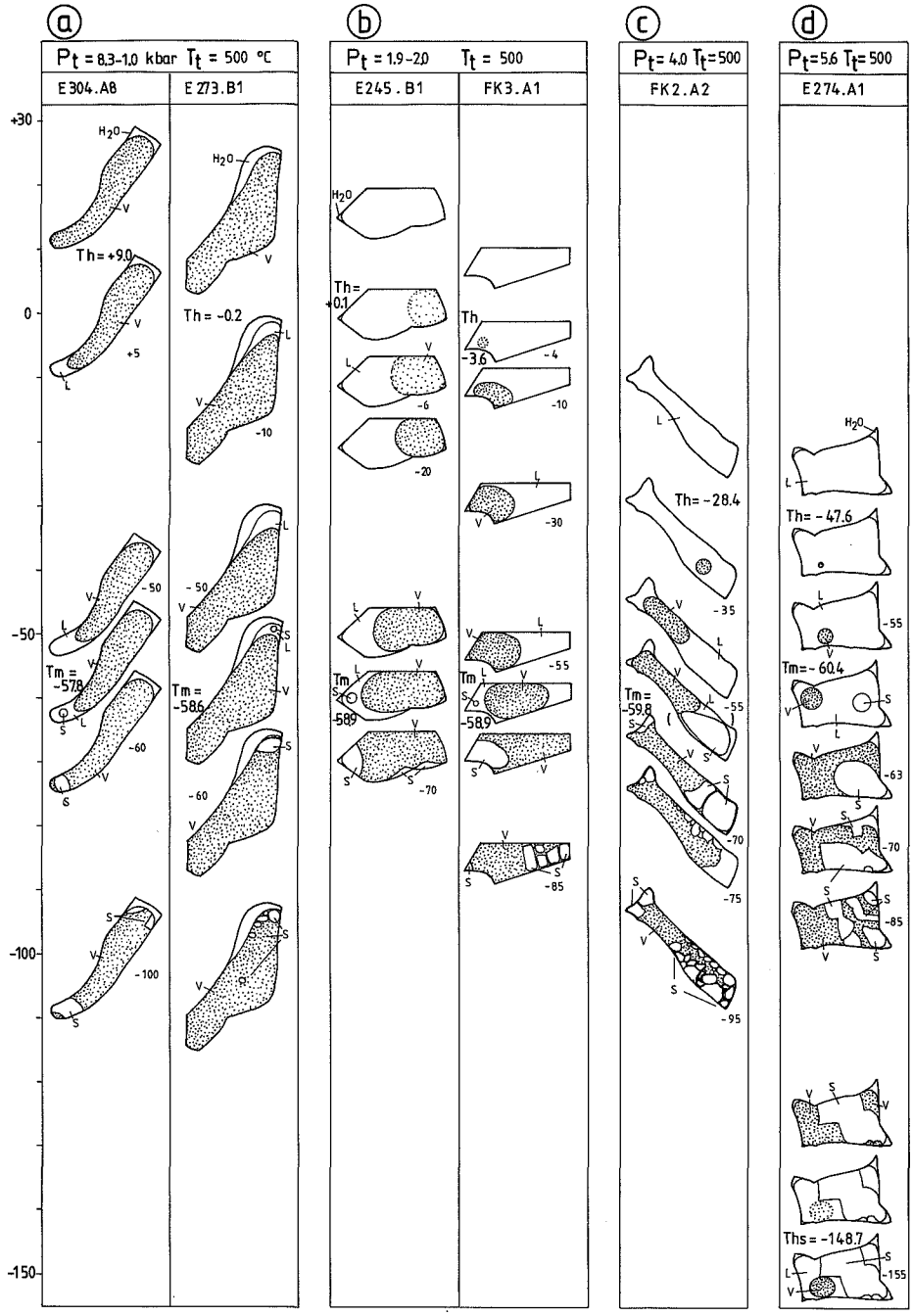
a
Pt = 8.3-10 kbar Tt = 500 °C
E304.A8
E273.B1
b
Pt = 1.9-2.0 Tt = 500
E245.B1
FK3.A1
c
Pt = 4.0 Tt = 500
FK2.A2
d
Pt = 5.6 Tt = 500
E274.A1
+30
0
-50
-100
-150
H2O
Th = +9.0
Th = -0.2
Th = +0.1
Th = -3.6
Th = -28.4
Th = -47.6
Ths = -148.7
Tm = -57.8
Tm = -58.6
Tm = -58.9
Tm = -59.8
Tm = -60.4

Fig.6.6.- Phase sequences during warming from -160°C, observed in fluid inclusions formed by experiments at 500°C with $AgNO_3$ and graphite. Dashed parts represent the vapour phase; other parts represent the liquid and solid phases. Type H3 inclusions formed around ***a)*** *1 kbar* ***b)*** *2 kbar and* ***c)*** *4 kbar; type H4 inclusions* ***(d)*** *only formed at the highest pressure (5.6 kbar).*

6.4.4. Microthermometry of CO_2-rich CO_2-N_2 inclusions

The gaseous parts of inclusions have been studied with the cooling stage in the low temperature range. The following phase transitions were observed: homogenization (T_h), melting (T_m) and partial homogenization (T_{hs}). The inclusions could be typified as H3 (lower densities) or H4 (higher densities) according to the classification proposed in Chap.III. The measurements are listed in Table 6.1.; examples of observed phase sequences are shown in Fig.6.6.

Homogenization temperatures

The variation of homogenization temperatures is in agreement with the experimental conditions: lowest T_h was found for inclusions formed at highest pressures; highest T_h for inclusions formed at lowest pressures. Variations of T_h within one sample is considerable, even for samples for which experimental pressures are known to be constant. This variation is generally less than 10 degrees for samples of lower P_t, but greater for inclusions formed at higher pressures and therefore containing higher density gases. It is assumed here that densities are constant during the experiment i.e. in equilibrium with the acting PT-conditions; therefore, partial leakage may have taken place for a number of inclusions after the experiment. Inclusions with lowest T_h are therefore taken as most representative for the experimental PT-conditions. No correlation was found between T_h and the water content of the inclusions.

Fig.6.7. shows homogenization temperatures (T_h) plotted against trapping pressures (P_t). A "best fitting" curve was drawn by connecting fluid inclusions of supposed highest density within one sample. The resulting T_h-P_t diagram is valid for inclusions trapped at 500°C. Temperatures marking homogenization to the vapour phase are inaccurate because of poor observations: the "true" homogenization points may be somewhat higher than recorded. The position of the T_h-P_t curve is roughly in agreement with available data and thermodynamic equations from the literature for the low (Darimont 1986) and the high PT ranges (Holloway

1977). The internal pressures (at 500°C) of some inclusions may have dropped drastically: from 5.6 to 3 kbar in sample E274 and from 4 to 3 kbar in sample FK2. Critical homogenization was found for inclusions trapped around 1.6 kbar and 500°C; T_h^C is between 0 and 5°C.

Retrograde condensation

Homogenization to the vapour phase is sometimes observed at higher temperatures than the critical point. T_h^C is therefore not the maximum homogenization temperature for the inclusions of present composition. This phenomenon has earlier been mentioned for both systems CO_2-CH_4 and CO_2-N_2 (Arai et al. 1971) and is known as "retrograde condensation". This term is defined as condensation on releasing pressure and is possible by the changing properties of the fluid (heat capacity and expansion coefficient). The following example is given as an illustration: imagine a closed vessel of given volume provided with a piston and filled with a critical fluid at 0°C. A lowering of the pressure by a volume increment will result to the condensation of a liquid. Evaporation of this liquid is possible by increasing the temperature. The 2 sketched situations can be compared with fluid inclusions characterized by a) critical homogenization at 0°C and b) higher homogenization temperatures to the vapour phase. The latter inclusions have higher molar volumes. During further expansion of the volume (and pressure release) of the cylinder of the example, a point should be reached where no condensation is possible without lowering the temperature. This point is defined as the critical point of the second order (Ypma 1963).

Melting temperatures

Recorded melting temperatures vary between -61 and -58°C; they are also correlated with trapping pressures (Fig.6.7). The correlation between T_m and P_t can be well approached by the empirical linear equation $T_m = -0.6 \times 10^{-3} \times P_t - 57.4$ (P_t in bar and T_m in centigrade). The lowest melting temperatures correspond to fluids of highest density and lowest homogenization temperatures.

Extrapolations show that T_m and T_h should become equal for inclusions formed at 6.4 kbar and 500°C. This point is defined by $T_m=T_h=-61$°C. Fluids of the present composition trapped at higher pressures than 6.4 kbar are characterized by sublimation ($T_h<T_m$).

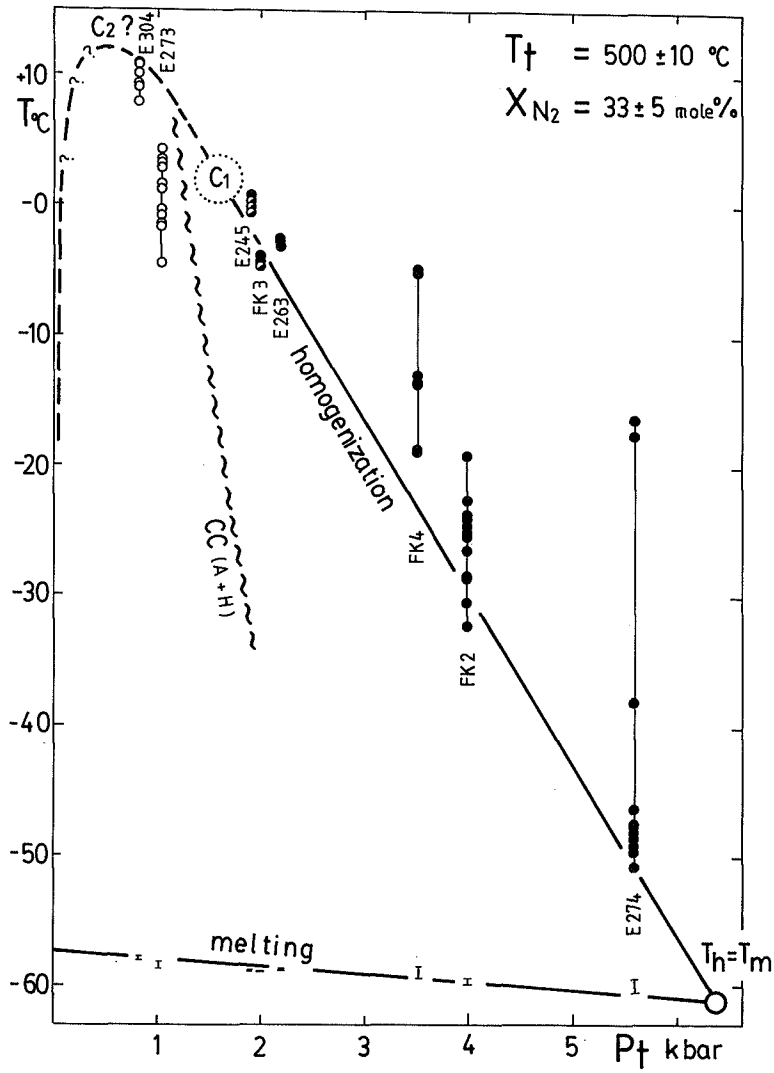

Fig.6.7.- *Homogenization and melting temperatures (T_h, T_m) of experimentally formed inclusions, plotted against trapping pressures (P_t). Black dots = T_h^L; partly filled circles = T_h^C; open circles = T_h^V. The curves shown are representative for the highest density inclusions within a sample; lower densities (higher T_h^L) are explained by partial leakage. C_1 denotes the critical point of the first order; the position of the critical point of the second order (C_2) is not exactly known. The critical curve as obtained from Arai et al. (1971) and the Holloway equation is indicated by a wavy curve, approximately intersecting the presently found position of C_1.*

Partial homogenization

Partial homogenization (T_{hs}) of the N_2-rich liquid and vapour (in the presence of solid CO_2) is only observed for inclusions of highest density (samples E274; FK2). These homogenizations are not observed for the other samples, although homogenizations to the vapour phase (T_{hs}^V) are suspected. Recorded partial homogenization temperatures range between -149/-148°C (critical or near critical) and about -150°C (vapour) i.e. around and below the critical temperature of nitrogen (Table 6.1).

Argon contamination

Argon was found as an additional gas species in one of the samples (E232). This gas is used as pressure medium and may intrude into the capsule in case of leakage during the experiment. The identification of argon is difficult because it cannot be detected by regular analytical techniques. The presence of argon became evident because of higher partial homogenization temperatures (T_{hs}) than the critical temperature of N_2 (in the absence of methane!). One inclusion which did not contain any CO_2, showed critical homogenization at -123.8°C i.e. near the critical temperature of Ar (-122.3°C). Both T_m and T_h appeared to be drastically lowered in CO_2-N_2-Ar inclusions with increasing Ar contents. Ar-bearing inclusions can be recognized by their strongly deviant microthermometric behaviour. There are no indications for argon in other samples than the one mentioned. The supposition that argon was also captured in other samples was one of the reasons why some experiments were carried out in Tübingen (M.P.I.) where CO_2 is used as a pressure medium.

6.4.5. Raman analysis of inclusions made by decomposition of silver-nitrate

The compositions of selected inclusions were measured by Raman analysis. The measurement results are listed in Table 6.1. CO_2 and N_2 are the only constituents of the gas phase (neither CH_4 nor other gases could be detected). Remarkable is the large compositional range between the 2 components (Fig.6.8.): N_2 contents were found between 22 and 39 mole% (mostly between 31 and 38 mole%). The Raman measurement of the "quartz

tube" (33 mole% N_2) is consistent with these data. The compositional variation within one sample mostly does not exceed 5 mole%. Measurements are more accurate for inclusions of higher density because of their stronger Raman signal (more molecules per unit volume): accuracies are estimated to be ±2 mole% for the high density inclusions and ±5 mole% for inclusions of lower density (pers. comm. Drs. E.A.J. Burke). Several inclusions produce lower Raman signals because of extremely flat shapes.

Leakage during the experiments with CO_2 as a pressure medium, is responsible for erroneous higher CO_2 contents (sample FK4). The N_2/CO_2-ratio is not influenced in the case of argon as a pressure medium: the fluid is only "diluted" then (sample E232).

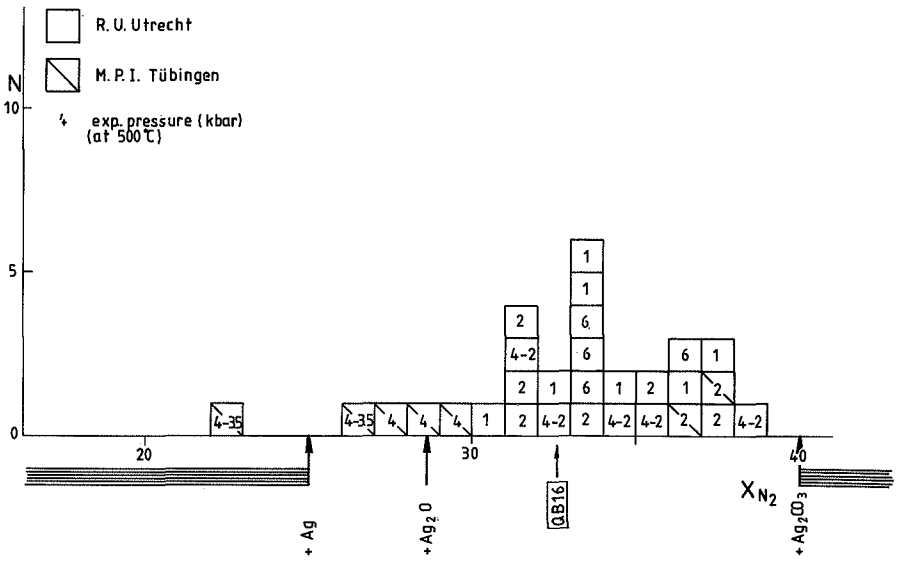

Fig.6.8.- *Histogram showing the results of Raman analysis (X_{N2}) for artificial inclusions, formed by the thermolysis of $AgNO_3$ (+graphite). The compositional distribution indicates that most inclusions formed during the stability of Ag_2CO_3. The (gradual) replacement of Ag_2CO_3 by silver (and/or silver oxides) results to CO_2-richer gas compositions. QB16 denotes the gas composition of a heated quartz tube, consistent with the mean fluid inclusion composition (33 mole% N_2).*

The mean gas composition of the inclusions formed by the thermolysis of $AgNO_3$ is 33 mole% N_2 with a variation of ±5 mole%. The N_2 content is significantly higher than calculated from the theoretical reaction equilibrium, taken silver as the only solid reaction product (25 mole% N_2, R.6.5a). Possible explanations for this discrepancy are given below:

a) Other solid reaction products than silver (Ag_2O and especially Ag_2CO_3) could be stable <u>during</u> the experiment, although these compounds could not be identified afterwards. "Quartz tube experiments" (section 6.4.1.) showed that the formation of silver proceeds very slowly (in the order of 1 or 2 days): at first, another reaction product is formed (most probably Ag_2CO_3) which is replaced by silver. The N_2 content of the gas phase should therefore be higher during the first days of the experiment (reaction 6.5c). The presently found compositions may therefore indicate that most inclusions already formed during the earliest stage and fluid films should be isolated from the surrounding gas. The compositional variation can be interpreted as a trapping time sequence.

b) The equilibria of reactions 6.5a-c are dependent on the acting gas pressure: Ag_2CO_3 should be favoured at higher (gas) pressures, silver at lower pressures. Ag_2CO_3 was possibly stable during the whole experimental run and silver formed just upon pressure release. However, such "retrograde" solid-solid reactions are not expected to proceed in a short time interval. Further, no distinct correlation between gas composition and experimental pressures was found.

c) CO_2 may be partly dissolved in the aqueous phase. However, there is no correlation between gas compositions and water contents. The capillary quartz tube of the "dry" HT-experiment contained gas of the same composition as the "wet" fluid inclusions.

d) The Raman analyses may be wrong because of incorrect values of the relative Raman cross-section (σ). For the present calculations, σ of N_2 and CO_2 were taken 1 and 1.21 respectively (sections 4.6.2; 4.6.3). The present samples (in particular quartz tubes) can be only used as a standard for the determination of σ, if gas compositions are determined independently. The relative Raman cross-section of a compound i, mixed with N_2 (σ = 1 by definition) is then calculated from the following equation.

$$\sigma_i \quad \frac{A^*_i}{A^*_{N2}} \cdot \frac{N_{N2}}{N_i} \qquad \text{(Eq.6.1.)}$$

where A^*_i denotes the peak integral for given laser power and integration time; N_i denotes the number of moles (cf. Eq.4.8). The ratio of the peak integrals was found to be about 2.4567 for the present samples. If X_{N2} = 0.25 is taken as the true composition of the fluid,

σ_{CO2} would be 0.82 (=2.4567 x 25/75). However, there are no indications for major deviations from the value published by Schrötter & Klöckner (1979) (section 4.6.3). Discrepancies between the theoretical and found compositions can therefore not be explained by the inaccuracy of the Raman cross-section.

e) Non-detectable compounds may be present.

The first mentioned possibility (a) seems to be most plausible because both the mean composition and the compositional variation (within the given limits) can be explained. It is therefore concluded that compositions of fluid inclusions are determined in the earliest experimental stage (during one or two days) at 500°C; although quartz healing is poor in this time interval, fluid transport is already very restricted. Possible later changes of the surrounding gas composition do hardly effect the composition of the ultimate inclusions.

6.4.6. Isochores in the high PT region

It has been shown in the foregoing how the trapping conditions of artificial fluid inclusions (T_t, P_t), homogenization temperatures (T_h) and compositions (X) are obtained from experimental runs, microthermometry and Raman analysis. It is now aimed at plotting high and low PT-conditions in one single diagram. P_h (the pressure at the homogenization point) cannot be measured, but it can be estimated from an available equation of state (Heyen 1980, 1981; Darimont & Heyen 1988): pressures are calculated to be 110 to 160 bar for inclusions of X_{N2} = 0.33 homogenizing to the liquid phase. These pressures are relatively low compared to the experimental pressures and they can therefore be accepted as a good approximation on a large PT-scale. A plot of both experimental and homogenization conditions is shown in Fig.6.9. The low and high PT-conditions are connected by straight lines. These tie-lines approximate the isochores for ideal (low density) gases and should be slightly curved for non-ideal (high density) gases. Inclusions trapped along the same isochore show the same phase behaviour at low temperatures. In this way it is possible to extend the knowledge for inclusions trapped at 500°C to lower and higher trapping temperatures.

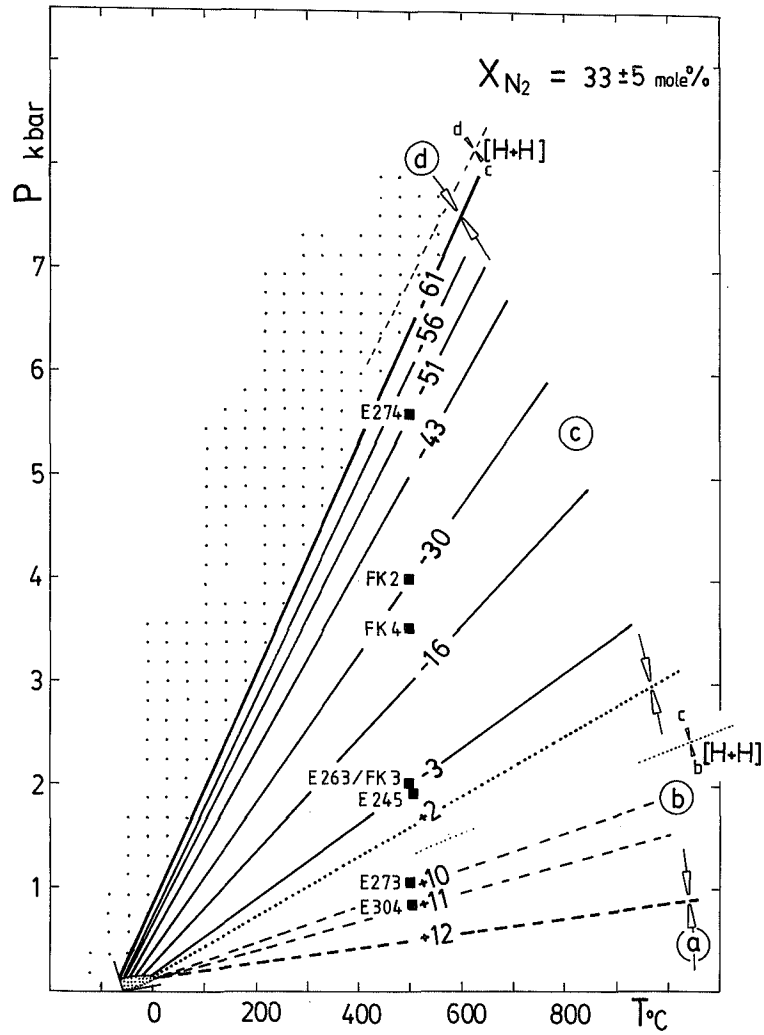

Fig.6.9.- *Experimentally derived isochores constructed by the connection of PT conditions in the low (multi-phase) and high (experimental) region. Numbers indicate homogenization temperatures (°C). Solid lines = homogenization to the liquid phase; dashed lines = homogenization to the vapour; dotted line = critical homogenization. Fluid inclusions formed at PT conditions in the stippled area, are characterized by sublimation ("$T_h<T_m$"). Denotations of phase behaviour (a, b, c and d) refer to the text. The critical curve and the curve $T_h=T_m$, estimated from the Heyen and the Holloway equation [H+H] are shown for comparison.*

Inclusions of the present composition can be grouped according to their phase behaviour at low temperatures. These inclusion types, in

order of decreasing molar volumes (increasing densities), are characterized by

a) melting and (stable) homogenization to the vapour phase;
b) melting and (stable) homogenization to the vapour phase with $T_h^V > T_h^C$ ("retrograde condensation");
c) melting and (stable) homogenization to the liquid phase;
d) sublimation and metastable homogenization to the liquid phase.
The trapping conditions of each type cover a well defined part of the PT-field (Fig.6.9).

For comparison, isochores were constructed from available equations of state (for high and low PT) (Fig.6.9): the MRK-equation as given by Holloway (1977) and the Heyen-equation; critical conditions are obtained from Arai et al. (1971). The results of available equations and the present experiments for the CO_2-rich compositions are, seen the accuracy of both sources, in reasonably good agreement.

6.5. Experiments with ammonium-nitrate and graphite

6.5.1. Decomposition reactions

Nitrogen-rich CO_2-N_2 mixtures were made by the thermolysis of NH_4NO_3 in the presence of graphite. Reactions were studied by heating capillary quartz tubes. Heating NH_4NO_3 only results to the forming of nitrogen oxides, nitrogen, oxygen, water and nitric acid.

The following observations were made on heating NH_4NO_3:
a) melting to a colourless liquid. The melting temperature of NH_4NO_3 at 1 atm. is +169.6°C (Weast 1975);
b) decomposition into nitrogen oxides. The gas composition at high temperature could not be determined, but it is assumed to be a mixture of one or more of the following compounds: N_2O, NO, NO_2, N_2O_4, N_2 and O_2. Only NO_2 could be discerned by its brown colour. The latter gas formed already shortly after melting, but the colour fades away on further heating (to about 380°C). The amount of liquid slowly decreases resulting to a single gas phase.

During subsequent cooling, a colourless liquid (nitric acid?) condensates and the gas turns to brown again. The liquid was found to be extremely acid with pH ~ 0. On further cooling to room temperature, the gas colour turns from brown to colourless (N_2O_4?). A solid phase does not form.

Raman analysis of the gas content of the tube shows a composition (in mole%) of $N_2O(76)$ $N_2(23)$ $O_2(2)$ (calculated for the 1285-peak of N_2O, σ = 1.96). The following

reaction equilibrium is suggested (at room temperature) after the decomposition of NH_4NO_3 into a gas and a liquid phase assumed that HNO_3 formed as a reaction product:

$$10\ NH_4NO_3 = 7.3\ N_2O + 2.2\ N_2 + 0.2\ O_2 + 19.5\ H_2O + 0.9\ HNO_3 \quad (R.6.6.)$$

Possible chemical equilibria at higher temperatures and pressures are given below, assumed that HNO_3 and H_2 do not form:

$$NH_4NO_3 = 2\ H_2O + N_2O \quad (R.6.7a)$$
$$= 2\ H_2O + NO + 1/2\ N_2 \quad (R.6.7b)$$
$$= 2\ H_2O + 1/2\ NO_2 + 3/4\ N_2 \quad (R.6.7c)$$
$$= 2\ H_2O + 1/2\ O_2 + N_2 \quad (R.6.7d)$$

The environment after decomposition is extremely acid and oxidizing. CO_2 should therefore be formed by the addition of graphite. The total reaction in its most simple form can be written as

$$NH_4NO_3 + 1/2\ C \rightarrow 2H_2O + 1/2\ CO_2 + N_2 \quad (R.6.8.)$$

Experiments in capillary quartz tubes have been done to verify this reaction. It has been observed at a temperature of 300°C that the brown gas (NO_2) grades to a colourless gas going to the graphite-bearing part of the tube. This observation is interpreted as evidence for the proceeding of the reaction

$$2\ N_2O + C = CO_2 + 2\ N_2 \quad (R.6.9)$$

The brown colour vanishes after a period of about 15 minutes. The amount of graphite diminishes in proportion.

A sample, put in a furnace for about 3 hours at 315°C, was analysed afterwards by Raman analysis. The measurement result for the gas phase is $N_2(77)CO_2(23)$. No other gaseous compounds (neither nitrogen oxides nor CH_4) could be detected. The CO_2 content appeared to be lower than expected from reaction 6.9. (23 mole% instead of 33 mole%). The following total reaction is therefore suggested, assumed that HNO_3 is also formed:

$$NH_4NO_3 + 0.3\ C \rightarrow 0.9\ N_2 + 0.3\ CO_2 + 1.9\ H_2O + 0.2\ HNO_3 \quad (R.6.10.)$$

6.5.2. HPT-experiments (P = 2 to 6 kbar; T = 500°C)

Fluid inclusions were made by healing "cracked" quartz in gold capsules as described in section 6.2. The used capsules are 0.45 cm in diameter and about 3 cm long and partly filled with NH_4NO_3 and a surplus

of graphite. The amount of water formed by decomposition is sufficient for quartz healing: 9 to 11 mg water is released from presently used 21 to 25 mg NH_4NO_3 (according R.6.10.). Some extra water (10 mg) was added for two experiments.

The experimental PT conditions were taken about 2, 4 and 6 kbar at 500°C; durations were about 2 weeks. Slightly wet graphite is the only non-gaseous constituent of the capsules (besides the quartz cylinders) after the experimental runs.

Many well developed inclusions formed (with an average size of 10-30μ) (Fig.6.5). Their water content varies between 10 and 30 vol%. "Daughter crystals" (salts) have not been observed.

6.5.3. Microthermometry of N_2-rich CO_2-N_2 inclusions

The phase behaviour of inclusions, produced by the ammonium-nitrate experiments, is characterized by sublimation (type S2); melting (type H3) is only suspected for some low density inclusions, but the amounts of liquid (on melting) are too small for clear observation. Low temperature phase behaviour of (the gaseous parts of) fluid inclusions is described below.

Cooling runs

Solidification ("freezing") of CO_2 has been observed on cooling between -90 and -120°C with a tendency of lower freezing temperatures with lower densities. A small amount of liquid condensates just before freezing in fluid inclusions formed above 4 kbar; liquid possibly also condensates in fluid inclusions formed at lower pressures. On continuing cooling, a bubble appears between -147 and -160°C. In summary, the phase transitions observed on cooling from room temperature to -160°C can be written as V → (V+L) → S+V → S+L+V. Solid CO_2 takes about 5 to 30 vol% of the cavities at the 3-phase stage for inclusions formed at 2 to 5.6 kbar (and 500°C) respectively; the respective bubble sizes are about 80 to 10 vol% (the relative amounts of solid and liquid are about constant in all inclusions at these low temperatures, but the volume of the vapour phase strongly varies).

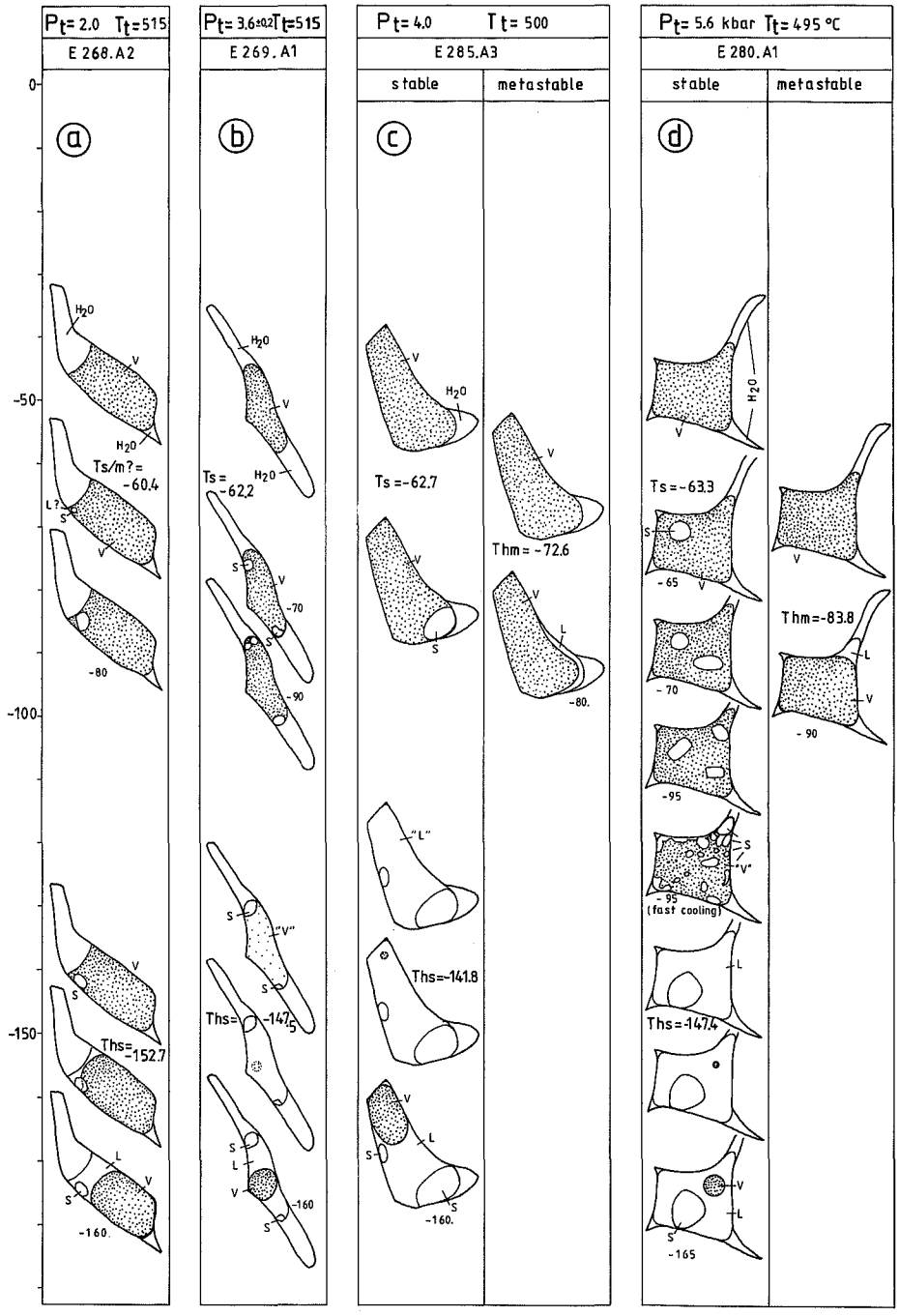
Pt= 2.0 Tt=515
E 268.A2
Pt= 3.6±0.2 Tt=515
E 269. A1
Pt= 4.0 Tt= 500
E 285.A3
stable
metastable
Pt= 5.6 kbar Tt= 495 °C
E 280.A1
stable
metastable
0
-50
-100
-150
a
b
c
d
H2O
V
L
S
Ts/m?= -60.4
-80
Ts= -62.2
-70
-90
"V"
Ths= -147.5
-160
Ts=-62.7
Thm= -72.6
"L"
Ths=-141.8
-160.
Ts=-63.3
-65
-70
-95
-95 (fast cooling)
Ths=-147.4
-165
Thm=-83.8
-90

Fig.6.10.- *Observed phase sequences at low temperatures in fluid inclusions formed by experiments at 500°C with NH_4NO_3 and graphite. Dashed parts represent the vapour phase, other parts the liquid and solid phases. All inclusions (a, b, c and d) are characterized by partial homogenization and subsequent sublimation (type S2) and formed around 2, 3.6, 4 and 5.6 kbar respectively. Melting of solid CO_2 and homogenization to the vapour phase (S+V → S+L+V → L+V → V) is suspected for inclusions formed at the lowest pressure (a), but the amount of liquid is too small to be observed. Metastable homogenization was detected for inclusions formed at higher pressures (c-d).*

Warming runs after cooling

Phase transitions observed on warming from -160°C are shown in Fig.6.10; measurement results are listed in Table 6.2. Partial homogenization (T_{hs}) has been observed for inclusions in all samples. These homogenizations are to the vapour, critical or liquid phase in order of increasing trapping pressures. Critical partial homogenization at -147°C (S+L+V → $S+V_{crit}$) has been recorded for inclusions formed around 3.5 kbar and 500°C. This temperature is equal to the critical temperature of pure N_2. Critical or near critical homogenization temperatures are difficult to be measured accurately. Temperatures marking homogenizations to the vapour phase (S+L+V → S+V) are significantly lower than T_{hs}^C (between -156 and -149°C). Partial homogenization to the liquid phase (S+L+V → S+L) was found for inclusions formed at 4 and 5.6 kbar. T_{hs}^L is higher than -147°C here (between -147 and -142°C). Higher partial homogenization temperatures than -147°C are due to the presence of methane (see sections 6.5.4. and 6.7.2.)

Just after partial homogenization, solid CO_2 coexists with a vapour, critical fluid or liquid. The character of the volatile phases becomes supercritical to higher temperatures. The amount of solid CO_2 decreases by evaporation on further warming until total disappearance (the sublimation point). Present sublimations were measured at temperatures between -68 and -60°C. The volume of solid CO_2 remains about constant for a large temperature range and suddenly shrinks at T_s. Brownian movements of the solid particle (!) have been observed (sample E268) just before sublimation. This is an indication for high fluid densities (approximating the density of the solid) and it can be concluded that the conditions around the sublimation point are not far from condensation (and melting) here. It is mostly difficult for these fluids (with T_h-T_m-T_s) to decide wether the solid phase disappears by melting (S+V →

S+L+V → L+V) or sublimation (S+V → V). Melting is favoured for inclusions formed at lower pressures (see below) with subsequent homogenization to the vapour phase, just after melting.

Metastable homogenization

Metastable homogenization (T_{hm}) can be observed for inclusions showing 2 phases (liquid and vapour) above the freezing point. Present T_{hm} was observed to the vapour phase at temperatures between -74 and -71°C (for inclusions trapped at 4.0 kbar) and between -89 and -81°C (for inclusions trapped at 5.6 kbar). The latter temperatures are very near to the freezing temperature and they represent the lowest possible T_{hm} which can be measured in CO_2-N_2 inclusions.

Correlations between microthermometry and experimental (trapping) conditions

Correlations between temperatures marking phase transitions (T_{hs}, T_{hm}, T_s and T_h) and trapping pressures (P_t) (at 500°C) are shown in Fig.6.11. Sublimation temperatures are lowered to higher trapping pressures and consequently higher densities. The best fitting correlation between T_s (partly T_m?) and P_t is given by the equation $T_{s/m} = -1.07xP_tx10^{-3} - 57.6$ (P_t in bar and $T_{s/m}$ in centigrade). This line is significantly steeper than calculated for CO_2-rich compositions (section 6.4.4.). The line is cross-cut by extrapolated homogenization points at P_t = 3.0 kbar where $T_h=T_s=T_m=-60.8$°C. It is remarkable that metastable homogenization temperatures to the vapour phase are lower to higher trapping pressures. These homogenizations should therefore represent conditions between the critical points of the 1st and 2nd order (C_1 and C_2) as was discussed for the inclusions made by $AgNO_3$. "Retrograde condensation" is the more typical for fluids of N_2-rich composition. Metastable homogenization to the liquid phase (L+V → L) is not possible for the present inclusions because the (1st order) critical point should be situated below the freezing temperature. It can be further stated that lowest T_{hm}^V within one sample corresponds to highest densities, most representative for the experimental conditions. Fluid inclusions of lower density than the density at C_2, will show "normal" phase behaviour i.e. lower homogenization temperatures (to the vapour phase) at lower densities. The

position of C_2 is estimated between -40 and -35°C for the present composition.

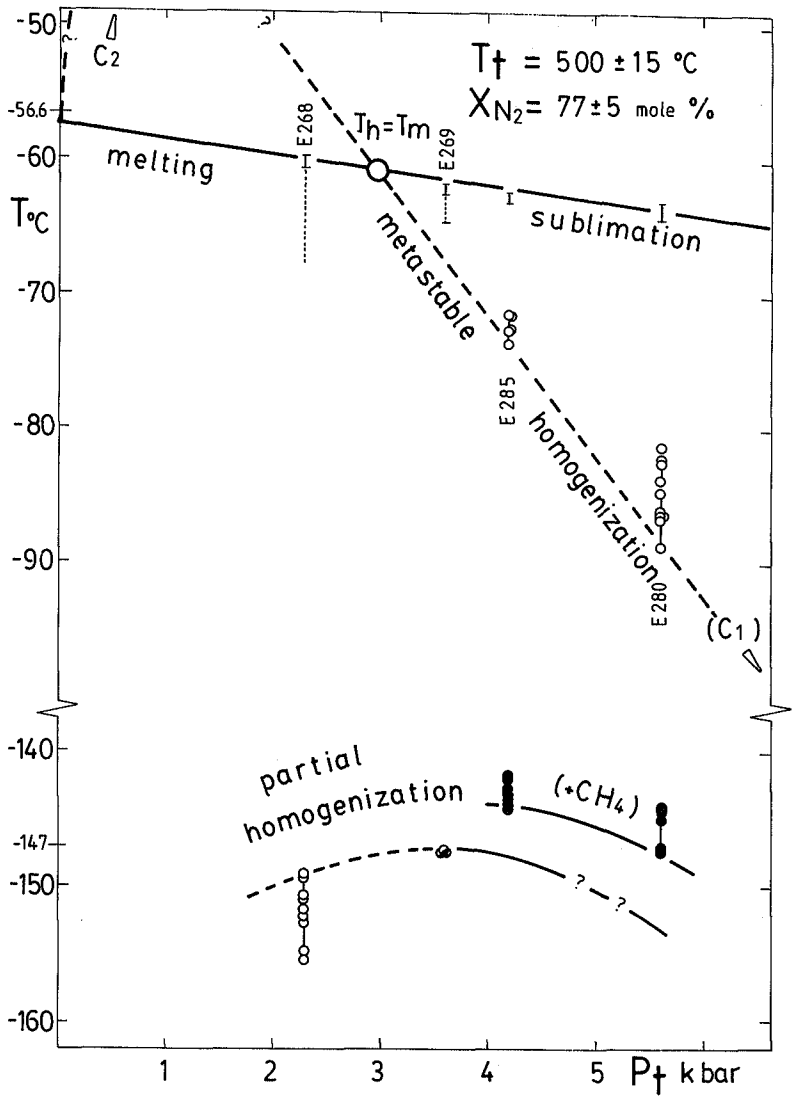

Fig.6.11.- *Temperatures of partial homogenization (T_{hs}), metastable homogenization (T_{hm}), sublimation (T_s) and melting (T_m) of artificial inclusions, plotted against trapping pressures (P_t). T_{hm} is only to the vapour phase; T_{hs} may be to the liquid (black dots), critical (partly filled circles) or vapour phase (open circles). The curves shown are representative for the highest density inclusions within a sample. The present fluid compositions are characterized by "retrograde condensation" (lower T_{hm}^V with higher densities). The position of the (metastable) critical point (C_1) is probably lower than the freezing*

point and cannot be reached. Higher partial homogenization than -147°C is due to the presence of 8 to 11 mole% CH_4.

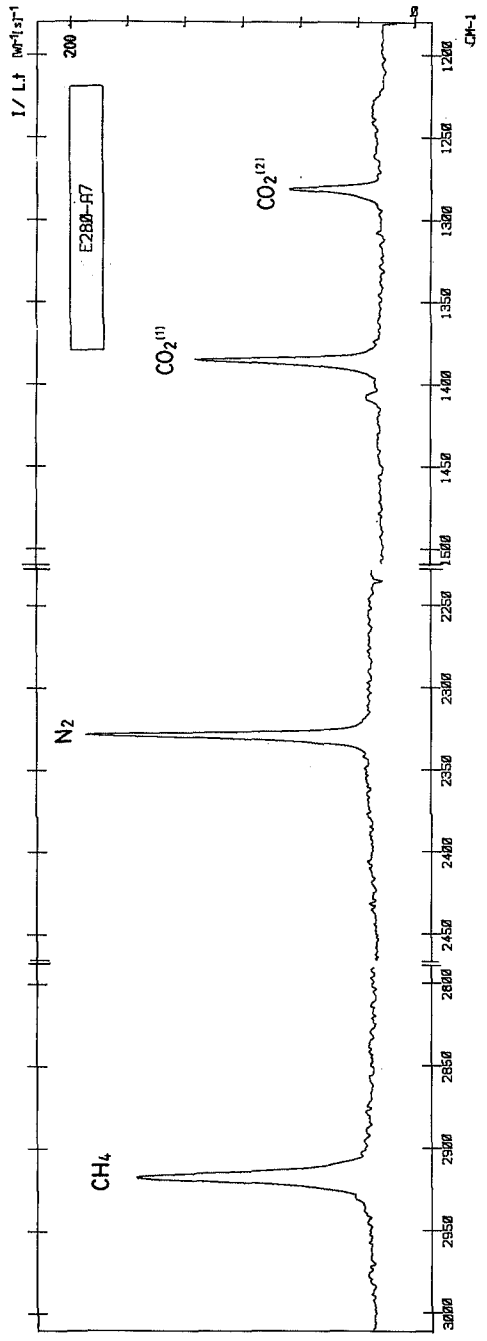

Fig.6.12.- *The Raman spectrum of an inclusion containing 60 mole% N_2, 29 mole% CO_2 and 11 mole% CH_4 formed at 500°C and 5.6 kbar (relative peak heights are to scale).*

Temperatures marking partial homogenization for CO_2-N_2 inclusions show maximum values at the critical fluid conditions (-147°C) (see section 6.7.2): P_t=3.5 kbar (T_t = 500°C). T_{hs} of 5°C above this temperature was noticed for inclusions containing about 10 mole% of methane (and trapped at 4 to 6 kbar, 500°C).

The phase behaviour as described above is unique for N_2-rich CO_2-N_2 inclusions and cannot be translated in terms of trapping conditions and molar volume by the existing models. The present observations of experimentally formed inclusions enable the determination of trapping pressures (at 500°C) from metastable homogenization and sublimation temperatures.

6.5.4. Raman analysis of inclusions made by decomposition of ammonium-nitrate

The gaseous parts of the present fluid inclusions have been analysed with the help of the Raman microspectrometer. The results of calculated compositions are presented in Table 6.2: N_2 contents are 60-79 mole%; CO_2 contents 21-32 mole%. Most remarkable is the presence of up to 11 mole% CH_4 in 3 of the 4 samples (Fig.6.12). Methane did not form in the other experimental inclusions discussed in this chapter. A graphical representation of the compositions is shown in Fig.6.13a. A tendency of higher CO_2 contents with increasing CH_4 was noticed. This can be best explained by a shift of the reaction

$$2\ C + 2\ H_2O \quad CH_4 + CO_2 \qquad \text{(R.6.11.)}$$

This reaction equilibrium is known to play an important role in general for CO_2-CH_4-H_2O inclusions. Proceeding of the reaction to the right will result to equal enrichment of the fluid in both CH_4 and CO_2. The present data affirm this assumption (Fig.6.13a). It can be further assumed that the measured gas compositions (at room temperature), represent compositions in equilibrium at the experimental conditions as the "retrograde" reaction is blocked because of the high nucleation energy of graphite (Kreulen 1987). Equivalent CO_2-N_2 compositions (i.e. if CH_4 would not be formed) can be calculated by subtracting equal amounts of CH_4 and CO_2 (Fig.6.13b). These "reduced" CO_2 contents show a frequency

maximum around X_{CO2} - 0.23 (X_{N2} = 0.77) which is in agreement with earlier measurements of the capillary quartz tubes. CH_4 was not detected in the latter tube. It can be concluded that CH_4 only forms in fluids of higher N_2/CO_2-ratio and not in CO_2-rich gases.

The present experiments indicate that reaction 6.11. is pressure dependent: the highest CH_4 contents were found for inclusions formed at the highest pressures. Contrary to the present findings, it might be expected from reaction 6.11. that the forming of CH_4 is favoured at lower pressures and the higher density phases (graphite and water) at higher pressures (Kreulen 1987). Further, increasing water contents should also favour the forming of CH_4. In the present samples however, higher CH_4 contents were found at lower H_2O contents. A sufficient explanation for the presence of CH_4 has not yet been found.

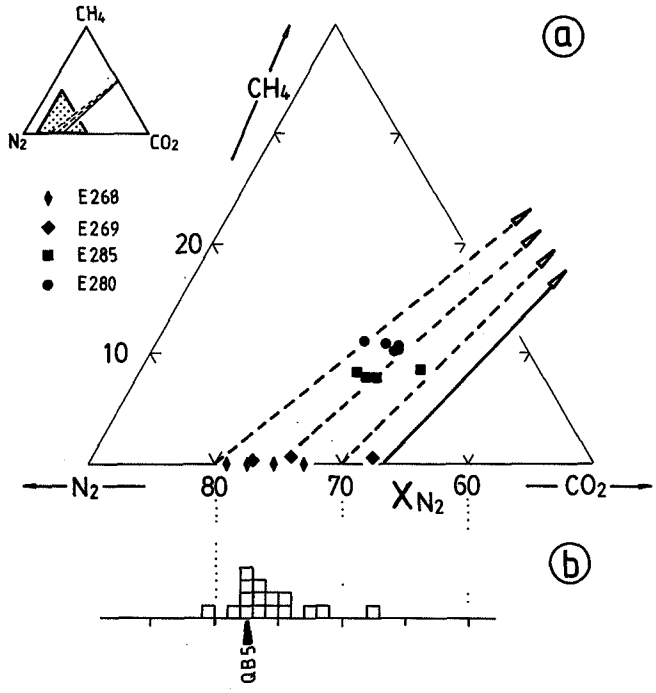

Fig.6.13.- *Gas compositions of 4 samples: the results of Raman analysis for fluid inclusions formed by experiments with NH_4NO_3 and graphite.*
a) *The triangular composition diagram CO_2-CH_4-N_2. Significant higher CO_2-contents are found for higher CH_4. Arrows indicate shifts of gas composition by proceeding of reaction $2C + 2H_2O = CO_2 + CH_4$.*
b) *Gas compositions with "reduced" CO_2-contents obtained from the equation: $X_{N2}' = X_{N2} / (X_{CO2}-X_{CH4}+X_{N2})$ (see text).*

6.5.5. Isochores in the high PT region

Isochores for inclusions of the present composition (X_{N2} = 0.77 ±0.05) are constructed by drawing tie-lines between the experimental conditions (T_t, P_t) and the homogenization points (T_h, P_h) (see section 6.1 and Fig.6.1). P_h can be estimated from the Heyen equation of state: the maximum internal pressure in multi-phase CO_2-N_2 inclusions is about 255 bar. The construction of isochores valid for the HPT range is allowed because P_h is very small compared to experimental pressures. The result is shown in Fig.6.14. This diagram was constructed with the help of the "best fitting curve" of Fig.6.11. For comparison, isochores and type distributions were calculated with the MRK-equation of state (Holloway 1977) and the Heyen equation. The discrepancy between calculated and experimental results is considerable: inclusions characterized by sublimation are much more common in the present samples. The phase behaviour for inclusions (of the present composition) can be grouped in order of increasing densities (Fig.6.14):

a) melting and (stable) homogenization to the vapour phase;

b) melting and (stable) homogenization to the vapour with $T_h^V > T_h^C$ ("retrograde condensation") (sample E268?);

c) sublimation and metastable homogenization ($T_h < T_m$) to the vapour phase (most common phase behaviour in the present samples: E280; E285; E269);

d) sublimation and metastable homogenization ($T_h < T_m$) to the liquid phase (probably not possible for the present composition as was mentioned in section 6.5.3).

Fig.6.14.- *Experimentally derived isochores constructed by connecting PT conditions in the low (multi-phase) and high (experimental) region. Numbers indicate homogenization temperatures (°C). Only homogenization to the vapour phase is possible for the present composition. Fluid inclusions plotting in the stippled area, are characterized by sublimation ("$T_h<T_m$"). Denotations of phase behaviour (a, b, c and d) refer to the text. The curve $T_h=T_m$ as estimated from the Heyen and the Holloway equation [H+H] is shown for comparison. Critical partial homogenization (T_{hs} = -147°C) corresponds to a (metastable) homogenization temperature of (T_{hm}^V) of about -68°C.*

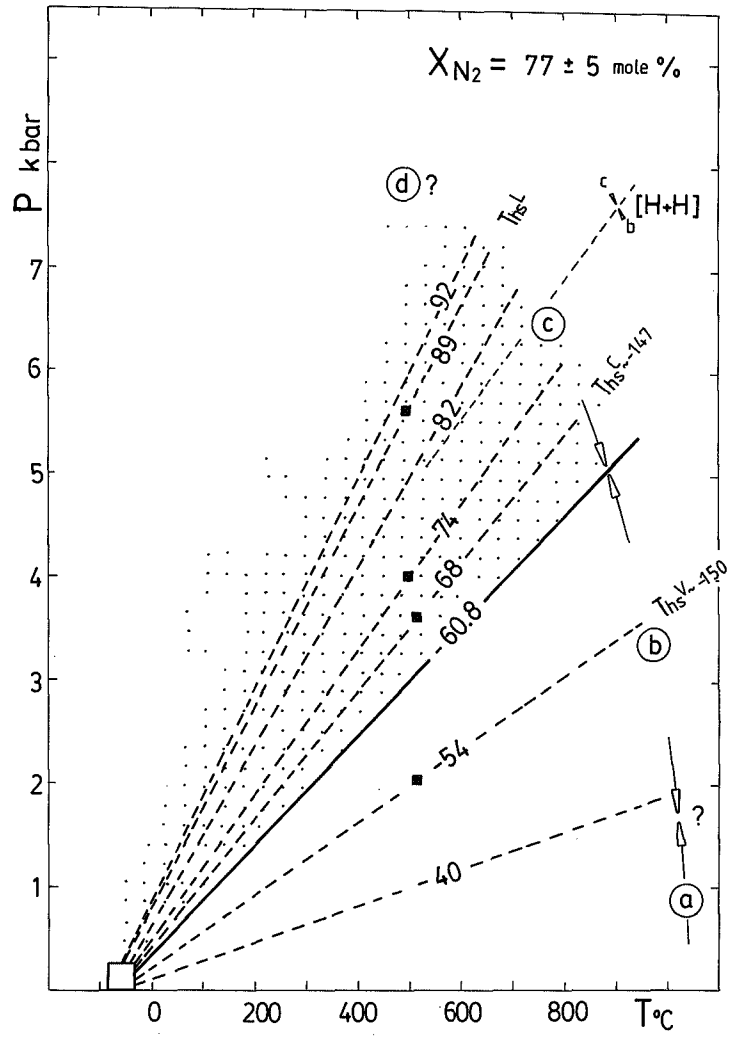

(Fig.6.14)

6.6. Inclusions containing about equal amounts of CO_2 and N_2

It has been shown in the foregoing how CO_2-N_2 inclusions of almost constant composition could be generated: inclusions with X_{N2} - 0.33 were made by using silver-nitrate as the main starting compound; inclusions with X_{N2} - 0.77 by using ammonium-nitrate. It is intended to establish a general model for the system CO_2-N_2, valid for the full compositional range. In particular, it was aimed at finding the point of coinciding critical and melting conditions (denoted as point Q, Chap.III). Mixtures of several starting materials are possible for the generation of fluids of intermediate composition. The two compounds ammonium-nitrate and

guanidine-nitrate are chosen here for the production of N_2. They were mixed with silver-oxalate which produces CO_2 on heating. Graphite was added for all experiments to ensure complete reduction of possible nitrogen-oxides. Wide compositional ranges of the produced gases can be achieved in this way. However, the present experiments were confined to a composition of $X_{N2} \sim 0.55$, most interesting for the characterization of the point $T_h^C = T_m$. The results of the experiments with ammonium-nitrate and silver-oxalate are in agreement with expectations based on earlier experiments; the results of the experiments with guanidine-nitrate are somewhat disappointing as it appeared not to be possible to produce high density inclusions by using this compound (see sections 6.6.2. and 6.8).

6.6.1. Experiments with ammonium-nitrate and silver-oxalate

It was demonstrated (section 6.5) that experiments with ammonium-nitrate (NH_4NO_3, M = 80) result to the production of CO_2-N_2 gases containing 77 ±5 mole% N_2. Higher CO_2 contents can be obtained by adding silver-oxalate ($Ag_2C_2O_4$, M = 303.76). A surplus of graphite was added as well. Small amounts of extra water (besides water released by decomposition) stimulate quartz healing.

Firstly, chemical reactions were tested by doing "quartz tube experiments" (as described in section 6.3.): the behaviour appeared to be about similar to that described for the decomposition of NH_4NO_3 only. In addition, decomposition of $Ag_2C_2O_4$ results to the precipitation of silver and other solid (intermediate) reaction products (Ag_2CO_3, Ag_2O_2).

Decomposition experiments of $Ag_2C_2O_4$ only show that this compound firstly transforms to a very dark brown compound (Ag_2O?) after 15 min. at 200°C. This colour turns to black afterwards (Ag_2O_2?) and subsequently shows a gradual transition into a beige-coloured (sometimes greenish white) compound (Ag_2CO_3?) after 45 min. at 200°C. CO_2 was detected by Raman analysis as the only present gaseous compound.

Another experiment, the decomposition of Ag_2CO_3, shows the following results: first the formation of a black compound (Ag_2O_2?) (after 15 min. at 400°C) and the subsequent formation of a white compound. A brown precipitate also formed in the latter case. The composition of the gas released from Ag_2CO_3 as measured by Raman analysis was CO_2(60) O_2(40); CO was not detected.

The HT-experiments show that decomposition of $Ag_2C_2O_4$ does not proceed in a simple way. However, by doing HPT-experiments (in gold tubes), only silver could be identified as the final solid reaction product: silver

formed as a precipitate on the walls or as graphite-silver aggregates. The most simple decomposition reaction of $Ag_2C_2O_4$ can be written as

$$Ag_2C_2O_4 \rightarrow 2\,Ag + 2\,CO_2 \qquad \text{(R.6.12.)}$$

It should be kept in mind that several other reaction products (Ag_2O, Ag_2O_2, Ag_2CO_3 and their mixtures) may be formed during the decomposition process.

It was shown earlier that 1 mole of NH_4NO_3 produces 1.2 mole of gas (0.9 mole N_2 and 0.3 mole CO_2) (R.6.10). The amounts of gas (in moles) produced by 1 mole of $Ag_2C_2O_4$ appeared to be the same because of a linear correlation between the mole fractions of starting compounds and the produced gases. This may stress the supposition that silver is not the only formed solid reaction product (a higher production of CO_2 is expected then). The ratio of the used starting compounds (in mole fractions) for a wished gas composition (X_{N2}^{gas}) are found from the following empirical equation

$$NH_4NO_3/(NH_4NO_3 + Ag_2C_2O_4) = X_{N2}^{gas} / 0.77 \qquad \text{(Eq.6.2.)}$$

where $0 < X_{N2}^{gas} < 0.77$. The amount of $Ag_2C_2O_4$ (in grams) to be added to 1 gram of NH_4NO_3 is given by the expression: $3.797(0.77 - X_{N2}^{gas}) / X_{N2}^{gas}$. As an example: 1.52 g $Ag_2C_2O_4$ is needed for 1 g NH_4NO_3 for the production of a CO_2-N_2 mixture containing 55 mole% N_2.

The HPT-experiments (as described in section 6.2.) were carried out for experimental pressures between 4.0 and 5.6 kbar at 500°C (E318; E332; E333). Time durations of 14 days appeared to be sufficient for the development of fluid inclusions. About 5 mg of extra water was added for the present experiments. The water content of the formed inclusions is mostly in the order of 60 vol%, but may show a great variation (some inclusions do hardly contain any visible water). This may indicate immiscibility of liquid and vapour during the experimental conditions.

It followed from microthermometric studies that all present inclusions can be classified as type H4 i.e. characterized by partial homogenization (T_{hs}) of liquid and vapour in the presence of solid CO_2 followed by melting (T_m) and subsequent homogenization (T_h) (Fig.6.15a). Partial homogenization (around -147°C) is to the vapour/critical (P_t = 4.0 kbar), critical (P_t = 5.0 kbar) or liquid phase (P_t = 5.6 kbar); final homogenization is into the vapour (P_t = 4.0 kbar), liquid to critical (P_t = 5.0 kbar) or liquid phase (P_t = 5.6 kbar). T_h ranges from -61 to -45°C. The measurement data are listed in Table 6.3. and plotted in a P_t-T_h diagram (Fig.6.16). The melting temperatures are -61 to -60°C. It is remarkable that melting trajectories are small (<0.5°C !) for the

present inclusions (with T_m not far from T_h). Critical homogenization temperatures (sample E332) are 5 to 12 degrees higher than the melting point. Sometimes (E333-B6) homogenization to the liquid was observed at only 0.1°C above T_m!: incipient melting (S+L → S+L+V) is not characterized by the forming of liquid, but by the forming of a small bubble (Fig.6.15a). The size of this bubble firstly increases and subsequently decreases within a temperature interval of a few 10ths of a degree. Solid CO_2 disappears just before homogenization (S+L+V → L+V → L). It is assumed that the "fluid" kept the character of a liquid between $T_{hs}{}^L$ and first melting. Inclusions with higher T_h (in the same sample) e.g.E333-B1 show "normal" melting behaviour i.e. the forming a liquid during the disappearance of the solid phase.

The results of Raman analysis are shown in Table 6.3, together with the microthermometric data. CO_2 and N_2 are the only detected gaseous compounds. The fluid composition of the present samples is 55 ±7 mole% N_2 (i.e. a range of about 14 mole%). The compositional variation within one sample was found to be less than 6 mole% i.e. within the supposed accuracy of Raman analysis in this range. Gas compositions within one sample can therefore be taken as constant.

The position of point Q ($T_h = T_m$) could be determined (by approximation) from the present experiments. The best fitting correlation of T_h with trapping pressures (P_t) is given by the equation $T_m = -0.67 \times 10^{-3} \times P_t \quad 57.5$ (P_t in bar). The intersection point with the homogenization points is found at $T_h = T_m = -61$°C for fluid inclusions (X_{N2} ~ 0.55) trapped at about 5.4 kbar (500°C) (Fig.6.16). Fluids showing critical homogenization ($T_h{}^C$ ~ -57°C) are trapped at a pressure of about 5.0 kbar (and 500°C). Inclusions characterized by melting into a critical fluid are expected to be somewhat richer in nitrogen (X_{N2} ~ 0.57) and probably formed at higher pressure (5.1 kbar) (see section 6.7).

Fig.6.15.- *Phase sequences at low temperatures, observed in fluid inclusions formed by experiments at 500°C with* **a)** NH_4NO_3 + $Ag_2C_2O_4$ *and graphite (3 examples for* P_t = *4, 5 and 5.6 kbar) and* **b)** *guanidine-nitrate +* $Ag_2C_2O_4$ *and graphite (5 kbar). Dashed parts mark the vapour phase; other parts mark the liquid and solid phases. All inclusions shown are of type H4. Phase behaviour shown in a) is representative for inclusions with properties around point Q (XN2 ~ 0.57;* $\bar{V}$ ~ *40* $cm^3/mole$*).*

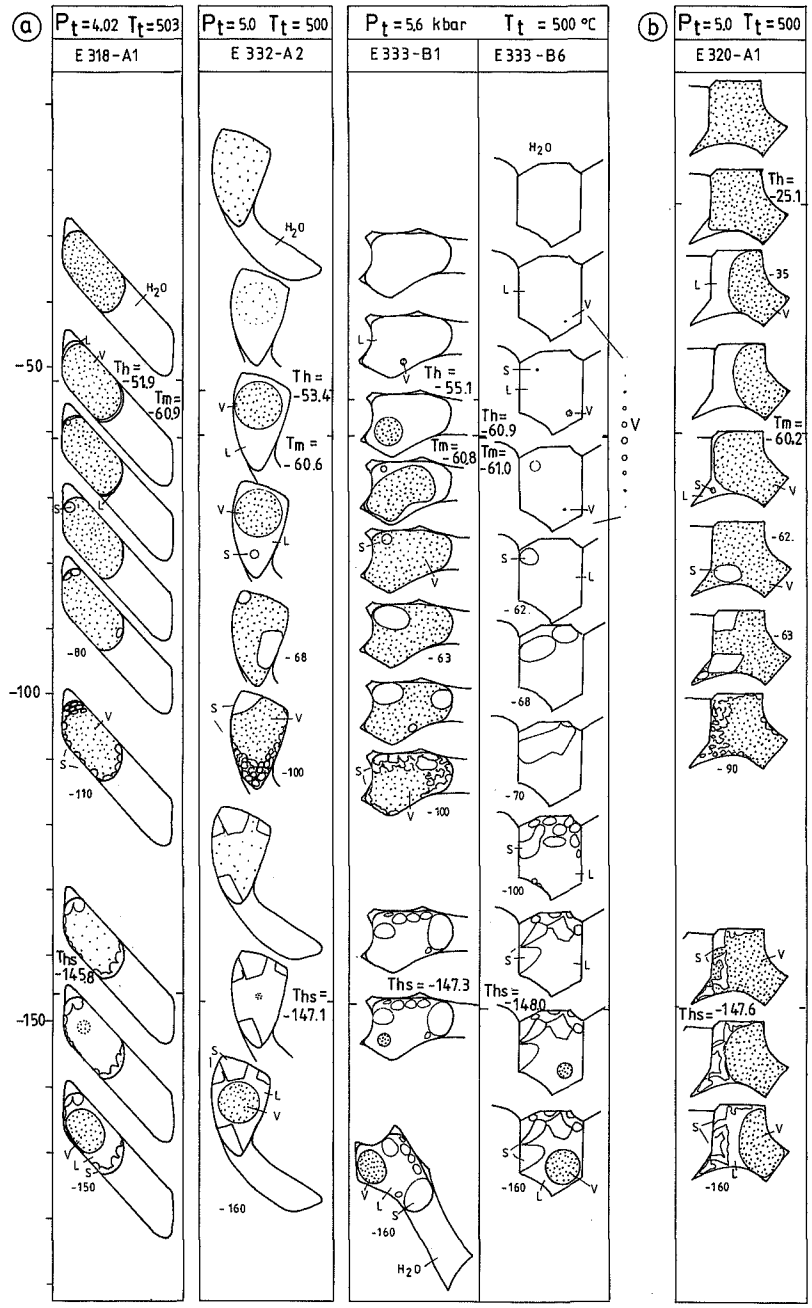
a
Pt=4.02 Tt=503
E 318-A1
Pt=5.0 Tt=500
E 332-A2
Pt=5.6 kbar Tt = 500 °C
E 333-B1
E 333-B6
b
Pt=5.0 Tt=500
E 320-A1
H2O
Th= -51.9
Tm= -60.9
Th= -53.4
Tm= -60.6
Th= -55.1
Tm= -60.8
Th= -60.9
Tm= -61.0
Th= -25.1
Tm= -60.2
Ths= -145.8
Ths= -147.1
Ths= -147.3
Ths= -148.0
Ths= -147.6
-50
-100
-150
-80
-110
-150
-68
-100
-160
-63
-100
-160
-62
-68
-70
-100
-160
-35
-62
-63
-90
-160

(Fig.6.15)

6.6.2. Experiments with guanidine-nitrate and silver-oxalate

The generation of CO_2-N_2 inclusions of intermediate composition has also been done by using an alternative starting compound: guanidine-nitrate ($NH_2C(=NH)NH_2.HNO_3$, M = 122.08) as a producer of N_2. This compound was proposed for fluid generation by Holloway & Reese (1974). However, decomposition reactions appeared to be much more complicated than mentioned in this paper. It is shown here that the results obtained from fluid inclusions formed in this way are deviant from the inclusions described in the foregoing sections.

The decomposition reaction of guanidine-nitrate is not exactly known. Some experiments have first been done by which guanidine-nitrate was heated in closed quartz tubes. The following phenomena are subsequently observed during heating up to 500°C: 1) melting (the melting point is 211 to 214°C at 1 atm.) and 2) evaporation and/or decomposition resulting into a single gas phase. During cooling, condensation was observed, followed by crystallization of fine white needles. This solid could not be identified, but its Raman spectrum is different from that of the starting compound. The gas composition appeared to consist of nitrogen only.

Guanidine-nitrate heated in a test-tube in the flame of a Bunsenburner shows melting and subsequent boiling: a colourless gas and (later) a white vapour is released. This vapour condensates in the coldest parts of the tube and crystallizes on further cooling. The strong smell of ammonia (NH_3) was noticed. The pH of the condensed vapour is 8 to 9 indicating a strongly reducing environment (contrary to decomposed NH_4NO_3 which results into an extremely acid environment). A white solid remains as a residue after boiling/decomposition. Continuing heating (to 900-1000°C) results into the forming of nitrogen oxides: brown NO_2 and N_2O (explosive!). Finally, a yellow to orange, partly sublimating, compound remains.

Some additional experiments were made by heating guanidine-nitrate in sealed gold-tubes (600°C, 0.6 bar). It was found that 1 g of guanidine-nitrate produces 0.3 g of gas. The gas composition is, considering the results given above, probably a mixture between N_2, NH_3 and H_2O. It cannot be explained why NH_3 (most probably present as dissolved NH_4^+) was not be detected by Raman analysis.

Several "quartz tube-experiments" have been done for mixtures of guanidine-nitrate and silver-oxalate to produce gas mixtures in the range between 45 and 100 mole% N_2. The tubes were heated up to 300-400°C. The decomposition processes of both compounds proceed as described above (for guanidine-nitrate) and as in section 6.6.1. (for silver-oxalate). N_2 and CO_2 were detected as the main gas species by Raman analysis (sometimes small amounts of N_2O occur). The amount of gas produced by 1 mole of guanidine-nitrate is higher (about 1.5x) than for $Ag_2C_2O_4$.

Fluid inclusions have been generated by means of HPT-experiments at 500°C and 2.0 to 5.5 kbar (E286; E320; E319). The experimental time duration was taken about 2 weeks. Fluid inclusions developed well in this time period. An amount of 10 mg water and a surplus of graphite was added for each experiment. The smell of ammonia was noticed by opening the gold tubes. Fluid inclusions may contain considerable amounts of water; daughter crystals have been observed in many of them.

The only gaseous compounds detected by Raman analysis are CO_2 and N_2. The N_2 content of the gas present in the three samples considered, ranges from 53 to 64 mole% (Table 6.4).

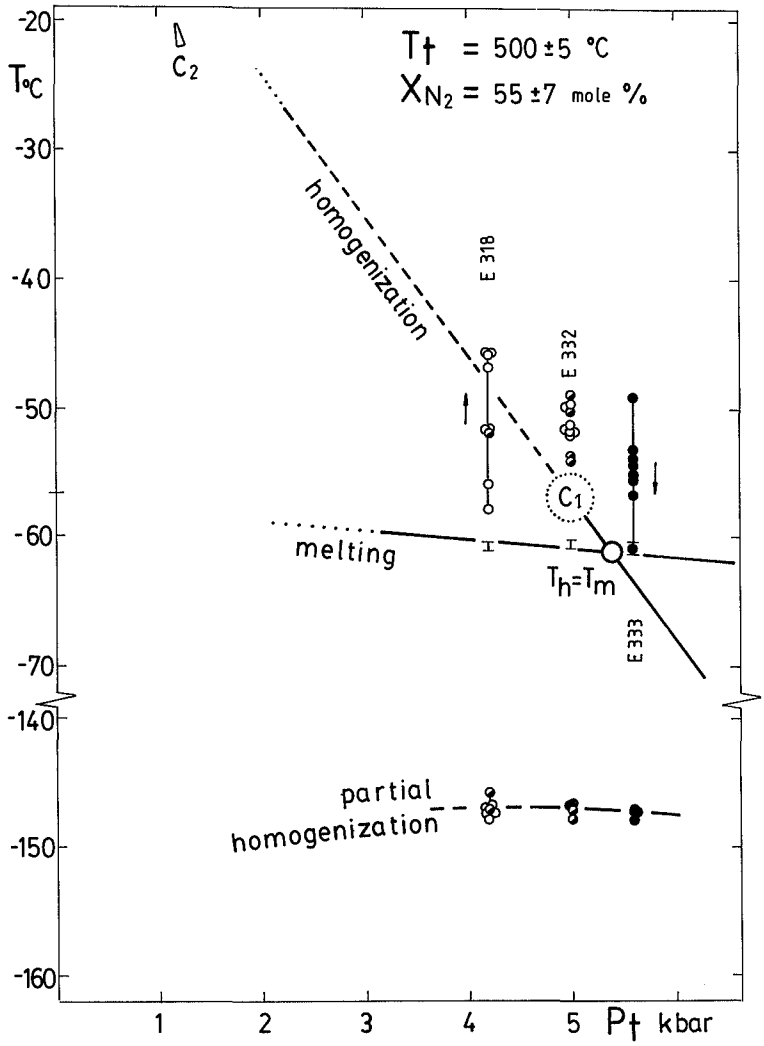

Fig.6.16.- *Temperatures of partial homogenization (T_{hs}), melting (T_m) and (final) homogenization (T_h) of artificial inclusions, plotted against trapping pressures (P_t). The gas compositions are produced by the decomposition of a mixture of NH_4NO_3 and $Ag_2C_2O_4$. Both T_h and T_{hs} may be to the liquid (black dots), critical (partly filled circles) or vapour phase (open circles). The position of critical point (C_1) is very near the point T_h=T_m. Curves for a mean composition of 55 mole% N_2 are tentatively drawn (compositions of samples E318 and E333 are about 5 mole% higher and lower respectively).*

Microthermometric observations show that homogenization temperatures do not agree with the values found for inclusions of comparable composition and trapping conditions described in the preceding section (6.5.3.): all homogenizations are to the vapour phase between -32 and -17°C (Fig.6.15b). These temperatures indicate low density of the gaseous fraction (Table 6.4). Partial homogenization (T_{hs}) is also to the vapour phase (between -149 and -147°C). Low densities are explained by the existence of one fluid phase (miscibility) at the experimental conditions; liquid and solid phases formed during cooling by condensation and crystallization (see section 6.8.). The presence of these phases in gaseous inclusions is a disturbing factor. In contrast, immiscibility during the experimental conditions could be assumed for inclusions formed by the decomposition of $AgNO_3$ and NH_4NO_3 ($\pm Ag_2C_2O_4$). The present results are not used for further interpretation because they are considered not to be representative for trapping conditions.

6.7. A model for the system CO_2-N_2

Many experimental results on the system CO_2-N_2 have been obtained by the generation of artificial fluid inclusions as described in the preceding sections of this chapter. A summary of the measured variables is given below.

From the experimental conditions can be obtained:
a) the trapping temperature (T_t) which was taken about 500°C for all experiments;
b) the trapping pressure (P_t) varying between about 1 to 6 kbar.

Microthermometric data of the formed inclusions comprise the following temperatures:
c) the homogenization temperature (T_h);
d) the melting (T_m) or sublimation (T_s) temperature;
e) the partial homogenization temperature (T_{hs});
f) a possible metastable homogenization temperature (T_{hm}).

Raman analysis, used for the determination of
g) the fluid composition (X):

Three compositional ranges can be distinguished by the choice of different starting compounds for fluid generation:

1) X_{N2} = 0.33 ±0.05 (fluids generated by the decomposition of silver-nitrate);

2) X_{N2} = 0.55 ±0.07 (fluids generated by the decomposition of ammonium-nitrate and silver-oxalate);

3) X_{N2} = 0.77 ±0.05 (fluids generated by the decomposition of ammonium-nitrate).

The only quantity which cannot be measured is the (molar) volume ($\bar{V}$). This is a disadvantage of the method. However, it is shown in the following sections that it is still possible to establish a model for the system CO_2-N_2 which can be used for the interpretation of data obtained from natural fluid inclusions.

6.7.1. Trapping conditions represented in a TX-diagram

The assembled compositions (X) and temperatures marking phase transitions (T_h, T_m, T_{hs}, T_{hm}) measured for the experimentally formed inclusions are plotted in a TX-diagram (Fig.6.17). The construction of curves ("isobars"), representing constant trapping pressures at 500°C, is possible now. Better fitting curves can be obtained by using mean values as already given in the P_t-T_h diagrams (Fig.6.7; 6.11; 6.16). The trapping conditions for the pure end-members are obtained from the literature (Angus et al. 1976a, 1976b, 1979; Shmonov & Shmulovich 1974; Malbrunot & Vodar 1972; Antanovish & Plotnikov 1976).

In the resulting TX-diagram (Fig.6.17) the following forms can be distinguished:

a) homogenization point curves representing the correlations X-T_h and X-T_{hm};

b) the critical curve of the 1st order (C_1). The present data are consistent with the critical data of Arai et al. (1971), given for $X_{N2}<0.4$;

Fig.6.17.- *The assembled microthermometric data of artificial CO_2-N_2 inclusions for the 3 compositional ranges A (X_{N2}=0.33 ±0.05), B (X_{N2}=0.55 ±0.07) and C (X_{N2}=0.77 ±0.05), plotted in a TX diagram. Black dots = homogenization (T_h or T_{hs}) to the liquid phase; partly filled circles = critical homogenization; open circles = homogenization to the*

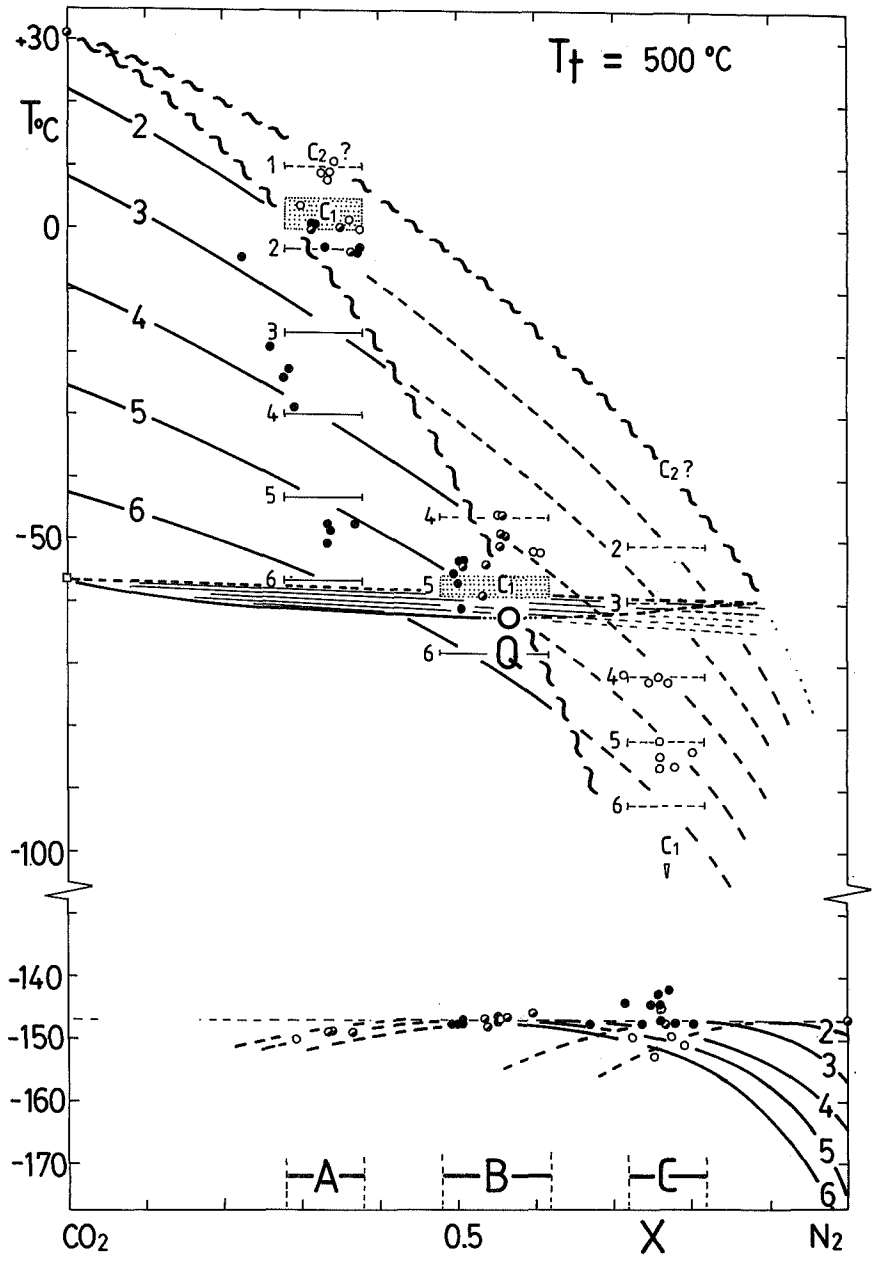

vapour phase. Numbers denote the interpreted trapping pressures (P_t in kbar) for each type of experiment; curves mark constant trapping pressures (for T_t=500°C). Values for the pure end-members are obtained from Angus et al. (1976, 1979). C_1 (stippled regions) present experimentally determined critical conditions; the two wavy curves are the critical curves of the first and second order. The intersection point of the critical curve and liquidus (T_h=T_m) is given by point Q.

c) melting (sublimation) lines ($X-T_m$ or $X-T_s$). This part of the diagram is represented in detail in Fig.6.18. The curve marking 3-phase equilibria is obtained by the intersection of homogenization and melting points ($T_h=T_m=T_s$). Of special interest is the point defined by $T_h^C=T_m=T_s$. This property is interpreted to be characteristic for inclusions with $X_{N2}=0.57$, trapped at 5.1 kbar and 500°C. They will show critical homogenization and simultaneous melting at -62°C;

d) partial homogenization point curves ($X-T_{hs}$). T_{hs} can only be measured for inclusions of N_2-richer compositions and higher densities (see section 6.7.2.);

e) the critical curve of the 2nd order is only roughly indicated.

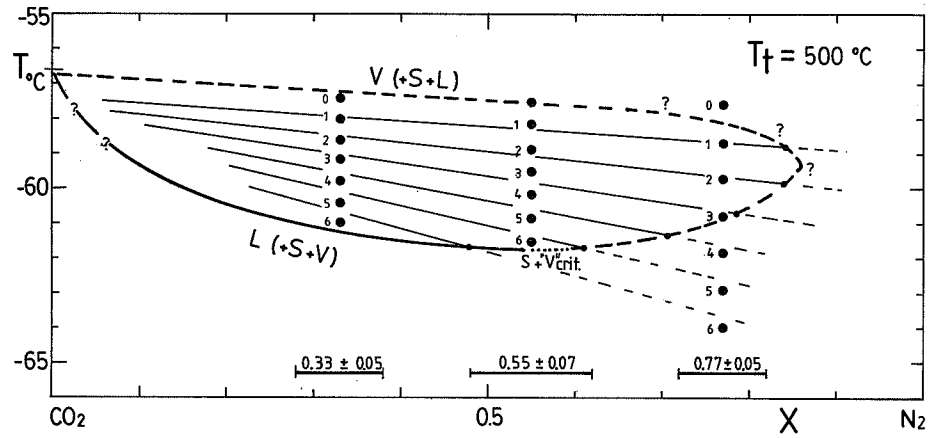

***Fig.6.18.**- Melting points determined by extrapolation of experimental data. Numbers denote trapping pressures (kbar) at 500°C. Curves L(+S+V) and V(+S+L) are constructed from the intersection points of homogenization and melting curves. Lowest melting temperature (for $S+V_{crit}$) is -61.9°C (X_{N2}~0.57).*

6.7.2. Partial homogenization (T_{hs})

Homogenization temperatures of the N_2-rich fraction (in the presence of solid CO_2) of both artificial and natural inclusions (Furua Granulite Complex, Tanzania; Pusula quarry, SW Finland) are not significantly higher than the critical temperature of N_2 (-147°C). Partial homogenization at -147°C is always (about) critical; T_{hs} to the liquid or vapour phase takes place at lower temperatures. In the case of higher T_{hs}, methane is present as an additional compound. It can therefore be stated that the amount of CO_2 dissolved in the volatile phases can be

neglected at low temperature. In contrast, this is not valid for inclusions of the system CO_2-CH_4: partial homogenization temperatures may indeed be nigher than the critical temperature of CH_4 (Appalachian Mountains). CO_2 should therefore be partly dissolved in the CH_4-rich liquid and vapour phases in this temperature range.

The assumption that all CO_2 is present in the solid phase and all N_2 in the volatile phases, allows the following calculation of partial homogenization temperatures as a function of composition and molar volume: the total molar volume ($\bar{V}_t$) of an inclusion is expressed as the sum of the partial molar volumes according

$$\bar{V}_t \quad X_{CO2}.\bar{V}_{CO2} + X_{N2}.\bar{V}_{N2} \qquad \text{(Eq.6.3.)}$$

The molar volume of solid CO_2 ($\bar{V}_{CO2}$) is 28.2 cm^3/mole (=M/d = 44/1.56). The mole fraction of CO_2 can be re-written as $1-X_{N2}$. Consequently, the molar volume of the N_2-rich fluid phase at low temperature can be expressed by the equation

$$\bar{V}_{N2} \quad \frac{\bar{V}_t + 28.2.X_{N2} - 1}{X_{N2}} \qquad \text{(Eq.6.4.)}$$

The corresponding homogenization temperatures can be find in the tables (Angus et al. 1979).

It was mentioned that T_{hs}^C = -147°C for all inclusions of the system CO_2-N_2. The critical molar volume of pure N_2 is 89.206 cm^3/mole (Angus et al. 1979). Higher amounts of CO_2 should be present in inclusions showing critical partial homogenization and lower total molar volume. The fluid composition of inclusions showing critical partial homogenization is given by

$$X_{N2} \quad (\bar{V}_t/61.0) - 0.462 \qquad \text{(Eq.6.5.)}$$

T_{hs} is plotted as a function of fluid composition in Fig.6.19. It can be seen that most partial homogenization temperatures approach -147°C except for fluids of extremely high or low density. An alternative representation of the same partial homogenization temperatures (in a $\bar{V}X$ diagram) was already shown in Fig.5.17a. It should be noted that T_{hs} to the vapour phase is difficult or impossible to observe for low density inclusions (section 5.3.2): partial homogenization cannot be observed

below -158°C for inclusions with rounded shapes, but at lower temperatures for irregular inclusions. T_{hs} can generally not be observed for CO_2-rich inclusions ($X_{N2} \lesssim 0.2$).

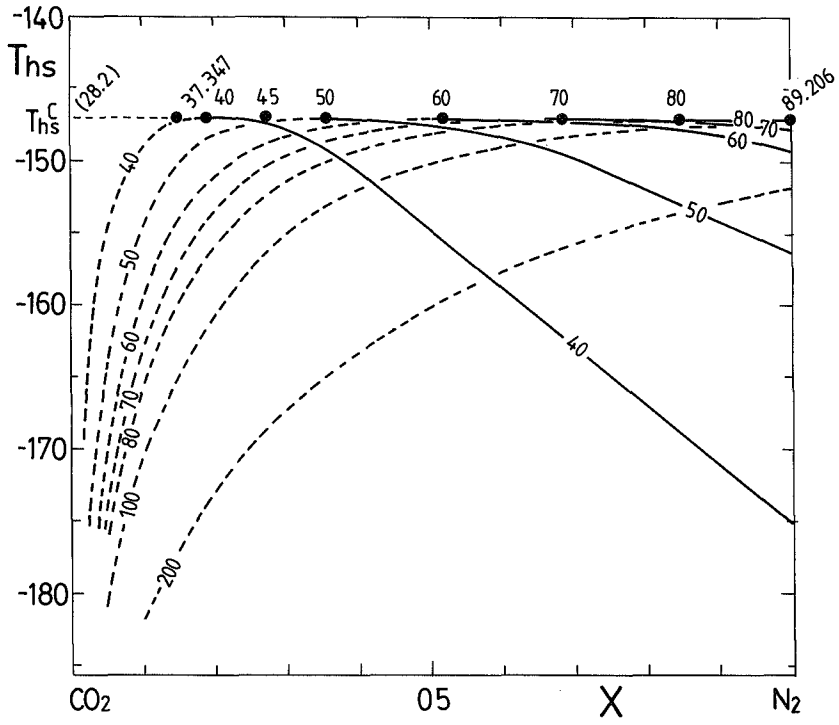

Fig.6.19.- *Calculated partial homogenization temperatures (T_{hs}) as a function of fluid composition at constant molar volumes (in cm^3/mole) (see text). Solid curves = T_{hs}^L; dashed curves = T_{hs}^V. Black dots mark critical partial homogenization (T_{hs}^C) at -147°C. No partitioning of CO_2 in the volatile phases is assumed.*

6.7.3. A model involving molar volume for the system CO_2-N_2

The determination of the trapping PT-conditions (P_t,T_t) is one of the main topics in fluid inclusion studies. It was demonstrated in section 6.7.1. how trapping pressures (for T_t=500°C) can be derived from the present data (Fig. 6.17). For the construction of a general model, valid at varying trapping temperatures, it is necessary to use an equation of state for the high PT-range. In this way, molar volumes are calculated at the trapping conditions (P_t, 500°C) and these values are subsequently extrapolated to low PT. This procedure is allowed as the assumption was

made that $\bar{V}$ remains constant during cooling (Chap.II). The MRK-equation as calculated by Holloway (1977) is chosen for the calculations. This equation finds a wide application, although it is known to be inaccurate for fluids of extreme density and N_2-rich compositions (Fig.6.9; Fig.6.14). Summarizing, the establishment of a model for the CO_2-N_2 system is made in two steps:

1) the construction of a X-T_h [P_t]-diagram for constant T_t (=500°C);
2) the construction of a X-T_h [$\bar{V}$]-diagram from the X-T_h diagram and the Holloway equation (or an alternative equation).

The result is shown in Fig.6.20. Note that the isochores in this diagram are (sub)parallel to the curves of constant P_t of Fig.6.17, except for extremely low molar volumes. Fig.6.20 can be used for the determination of the molar volume of fluid inclusions by measuring T_h and composition. It is noted that the calculation of trapping conditions (calculated from $\bar{V}$ and an equation of state) is only allowed if the same equation is applied as used for the construction of the diagram (in casu the Holloway equation).

6.7.4. A comparison with other models

The isochoric TX-diagram (Fig.6.20) established from experimentally generated fluid inclusions can be compared with already available models. A recapitulation of the models presently known for the system CO_2-N_2 is given below.

a) the experimental PVTX-data (limited range) of liquid-vapour equilibria published by Arai et al.(1971);
b) the Heyen equation of state (Heyen 1980; Heyen 1981; Darimont 1986; Darimont & Heyen 1988);
c) a model obtained from natural fluid inclusions with a molar volume of about 40 cm^3/mole (Furua Granulite Complex, van den Kerkhof 1988).

Differences between the models are considerable. It should be kept in mind that the data of Arai et al. (1971) are the only data available which include the molar volume. The isochoric homogenization point curves as obtained from the Heyen equation are known to deviate from these data (see section 5.3.2). However, the present model, obtained from artificial fluid inclusions, also deviates from these data and even approximates

the Heyen equation to a large extend. This can be explained by the role of water during fluid trapping (see section 6.8.). Molar volumes found with the help of the present model are somewhat too low: a fluid with X_{N2} = 0.33 and T_h = -28°C has a molar volume of about 50 cm^3/mole according to extrapolations of the data of Arai et al. (1971), but a molar volume of about 44 cm^3/mole according to the present model. It is possible to estimate the amount of water present in the fluid at the time of trapping: a fluid with $\bar{V}$ = 50 cm^3/mole and X_{N2} = 0.33 has a homogenization temperature of -11°C according to the present model. This point corresponds to a molar volume of 65 cm^3/mole according to Arai et al. (1971). The found higher values for the molar volume can be explained by the withdrawal of water from the vapour phase upon cooling. For example: for an inclusion with total molar volume ($\bar{V}_t$) of 50 cm^3/mole and molar volume of the gas fraction ($\bar{V}_G$) of 65 cm^3/mole, the amount of condensed water is calculated to be in the order of 30 mole% (=10 vol%) (see Appendix 2).

The modification of the high density part of the model as was done by means of fluid inclusions from the Furua Granulite Complex (van den Kerkhof 1988) is supposed to be reliable because these fluids do most probably not contain any water. Furthermore, the constructed homogenization point curve for $\bar{V}$ = 40 cm^3/mole is about parallel to the curves obtained from the data of Arai et al. (1971).

The critical data obtained from artificial inclusions are consistent with the data of Arai et al. (1971). This may stress the reliability of the critical curve as shown in Fig.6.17 and 6.20.

The most striking deviation between the Heyen equation and the present model concerns the characterization of the melting conditions and the 3-phase equilibria: the lowering of the melting temperatures with increasing N_2 contents is much less for the present model (lowest T_m = -62°C) than for the Heyen equation (lowest T_m = -70°C). The point $T_h^C = T_m$ should be situated to lower N_2 contents (X_{N2} = 0.57) than expected from the Heyen equation (X_{N2} = 0.75).

Fig.6.20.- *The isochoric TX diagram (cm^3/mole): a model for the system CO_2-N_2 established from the combined experimental data and the Holloway equation (see text). Solid and dashed curves indicate homogenization (partial or final) to the liquid or vapour phase respectively. The 5 phase fields are also presented. The stippled regions indicate the maximum extension of TX-conditions for fluid inclusions containing a bubble (S+L+V and L+V).*

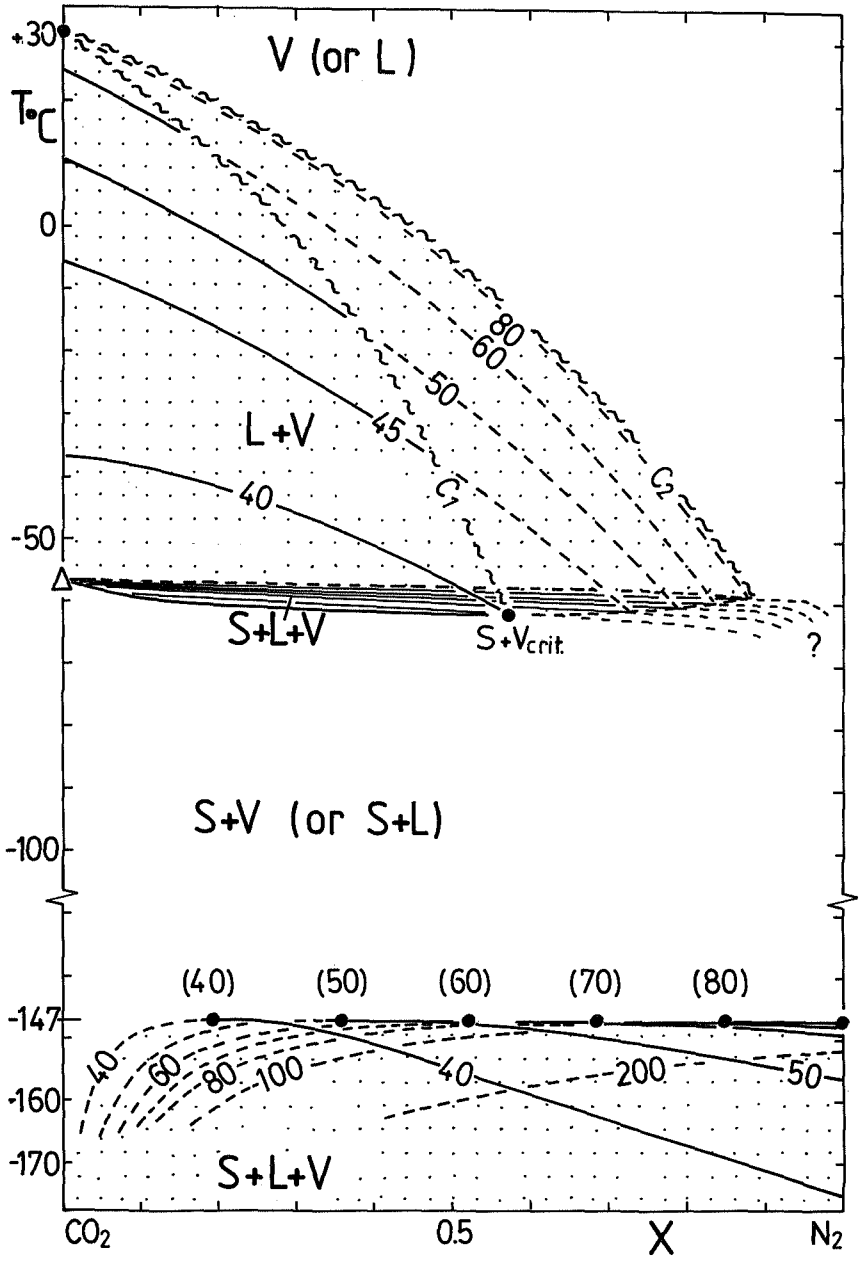
+30
T°C
0
-50
-100
-147
-160
-170
V (or L)
L+V
S+L+V
S+Vcrit.
S+V (or S+L)
S+L+V
40
45
50
60
80
C1
C2
?
(40)
(50)
(60)
(70)
(80)
40
60
80
100
40
200
50
CO2
0.5
X
N2

6.8. Limitations of the experimental method

It became evident in the preceding sections that the present method for the characterization of the system CO_2-N_2 by making artificial fluid inclusions has its limitations: the fact that molar volumes cannot be measured directly is inherent to the method and implies that isochores should be calculated by means of an independent equation.

Fluid inclusions mostly show a range in density within a sample. This variation results to lower accuracies. The consistency of molar volumes and trapping PT-conditions is a matter of discussion. The assumption was made here that inclusions of highest density are most representative for the experimental forming conditions. Lower densities are explained by partial leakage.

The influence of non-gaseous phases (in particular water) on the molar volume of the vapour phase was mentioned earlier in section 6.6.2. It can be stated in general that the liquid to vapour ratio is not the same at high PT and at room temperature. The result is a lower density of gaseous inclusions. This became evident from the misfit of the presently established model and data on the "dry" CO_2-N_2 system (section 6.7.4.). However, water is indispensable for the healing of quartz and therefore for the forming of fluid inclusions.

Textural evidence have been found for gas-liquid immiscibility during the forming conditions of fluid inclusions during the experiments with silver-nitrate, ammonium-nitrate and silver-oxalate. Here, the liquid phases consist of concentrated solutions. In the case of complete miscibility, it would be impossible to form high density gaseous inclusions. The experiments with guanidine-nitrate resulted to the forming of low density inclusions probably because of the presence of a single phase at the experimental conditions and subsequent condensation and crystallization of liquid and solid phases. It should be kept in mind that even in the case of immiscibility at high temperature, the activity of water in the gas phase is much higher than at room temperature (and lower temperatures). This problem does not only rise for the experimentally generated inclusions, but also for inclusions formed during natural processes. The assumption that the molar volume of gaseous inclusions is equal to the total molar volume may lead to a deviant interpretation of trapping conditions. Note that 10 vol% of liquid water in gaseous inclusions can generally not be observed. The (molar) amount

of water relative to gas in a fluid inclusion may therefore be considerable, especially for low densities of the gas fraction.

It followed from the experiments with ammonium-nitrate that chemical equilibria within the system C-O-H-N may change for different trapping pressures: additional amounts of CH_4 formed in CO_2-N_2 fluids with X_{N2} - 0.77 at higher P_t. Fluid compositions as measured by Raman analysis represent chemical equilibria at room temperature; compositions at the experimental PT-conditions cannot be measured (but can be calculated). A shift of chemical equilibria going from high to low temperature, may also have implications for the molar volume.

6.9. Conclusion: a model for the system CO_2-N_2

Models which are available until now for the determination of the molar volume of mixed CO_2-N_2 inclusions and therefore of their trapping conditions, could only rely on the PVTX data with a limited range of application (Muirbrook 1964; Arai et al. 1971). Deduced equations of state are therefore inaccurate to higher nitrogen contents and higher densities. In this chapter, new PTX data are presented which improve the knowledge of CO_2-N_2 system for a much wider range. A model could be established showing the relations between phase behaviour and trapping conditions at 500°C (Fig.6.17). An universal model, valid for other trapping temperatures was also established (Fig.6.20): molar volumes (consistent with the Holloway equation) can be determined from the homogenization temperature (T_h) and checked by melting (T_m) or sublimation temperatures (T_s) and partial homogenizations (T_{hs}). Especially melting and sublimation temperatures could be determined more precisely (data have been lacking completely until now). Molar volumes of inclusions of higher N_2-contents can be determined from metastable homogenization (T_{hm}) and/or sublimation (T_s), and partial homogenization temperatures (T_{hs}). Partial homogenization could be quantified as it became evident from "microthermometry" that the solubility of CO_2 in N_2 is nihil below -147°C. Although the presently applied experimental method has several limitations as mentioned in section 6.8, the resulting measurement results are the best and only data available for N_2-rich inclusions.

(Table 6.1.)

Incl.nr.	type	hm	L/C/V	$T_{h.hm}$	m/s	$T_{m.s}$	L/C/V	T_{hs}	H_2O	s	CO_2	N_2	CH_4
E304	T_t = 504°C P_t = 830 bar				$AgNO_3$ = 44.9 mg H_2O = 10 mg				time = 14 days				
E304-A1	H3		V	+9.5					(+)	-			
A2	H3		V	+9.4					(+)	-			
A3	H3		V	+10.8	M	-57.8			(+)	-	65.6	34.4	
A4	H3		V	+10.4					(+)	-			
A5	H3		V	+10.0	M	-58.0			(+)	-			
A6	H3		V	+8.9					(+)	-			
A7	H3		V	+10.1					(+)	-			
A8	H3		V	+9.0	M	-57.8			(+)	-	66.3	33.7	
A9	H3		V	+9.4					(+)	-			
B1	H3		V	+10.3	M	-57.9			(+)	-			
B2	H3		V	+8.9	M	-58.1			(+)	-	67.4	32.6	
B3	H3		V	+7.8	M	-58.0			(+)	-	66.6	33.4	
B4	H3		V	+10.0					(+)	-			
B5	H3		V	+10.9					(+)	-			
B6	H3		V	+9.1					(+)	-			
E273	T_t = 497°C P_t = 1040 bar				$AgNO_3$ = 40.1 mg H_2O = 10 mg				time = 15 days				
E273-A1	H3		V	+1.2	M	-58.2			(+)	-			
A2	H3		V	+3.5	M	-58.2			(+)	-			
A3	H3		V	+2.8					(+)	-			
A4	H3		V	+1.3	M	-58.2			(+)	-	63.8	36.2	
A5	H3		V	+4.3					-	-			
A6	H3		V	+3.6					(+)	-			
A7	H3		V	+3.5	M	-58.2			(+)	-	69.9	30.1	
B1	H3		V	-0.2	M	-58.6			+	-	62.4	37.6	
B2	H3		V	-4.5					(+)	-			
B3	H3		V	-1.4	M	-58.6			-	+			
B4	H3		V	-1.3					-	+			
B5	H3		V	-1.8					-	+			
B6	H3		V	-4.5	M	-58.7			-	-			
B7	H3		V	-0.7									
E245	T_t = 507°C P_t = 1912 bar				$AgNO_3$ = 432 mg H_2O = 100 mg				time = 7 days				
E245-A1	H3		L	+0.6	M	-58.8		-	(+)	-	68.1	31.9	
A2	H3		L	+0.8	M	-58.8		-	(+)	-	68.6	31.4	
A3	H3		L	+0.8				-	(+)	-			
A4	H3		C	-0.6	M	-58.8		-	(+)	-			
A5	H3		C	+0.3					(+)	-			
A6	H3		C	+0.4					(+)	-			
B1	H3		C	+0.1	M	-58.9		-	(+)	-	64.9	35.1	
B2	H3		C	+0.7	M	-58.8		-	(+)	-			
B3	H3		C	-0.2				-	(+)	-			
B4	H3		C	+0.0				-	(+)	-			
B5	H3		C	-0.1	M	-58.8			(+)	-	68.6	31.4	

B6	H3	C	-0.1					(+)	·			
E263	T_t = 498°C P_t = 2020 bar			$AgNO_3$ = 573.5 mg H_2O = 20.6 mg				time = 14 days				
E263-A1	H3	L	-2.4	M	-58.7			(+)	-			
A2	H3	L	-3.1	M	-58.7			(+)	-		62.4	37.6
A3	H3	L	-3.0	M	-58.8			-	-		66.9	33.1
A4	H3	L	-2.6					-	-			
A5	H3	L	-3.0					(+)	-			
A6	H3	L	-3.0					(+)	·			
FK3	T_t = 503°C P_t = 2000 bar			$AgNO_3$ = 498.87 mg H_2O = 20.46 mg				time = 8 days				
FK3-A1	H3	L/C	-3.6	M	-58.9			-	-		63.6	36.4
A2	H3	L/C	-3.9					-	-			
A3	H3	C	-3.9					(+)	-			
A4	H3	C	-4.6	M	-58.9			(+)	-			
A5	H3	L	-3.6	M	-58.9			-	-		62.6	37.4
A6	H3	L	-4.3					-	-			
A7	H3	L/C	-3.7									
E232	T_t = 510°C P_t = 4010 → 1960 bar			$AgNO_3$ = 400 mg H_2O = 10 mg				time = 5 days Rem.: leaked + Argon				
E232-A1	H4	L	-27.0	M	-60.6	V/C	-136.9	(+)	-		64.2	35.8
A4	H4	L	-16.9	M	-60.3	C/V	-137.5	(+)	-		67.3	32.7
A5	H4	L	-20.6	M	-60.4			(+)	-			
A8	H1?		-		-	L	-131.0	(+)	-		65.8	34.2
A9	H4	L	-28.0	M	-60.8	V	-135.9	(+)	-			
B1	H4	V/C	-6.7	M	-59.3	V	-141.7	++	++			
B2	H4	L	-42.4	M	-60.9	C/V	-135.7	(+)	-		61.8	38.2
B3	H4	C	-7.9	M	-59.4			(+)	-			
B4	H4	L	-45.5	M	-60.9	V	-136.6	(+)	-			
B5	H4	C	-32.	M	-60.6			(+)	-			
C1	H4	V	-55.3	M	-62.0	L	-128.4	(+)	-		68.5	31.5
C2	H3?	L/C	-21.0	M	-60.5		-	-	-			
C3	H3?	V	-14.2	M	-60.0		-	-	-			
C4	H1					L	-123.8	(+)	·			
FK4	T_t = 498°C P_t = 4000 → 3520 bar			$AgNO_3$ = 509.93 mg H_2O = 10.53 mg				time = 8 days Rem.: leaked + CO_2				
FK4-A1	H3	L	-14.5	M	-59.4			-	-			
A2	H3	L	-18.9	M	-59.4						73.9	26.1
A3	H3	L	-4.7	M	-58.9						77.4	22.6
A4	H3	L	-5.2	M	-58.5							
A5	H3	L	-13.7						-			
A6	H3	L	-18.6	M	-59.2				-			
A7	H3	L	-12.9	M	-59.0			-				
A8	H3	L	-13.5					-				
A9	H3	L	-14.6	M	-59.0							

FK2	T_t = 501°C P_t = 4000 bar				$AgNO_3$ = 496.51 mg H_2O = 20.95 mg			time = 9 days			
FK2-A1	H3	L	-22.6	M	-59.8		-	-	-	71.4	28.6
A2	H3	L	-28.4	M	-59.8		-	-	-		
A3	H4	L	-28.6			V/C	-150.0	-	-	70.7	29.3
A4	H3	L	-30.5				-	-	-		
A5	H3	L	-32.3	M	-59.9		-		-		
A6	H3	L	-19.0				-		-		
B1	H3	L	-25.2	M	-59.4			-	-		
B2	H3	L	-24.6	M	-59.5			-	-		
B3	H3	L	-23.7				-	-	-		
B4	H3	L	-25.0				-	-	-		
B5	H3	L	-24.9				-	-	-		
B6	H3	L	-24.5				-	-	-		
B7	H3	L	-26.5	M	-59.4		-		-		
B8	H3	L	-24.0	M	-59.6					72.1	27.9

E274	T_t = 498°C P_t = 5600 bar				$AgNO_3$ = 188.1 mg H_2O = 10 mg			time = 15 days			
E274-A1	H4	L	-47.6	M	-60.4	C	-148.7	(+)	-		
A2	H4	L	-49.2					(+)	-		
A3	H4	L	-47.2	M	-60.4			(+)	-		
A4	H4	L	-47.4	M	-60.4	C	-149.0	(+)	-	63.1	36.9
A5	H4	L	-47.4	M	-60.4	C	-148.9	(+)	-	66.5	33.5
A6	H4	L	-47.3					(+)	-		
A7	H4	L	-47.5					(+)	-		
A8	H4	L	-47.8					(+)	-		
A9	H4	L	-46.2					(+)	-		
B1	H4	L	-49.5	M	-60.2			(+)	+		
B2	H4	L	-49.0					(+)	-		
B3	H4	L	-48.3	M	-60.3			(+)	-		
B4	H4	L	-50.7	M	-60.5	C	-149.2	(+)	-	66.5	33.5
B5	H4	L	-49.3	M	-60.4			(+)	-		
B6	H4	L	-38.0	M	-59.5			(+)	-		
B7	H4	L	-16.2	M	-59.4	V	-149.8	(+)	-		
B8	H4	L	-17.4	M	-59.6			(+)	(+)		
B9	H4	L	-17.4					(+)	-		
B10	H4	L	-48.0					(+)	-		
B11	H4	L	-48.3	M	-60.3	C	-148.6	(+)	-	66.1	33.9

(Table 6.2.)

E268	T_t = 515°C P_t = 2030±50 bar (var.)			NH_4NO_3 = 21.5 mg H_2O = 10 mg				time = 15 days			
E268-A1	S2/H3?			S/M?	-60.2	V	-149.6	+	-	27.5	72.5	-
A2	S2/H3?			S/M?	-60.4	V	-152.7	+	-	24.7	75.3	
A3	S2/H3?					V	-152.2	+	-			
A4	S2/H3?					V	-154.8	+	-			
A5	S2/H3?					V	-155.5	+	-			
B1	S2/H3?			S/M?	-60.0			+	-			
B2	S2/H3?			S/M?	-60.0	V	-151.8	+	-			
B3	S2/H3?			S/M?	-68.2	V	-149.5	+	-	22.5	77.5	
B4	S2/H3?			S/M?	-60.0	V	-150.9	+	-	21.0	79.0	
B5	S2/H3?			S/M?	-63.0	V	-149.3	+	-			
B6	S2/H3?			S/M?	-60.0	V	-151.1	+	-			
B7	S2/H3?					V	-149.1	+				

E269	T_t = 516°C P_t = 3610±170 bar			NH_4NO_3 = 23.4 mg H_2O = 10 mg				time = 15 days				
E269-A1	S2		-	S	-62.2	L/C	-147.5	+	-	32.3	67.2	0.5
A2	S2		-	S	-63.0	L/C	-147.4	+	-			
A3	S2		-	S	-64.4	C/L	-147.5	+	-	22.9	76.8	0.4
A4	S2		-	S	-61.9	L/C	-147.5	+	-	25.7	73.7	0.6
A5	S2		-	S	-62.1	L/C	-147.5	+	-			
A6	S2		-	S	-62.4	L/C	-147.6	+	-			
A7	S2					C/L	-147.6	+				

E285	T_t = 499°C P_t = 4020 bar			NH_4NO_3 = 25.2 mg no H_2O				time = 13 days				
E285-A1	S2	hm V	-73.6	S	-62.9	L	-143.0	+	-			
A2	S2	hm V	-71.6	S	-62.9	L	-142.7	+	-	28.1	64.1	7.8
A3	S2	hm V	-72.6	S	-62.7	L	-141.8	+	-	27.3	64.5	8.2
A4	S2			S	-62.7	L	-142.2	+	-			
B1	S2	hm V	-72.6	S	-62.9	L	-144.3	+	-	29.0	63.3	7.7
B2	S2	hm V	-71.4	S	-62.9	L	-144.0	+	-	32.1	59.5	8.4
B3	S2			S	-62.6	L	-143.2	+	-			
B4	S2					L	-144.0	+	-			
B5	S2			S	-62.7	L	-143.6	+				

E280	T_t = 495°C P_t = 5620 bar			NH_4NO_3 = 23.0 mg no H_2O				time = 14 days				
E280-A1	S2	hm V	-83.8	S	-63.3	L	-147.4	+	-	26.4	62.5	11.1
A2	S2	hm V	-82.1	S	-63.2	L	-144.3	+	-	29.2	60.6	10.1
A3	S2	hm V	-81.3	S	-63.6	L	-144.0	+	-			
A4	S2	hm V	-82.5	S	-63.5	L	-143.9	+	-			
A5	S2	hm V	-86.8	S	-63.3	L	-145.1	+	-			
A6	S2	hm V	-88.7	S	-63.8	L	-144.4	+	-			
A7	S2	hm V	-84.6	S	-63.8	L	-145.0	+	-	29.4	59.9	10.7
B1	S2	hm V	-86.2	S	-64.1	L	-147.1	+				

B2	S2	hm V	-86.2	S	-63.9	L	-147.3	+		28.2	60.9	10.9
B3	S2	hm V	-85.9	S	-64.0			+	-			
B4	S2	hm V	-86.5	S	-63.9	L	-147.1	+		29.4	60.1	10.5

(Table 6.3.)

E318	T_t = 503°C P_t = 4020 bar			NH_4NO_3 = 16.6 mg $Ag_2C_2O_4$ = 20.0 mg H_2O = 5.2 mg				time = 14 days				
E318-A1	H4	V	-51.9	M	-60.9	C/L	-145.8	++	-	40.2	59.8	-
A2	H4	V	-55.9			C	-145.8	++	-			
A3	H4	V	-57.9			C	-146.7	++	-			
A4	H4	V	-51.9	M	-60.9			++	-	39.3	60.7	
A5	H4	V	-51.9	M	-60.9	C	-147.2	++	-			
B1	H4	V	-45.6			V/C	-147.3	++	-			
B2	H4	V/C	-45.8	M	-60.6	V/C	-147.3	(+)	-	44.2	55.8	
B3	H4	V	-45.7			V/C	-147.9	++	-			
B4	H4	V	-46.8	M	-60.6	V/C	-147.0	++	-			
B5	H4	V	-45.9	M	-60.5	V/C	-146.9	++		44.3	55.7	

E332	T_t = 500°C P_t = 5000 bar			NH_4NO_3 = 15.5 mg $Ag_2C_2O_4$ = 22.9 mg H_2O = 5.5 mg				time = 14 days				
E332-A1	H4	C/L	-54.1	M	-60.6	L/C	-146.9	++	-	49.2	50.8	-
A2	H4	C	-53.4	M	-60.6	L/C	-147.1	++	-	44.4	55.6	
A3	H4	C/V	-49.4	M	-60.5	L/C	-146.7	++	-			
A4	H4	C/L	-51.6					++	-			
A5	H4	C/L	-51.4	M	-60.7	L/C	-146.6	++	-	44.3	55.7	
A6	H4	C	-50.2					++				
B1	H4	C/L	-54.1	M	-60.6	C	-147.1	++				
B2	H4	C/L	-51.7	M	-60.5	C/L	-146.9	++	-	43.6	56.4	
B3	H4	C/L	-51.6	M	-60.6			++	-			
B4	H4	C	-49.5					++	-			
B5	H4	C/L	-53.7			C	-148.0	(+)	-	46.1	53.9	
C1	H4	C/L	-48.9	M	-60.6	C/L	-146.7	++	-	46.7	53.3	
C2	H4	C	-51.1	M	-60.7			++	-			
C3	H4	C/L	-49.8					++	-			
C4	H4	C	-52.0					++				

E333	T_t = 500°C P_t = 5600 bar			NH_4NO_3 = 14.3 mg $Ag_2C_2O_4$ = 28.0 mg H_2O = 5.1 mg				time = 14 days				
E333-A1	H4	L	-53.4	M	-60.6	L	-147.3	++	-	49.6	50.4	
A2	H4	L	-54.5	M	-60.7	L	-147.4	++	-	49.0	51.0	
A3	H4	L	-53.2	M	-60.7	L	-147.1	++	-			
A4	H4	L	-53.9					++	-			
A5	H4	L	-53.3					++	-			
A6	H4	L	-49.2					++	-			
B1	H4	L	-55.1	M	-60.8	L/C	-147.3	++	-	50.7	49.3	
B2	H4	L	-53.8	M	-60.7	L/C	-147.4	++				

B3	H4	L	-55.5					++				
B4	H4	L	-54.4			L/C	-147.3	++	-			
B5	H4	L	-56.8	M	-60.9	L/C	-147.5	++		49.9	50.1	
B6	H4	L	-60.9	M	-61.0	L	-148.0	++		49.5	50.5	

(Table 6.4.)

E286	T_t = 504°C P_t = 2020 bar			Guanidine-nitrate = 11.3 mg $Ag_2C_2O_4$ = 28.0 mg H_2O = 10.0 mg				time = 13 days				
E286-A1	H3	V	-17.	M	-58.7		-	+	-	47.1	52.9	-
A2	H3	V	-20.	M	-58.5		-	+	-			
A3	H3			M	-58.6			+				
E320	T_t = 500°C P_t = 5000 bar			Guanidine-nitrate = 14.1 mg $Ag_2C_2O_4$ = 28.6 mg H_2O = 10.0 mg				time = 15 days				
E320-A1	H4	V	-25.1	M	-60.2	V	-147.6	(+)	+			
A2	H4	V	-25.7					+	+			
A3	H4	V	-23.9	M	-60.1	V	-148.7	+	+			
A4	H4	V	-23.0					+	+			
A5	H4	V	-24.8			V	-146.8	+	+			
A6	H4	V	-26.0	M	-60.1	V	-147.1	+	-	36.4	63.6	
A7	H4	V	-27.7					+	-			
A8	H4	V	-28.6					+	+			
E319	T_t = 500°C P_t = 5480 bar			Guanidine-nitrate = 15.7 mg $Ag_2C_2O_4$ = 31.9 mg H_2O = 10.0 mg				time = 14 days				
E319-A1	H4	V	-30.4	M	-60.3	V	-147.4	(+)	-	41.4	58.6	-
A2	H4	V	-31.8					(+)	-			
A3	H4	V	-30.9			V	-149.2	(+)	-			
A4	H4	V	-30.5	M	-60.4	V	-147.9	(+)	+			
B1	H4	V	-31.8	M	-60.6	V	-147.5	(+)	-	38.2	61.8	

Table 6.1-4.- *Microthermometric data and Raman analyses measured for artificial inclusions containing fluids produced by the decomposition of*

6.1. *$AgNO_3$ in the presence of graphite;*
6.2. *NH_4NO_3 in the presence of graphite;*
6.3. *NH_4NO_3 and $Ag_2C_2O_4$ in the presence of graphite;*
6.4. *mixtures of guanidine-nitrate ($NH_2C(=NH)NH_2.HNO_3$ and $Ag_2C_2O_4$ in the presence of graphite.*

The experimental parameters (temperatures (T_t), pressures (P_t), time durations and the amounts of used starting material and added water) are also presented. The accuracy of the experimental temperatures and

pressures are about 5°C and 30 bar respectively.

The "microthermometric" data comprise: a) the inclusion type (H and S-types) b) the homogenization temperature, stable (T_h) or metastable (T_{hm}) to L(iquid), C(ritical) or V(apour) c) the melting (T_m) or sublimation (T_s) temperature (M or S) to L/C/V. Also indicated (by observation) are the presence of water and of daughter crystals in the inclusions.

Compositions are measured by Raman analysis and are given by the relative amounts of N_2, CO_2 and CH_4 (in mole%).

REFERENCES

ALPERT N.L., W.E. KEISER & H.A. SZYMANSKI (1970) Theory and practise of infrared spectroscopy. Plenum Press - New York (2nd ed.), 380 p.

AMAT G. & M. PIMBERT (1965) On Fermi resonance in carbon dioxide. J. Molecular Spectrosc., 16, 278-290.

ANGUS S., B. ARMSTRONG & K.M. de REUK, V.V. ALTUNIN, O.G. GADETSKII, G.A. CHAPELA & J.S. ROWLINSON (1973, 1976a) International thermodynamic tables of the fluid state, vol.3: Carbon Dioxide. Pergamon Press - Oxford, 385 p.

ANGUS S., B. ARMSTRONG & K.M. de REUK (1976b) International thermodynamic tables of the fluid state, vol.5: Methane, Pergamon Press - Oxford.

ANGUS S., B. ARMSTRONG & K.M. de REUK (1979) International thermodynamic tables of the fluid state, vol.6: Nitrogen, Pergamon Press - Oxford.

ANTANOVISH A.A. & M.A. PLOTNIKOV (1976) Experimental determination of the density of nitrogen at high pressures and temperatures. Sov. Phys. Dokl., 21, 99-100.

ARAI Y., G. KAMINISHI & S. SAITO (1971) The experimental determination of the PVTX-relations for the carbon dioxide -nitrogen and the carbon dioxide - methane systems. J. Chem. Eng. Jap., 4, 113-122.

BARBILLAT J. (1983) Étude d'une seconde génération de microsonde optique à effet Raman mettant à profit les avantages de la détection multicanale. Thèse Doct., Univ. Lille, 171 p.

BÉNY C., N. GUILHAUMOU & J-C. TOURAY (1982) Native sulphur-bearing fluid inclusions in the CO_2-H_2S-S system - microthermometry and Raman microprobe (MOLE) analysis - thermochemical interpretations. Chem. Geology, 37, 113-127.

BODNAR R.J., C.W. BURNHAM & S.M. STERNER (1985) Synthetic fluid inclusions in natural quartz III: Determination of phase equilibrium properties in the system H_2O-NaCl to 1000°C and 1500 bars. Geochim. Cosmochim. Acta, 49, 1861-1874.

BOS A., G.J.L.M. de HAAS, J.H.L. VONCKEN, A.M.J. van der EERDEN & J.B.H. JANSEN (1987) Hydrothermal synthesis of ammonium-phlogopite. Geologie en Mijnbouw, 66, 251-258.

BOTTINGA Y. & P. RICHET (1981) High pressure and temperature equation of state and calculation of the thermodynamic properties of gaseous carbon dioxide. Am. J. Sci., 281, 615-660.

BOWERS T.S. & H.C. HELGESON (1984) Calculation of the thermodynamic and geochemical consequences of non-ideal mixing in the system H_2O-CO_2-NaCl on phase relations in geologic systems: metamorphic equilibria of high pressures and temperatures. Amer. Mineral., 68, 1059-1079.

BOWERS T.S. & H.C. HELGESON (1985) Fortran programs generating fluid inclusion isochores and fugacity coefficients for the system H_2O-CO_2-NaCl at high pressures and temperatures. Computers and Geosciences, 11, 203-213.

BRAME E.G. & J. GRASSELLI eds. (1976) Infrared and Raman spectroscopy (part A). Marcel Dekker Inc. - New York-Basel, 345 p.

BREWSTER D. (1826) On the existence of two new fluids in the cavities of minerals, which are immiscible, and possess remarkable physical properties. Royal Soc. Edinburgh Trans., 10, 1-41.

BURKE E.A.J. & W.J. LUSTENHOUWER (1987) The application of a multichannel laser Raman microprobe (Microdil-28) to the analysis of fluid inclusions. Chem. Geology, 61, 11-17.

BURRUSS R.C. (1981a) Analysis of fluid inclusions: phase equilibria at constant volume. Am. J. Sci., 281, 1104-1126.

BURRUSS R.C. (1981b) Analysis of phase equilibria in C-O-H-S fluid inclusions. In: L.S. Hollister & M.L. Crawford (eds.) Short course

in fluid inclusions: applications to petrology. Mineral. Ass. Canada, 39-74.

CAMPBELL A.N. & N.O. SMITH (1951) Phase rule (A. Findlay ed.) Dover Publications Inc., 494 p.

CAMPION A. & W.H. WOODRUFF (1987) Multichannel Raman Spectroscopy. Analytical Chemistry, 59-22, 1299-1308.

COOLEN J.J.M.M.M. (1980) Chemical petrology of the Furua Granulite Complex, southern Tanzania. GUA Papers of geology (Univ. Amsterdam), series 1, 13, 258 p.

CRAWFORD M.L. (1981) Phase equilibria in aqueous fluid inclusions. In: L.S. Hollister & M.L. Crawford (eds.) Short course in fluid inclusions: applications to petrology. Mineral. Ass. Canada, 75-100.

CRAWFORD M.L. & L.S. HOLLISTER (1986) Metamorphic fluids: the evidence from fluid inclusions. In: J.V. Walther & B.J. Wood (eds.) Fluid-rock interaction during metamorphism. Advances in Phys. Geochemistry (Springer Verlag), vol.5, 1-35.

DARIMONT A. (1986) Genèse des filons transverses du Paléozoïque belge. Inclusions fluides. Thèse Doct. Sciences, Univ. Liège, 138 p.

DARIMONT A. & G. HEYEN (1988) Simulation des équilibres de phases dans le système CO_2-N_2: application aux inclusions fluides. Bull. Minéral., 111, 179-182.

DAVIS J.A., N. RODEWALD & F. KURATA (1961) Solid-liquid-vapor phase behavior of the methane - carbon dioxide system. A. I. Ch. E. Journal, 8-4, 537-539.

DAVY Sir H. (1822) On the state of water and aeriform matter in cavities found in certain crystals. Royal Soc. London Philos. Trans., 2, 367-376.

DELHAYE M., J. BARBILLAT & P. DHAMELINCOURT (1980) Indentification of inclusions and particles by Raman microprobe. In: J. Albaiges (ed.) Analytical techniques in environmental chemistry, 3. Pergamon Press - Oxford, 515-522.

DELHAYE M. & P. DHAMELINCOURT (1975) Raman microprobe and microscope with laser excitation. J. Raman Spectrosc., 3, 33-43.

DHAMELINCOURT P. (1979) Étude et réalisation d'une microsonde moléculaire à effet Raman. Quelques domaines d'application. Thèse l'Univ. des Sciences et Techniques de Lille.

DHAMELINCOURT P., J.M. BÉNY, J. DUBESSY & B. POTY (1979) Analyse d'inclusions fluides à la microsonde MOLE à effet Raman. Bull. Minéral., 102, 600-610.

DONNELY H.G. & D.L. KATZ (1953) Phase equilibria in the carbon dioxide-methane system. Indus. Eng. Chem., 46, 511-517.

DUBESSY J. (1984) Simulation des équilibres chimiques dans le système C-O-H. Conséquences méthodologiques pour les inclusions fluides. Bull. Minéral., 107, 155-168.

DUBESSY J. (1985) Contribution à l'étude des interactions entre paléo-fluides et minéraux à partir de l'étude des inclusions fluides par microspectrométrie Raman - Conséquences métallogéniques. Thèse Doct. Inst. National Polytechnique de Lorraine, Nancy, 198 p.

DUBESSY J., D. AUDEOUD, R. WILKINS & C. KOSZTOLANYI (1982) The use of the Raman microprobe MOLE in the determination of the electrolytes dissolved in the aqueous phase of fluid inclusions. Chem. Geol., 37, 137-150.

DUBESSY J., N. GUILHAUMOU, J. MULLIS & M. PAGEL (1984) Reconnaissance par microspectrométrie Raman dans les inclusions fluides de H_2S et CO_2 solides à domaine de fusion comparable. Bull. Minéral., 107, 189-192.

FABRE D. & R. COUTY (1986) Étude par spectroscopie Raman, du methane comprimé jusqu'à 3 kbar. Application à la mesure de pression dans

les inclusions fluides contenues dans les mineraux. C.R. Acad. Sci. Paris, t.303, serie II, 14, 1305-1308.

FARMER V.C. ed. (1974) The infrared spectra of minerals. Mineralogical Society Monograph, 4, Adlard & Son Ltd. - Dorking, Surrey (England).

FISHER J.R. (1976) The volumetric properties of H_2O - a graphical portrayal. U.S. Geol. Survey J. Res., 4, 189-193.

FRASER D.G. ed. (1977) Thermodynamics in geology. Proceedings of the NATO Advanced Study Institute. D. Reidel Publ.-Dordrecht, 410 p.

GMELIN'S HANDBUCH DER ANORGANISCHEN CHEMIE (1971) System Nr.61, Teil B1/B3. Gmelin Institut. Verlag Chemie GmbH - Weinheim (8. Auflage).

GRIFFITH W.P. (1974) Raman spectra of minerals. In: V.C. Farmer (ed.) The infrared spectra of minerals. Mineralogical Society Monograph, 4, Adlard & Son Ltd. - Dorking, Surrey (England), 119-136.

GRIFFITH W.P. (1975) Raman spectroscopy of terrestrial minerals. In: C. Karr (ed.) Infrared and Raman spectroscopy of lunar and terrestrial minerals. Academic Press - New York-San Francisco-London, 299-323 (Chap. 12)

GUILHAUMOU N. (1982) Analyse ponctuelle des inclusions fluides par microsonde moléculaire à laser (MOLE) et microthermométrie. Traveaux Lab. Geol., 14. Presses de l'École Normale Supérieure, Paris, 78 p.

GUILHAUMOU N., P. DHAMELINCOURT, J-C TOURAY & J. TOURET (1981) Étude des inclusions fluides du système N_2-CO_2 de dolomites et de quartz de Tunisie septentrionale. Données de la microcryoscopie et de l'analyse à la microsonde à effet Raman. Geochim. Cosmochim. Acta, 45, 657-673.

GUILHAUMOU N., B. VELDE & C. BÉNY (1984) Raman microprobe analysis of gaseous inclusions in diagenetically recrystallized calcites. Bull. Minéral., 107, 193-202.

HALBACH H. & N.D. CHATTERJEE (1982) An empirical Redlich-Kwong type equation of state for water to 1000°C and 200 kbar. Contrib. Mineral. Petrol., 79, 337-345.

HARTLEY W.N. (1876) On variations in the critical point of carbon dioxide in minerals, and deductions from these and other facts. J. Chem. Soc., 31, 241-249.

HERSKOWITZ M. & H.J. KISCH (1984) An algorithm for finding composition, molar volume and isochores of CO_2-CH_4 fluid inclusions from T_h and T_{fm} (for $T_h < T_{fm}$). Geochim. Cosmochim. Acta, 48, 1581-1587.

HEYEN G. (1980) Liquid and vapor properties from a cubic equation of state. In: Phase equilibria and fluid properties in the chemical industry. EFCE Publication, series 11, 9-13.

HEYEN G. (1981) A cubic equation of state with extended range of application. Proc. 2nd World Congres Chem. Eng., Montreal, paper 8.2.6.

HEYEN G., C. RAMBOZ & J. DUBESSY (1982) Simulation des équilibres de phases dans le système CO_2-CH_4 en dessous de 50°C et de 100 bar. Application aux inclusions fluides. C. R. Acad. Sc. Paris, t. 294, série II, 203-206.

HIBBEN J.H. (1939) The Raman effect and its chemical applications. Reinhold Publishing Corporation - New York, 544 p.

HOLLISTER L.S. (1981) Information intrinsically available from fluid inclusions. In: L.S. Hollister & M.L. Crawford (eds.) Short course in fluid inclusions: applications to petrology. Mineral. Ass. Canada, 1-12.

HOLLISTER L.S., R.C. BURRUSS, D.L. HENRY & E.M. HENDEL (1979) Physical conditions during uplift of metamorphic terranes, as redorded by fluid inclusions. Bull. Minéral., 102, 555-561.

HOLLISTER L.S. & M.L. CRAWFORD eds.(1981) Short course in fluid inclusions: applications to petrology. Mineral. Ass. Canada., 304 p.

HOLLOWAY J.R. (1977) Fugacities and activity of molecular species in supercritical fluids. In: D.G. Fraser (ed.) Thermodynamics in geology, 161-181.

HOLLOWAY J.R. (1981) Compositions and volumes of supercritical fluids in the earth's crust. In: L.S. Hollister & M.L. Crawford (eds.) Short course in fluid inclusions: applications to petrology. Mineral. Ass. Canada, 13-38.

HOLLOWAY J.R. & R.L. REESE (1974) The generation of N_2-CO_2-H_2O fluids for use in hydrothermal experimentation: I. Experimental method and equilibrium calculations in the C-O-H-N system. Amer. Mineral., 59, 587-597.

HONMA H. & Y. ITIHARA (1981) Distribution of ammonium in minerals of metamorphic and granitic rocks. Geochim. Cosmochim. Acta, 45, 983-988.

HOWARD-LOCK H.E. & B.P. STOICHEFF (1971) Raman intensity measurements of the Fermi diad ν_1, $2\nu_2$ in $^{12}CO_2$ and $^{13}CO_2$. J. Molecular Spectrosc., 37, 321-326.

HWANG S.-C., H.-M. LIN, P.S. CHAPPELEAR & R. KOBAYASHI (1976) Dew point study in the vapor-liquid region of the methane - carbon dioxide system. J. Chem. Eng. Data, 21-4, 493-497.

JUZA J, V. KMONICEK & O. SIFNER (1965) Measurements of the specific volume of carbon dioxide in the range of 700 to 4000 bar and 50 to 475°C. Physica, 31, 1735-1744.

KADIK, A.A. & O.A. LUKANIN (1973) The solubility dependent behaviour of water and carbon dioxide in magmatic processes. Geochem. Intern., 10, 115-129.

KADIK A.A. & D.H. EGGLER (1976) The behaviour of water and carbon dioxide during formation of acidic magmas. Geokhimia, 8, 1167-1174 (in Russian).

KERKHOF, A.M. van den (1987) The fluid evolution of the Harmsarvet ore deposit, central Sweden. G.F.F., 109, 1-12.

KERKHOF, A.M. van den (1988) Phase transitions and molar volumes of CO_2-CH_4-N_2 inclusions. Bull. Minéral., 111-3/4 (in press).

KERRICK D.M. & G.K. JACOBS (1981) A modified Redlich-Kwong equation for H_2O, CO_2 and H_2O-CO_2 mixtures at elevated pressures and temperatures. Am. J. Sci., 281,735-767.

KREULEN R. & R.D. SCHUILING (1982) N_2-CH_4-CO_2 fluids during formation of the Dôme de l'Agout, France. Geochim. Cosmochim. Acta, 46, 193-203.

KREULEN R. (1987) Thermodynamic calculations of the C-O-H system applied to fluid inclusions: are fluid inclusions unbiassed samples of ancient fluids? Chem. Geology, 61, 59-64.

LANDOLT - BÖRNSTEIN (eds.) (1960) Zahlenwerte und Funktionen, Band II, Teil 2, 431-433.

LASNIER B. (1976) Persistence d'une série granulitique au coeur du Massif Central Française (Haut Allier) - Les termes basiques, ultrabasiques et carbonates. Thèse Univ. Nantes.

LEEDER O., R. THOMAS & W. KLEMM (1987) Einschlüsse in Mineralien. VEB Deutscher Verlag für Grundstoffindustrie - Leipzig, 180p.

LEMMLEIN G.G. & M.O. KLIYA (1952) Distinctive features of the healing of a crack in a crystal under conditions of declining temperature. Akad. Nauk. SSSR Dokl., 87, 957-960 (Transl.: 1960) Int. Geol. Rev., 2, 125-128.

LONG D.A. (1977) Raman spectroscopy. McGraw-Hill XIV, 276 p.

MALBRUNOT P. & B. VODAR (1973) Experimental PVT data and thermodynamic properties of nitrogen up to 1000°C and 5000 bar. Physica, 66, 351-363.

MRAW S.C., S.-C. HWANG & R. KOBAYASHI (1978) Vapor-liquid equilibrium of

the CO_2-CH_4 system at low temperatures. J. Chem. Eng. Data, 23-2, 135-139.

MAY A.D., J.C. STRYLAND & H.L. WELSH (1959) Raman spectra of H_2 and CH_4 at high pressures. J. Chem. Phys., 30, 1099-1101.

MICHEL-LEVY M.C. & LAUTIE (1981) Microanalysis by Raman spectroscopy of carbon in the Tieschitz chondrite. Nature, 292, 321-322.

MUIRBROOK N.K. (1964) Experimental and thermodynamic study of the high-pressure vapor - liquid equilibria for the N_2-O_2-CO_2 system. University of California, Berkeley Ph.D. Thesis.

OMAR H.O. (1962) Phase equilibria of some binary systems at low temperatures. Ph.D. Thesis Univ. Leiden.

PENG D.Y. & D.B. ROBINSON (1976) A new two-constant equation of state. Ind. Eng. Chem. Fundam., 15, 59-64.

PICHAVANT M., C. RAMBOZ & A. WEISBROD (1982) Fluid immiscibility in natural processes: use and misuse. I: Phase equilibria analysis - a theoretical and geometrical approach. Chem. Geology, 37, 1-27.

PLACZEK G. (1934) Rayleigh-Streuung und Raman Effekt. In: E. Marx (ed.) Handbuch der Radiologie, vol. 6, pt.2., 205-374. Akademische Verlagsgesellschaft - Leipzig.

POTY B., J. LEROY & L. JACHIMOWICZ (1976) A new device for measuring temperatures under the microscope: the Chaixmeca microthermometry apparatus. Bull. Soc. française Mineral. Cristallogr., 99, 182-186.

POTY B., H.A. STALDER & A. WEISBROD (1974) Fluid inclusion studies in quartz from fissures in Western and Central Alps. Schweiz. Mineral. Petrogr. Mitt., 54, 717-752.

RAMBOZ C., D. SCHNAPPER & J. DUBESSY (1984) The P-$\bar{V}$-T-X-fO_2 evolution of H_2O-CO_2-CH_4-bearing fluid in a wolframite vein: reconstruction from fluid inclusion studies. Geochim. Cosmochim. Acta, 49, 205-219.

REDLICH, O & J.N.S. KWONG (1949) On the thermodynamics of solutions V: An equation of state. Fugacities of gaseous solutions. Chem. Rev., 44, 233-244.

ROEDDER E. (1984) Fluid inclusions. Reviews in Mineralogy (P.H. Ribbe ed.) vol. 12. Mineral. Soc. America, 644 p.

ROEDDER E. & R.J. BODNAR (1980) Geologic pressure determinations from fluid inclusion studies. Ann. Rev. Earth Planet. Sci., 8, 263-301.

ROSASCO G.J. (1980) Raman microprobe spectroscopy. In: R.J.H. Clark & R.E Hester (eds.) Advances in Infrared and Raman Spectroscopy, vol.7. Heyen Co. London, 223-282.

ROSASCO G.J. & E. ROEDDER (1975) Laser excited Raman spectroscopy. Science, 190, 557-560.

ROSASCO G.J. & E. ROEDDER (1979) Application of a new Raman microprobe spectrometer to nondestructive analysis of sulphate and other ions in individual phases in fluid inclusions in minerals. Geochim. Cosmochim. Acta, 43, 1907-1915.

ROSENBUSCH H. (1923) Mikroskopische Physiographie des Petrographisch wichtigen Mineralien. 5. Auflag, O. Mügge - Stuttgart, 5 vol.

SANTIS R. de, G.J.F. BREEDVELD & J.M. PRAUSNITZ (1974) Thermodynamic properties of aqueous gas mixtures at advanced pressures. Ind. Eng. Chem. Process Des.Dev., 13, 374-377.

SAXENA S.K. & Y. FEI (1987) Fluids at crustal pressures and temperatures. I. Pure species. Contrib. Mineral. Petrol., 95, 370-375.

SCHREURS (1985) The West Uusimaa Low Pressure Thermal Dome, SW Finland. Ph.D. Thesis, Free Univ. Amsterdam.

SCHRÖTTER H.W. & H.W. KLÖCKNER (1979) Raman scattering cross-sections in gases and liquids. In: A. Weber (ed.) Raman spectroscopy of gases and liquids. Springer Verlag, 123-166.

SHELTON K.L. & P.M. ORVILLE (1980) Formation of synthetic fluid inclusions in natural quartz. Amer. Mineral., 65, 1233-1236.

SHEPHERD T.J., A.H. RANKIN & D.H. ALDERTON (1985) A practical guide to fluid inclusion studies. Blackie & Son Ltd., 239 p.

SHMONOV V.M. & K.I. SHMULOVISH (1974) Molal volumes and equations of state of CO_2 at temperatures from 100 to 1000°C and pressures from 2000 to 10,000 bar. Dokl. Akad. Nauk. S.S.S.R., 217-4, 935-938.

SMITH D.C. & J. DUBESSY (1987) Georaman-86: Raman spectroscopy in the earth sciences. Terra Cognita, 7, 27-30.

SMITH D.L. & B. EVANS (1984) Diffusional crack healing in quartz. J. Geophys. Research, 89 no.B6, 4125-4135.

SMITH F.G. (1963) Physical Geochemistry vol.1. Addiston-Wesley Publ., 624 p.

SORBY H.C. (1858) On the microscopic structure of crystals, indicating the origin of minerals and rocks. Geol. Soc. London Quart. J., 14, pt. 1, 453-500.

SPEAR F.S. & J. SELVERSTONE (1983) Water exsolution from quartz: implications for the generation of retrograde metamorphic fluids. Geology, 11, 82-85.

STEPHEN H. & T. STEPHEN (eds.) (1963), reprint 1979) Solubilities of inorganic and organic compounds. vol.1, part 1. Binary systems. Table 1781.

SWANENBERG H.E.C. (1979) Phase equilibria in carbonic systems and their application to freezing studies of fluid inclusions. Contr. Mineral. Petrol., 68, 303-306.

SWANENBERG H.E.C. (1980) Fluid inclusions in high-grade metamorphic rocks from S.W.Norway. Geologica Ultraiectina, 25 (Univ. Utrecht), 146 p.

TIMMERMANS J. (1960) The physico-chemical constants of binary systems in concentrated solutions. vol.4. Systems with inorganic + organic or inorganic compounds. Interscience Publ. Inc. - New York, p.676.

TOBIAS R.S. (1967) Raman spectroscopy in inorganic chemistry. I: Theory. J. Chem. Educ., 44, 2-8.

TOMILENKO A.A. & V.P. CHUPIN (1983) Thermobarochemistry of metamorphic complexes. Acad. Sci. S.S.S.R. Siberian branch 524, 200 p.

TOURAY J-C. (1968) Recherches geochimique sur les inclusions à CO_2 liquide. Bull. Soc. française Minéral. Cristallogr., 91, 367-382.

TOURAY J.C., C. BÉNY, J. DUBESSY & N. GUILHAUMOU (1985) Microcharacterization of fluid inclusions in minerals by Raman microprobe. Scanning Electron Microscopy, 103-118.

TOURET J.L.R. (1977) The significance of fluid inclusions in metamorphic rocks. In: D.G. Fraser (ed.) Thermodynamics in geology. Reidel Publ. Co. - Dordrecht, 203-227.

TOURET J.L.R. (1981) High grade metamorphic rocks In: L.S. Hollister & M.L. Crawford (eds.) Short course in fluid inclusions: applications to petrology. Mineral. Ass. Canada, 182-208.

TOURET J.L.R. (1982a) An empirical phase diagram for a part of the N_2-CO_2 system at low temperature. Chem. Geology, 37, 49-58.

TOURET J.L.R. (1982b) Les effluves de la terre. Inaugural. Free University - Amsterdam, 22 p.

TOURET J.L.R. (1984) Les inclusions fluides: histoire d'un paradoxe. Bull. Minéral., 107, 125-137.

TOURET J.L.R. (1987) Fluid inclusions and pressure-temperature estimates in deep-seated rocks. In: H.C. Helgeson (ed.) Chemical transport in metasomatic processes. NATO ASI Series (C): Mathemathecal and Physical Sciences. vol.218, 91-121.

TOURET J.L.R. & Y. BOTTINGA (1979) Équation d'état pour le CO_2: application aux inclusions carboniques. Bull. Minéral., 102, 577-583.

TOURET J.L.R. & A.M. van den KERKHOF (1986) High density fluids in the lower crust and upper mantle. Physica, 139 & 140B, 834-840 (Proceedings of the Xth AIRAPT International High Pressure Conference).

TSIKLIS D.S. & E.V. POLYAKOV (1968) Measuring the compressibility of gases by the displacement method. Nitrogen compressibility at pressures up to 10,000 atm. and temperatures to 400°C. Dokl. Akad. Nauk., Soviet Physics, 12-9, 901-904.

TSU R., J.H. GONZALES & I.C. HERNANDEZ (1978) Observations of splitting of the E_{2g} mode and two-phonon spectrum in graphites. Solid state communications. Pergamon Press Ltd., vol. 27, 507-510.

TUINSTRA F. & KOENIG (1970) The Raman spectrum of graphite. J. Chem. Phys., 53, 1126-1130.

TUTTLE O.F. (1949) Two pressure vessels for silicate-water studies. Geol. Soc. Amer. Bull., 60, 1727-1729.

VAGARFTIK N.B. (1972) Tables of thermodynamic properties of gases and liquids. Izd. Nauka - Moscow, 720 p.

VOGELSANG H. & GEISSLER H. (1869) Über die Natur der Flüssigkeitseinschlüsse in gewissen Mineralien. Ann. Physik. Chemie, 137, ser. 5, 17, 56-75.

WAGNER A., M. FREY, F. QUADRIO, J. SCHWARZKOPFF & H.A. STALDER (1972) Die Mineralfundstellen von Camperio und Campo Blenio, Kanton Tessin. Jahrbuch Naturhist. Museum der Stadt Bern.

WALTHER J. (1981) Fluide Einschlusse im Apatit des Carbonatits vom Kaiserstuhl (Oberrheingraben): ein Beitrag zur Interpretation der Carbonatitgenese. Dissertation Univ. Karlsruhe.

WEAST R.D. ed. (1975) Handbook of chemistry and physics (56th ed.) CRC Press Inc.

WHITE W.B. (1975) Structural interpretation of lunar and terrestrial minerals by Raman Spectroscopy. In: C. Karr (ed.) Infrared and Raman Spectroscopy of lunar and terrestrial minerals. Academic Press - New York-San Fransisco-London (Chap.13).

WOOD B.J. & D.G. FRASER (1978) Elementary thermodynamics for geologists. Oxford University Press, 303 p.

WOPENKA B. & J.D. PASTERIS (1985) Limitations to quantitative analysis of fluid inclusions in geological samples by laser Raman microprobe spectroscopy. Applied Spectroscopy, 40, 144-151.

WILLIAMS D.H., I. FLEMMING (1971) Spekroskopische Methoden in der Organischen Chemie. Georg. Thieme Verlag - Stuttgart, 346 (translated by B. Zeeh).

YPMA P.J.M. (1963) Rejuvenation of ore deposits as examplified by the Belledonne metalliferous province. Thesis Univ. Leiden, 209 p.

ZIRKEL F. (1873) Die mikroskopische Beschaffenheit der Mineralien und Gesteine. W. Englemann - Leipzig, 502 p.

APPENDICES

Appendix 1. The filling degree of 2-phase inclusions

The total molar volume ($\bar{V}_t$) of a 2-phase inclusion (containing liquid and vapour) can be expressed as a function of molar volume of the single phases ($\bar{V}_L$ and $\bar{V}_V$) and the filling degree (DF). The filling degree is defined as follows:

$$DF \quad V_L / V_t \quad V_L / (V_L + V_V) \qquad \text{(Eq.A.1)}$$

where V_L, V_V and V_t denote the absolute volumes of the liquid and vapour phases and total volume respectively. V_t is taken as 1 and Eq.A.1 reduces to

$$DF \quad V_L \qquad \text{(Eq.A.2)}$$

(DF is a number between 0 and 1).

The absolute volumes of the phases are expressed by the equations:

$$V_L \quad \bar{V}_L \cdot n_L \quad \text{and} \qquad \text{(Eq.A.3a)}$$
$$V_V \quad \bar{V}_V \cdot n_V \qquad \text{(Eq.A.3b)}$$

where n_L and n_V denote the number of moles present in the liquid and vapour phases respectively. Now, the total molar volume can be expressed by

$$\bar{V}_t \quad \frac{V_L + V_V}{n_L + n_V} \qquad \text{(Eq.A.4)}$$

By filling in Eqs A.1, 2 and 3 in Eq.A.4, the total molar volume at a given temperature is expressed by

$$\boxed{\bar{V}_t \quad \frac{\bar{V}_L \cdot (1/DF)}{1 + (\bar{V}_L/\bar{V}_V)(1/DF - 1)}} \qquad \text{(Eq.A.5)}$$

If DF approaches zero, $\bar{V}_t$ reduces to the molar volume of the vapour ($\bar{V}_V$);

if DF approaches unity, $\bar{V}_t$ reduces to the molar volume of the liquid phase ($\bar{V}_L$).

Application 1 (minimum T_h^V observed in CO_2 inclusions)

Calculate the minimum homogenization temperature to be measured in a CO_2 inclusion, homogenizing to the vapour phase. It is assumed that the minimum amount of liquid which can be observed in a (spherical) fluid inclusion is 10 vol% (DF = 0.1). Observation at the temperature of the triple point of CO_2 (-56.6°C) is considered. The molar volumes can be found from thermodynamic tables (Angus et al. 1976a): $\bar{V}_L$ = 37.347 and $\bar{V}_V$ = 3134.2 cm^3/mole. The total molar volume of the inclusion containing 10 vol% liquid and -56.6°C is given by Eq.A.5:

$$\bar{V}_{CO2} = \frac{37.347\ (1/0.1)}{1 + (37.347/3134.2)(1/0.1\ -1)} \quad 337.3\ cm^3/mole.$$

It is found in the same table as mentioned above that the corresponding homogenization temperature is +9°C. Homogenization temperatures below this value can therefore generally not be observed and inclusions seem to be empty.

Application 2 (minimum T_{hs}^V observed in N_2 ($\pm CO_2$) inclusions)

Find the minimum homogenization temperature to the vapour phase (minimum density) of a pure nitrogen inclusion or of a mixed CO_2-N_2 inclusion. In the latter inclusions, no solubility of CO_2 in fluid N_2 is assumed at temperatures below the critical temperature of N_2 (-147°C). The minimum amount of liquid which is possible to observe in an inclusion containing N_2 (with or without solid CO_2) is assumed to be 10 vol% (DF = 0.1). The temperature considered is -180°C, the minimum temperature which can normally be reached by cooling with liquid nitrogen. The molar volumes of the liquid and vapour phases are found in Angus et al. (1979): $\bar{V}_L$ = 38.393 and $\bar{V}_V$ = 1464.5 cm^3/mole. The total molar volume is calculated according Eq.A.5:

$$\bar{V}_{N2} = \frac{38.393\ (1/0.1)}{1 + (38.393/1464.5)(1/0.1\ -1)} \quad 310.6\ cm^3/mole.$$

Nitrogen of this molar volume will show T_h^V (or Ths^V) = -158°C. Inclusions showing lower homogenization temperatures seem to be empty. The boundary between (apparent) H3 and H4 inclusions of the system CO_2-N_2 is represented by the tie-line between solid CO_2 and the homogenization point of the N_2 fraction in a $\bar{V}X$ diagram (line 1 in Fig.5.17b). This line is expressed by an equation found by filling in the find value for $\bar{V}_{N2}$ in Eq.6.3; the molar volume of solid CO_2 is taken 28.2 cm^3/mole:

$$\bar{V}_t \quad X_{CO2} \cdot 28.2 + X_{N2} \cdot 310.6 \quad : \quad 282.4\ X_{N2} + 28.2$$

Inclusions with $\bar{V}_t > 282.4\ X_{N2} + 28.2$ (plotting at the high $\bar{V}$ side of the line) are observed as type H3; inclusions with $\bar{V}_t < 282.4\ X_{N2} + 28.2$ are characterized by observed partial homogenization of the N_2 fraction (T_{hs}).

Application 3 (minimum amount of solid CO_2 observed in CO_2 ($\pm N_2$) inclusions)

Calculate the highest molar volume of a CO_2 inclusion in which the solid content can be observed at -180°C. Eq.A.5 can be re-written for a cavity containing a solid and a vapour phase:

$$\bar{V}_t \quad \frac{\bar{V}_S\ (1/VS)}{1 + (\bar{V}_S/\bar{V}_V)(1/VS - 1)} \qquad \text{(Eq.A.6)}$$

where VS = the volume proportion of the solid particle; $\bar{V}_S$ = molar volume of the solid = 28.2 cm^3/mole and $\bar{V}_V$ = is the molar volume of the vapour phase. The latter quantity is considered as very high compared to $\bar{V}_S$ and Eq.A.6 reduces to

$$\bar{V}_t \quad \bar{V}_S/VS \quad 28.2/VS \qquad \text{(Eq.A.7)}$$

Assumed that less than 1 vol% of solid CO_2 is not visible, it follows from Eq.A.7 that $\bar{V}_t$ = 28.2/0.01 = 2820 cm^3/mole. This value indicates that even very small amounts of CO_2 can be observed by freezing, for inclusions of high molar volume (low density).

In the system CO_2-N_2, no solubility of CO_2 in the vapour is assumed at -180°C. Fluid inclusions of mixed composition containing 1 vol% of solid

CO_2 at this temperature plot on a line in the $\bar{V}X$ diagram (line 2 in Fig.5.17b) connecting the point $X_{N2} = 0.99$, near the triple point of N_2, and the point $X_{N2} = 0$ ($\bar{V} = 2820$ cm^3/mole).

Appendix 2. Molar volume of inclusions containing gas and water

The correlation between total and partial molar volumes of fluid inclusions containing water and a gas phase is calculated by assuming that all water is present in the liquid phase and that gas species do not dissolve in water.

Definitions:

$\bar{V}_t$ = total molar volume;
$\bar{V}_{H2O}$ = partial molar volume of the water phase (=18.01 cm^3/mole for liquid H_2O and 19.65 for ice);
$\bar{V}_G$ = partial molar volume of the gas phase;
X_{H2O} = the mole fraction of H_2O;
X_G = the mole fraction of gas;
C_{H2O} = filling degree of water (in volume proportions);
r_1 = the radius of a (spherical) bubble (gas phase);
r_2 = the radius of a spherical inclusion.

Equations:

The correlation between $\bar{V}_G$ and $\bar{V}_t$ are deduced from $\bar{V}_t = \bar{V}_G.X_G + \bar{V}_{H2O}.X_{H2O}$ and $X_{H2O} + X_G = 1$:

$$\bar{V}_G \qquad \frac{\bar{V}_t - \bar{V}_{H2O}.X_{H2O}}{1 - X_{H2O}} \qquad \text{or} \qquad X_{H2O} \qquad \frac{\bar{V}_G - \bar{V}_t}{\bar{V}_G - \bar{V}_{H2O}} \qquad \text{(Eg.A.8.)}$$

Filling degrees are related to molar water fractions according

$$C_{H2O} = \frac{\bar{V}_{H2O}}{\bar{V}_t} \cdot X_{H2O} \qquad \text{(Eq.A.9)}$$

The size of the bubble in a spherical inclusion is calculated as a function of the filling degree:

$$r_1 \qquad \sqrt[3]{1 - C_{H2O}} \cdot r_2 \qquad \text{(Eq.A.10)}$$

Appendix 3. Review of studied natural inclusions

High-grade metamorphic rocks from SW Norway (Rogaland)

The samples are obtained from the study of Swanenberg (1980) of the Rogaland and Vest-Agder area. Here, the main metamorphic episode was superimposed on older metamorphic rocks (1500-1200 Ma). The PT-conditions ranged between 650-1050°C and 3-7 kbar during a complex metamorphic path. Higher metamorphic pressures (up to 10 kbar) are rejected by including present Raman data which show the impurity of the fluids.

Non-aqueous fluid compositions are representative for (the full ranges of) the 3 systems CO_2-CH_4, CO_2-N_2 and CH_4-N_2. Inclusions could be classified according to their microthermometric behaviour as type H3, S2, H4, H1 and H5 (in order of decreasing frequency). Lowest molar volumes (highest densities) are found for the CO_2-rich fluids ($\bar{V}$ = 41 to 55 cm^3/mole); CH_4 and N_2 have higher molar volumes (from critical $\bar{V}$, 99-89, to about 53 cm^3/mole). The latter gas species most probably represent late fluids. A mixing trend could be recognized between highest density CO_2 and CH_4: intermediate compositions show lower molar volumes with a maximum around the 50-50 mole% composition ($\bar{V}$ - 80 cm^3/mole). This is an indication for the proceeding of a retrograde graphite-forming reaction. Small amounts of graphite (detected by Raman analysis) formed in all inclusions except in the members of the CO_2-N_2 range. There is evidence for a contemporaneous fluid evolution from high to low density CO_2 and a (local) change in fluid composition to CH_4 and N_2.

"Carbonic" inclusions showing metastable homogenization or only "dissolution" of solid CO_2, as described by Swanenberg (1980, p.22-23 and 92-94), appeared to contain 15-83 mole% CH_4 and 5-82 mole% N_2. The non-purity of CO_2 is also evident from low melting and sublimation temperatures and from the occurrence of type H4 and H5 inclusions.

Nitrogen-bearing fluids in marbles from Pusula (SW Finland)

The studied samples are taken from the small quarry of Pusula, about 50 km NW of Helsinki. The marbles are situated within the so-called West Uusimaa Granulite Complex (700-825°C and 3-5 kbar, Schreurs 1985). The marbles are poor in magnesia, but locally rich in silica: the main

minerals in the impure marbles are wollastonite, diopside, tremolite, phlogopite, olivine and locally graphite. Quartz veins of some mm's to dm's thick show the enrichment of wollastonite and diopside.

Gaseous inclusions (found in quartz) are representative for the system CO_2-N_2, but the amounts of H_2S may be considerable (up to 24 mole%); the content of hydrocarbons is less than 5 mole% in all samples. There is a tendency of lower H_2S and higher CH_4 to higher CO_2-contents. The phase behaviour of fluid inclusions is classified as type H3, H1, S2 and H4. Both CO_2 and N_2-rich inclusions have a mean molar volume of about 70 cm^3/mole and are not consistent with regional metamorphic conditions.

The origin of CO_2 and N_2 is probably different seen the local enrichment of CO_2 in veins of a different generation: CO_2 is supposed to be mainly of metamorphic origin; N_2 (and H_2S) was most probably produced by biochemical processes during the sedimentary stage.

The Furua Granulite Complex (Tanzania)

The Furua Granulite Complex consists of high-grade metamorphic volcano-sedimentary rocks of Precambrian age. The area was studied in detail by Coolen (1980). The highest density CO_2-inclusions show a primary character (isolated, and a negative crystal shape). Although most carbonic inclusions are pure in CO_2, some samples (grossularite-diopside rocks) show high N_2-contents. Fluid inclusions mainly developed in quartz grains. The metamorphic pressure was calculated to be 6.5 to 8.5 kbar at 650-850°C; earlier calculations, indicating higher pressures (up to 15 kbar), are rejected by the present data (including Raman analysis).

Microthermometric studies show H3, S1, S2, S3 and S4 behaviour (in order of decreasing frequency of occurrence) of fluid inclusions. N_2-contents range from 3 to 54 mole%. The molar volume is about 40 cm^3/mole for all inclusions. Lower molar volumes (higher densities) as described by Coolen for the S-type inclusions are not realistic, because the lowest homogenization temperatures are due to high N_2-contents.

The present data could be used for the construction of the high density part of the isochoric TX diagram (van den Kerkhof 1988).

Dôme de l'Agout (France)

The area is located in the southern part of the Massif Central and it is an example of a thermal dome, superimposed on low-grade metamorphic rocks. Fluid inclusions were studied by Kreulen & Schuiling (1982). The same samples were presently studied by Raman analysis.

Fluid inclusions are of type H3, H1, H2, S2 and S1. They are mainly restricted to CO_2-CH_4 and CH_4-N_2 compositions. Raman analysis shows that members of both ranges may occur in one sample. These results are generally consistent with earlier published bulk compositions, measured by gas chromatography (Kreulen & Schuiling 1982). Hydrogenated sulphur occurs in accessory amounts; graphite is absent. Molar volumes are high in the central part of the dome (100 to 400 cm^3/mole) and lower in the outer parts (52 to 100 cm^3/mole). However, both volumetric ranges are not consistent with the regional metamorphic PT-conditions as calculated from mineral stability reactions by Kreulen & Schuiling (4-5 kbar, 500-700°C). This can be explained by the presence of water in the "gaseous" inclusions and miscibility of the phases at the time of trapping.

Granulites from Haut Allier (France)

The studied rock is a basic granulite (quartz-bearing "pyrigarnite") which is supposed to be an equivalent of eclogite. The petrographic aspects of the rock were extensively studied by Lasnier (1976).

Fluid inclusions are of type S2 and H3. Most inclusions (type S2) are rich in N_2 with a mean composition (in mole percent) of $N_2(77)CH_4(15)CO_2(8)$; some inclusions (type H3) are CO_2-rich: about $N_2(10)CH_4(15)CO_2(75)$. Molar volumes range from 75 to 90 cm^3/mole and the present inclusions apparently do not originate from a high-grade metamorphic stage.

The coal basins of the Appalachian

The samples, provided by Dr. H. Kisch, were taken from the anchimetamorphic terrains in the Great Valley and anthracite fields in the external zones of the central Appalachian. The phase behaviour of

fluid inclusions (with "$T_h<T_m$") was earlier described by Herskowitz & Kisch (1984).

In the present study, the following types of phase behaviour were distinguished: S2, H1 and H2. The fluids are mixtures between CH_4 and CO_2 (from 0 to 22 mole%); amounts of N_2 and HS^- are generally less than 1 mole%. Type S2 and H2 inclusions have low molar volumes (41 to 67 cm^3/mole); the molar volumes of type H1 inclusions are much higher. Trapping pressures are calculated to be 3 to 1 kbar at 300°C.

The Harmsarvet ore deposit (central Sweden)

The samples, provided by Dr. C. Kieft, are taken from quartz veins in the silver-rich zinc-lead deposit. Gaseous inclusions consist of 3 components: CO_2, CH_4 and N_2; aqueous inclusions are complex brines of varying composition. Gaseous inclusions could be classified as H3, H1 or S1. Most frequent are CO_2-inclusions with up to 30 mole% CH_4; CH_4 and N_2 inclusions are free of any CO_2 (van den Kerkhof 1987). Remarkable is the occurrence of sharp trails which contain late phase ore minerals (e.g. acanthite) and associated CH_4-rich inclusions. A change in fluid composition from CO_2 to more CH_4-rich is proposed from the peak of metamorphism (600°C, 3 kbar) to late (retrograde) PT-conditions (200°C, <0.5 kbar); aqueous inclusions evolved contemporaneously from extremely salt (47 wt% NaCl-equivalents) to low salt contents. The deposition of different ore minerals (early and late) could be related to several stages of fluid evolution.